DESIGN OF MOMENT CONNECTIONS FOR COMPOSITE FRAMED STRUCTURES

by

Gregory G. Deierlein
Joseph A. Yura
James O. Jirsa

National Science Foundation
Grant No. MSM-8412111
American Institute of Steel Construction
CBM Engineers, Inc.

Phil M. Ferguson Structural Engineering Laboratory
Bureau of Engineering Research
The University of Texas at Austin

PMFSEL REPORT NO. 88-1

MAY 1988

Any opinions, findings, and conclusions or recommendations expressed in this publication are those of the authors and do not necessarily reflect the views of the National Science Foundation.

ABSTRACT

Increasingly, engineers are designing composite and mixed building systems of structural steel and reinforced concrete to produce more efficient structures than either material alone affords. Recent literature has pointed the out need for design guidelines in several areas related to composite structural systems. One such area is in detailing of moment connections in composite framed structures which consist of steel beams and reinforced concrete or composite columns. Such composite frames have been employed for buildings in the 40 to 70 story height range.

Based on experimental research conducted at The University of Texas, the design of moment connections between steel beams and reinforced concrete or composite columns is addressed. An analytic model for calculating joint strength and design recommendations are developed from test data for composite connections and design recommendations for structural steel and reinforced concrete joints. Experimental results are reported for eight 2/3 scale interior composite joint specimens tested under reverse cyclic loading. Also summarized are results from nine composite joint specimens tested in an earlier phase of the research. The aim in the tests is to gain understanding of connection behavior by examining the influence of various joint details in mobilizing shear capacity of concrete in the connection. Attention is focussed on formation of internal mechanisms which transfer load between the steel beam and reinforced concrete.

ACKNOWLEDGMENTS

This report is the Ph.D. dissertation of Gregory G. Deierlein, under the direction of Professors Joseph A. Yura and James O. Jirsa. The material is based upon work supported primarily by the National Science Foundation under Grant No. MSM-8412111 and by the University of Texas through university fellowship support. The American Institute of Steel Construction and CBM Engineers, Inc., of Houston, Texas, provided funds to initiate the project. This research is a continuation of work initiated at the University of Texas by Dr. Tauqir Sheikh.

The experimental work was conducted in the Ferguson Structural Engineering Laboratory of The University of Texas at Austin. The help of the many graduate students who assisted in the construction of the test specimens and the actual testing, and the technical and administrative staff of the Laboratory is greatly appreciated. Carol Booth typed the report.

TABLE OF CONTENTS

CHAPTER 1 - INTRODUCTION

A significant development in the evolution of building design has been innovative use of composite and mixed construction of structural steel and reinforced concrete to achieve greater efficiency than either material alone can provide. In one sense, mixed systems are not new since structural steel buildings have to some extent always incorporated reinforced concrete components. Recently, however, designers and contractors are pioneering structural systems which utilize unprecedented interaction of steel and concrete elements. Rapid development of these composite structures has created need for research in several areas to provide better understanding of composite behavior.

One area of needed research is in moment connections (termed composite connections) between steel beams and reinforced concrete or composite columns. Such connections are an integral part of so called composite framed structures which have been employed in buildings ranging from 40 to 70 stories. The composite frame is a system of steel beams and reinforced concrete or composite columns which carry vertical or horizontal loads through frame action.

This report presents an examination of composite connection behavior based on an experimental research program conducted at the University of Texas. Two aims of the study are to first, identify the internal mechanisms which carry loads through the joint, and second, develop design models to calculate the strength of such mechanisms. These aims lead towards a general goal of developing guidelines to aid practicing engineers in designing composite connections with greater certainty. The analysis and recommendations presented are based primarily on results from an experimental program conducted in two phases. The first phase includes tests of 9 specimens which have been reported previously by Sheikh,[1] and the second phase includes tests of 8 specimens documented herein.

1.1 Composite Framed Structures

In the United States the composite frame has evolved for buildings where traditionally structural steel moment resisting frames offered a convenient and cost effective lateral force system. Such buildings, typically in the range of

40 to 70 stories, are designed with perimeter framed tube systems. Substitution of the steel columns with reinforced concrete or composite columns offers an attractive alternative since concrete columns are roughly 8 to 11 times more cost effective[2] than structural steel columns based on strength and stiffness. This cost differential results in significant savings for medium and high rise buildings where columns represent a larger portion of the total structural cost.

Typically, composite framed structures are built by erecting a steel frame in which light steel erection columns are later encased by reinforced concrete columns. As shown in Figs. 1.1a and b the steel erection usually advances roughly 10 to 12 stories ahead of the concrete columns. This construction sequence is an integral ingredient for the economy of such systems as one designer notes, "Besides the economy of materials, composite structures have the advantage of speed of construction by allowing a vertical spread of construction activity so that numerous trades can engage simultaneously in the construction of the building."[2] Further discussion of advantages with composite framed structures and examples of where they have been used are presented in references 1, 3, 4, and 5.

1.2 Composite Connection

1.2.1 Description. This report addresses the design and behavior of composite connections configured as interior joints in frames subjected to lateral loading. Figure 1.2a shows the classic deflected shape of such a frame in which the member force distribution is characterized by inflection points near the midpoint of the beams and columns with the maximum moments occurring at the connection. In Fig. 1.2b an interior joint is extracted from the frame and shown with the resulting beam and column forces acting at the connection. As shown, the steel beam is continuous through the concrete column. Where used the embedded steel erection column offers only a minimal strength contribution to the concrete column owing to their relative sizes, however, as will be discussed the column offers a significant benefit locally at the connection. While this study directly addresses interior planar cruciform connections, the results can be applied to other configurations such as exterior, corner, and three dimensional joints.

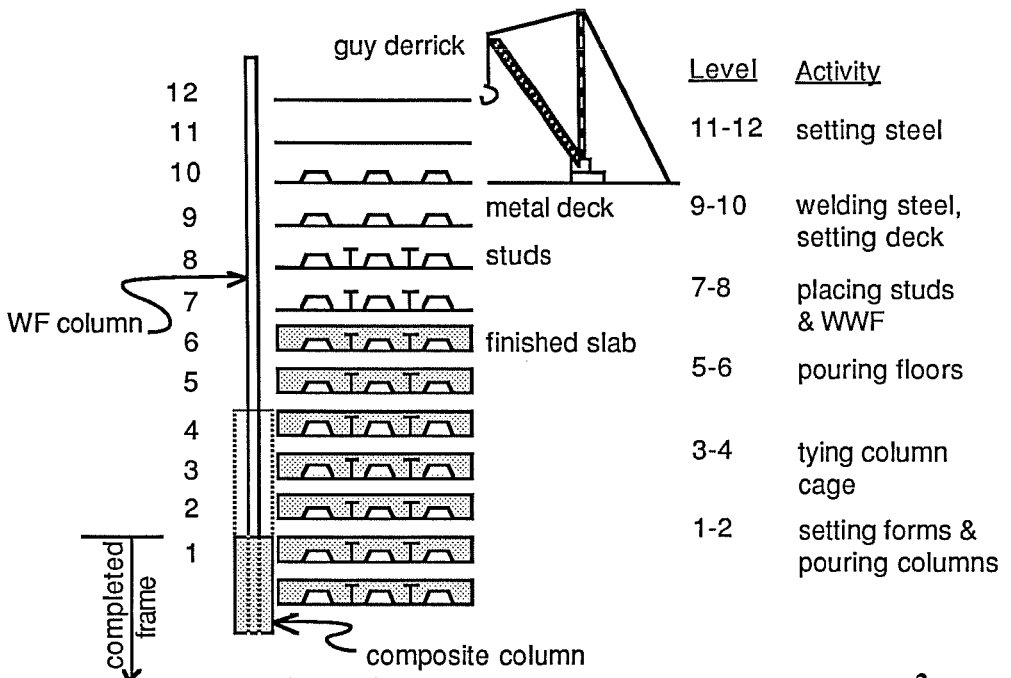

Fig. 1.1a Composite Frame Construction Sequence [2]

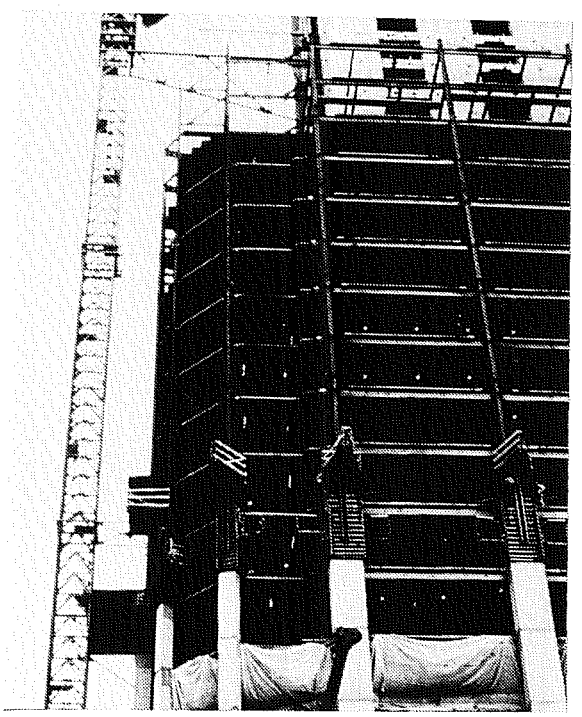

Fig. 1.1b Forty-nine Story First City Tower, Houston [2]
(Courtesy of Walter P. Moore & Associates)

The primary function of connections such as that shown in Fig. 1.2b is to transfer large unbalanced moments between the beams and columns. Proper connection design should insure satisfactory response of the structure under both service and ultimate conditions. At service loads the joint should have adequate stiffness so as to limit wind and earthquake induced drifts to acceptable levels. The connection must also resist ultimate design loads at reasonable deformation levels. The ultimate connection design forces may be factored service loads as in the case of wind loading, or forces associated with hinging of adjacent beams which provide an upper bound on connection forces for inelastic seismic response. Joint deformations should be controlled at ultimate loads to prevent excessive building drift which could lead to lateral instability.

1.2.2 Current Practice. The current state of practice for design of composite beam-column joints relies heavily on individual designer's judgment based on existing information and specifications for structural steel and reinforced concrete connections. Owing to traditional separation of research and specifications for structural steel and reinforced concrete, established design guidelines for composite structures have not evolved in a systematic fashion. In the United States there has been little if any published research directly addressing the composite connection. The closest applicable research and standards are those addressing embedded steel shapes used as brackets in precast concrete construction. In Phase I of this project Sheikh[1] presented research and specifications pertinent to composite beam-column joints. Sheikh's review includes references from the United States, Japan and Australia.

In Japan a type of composite construction called Steel Reinforced Concrete (SRC) has been popular for many years and has generated considerable research on composite connections. In addition, the Architectural Institute of Japan (AIJ) has published SRC design standards which include recommendations for composite connections. However, due to several basic differences between the evolution of composite systems in the U.S. and Japan, much of the Japanese work is not directly applicable to the composite connections addressed in this report.

SRC structures gained in popularity in Japan after the 1923 Kanto earthquake by providing enhanced ductility of reinforced concrete frames in low and medium rise structures.[6] Traditional SRC structures consist of framed systems where both the steel beams and columns are encased by concrete. Early SRC structures in Japan were similar to schemes for reinforced concrete built in the U.S. during the early 1900's where built-up open web structural steel members served as the primary reinforcement in concrete. More recently, Japanese SRC structures are evolving to resemble U.S. composite systems where rolled column shapes are encased in concrete and steel beams remain unencased. However, due to its emphasis on ductility the AIJ standard places the following restriction on the minimum moment capacity of the embedded column:[7]

$$0.5\, M_b \leq M_c \leq 2.0\, M_b \tag{1.1}$$

Here M_b and M_c are the moment capacities of the steel beam and column respectively. This requirement is contrary to U.S. practice where the steel column is small relative to the steel beam and the reinforced concrete provides most of the column capacity.

1.2.3 Internal Mechanisms. The two basic modes of failure observed in composite connections are joint shear failure and compressive crushing or bearing failure. Fig. 1.3a indicates the deformation associated with joint shear failure. As will be described throughout this report, an important distinction regarding shear failure in composite connections is that several different mechanisms resist shear in different regions of the connection. The different zones do not deform equally and hence their contribution to the capacity varies depending on the joint detailing used. Figure 1.3b shows the compression or bearing failure, evidenced by concrete crushing and gaps opening against the beam flanges.

Figures 1.4a through 1.4c show the three basic mechanisms which resist joint shear. In visualizing joint shear mechanisms it is useful to consider their role in preventing horizontal movement of the beam flanges which tend to push through the joint due to the axial flange forces shown. These flange forces

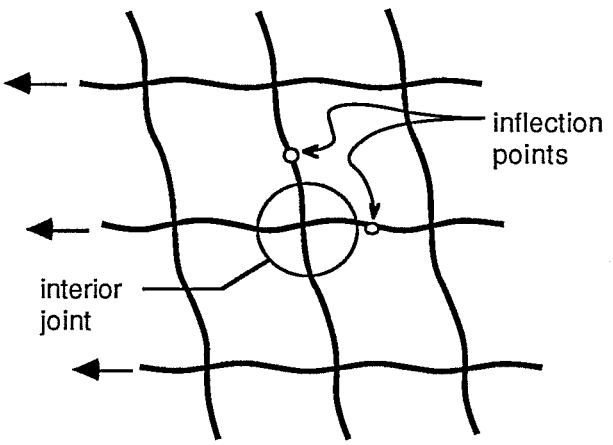

Fig. 1.2a Frame Subjected to Lateral Loading

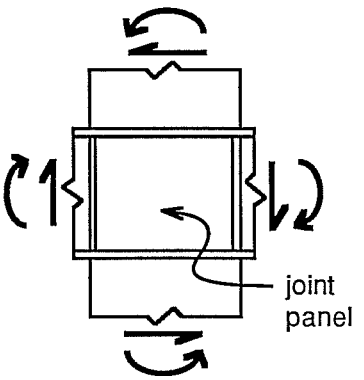

Fig. 1.2b Forces on Interior Joint

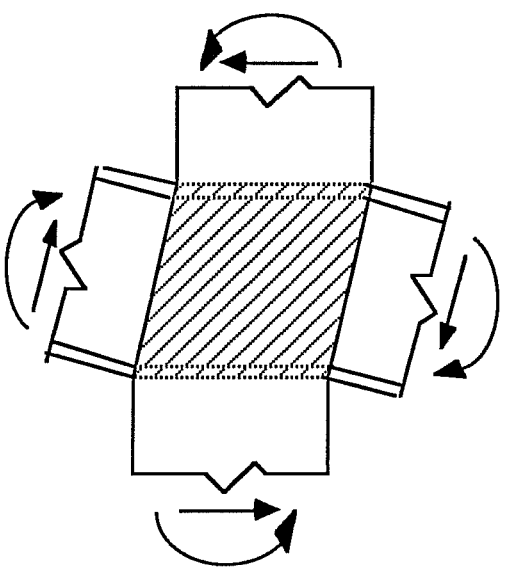

Fig. 1.3a Joint Shear Failure

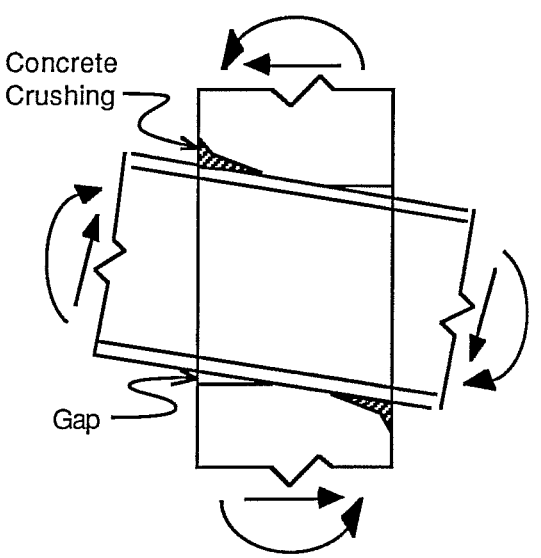

Fig. 1.3b Joint Bearing Failure

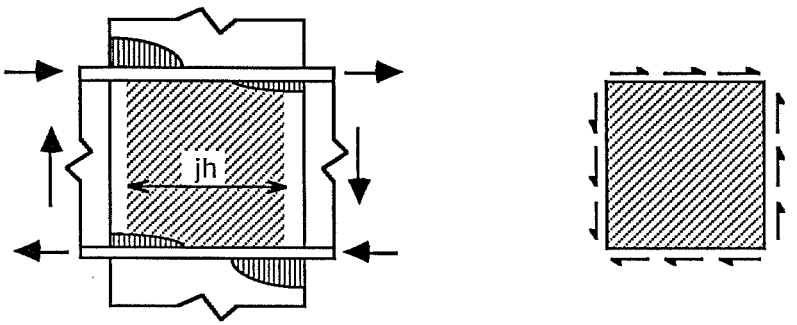

Fig. 1.4a Steel Web Panel

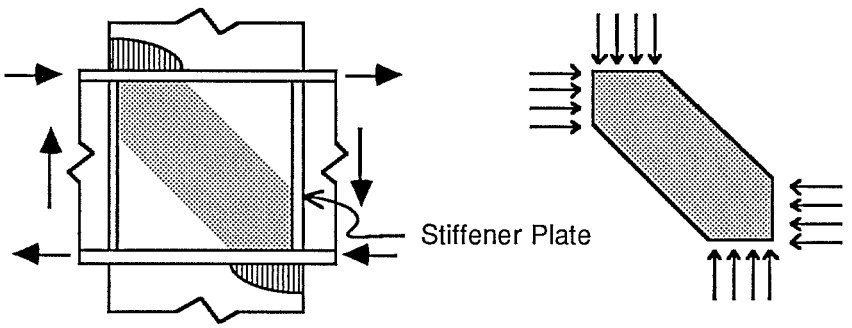

Fig. 1.4b Concrete Compression Strut

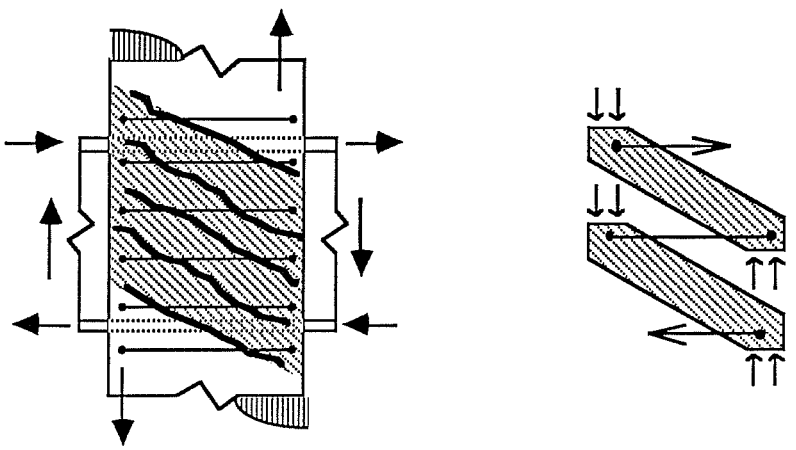

Fig. 1.4c Concrete Compression Field

are simply the horizontal force couple equivalent to the applied beam moment adjacent to the connection.

In Fig. 1.4a the steel web panel resists joint shear in a similar manner as joint panels in structural steel connections. One complication in composite joints is evaluation of the effective web panel width, jh, which is determined by the location of the vertical bearing force resultant.

Figures 1.4b and c show two means by which concrete carries joint shear forces. In Fig. 1.4b a single diagonal compression strut forms between the beam flanges through bearing against the vertical stiffener plates shown. This strut model is similar to that currently viewed in U.S. practice as the primary joint shear mechanism in reinforced concrete joints.[8] Figure 1.4c shows the compression field or truss mechanism where a system of diagonal compression struts and horizontal tension ties carry shear through the joint. This mechanism is similar to that for modeling shear in reinforced concrete members. Also, contrary to current U.S. practice, the compression field model is viewed by some researchers[9] and specification committees as the primary shear mechanism in reinforced concrete joints. In the composite connection each of these two mechanisms, the compression strut and compression field, carry joint shear in different regions of the connection.

Models for evaluating the second mode of failure, joint bearing, are shown in Figs. 1.5a and b. Figure 1.5a shows regions of high concrete bearing stresses which develop against the flanges as the beam tends to rotate within the column. Stresses develop against both flanges (top and bottom), although as shown in Fig. 1.5a, stresses outside the beam depth are greater. Concrete bearing capacity is assessed using an equivalent rectangular stress block similar to that used for compressive flexural stresses in concrete members. Figure 1.5b indicates how vertical joint reinforcement strengthens the concrete bearing region and also transfers tension directly into the column. Such reinforcement typically consists of reinforcing bars attached to the beam using a welded or other mechanical detail.

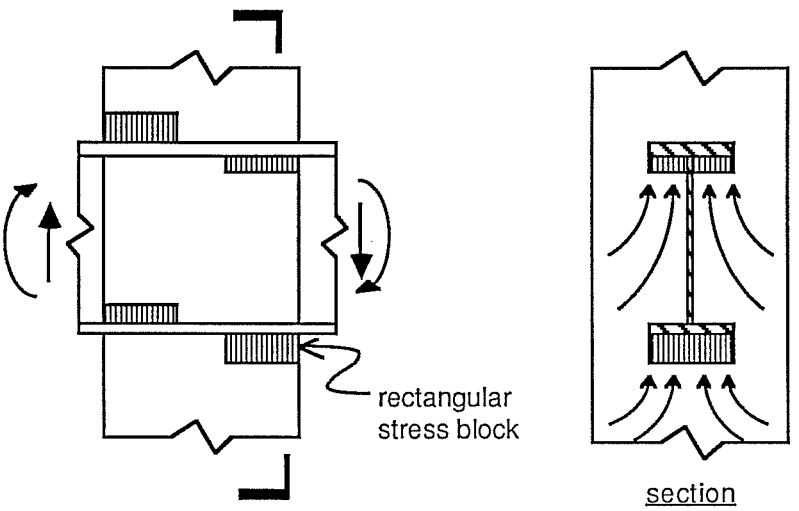

Fig. 1.5a Flange Bearing

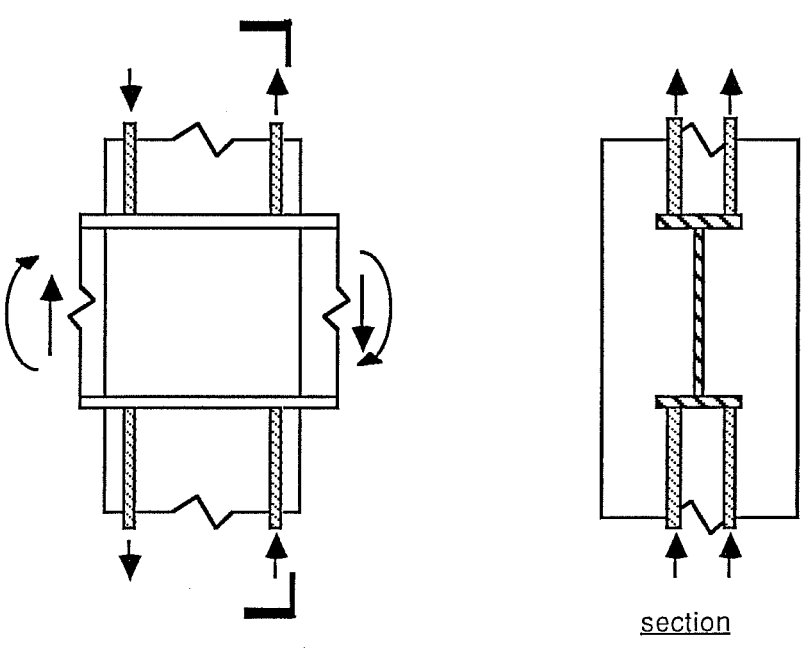

Fig. 1.5b Vertical Joint Reinforcement

1.2.4 Steel Details. The primary experimental test variable involves changing the structural steel details to assess their influence on the connection strength. Figures 1.6 through 1.8 show several steel details considered in this study. In general, these details enhance joint capacity by mobilizing a greater region of concrete to carry joint shear. As described previously, concrete participation is achieved through steel elements which bear against the concrete and restrain horizontal beam flange movement through the joint.

Figure 1.6 shows several configurations of stiffener plates which may be used to mobilize concrete between the beam flanges. In one case stiffener plates are located at the column face and are referred to as Face Bearing Plates (FBP). In an alternate case, the stiffeners are inset to a location which lines up with the flanges of a steel erection column. Stiffeners in this location are referred to as Web Stiffener Plates (WSP). Referring to the section view in Fig. 1.6, the stiffener plate widths may be smaller or larger than the beam flange width which influences the region of concrete mobilized. Also, as shown in the figure the plates may be split for easier fabrication.

Figure 1.7 shows two details which mobilize concrete outside the beam depth. The extended FBP detail forms in a sense a haunched beam at the connection. The steel column acts as inset extended FBPs which through bearing transfer beam flange forces into concrete above and below the beam. The steel column detail is probably one of the most common details owing to the column's role in the composite frame erection sequence described previously.

Finally, Fig. 1.8 shows a welded shear stud detail which offers another means of transferring load from the beam flange into the concrete. The welded studs offer an economical and convenient detail since a typical steel beam will already have studs attached along its length in order to develop composite action with the floor slab.

1.3 Summary of Phase I

1.3.1 General. The research presented in this report is a continuation of a project begun at the University of Texas by Sheikh.[1] The experimental tests

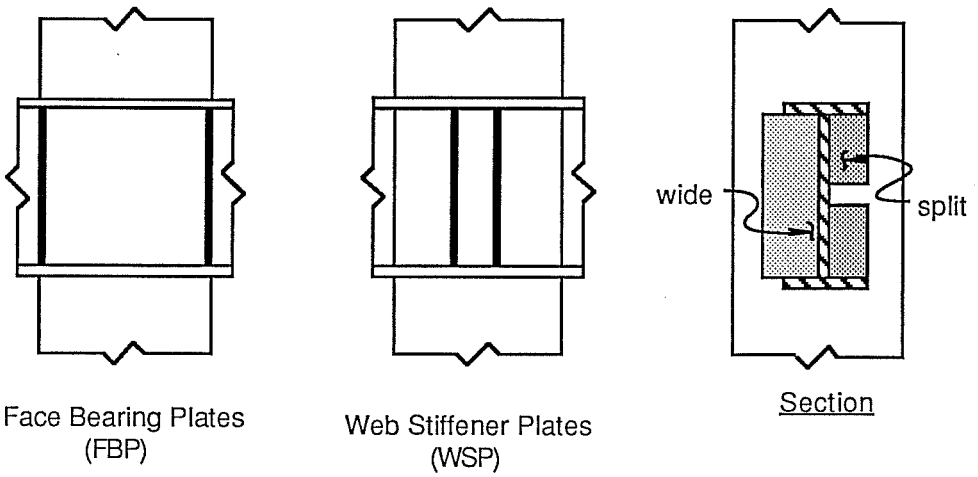

Fig. 1.6 Stiffener Plate Details

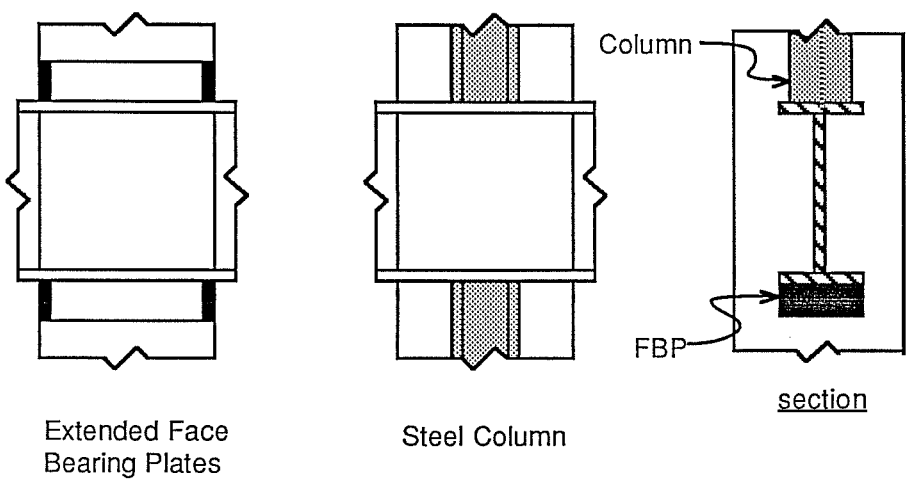

Fig. 1.7 Extended FBP and Steel Column Details

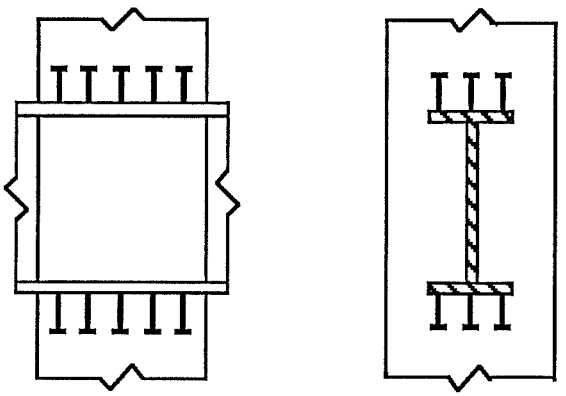

Fig. 1.8 Welded Shear Stud Detail

and conclusions reported by Sheikh comprise Phase I of the work while this report comprises Phase II. The main objective in Phase I was to gain general understanding of the composite connection behavior and identify the primary modes of failure which govern its strength. In particular, tests conducted in Phase I were designed to evaluate FBP effectiveness in mobilizing the concrete compression strut mechanism. In both Phase I and Phase II tests the primary experimental variable involved changing the structural steel details to identify internal force mechanisms which form in the joint. In Phase I, Sheikh presents a design model to calculate the joint capacity and outlines various detailing recommendations.

1.3.2 Phase I: Experimental Program. The Phase I experimental program consisted of nine 1/2 and 2/3 scale test specimens which modeled planar cruciform connections such as shown previously in Fig. 1.2b. A summary of the Phase I tests and results is presented in Appendix A1 of this report. The first two of the nine tests were 1/2 scale specimens which served as a pilot study to evaluate the potential strength increase provided by the FBP detail. In the pilot specimens addition of FBPs increased connection strength by roughly 40%

above the plain steel beam. Based on these tests, seven 2/3 scale specimens were designed to isolate different modes of failure in the connection and evaluate parameters affecting the FBP contribution. In Phase I, testing consisted of monotonically loading specimens to failure first in one direction followed by loading in the reverse direction. Loads were applied to simulate connection forces shown in Fig. 1.2b.

1.3.3 Phase I: Conclusions. The primary conclusion from Phase I is that FBP details increase joint shear capacity significantly by mobilizing concrete in the joint region. Various configurations of FBPs resulted in strength gains of 70% to 190% above the plain steel beam. Specific information regarding the relative strength increases is given by Sheikh. Also, in Chapter 3 of this report comparison of relative connection capacities is included for Phase I along with Phase II tests.

Sheikh developed a design model for connection strength in which the structural steel and concrete contributions are summed. The steel contribution is given as the capacity of the steel beam web in pure shear. The concrete contribution is calculated based on a diagonal compression strut between the beam flanges. In the design model, joint capacity as governed by concrete crushing against the beam flanges is also checked.

1.4 Objective and Scope

The primary objective in this phase is to gain further understanding of composite joint behavior by continuing and expanding the work begun in Phase I. Comprehensive and practical guidelines are developed which address design concerns for a wide range of composite joint details and configurations. Formulation of an analytic design model for calculating the composite joint capacity is an important component of these guidelines.

Experimental research from the first phase is extended in two areas. First, additional joint details are tested in order to refine and enhance understanding of the internal mechanisms controlling joint strength. The major details examined in this phase include the embedded steel column (Fig. 1.7), welded

shear studs (Fig. 1.8), and vertical joint reinforcement (Fig. 1.5b). The second extension of the research is examination of joint response under reverse cyclic loading in the inelastic range. This will provide information which begins to address design concerns and suitability of composite connections for seismic applications.

The Phase II experimental program consists of eight 2/3 scale cruciform specimens with the same geometry as the 2/3 scale specimens tested previously. The test program description and procedure is described in Chapter 2. In Chapter 3 the results of the eight tests are summarized along with a comparison of relative strengths for all 2/3 scale specimens from Phases I and II.

Analysis of the joint response, which focuses on development of an analytic design model, is presented in Chapter 4. The development in Chapter 4 draws in part from a design model proposed by Sheikh and from recommendations for design of structural steel and reinforced concrete joints. In development of the analytic model two points are emphasized: first, the analysis is kept simple and straightforward while preserving an appropriate degree of precision, and second, joint capacity is calculated by analysis of internal mechanisms which follow logically from mechanics.

In Chapter 5 design and detailing recommendations for composite connections are presented. A simplified version of the analytic model from Chapter 4 is a central component of the guidelines for calculating the connection capacity. Accuracy of the simplified model is checked by comparing calculated results with the Chapter 4 analysis and with test results. The recommendations include a design methodology consistent with the load and resistance factor approach used in the AISC-LRFD[10] specification. Detailing recommendations address requirements for horizontal reinforcing bar ties, vertical reinforcing bars sizes and layout, and structural steel detailing peculiar to composite joints. Finally, Chapter 5 also includes information related to design of alternate joint configurations. Chapter 6 provides a summary and conclusions of the report.

Three appendices present supplemental information to the report. As noted previously, in Appendix A1 the scope and results of Phase I tests are

summarized. In Appendix A2 a satellite study which examines the ultimate behavior of shear studs in the joint region is presented. Results of this study are incorporated in the design recommendations of Chapter 5. Finally, sample calculations for two connection examples are presented in Appendix A3.

CHAPTER 2 - EXPERIMENTAL PROGRAM

2.1 General

The experimental program consists of eight 2/3 scale composite joint specimens which were built and tested at the Ferguson Structural Engineering Laboratory at The University of Texas. These tests are designed as a follow up to Phase I tests reported by Sheikh.[1] The specimens reported herein comprise Phase II of the composite joint study, and are numbered 10 through 17 to follow in sequence with Specimens 1 through 9 from Phase I. With the exception of pilot Specimens 1 and 2 from Phase I, all specimens are the same size and geometry and have similar reinforcing bar arrangements. The main test variable consists of using different structural steel details in the joint.

The primary differences between Specimens 10 through 17 are structural steel attachments to the beam. Details evaluated in the tests include FBPs, vertical joint reinforcement, steel doubler plates, welded shear studs, embedded steel columns and steel clip angles. Along with evaluating contribution of these details individually, several of the specimens are designed to examine the interaction of different details. The specimens are loaded with reverse cyclic loads which simulate joint forces due to lateral frame loading.

2.2 Description of Specimens

2.2.1 Typical Details. The overall specimen geometry and loading configuration are shown in Fig. 2.1. The specimens are planar cruciform beam-column connections with 20 in. square columns and built-up W18 steel beams continuous through the joint. As shown in Fig. 2.1, loads at the beam ends simulate member shears at inflection points which occur under lateral loading of the frame.

The steel beam in the specimens is a built-up section consisting of 7/8 $\times$ 8 in. flange plates ($F_y = 50$ ksi) and a 1/4 $\times$ 16 in. web plate ($F_y = 36$ ksi). The hybrid section is weak in shear relative to bending to insure that beam capacity outside the joint will exceed the largest anticipated joint capacity, thus forcing failure to occur in the joint. The thin web reduces the steel panel contribution

to the joint strength and, therefore, also accentuates load carried by the concrete panel. The philosophy of forcing failure in the joint is followed for experimental purposes, and is opposite to design practice where preferably failure occurs in the members. Finally, as shown in Fig. 2.1, reusable extension beams are attached to the beam outside the joint region to facilitate handling of the specimens and reduce the steel beam cost.

The reinforcing steel layout is essentially the same in all specimens, except that, as will be described later, additional horizontal ties are added in Specimens 12 and 13. Like the steel beam, the column is designed such that its shear and moment capacities insure that failure will occur in the joint. As shown in Fig. 2.2 the vertical column reinforcement consists of twelve #10 bars which provide a longitudinal steel area equal to 3.7% of the gross column area. The longitudinal bars are located near the column corners as shown, allowing clearance for steel beams as is typical in practice.

As shown in Fig. 2.2, cap ties are used within the beam depth and rectangular hoops are used outside the beam. The outer set of cap ties pass though holes in the beam web and are developed in tension through lap splices. In the joint region all ties are #3 bars, whereas, outside the joint #4 bars are used for the outer hoop to allow greater tie spacing. Ties within the beam depth are designed using the ACI-ASCE Committee 352 recommendations[8] for reinforced concrete joints in regions of high seismic risk. This criteria is used, not because the specimens are specifically intended for seismic design, but rather to insure that ties provided will not limit the joint shear capacity. Since the specimens represent 2/3 of full scale, tie spacings and concrete cover dimensions are proportionally smaller than would be used in standard construction practice.

2.2.2 Specimen Details. Figure 2.3 summarizes the joint details in Specimens 10 through 17, which comprise Phase II of the composite joint project. Appendix A1 includes a similar summary for Phase I.

Specimen 10, FBP (Split). Specimen 10 consists of a plain steel beam with 3/8 in. thick split FBPs as shown in Fig. 2.4a. The FBPs are intended to mobilize a diagonal compression strut in the concrete between the flanges. Through

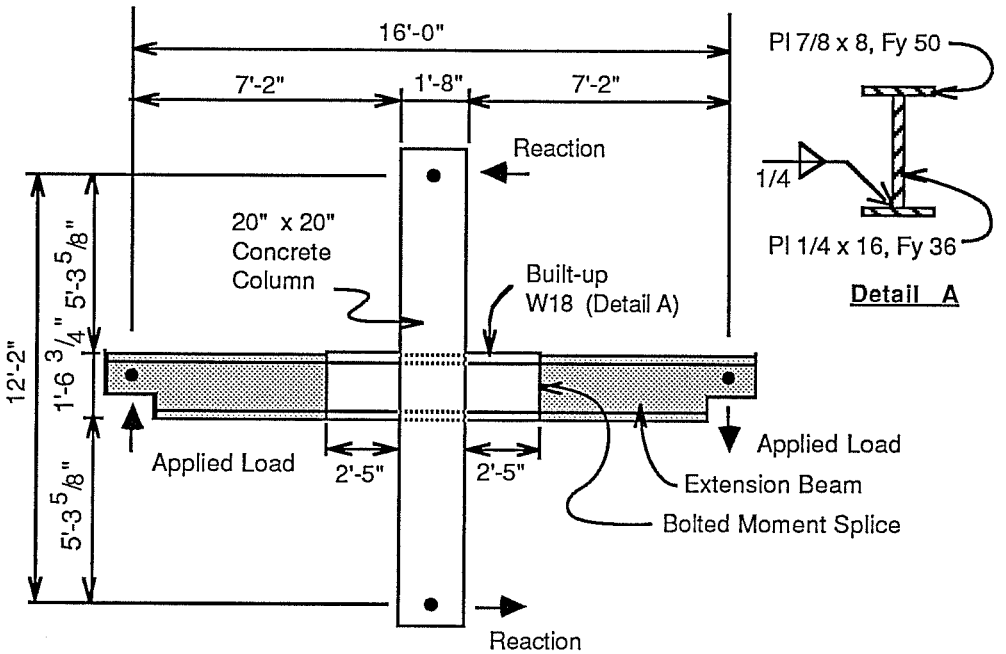

Fig. 2.1 Typical Test Specimen

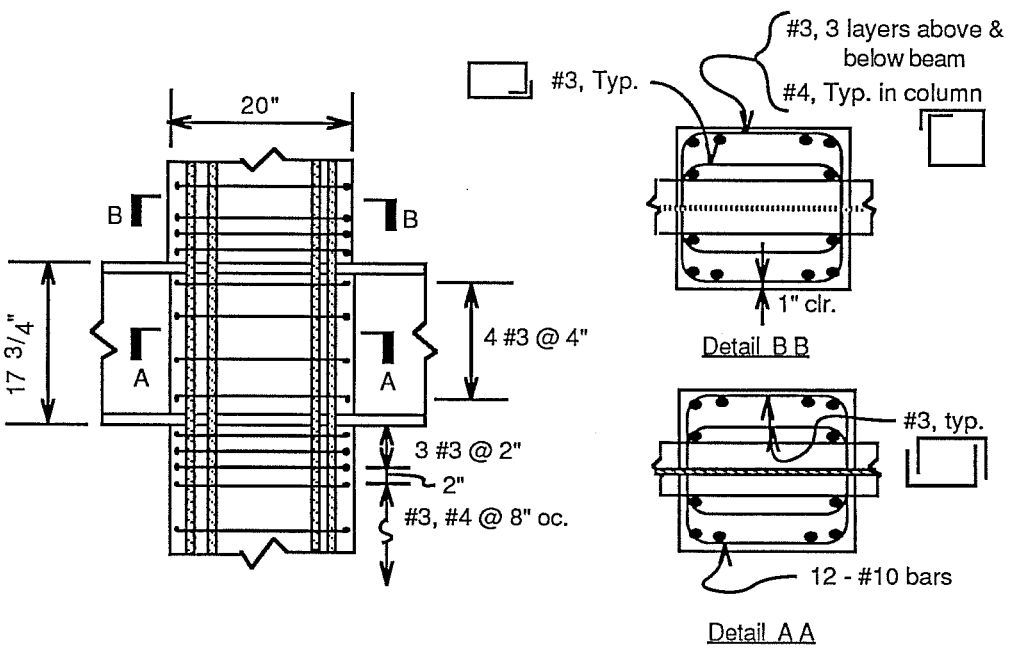

Fig. 2.2 Typical Reinforcing Steel Detail

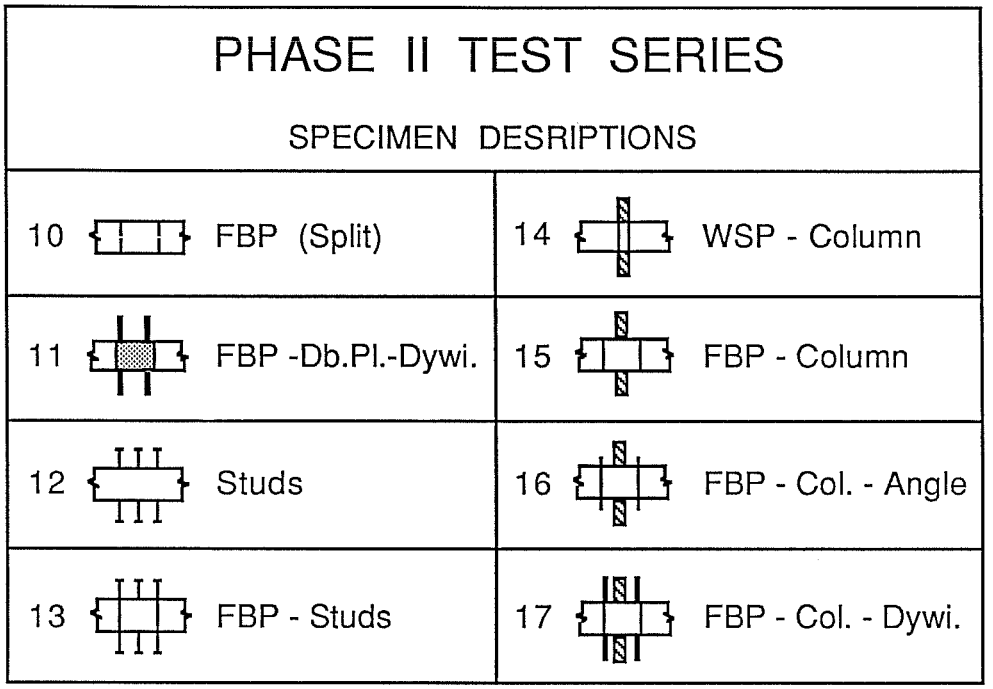

Fig. 2.3 Summary of Phase II Specimens

comparison with specimens with full height FBPs, Specimen 10 should indicate whether splitting the FBP has a detrimental effect on strength by increasing the plate's flexibility. The motivation for splitting the stiffener is the reduction of fabrication costs by eliminating close fit up required with full height stiffeners. Also shown in Fig. 2.4a are 7/8 in. diameter holes typical in all specimens which provide passage for the #3 cap ties through the web.

Specimen 11, FBP-DbPl-Dywi. Specimen 11 is designed to examine effectiveness of vertical joint reinforcing for strengthening when concrete crushing against the beam flanges controls the design. The vertical joint reinforcement consists of eight Dywidag bars (#8 - 3 ft 0 in., Gr. 60) as shown in Fig. 2.4b. These bars are attached through threaded couplers welded to the beam flanges. Web doubler plates and FBPs are also provided to increase the joint shear panel capacity above that governed by concrete bearing failure. The doubler plate

thickness provides a shear to moment capacity ratio in the beam similar to that for rolled W18 shapes.

Specimen 12, Studs. Specimen 12 is the first of two specimens where shear studs welded to the flanges provide a means of transferring horizontal force to concrete outside the beam depth. As shown in Fig. 2.4c fifteen $1/2 \times 4$ in. headed studs are welded to each flange in 5 rows of 3 studs per row. The $1/2$ in. diameter studs are chosen as scale versions of $3/4$ in. diameter studs common in construction practice. Three additional layers of horizontal ties (#3 bars) are provided around the studs as shown in Fig. 2.4c. These ties are intended to aid in carrying stud shear into the surrounding concrete, particularly for studs near the column face where concrete cover is inadequate.

Specimen 13, FBP-Studs. Specimen 13, shown in Fig. 2.4d, is identical to Specimen 12 except for the addition of full height FBPs. A comparison between Specimens 12 and 13 will demonstrate whether the strength gain achieved by FBPs is additive with that provided by shear studs.

Specimen 14, WSP-Column. Specimen 14 is the first of four specimens with an embedded steel column attached to the steel beam. As shown in Fig. 2.4e the column is a W5 $\times$ 19 (F_y = 50 ksi) rolled shape which represents a W8 erection column in full size composite frames. As noted previously, the relative sizes of the steel and reinforced concrete columns are such that the steel column's axial and bending capacity is negligible with respect to the overall composite column. The steel column has bending and axial capacities equal to roughly 8% and 12% of the reinforced concrete section. Locally, however, the steel column contributes significantly to the connection force transfer.

For ease of laboratory fabrication the steel column extends only 30 inches above and below the beam, whereas, in real structures it would run the full column height. Based on crack patterns observed in previous tests (Phase I), the 30 in. length should insure that the steel column extends beyond the region influencing joint behavior. Finally, in Specimen 14 stiffener plates are located in line with the column flanges. These plates, referred to as Web Stiffener Plates

(WSP), function in a similar fashion to the FBP in mobilizing shear resistance of concrete inside the beam flanges.

Specimen 15, FBP-Column. Specimen 15, shown in Fig. 2.4f, is the same as Specimen 14 except that FBPs are used instead of WSPs. As will be discussed in subsequent chapters, FBPs are expected to be more effective than the WSPs. Perhaps more than other specimens tested, Specimens 14 and 15 represent the most likely combination of details to be used in practice.

Specimen 16, FBP-Column-Clip Angle. Specimen 16, shown in Fig. 2.4g, is the same as Specimen 15 with the addition of light clip angles welded above and below the flanges at the column face. The angles (L $4 \times 4 \times 3/8$, $F_y =$ 36 ksi) are intended to improve performance by confining concrete in the highly stressed bearing zone. This detail was suggested by Griffis,[11] as an economical alternative to vertical joint reinforcement for strengthening and stiffening the concrete bearing region. Clip angles also serve as an addition means to the steel column for transferring horizontal beam flange force into the concrete.

Specimen 17, FBP-Col.-Dywi. Specimen 17 which is shown in Fig. 2.4h is the same as Specimen 15 with the addition of Dywidag bars (vertical joint reinforcement). The Dywidag bar configuration is the same as that described for Specimen 11. Preliminary design calculations for Specimen 17 indicate that ultimate strength is not controlled by concrete bearing, but rather joint shear. The purpose of Specimen 17 is to ascertain whether vertical joint reinforcement will significantly increase connection stiffness. Previous tests showed considerable rigid body rotation of the beam within the column, presumably due to high concrete strains in the bearing region. Since the useful capacity is a function of joint deformation, additional stiffness would increase the joint design capacity. Specimen 17 will be used for comparison with Specimens 15 and 16 to determine differences in behavior obtained by relative enhancements of the concrete bearing region.

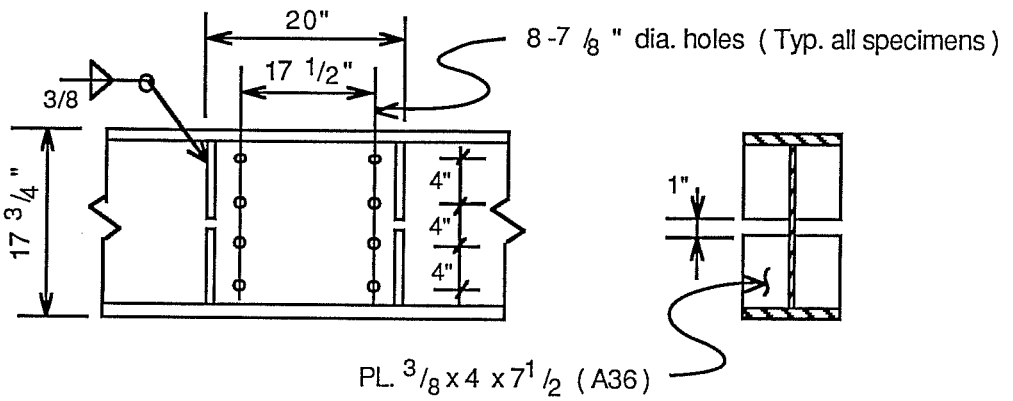

Fig. 2.4a Specimen 10: Split Face Bearing Plates

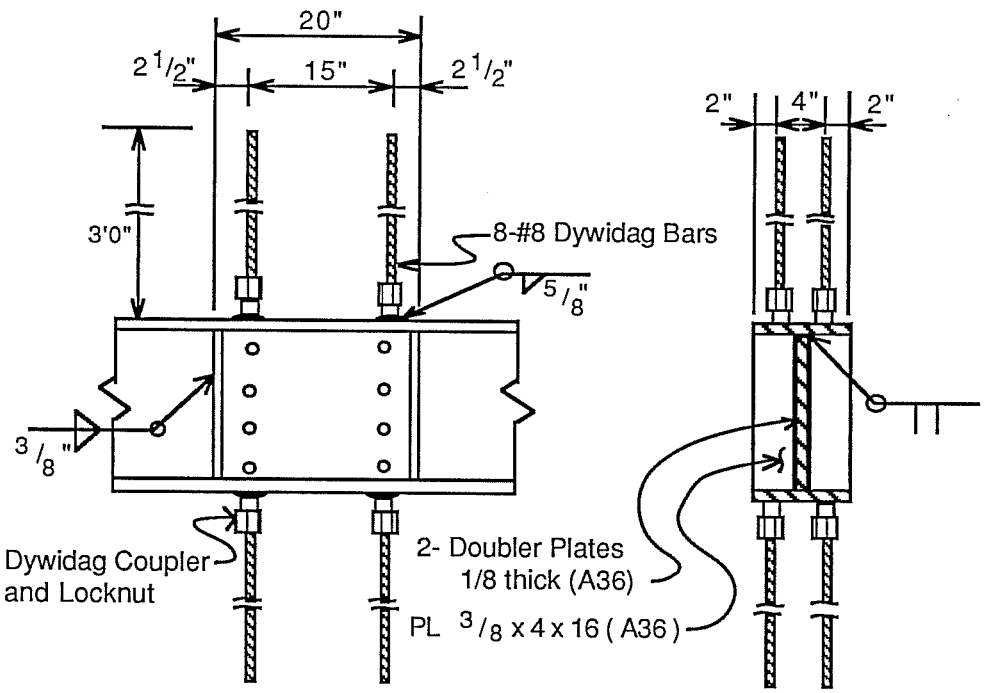

Fig. 2.4b Specimen 11: Face Bearing Plates, Doubler Plates and Dywidag Bars

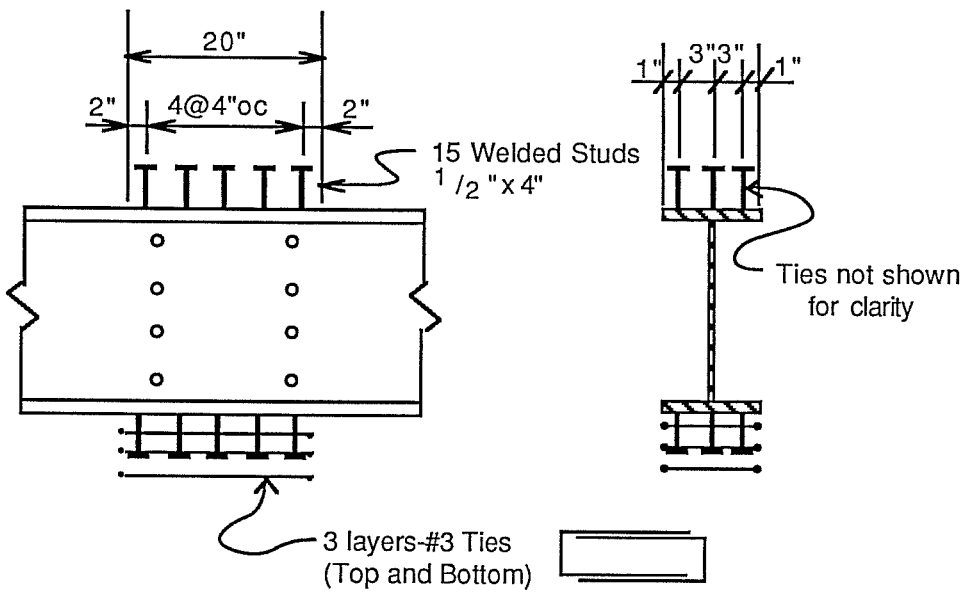

Fig. 2.4c Specimen 12: Shear Studs

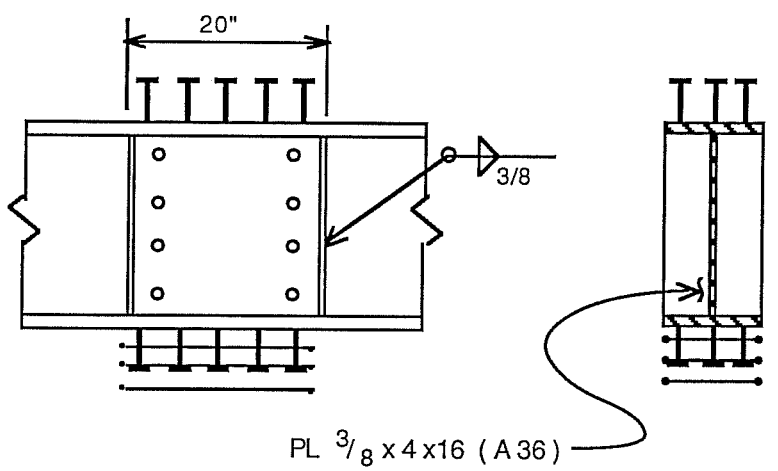

For information not shown see Fig. 2.4c

Fig. 2.4d Specimen 13: Face Bearing Plates and Shear Studs

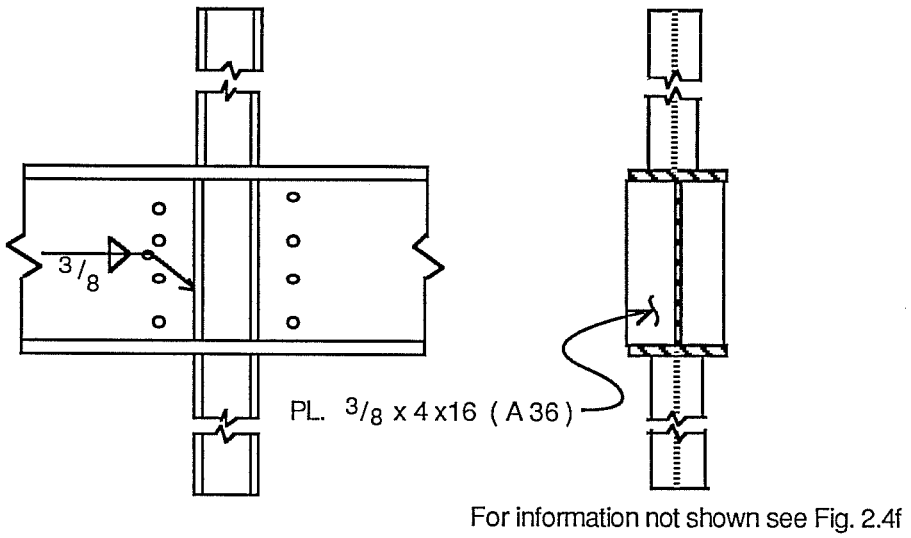

Fig. 2.4e Specimen 14: Web Stiffener Plates and Column

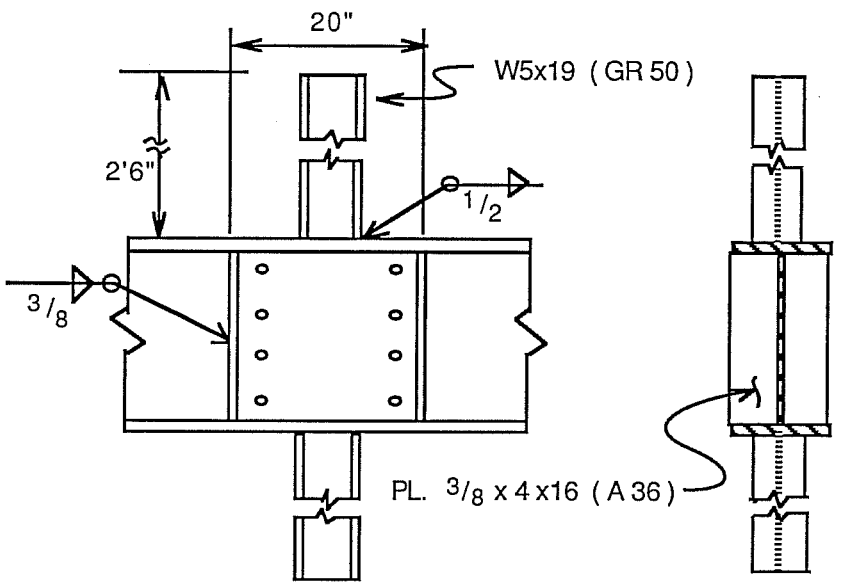

Fig. 2.4f Specimen 15: Face Bearing Plates and Column

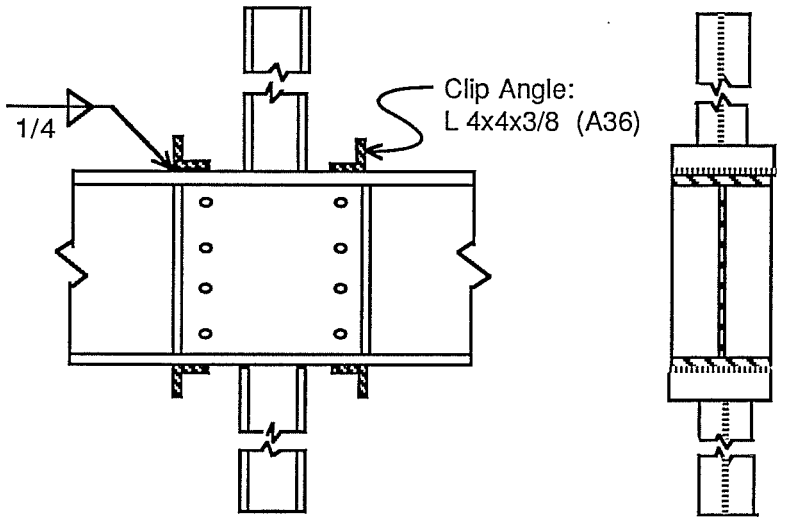

Fig. 2.4g Specimen 16: Face Bearing Plate, Column and Clip Angle

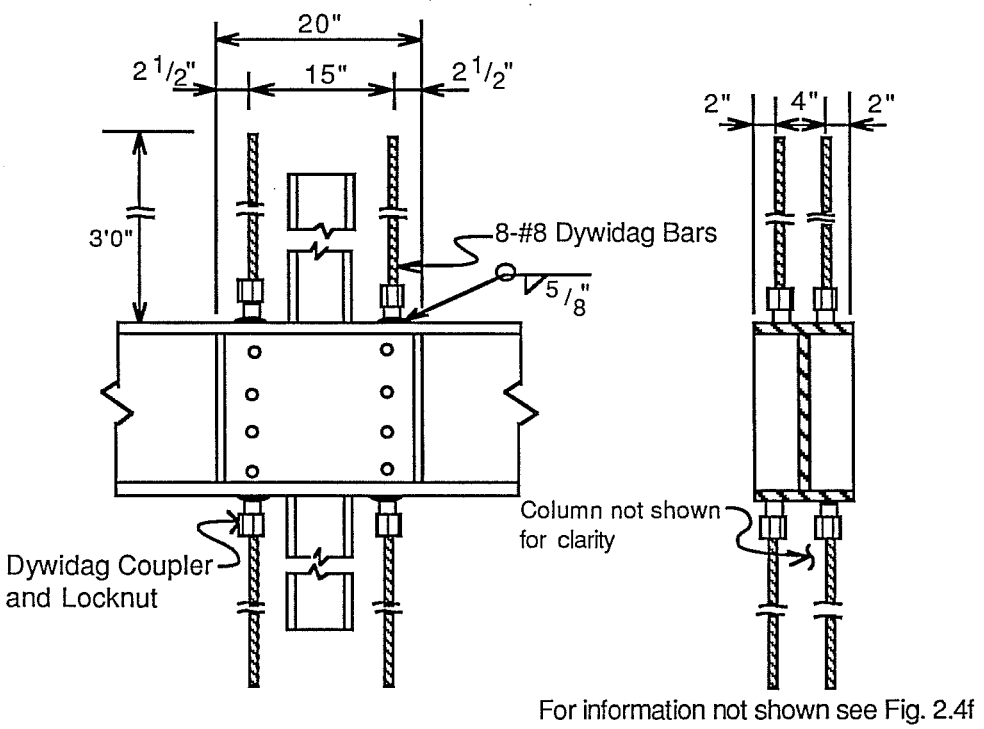

Fig. 2.4h Specimen 17: Face Bearing Plates, Column and Dywidag Bars

2.3 Specimen Fabrication

The specimen fabrication and construction sequence is the same as that described in detail by Sheikh[1] in Phase I. Only aspects of importance in the construction sequence are discussed here. As shown in Fig. 2.5, specimens were erected and cast in a vertical position as would occur in practice. Casting position is important since it influences the insitu concrete properties. In particular, concrete cast beneath the beam flanges is weakened by small air voids, consolidation, and trapped bleed water. Such conditions cannot economically be eliminated in practice, and hence should be replicated in experiments.

Figure 2.6 shows the joint detail and reinforcement in Specimen 10, indicating the degree of congestion in the joint region which necessitates careful concrete placement. In the laboratory concrete was placed with slumps of 6 to 7 in. which are higher than in normal practice, but were required to insure against formation of voids. Immersion vibrators (2 in. diameter) were used for consolidating concrete after placing each lift (lift heights were approximately 12 in.).

2.4 Material Properties

The static yield stress, ultimate stress and percent elongation are reported for the structural and reinforcing steel components in Table 2.1. Static yield stress provides a lower bound for yielding which corresponds well with quasi-static loading of the joint specimens. Table 2.1 also includes strain at commencement of strain hardening and the strain hardening modulus for the structural steel elements which may undergo large strains in the tests. Procedures and specifications for the material tests are the same as those reported by Sheikh.[1]

Table 2.2 lists concrete compressive strengths based on 6 $\times$ 12 in. cylinder tests along with concrete mix proportions. As noted, compressive strengths on the day of testing ranged between 3.8 ksi to 5 ksi. The water contents listed in Table 2.2 are based on batch plant reports for quantity of mix water and fine aggregate moisture content. The calculated water-cement ratios do not always

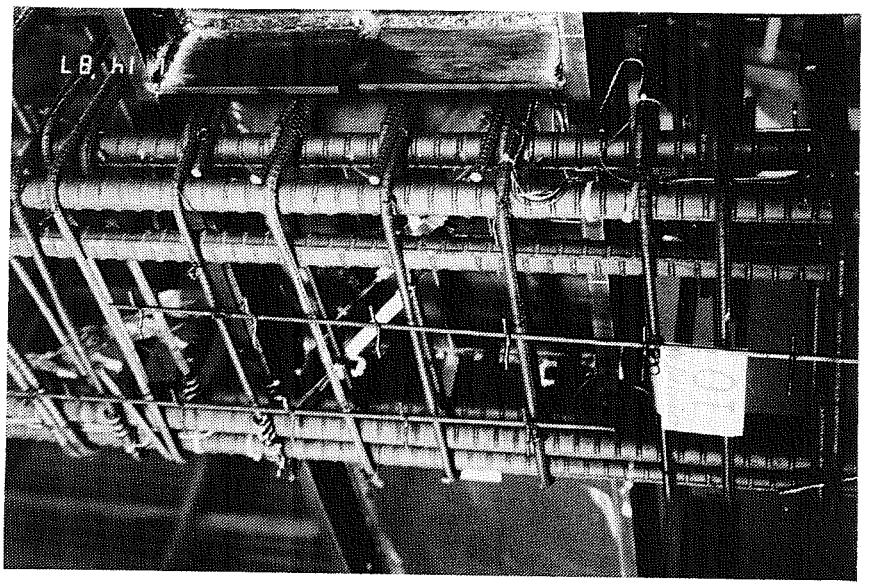

Fig. 2.6 Specimen 10: Joint Detail

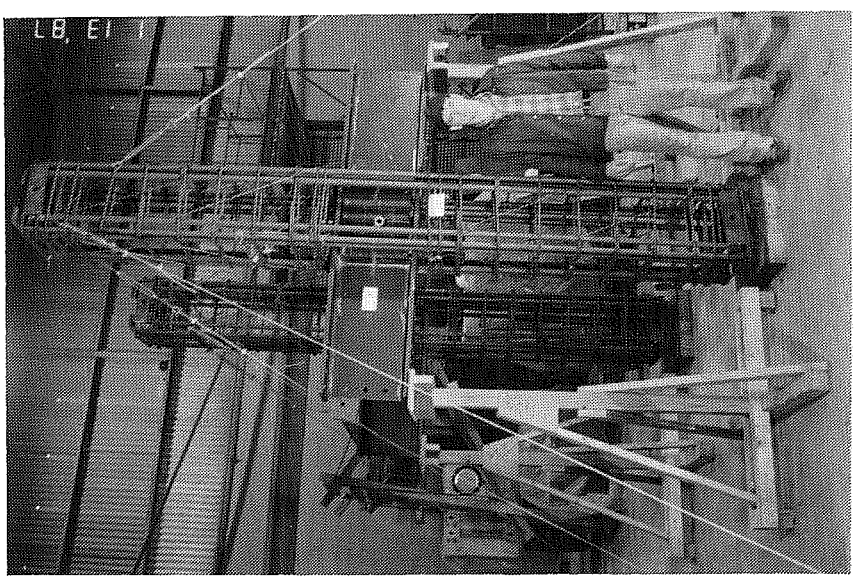

Fig. 2.5 Specimen Fabrication

Table 2.1 Structural and Reinforcing Steel Properties

Item	t (in.)	σ_y (ksi)	σ_u (ksi)	Gage Length (in.)	% Elong.	ϵ_{sh} (in./in.)	E_{sh} (ksi)
Flange Plate $\frac{7}{8} \times 8$ in.	0.882	49.0	75.2	8	27	0.016	530
Web Plate $\frac{1}{4} \times 16$ in.	0.263	36.2	60.0	2	38	0.020	540
Web Dblr. Pl. $\frac{1}{8} \times 16$ in.	0.132	35.8	50.4	2	38	0.019	260
FBP $\frac{3}{8} \times 4$ in.	0.372	43.8	68.8	2	39	0.019	580
Angle $4 \times 4 \times \frac{3}{8}$	0.394	55.5	74.8	2	35	0.019	430
Column-Flange W5 $\times$ 18.5	–	47.5	69.2	8	28	0.011	440
Column-Web W5 $\times$ 18.5	–	47.8	66.7	8	29	0.025	330
#3 Rebar	–	61.1	101.9	8	13	–	–
#4 Rebar	–	64.5	101.5	8	16	–	–
#10 Rebar	–	60.6	101.5	8	19	–	–
#8 Dywidag (Spec. 11)	–	61.7	101.6	8	18	–	–
#8 Dywidag (Spec. 14)	–	66.6	111.0	8	15	–	–

Notes:

t = measured plate thickness (in.)
σ_y = static yield stress (ksi)
σ_u = ultimate stress (ksi)
ϵ_{sh} = strain at commencement of strain hardening (in./in.)
E_{sh} = strain hardening modulus (ksi)

correlate well with the relative ratios anticipated considering the strength and slump data. Presumably, this is due to excess water in the mix.

2.5 Experimental Setup

2.5.1 Overview and Loading System. A schematic view of the test setup and loading system is shown in Fig. 2.7. Also, a photograph of the setup is shown in Fig. 2.8. The specimen was loaded by 100 kip hydraulic rams at the beam ends where one ram acts in tension (pulling downward) while the second was in compression (pushing upward). The multi-pressure load maintainer controls the hydraulic line pressures such that the rams have equal loads. At each load stage shutoff valves in the hydraulic lines were closed to lock the rams

Table 2.2 Concrete Strengths and Mix Properties

Specimen	Test Age (days)	Date f'_c (ksi)	28-day f'_c (ksi)	Mix Proportions (per cu. yd.) CA (lb)	FA (lb)	Cement (lb)	Water (lb)	W/C	Slump (in.)
10	39	4.7	4.6	1830	1440	400	250	0.63	7
11	87	4.7							
12	47	5.0	4.8	1860	1430	420	270	0.65	6
13	60	5.0							
14	67	4.1	4.0	1820	1440	400	270	0.67	$7\frac{1}{2}$
15	75	4.1							
16	32	3.8	3.7	1900	1370	430	270	0.64	8
17	42	3.9							

at given displacements. In this manner, tests were run by displacement control although during each step, loads were applied by increasing ram pressures while monitoring load-displacement response.

Applied ram loads were monitored through hydraulic line pressures measured by the dial gages and transducers shown in Fig. 2.7. Hydraulic pressures were converted to ram loads based on a calibration in which ram loads were measured independently by electronic load cells. Based on the calibration the reported ram loads are within roughly $\pm 3\%$ of the true loads.

2.5.2 Deformation Measurement. Together with applied load, joint deformation is the most important parameter for evaluating behavior. In the test setup joint deformations were measured by two independent sets of instrumentation. One set records deformation in terms of total specimen drift. The second measures angular joint distortion directly and provides a breakdown of the total distortion into its component parts.

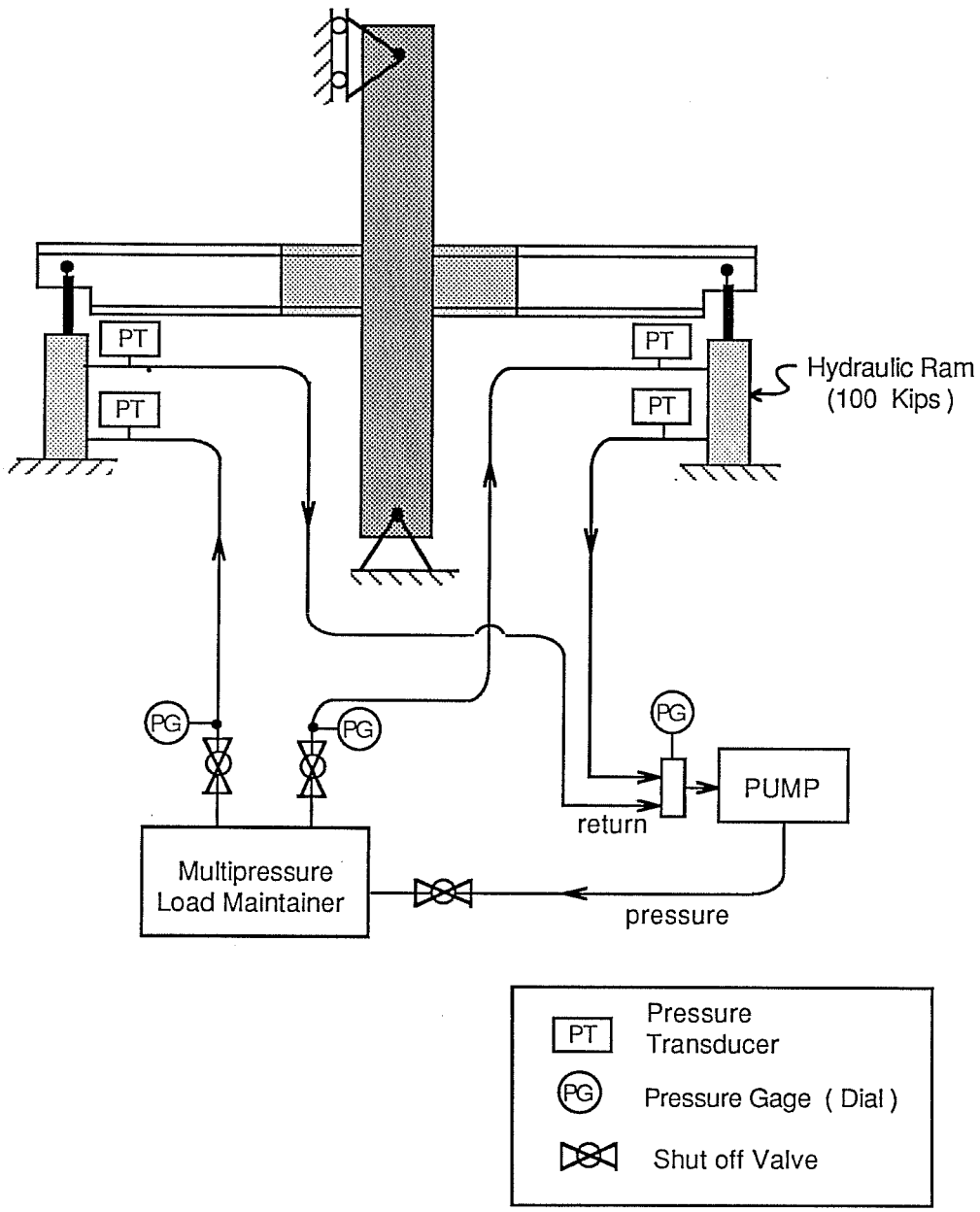

Fig. 2.7 Schematic of Test Setup and Loading System

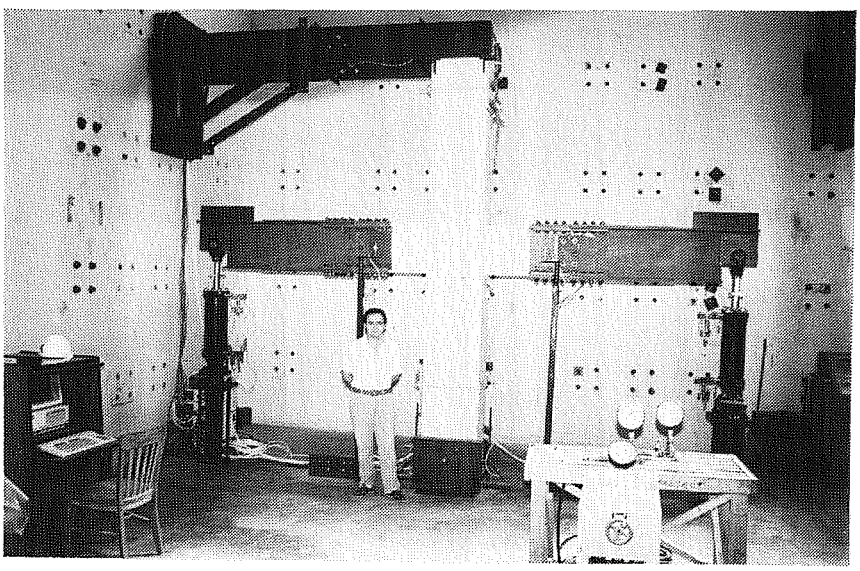

Fig. 2.8 Experimental Test Setup

Figure 2.9 describes specimen drift which is analogous to inter-story drift in framed structures. In the left side of Fig. 2.9 displacements used to calculate the drift are shown. These displacements were measured relative to a fixed reference using several 2 inch stroke linear potentiometers, details of which are described by Sheikh.[1] The right side of Fig. 2.9 shows the deformed shape, redrawn to indicate how test setup displacements correspond to inter-story drift in frames. As indicated by the deflected shape, drift measurements include both member deformations in the beams and columns and an angular distortion of the joint. Where flexural and shear distortions of the members are small, the drift angle is equal to the angular joint distortion. Drift is reported as a percentage where 1% equals a drift ratio (sway/height ratio) of 1/100. Referring to Fig. 2.9,

a drift ratio of 1% corresponds to an angular distortion of 0.010 radians between the member reference lines (shown dashed).

A more direct measure of angular joint distortion is made using the instrumentation shown in Figs. 2.10 and 2.11. Total angular joint distortion (TJD) is given by the difference in rotations of the steel beam and concrete column adjacent to the joint. Member rotations were measured using an electronic micro-level (see Fig. 2.11) with a resolution of 8×10^5 radians (0.008%). Six angular rotations were measured (two beam measurements and four column measurements) on brackets attached to the beam and column in locations shown in Fig. 2.10. Micro-level brackets on the beam were bolted to the web while column brackets were attached with embedded thread bars. As shown in Detail A (Fig. 2.10), a soft neoprene fill isolates the embedded thread bars are from the concrete cover so that the measurements reflect distortion of the concrete core. Also indicated in Fig. 2.10 are displacement transducers (2 inch linear potentiometers) which measure diagonal deformations across the joint and relative vertical movement of the beam and column.

Using the measurements described in Fig. 2.10 joint distortions shown in Fig. 2.12 are calculated. As noted previously, total joint distortion (TJD) is the relative angular rotation of the beam and column measured near the joint. Total joint distortion is equal to the sum of component distortions as follows:

$$TJD = CPS + LFB + SPS \tag{2.1}$$

TJD = Total Joint Distortion
CPS = Concrete Panel Shear
LFB = Local Flange Bearing
SPS = Steel Panel Shear

The concrete panel shear (CPS) is the shear distortion of the concrete column in the joint region, measured using the diagonal displacement transducers

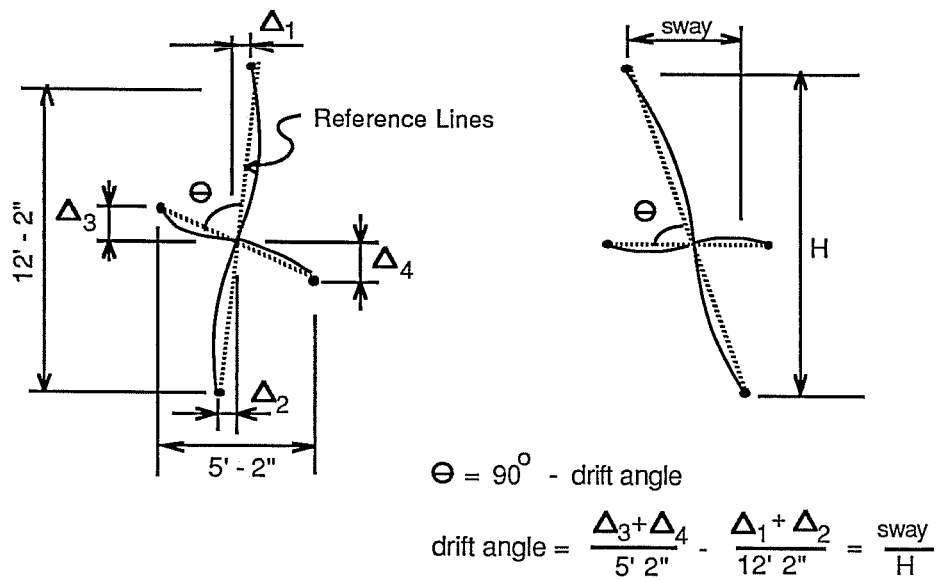

Fig. 2.9 Measurement and Calculation of Drift

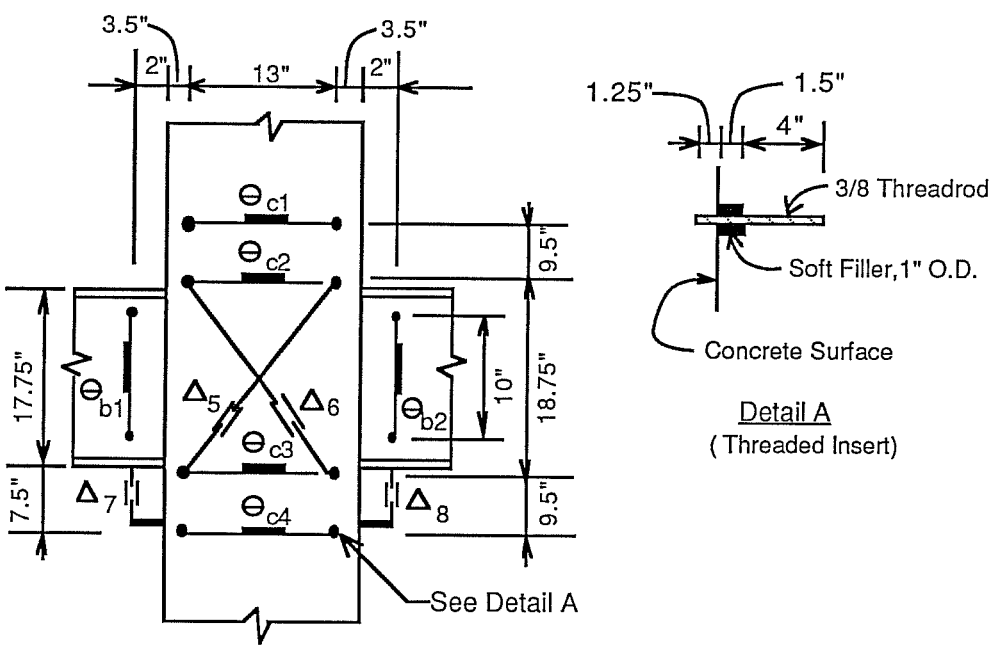

Fig. 2.10 Instrumentation for Joint Distortion

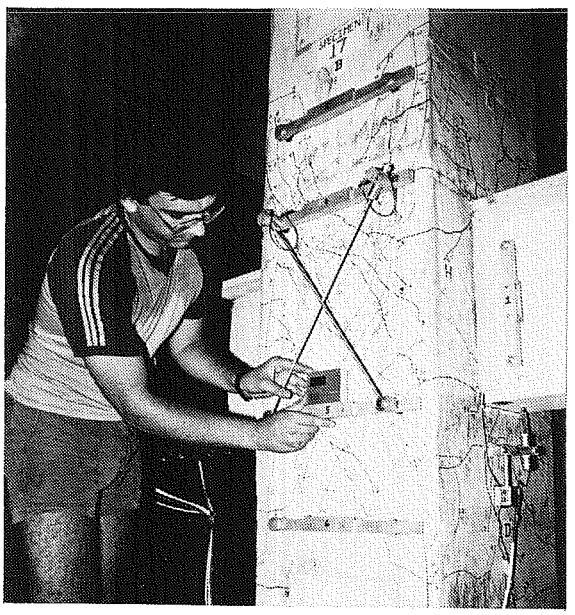

Fig. 2.11 Joint Deformation Instrumentation

(Fig. 2.10). The local flange bearing (LFB) measures rigid body rotation of the beam inside the column resulting from high strains in the concrete bearing region. The high bearing strains are also evidenced by gaps which open against the tension flanges opposite to the bearing zone. LFB is calculated using the relative vertical displacements between the beam flange and concrete column. The steel panel shear (SPS) is the shear deformation of the beam web panel inside the joint. If the entire joint region would act as a single unit the steel panel and concrete panel shears would be identical. However, as noted by Sheikh,[1] typically the steel panel distortion is greater than the concrete panel distortion. In the tests SPS was not measured independently, but, is calculated as the difference between the TJD and the sum of CPS and LFB. Strictly speaking the total shear in the steel panel is the sum of CPS and SPS. However, in this and subsequent

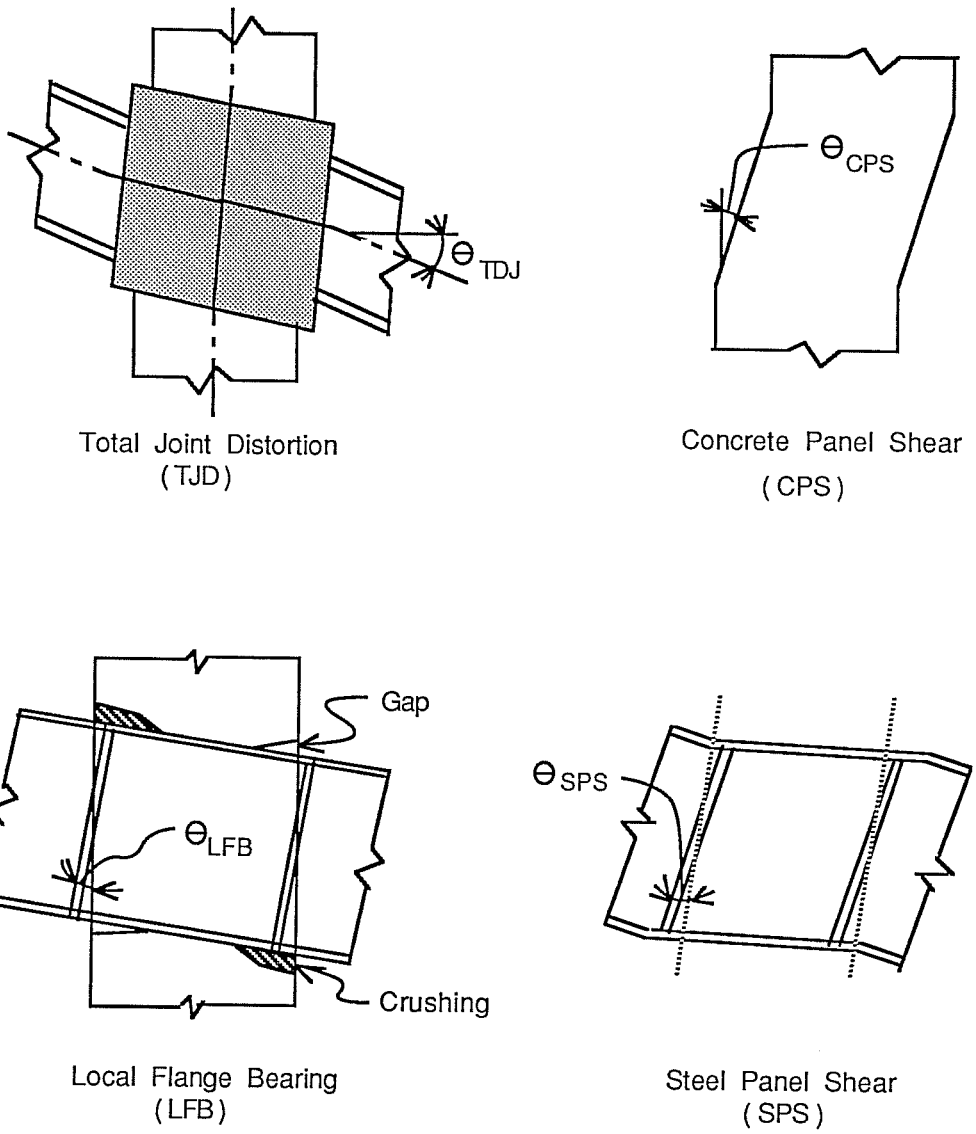

Fig. 2.12 Components of Joint Distortion

discussions, following Eq. 2.1, SPS refers to steel shear panel distortion in excess of concrete panel distortion.

2.5.3 Strain Measurement. Internal strains offer a means of verifying how forces distribute through the joint region. Resistance strain gages attached to both structural and reinforcing steel elements together with concrete embedment strain gages were used to monitor internal strains. Steel strains were measured by epoxy carrier foil strain gages (6 mm gage length) in single, cross and 45 degree rosette configurations. Concrete strains were measured by embedment gages (60 mm gage lengths) encased in polyester/resin molds (125 × 13 × 5 mm) with a coarse grit surface.

Figures 2.13 through 2.15 show strain gage locations on the structural steel elements. In Fig. 2.13 gages along the beam flange measure dissipation of axial forces out of the flange through the joint region. The rosette gage measures shear strains in the web and the cross gage measures bending in the face bearing plate. In Fig. 2.14 cross gages on the column flanges and clip angles measure bending in those elements due to concrete bearing stresses. Finally, Fig. 2.15 shows strain gages attached to the welded studs which indicate the studs' relative participation in transferring horizontal loads.

Figures 2.16 and 2.17 show gage locations for the reinforcing bars. In Fig. 2.16 gages were located so as to measure the axial stresses along Dywidag bars which serve as vertical joint reinforcement. Near the base, two gages were used on opposite sides of the bars to distinguish axial and bending stresses. In Fig. 2.17 gage locations are shown for both transverse column ties and vertical column bars. On some ties two gages were installed at each location, again, to distinguish between axial and bending stresses.

Concrete embedment gage locations are shown in Fig. 2.18. These gages measure axial compressive strains along the joint diagonal as shown. One gage was located inside the beam flanges and one outside to evaluate relative concrete participation through the column width. These gages were intended to function only during initial loading in one direction since under reversed loading

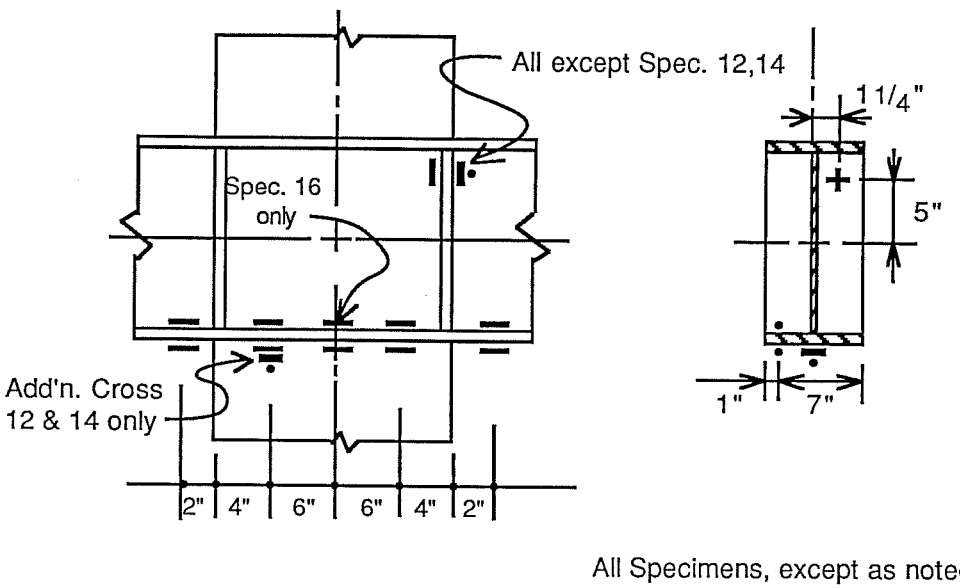

Fig. 2.13 Strain Gages: Web, Flange, and Face Bearing Plate

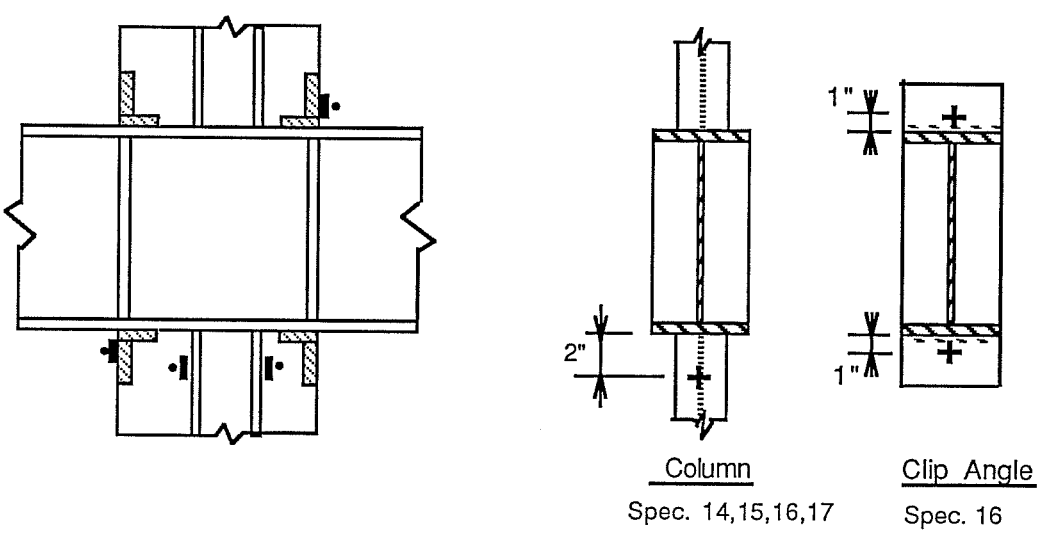

Fig. 2.14 Strain Gages: Steel Column and Clip Angle

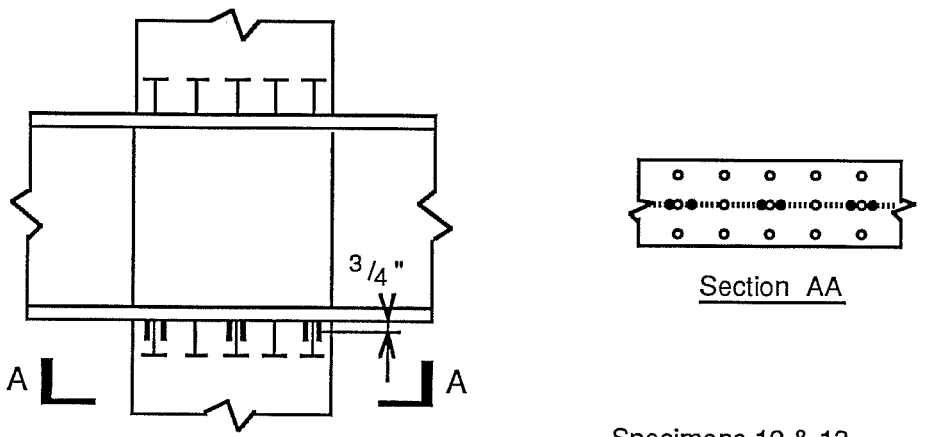

Fig. 2.15 Strain Gages: Shear Stud s

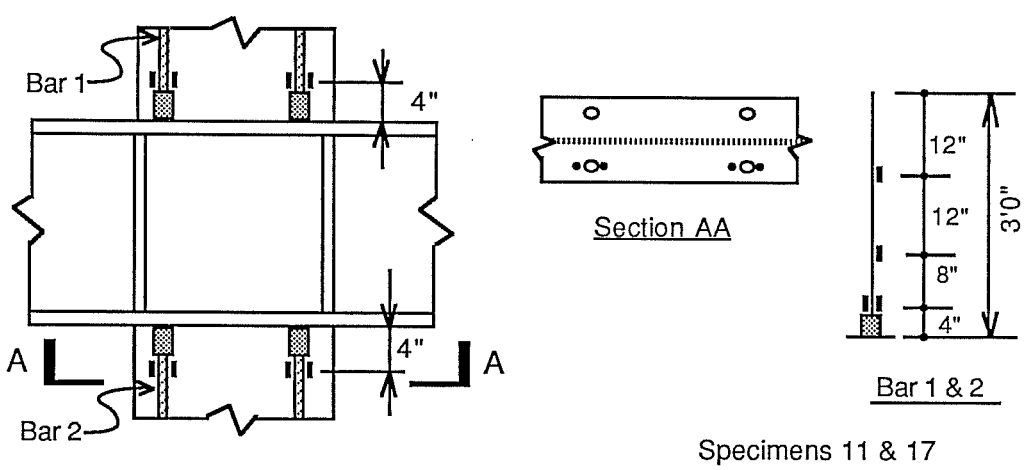

Fig. 2.16 Strain Gages: Dywidag Bars

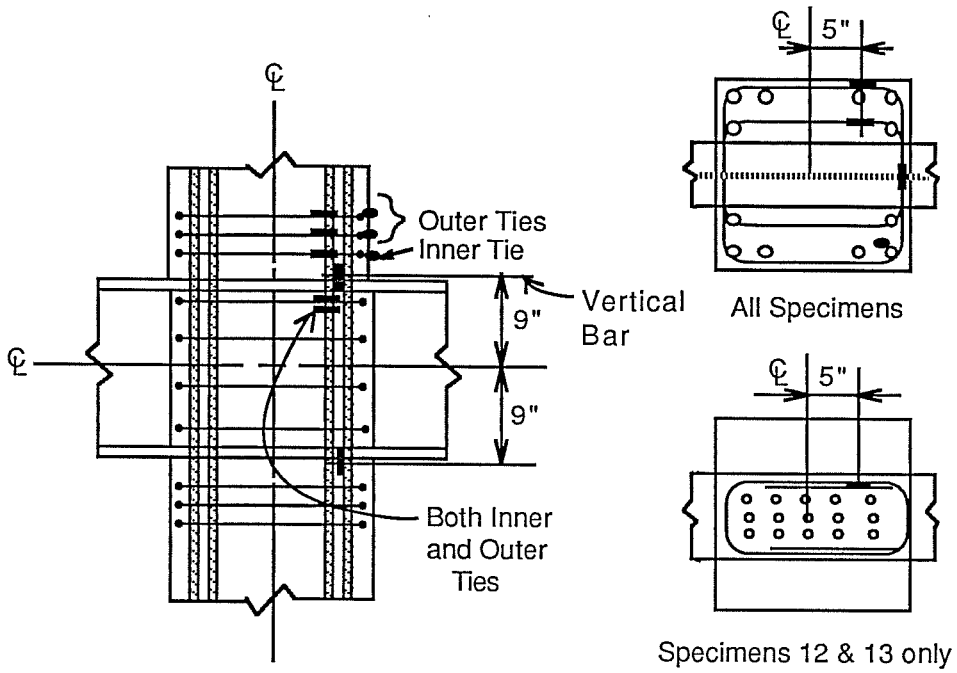

Fig. 2.17 Strain Gages: Reinforcing Bars

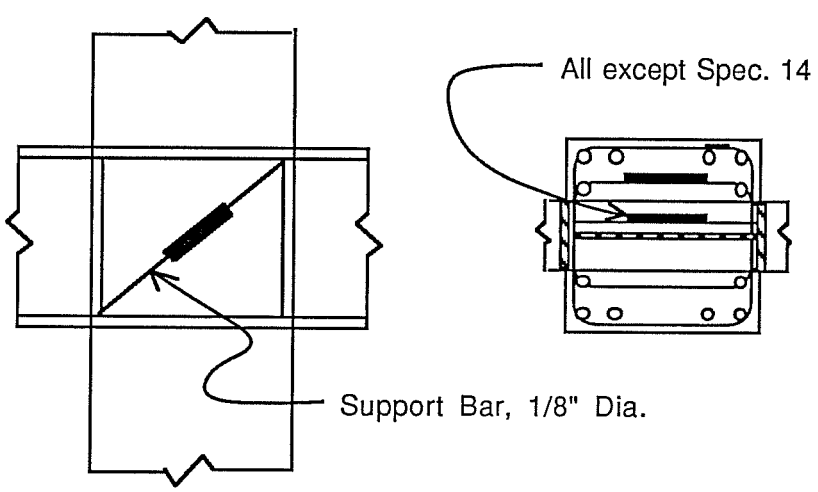

Fig 2.18 Concrete Embedment Strain Gages

tension cracks may open perpendicular to the gage which will distort strain measurements.

2.5.4 Data Acquisition. Data were recorded through a combination of visual and electronic means. Visual inspection included marking concrete cracks, and noting concrete spalling and formation of yield lines on the structural steel. To highlight yield lines, the steel beam was coated with a light lime whitewash prior to testing. Manual readings included those for hydraulic pressure measured with dial gages and joint rotations measured with the electronic micro-level. Finally, a personal computer based data acquisition system monitored voltage output from pressure transducers, displacement transducers, and resistance strain gages. Also, during the test a X-Y pen plotter recorded the force and displacement in the hydraulic ram pushing upward in compression.

2.6 Test Procedure

Specimens were loaded in a quasi-static fashion according to the loading agenda shown in Fig. 2.19. All of the specimens were loaded first to a low stress level where concrete cracks began opening at roughly 25% to 40% of the ultimate joint. Following this specimens were loaded through 2 complete cycles to 1% TJD and 2 cycles to 2% TJD. The test concluded by loading specimens to a final deformation of roughly 4% TJD. The final loading sequence for Specimen 10 was cut short by 1/2 cycle due to scheduling and time constraints in the laboratory.

As discussed previously, tests were displacement controlled by locking off ram displacements at each loading increment. Data was collected at each load step after waiting 5 to 15 minutes for the structure to reach steady state equilibrium. This delay allowed for time dependent concrete cracking and steel yielding. Difference between the static and real time response is demonstrated by the plot in Fig. 2.20. As shown, at each load stage displacement is fixed while load drops off due to relaxation in the structure. In the elastic range the load drop is negligible while in the inelastic range the load drops 5% to 15% at each step. Plots such as that in Fig. 2.20 were recorded during testing using an X-Y pen plotter. The lower bound response given by the static load points is used for interpretation and analysis of the data.

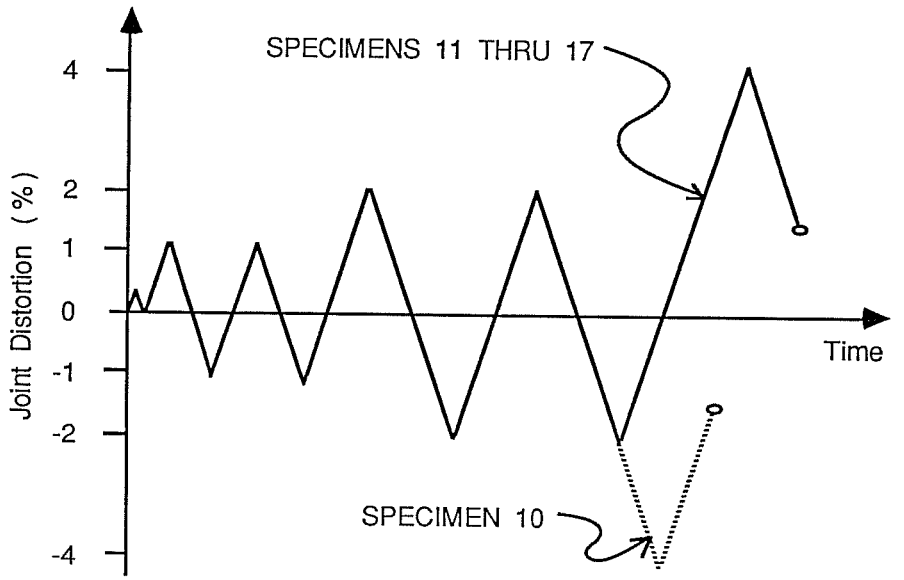

Fig. 2.19 Loading Agenda

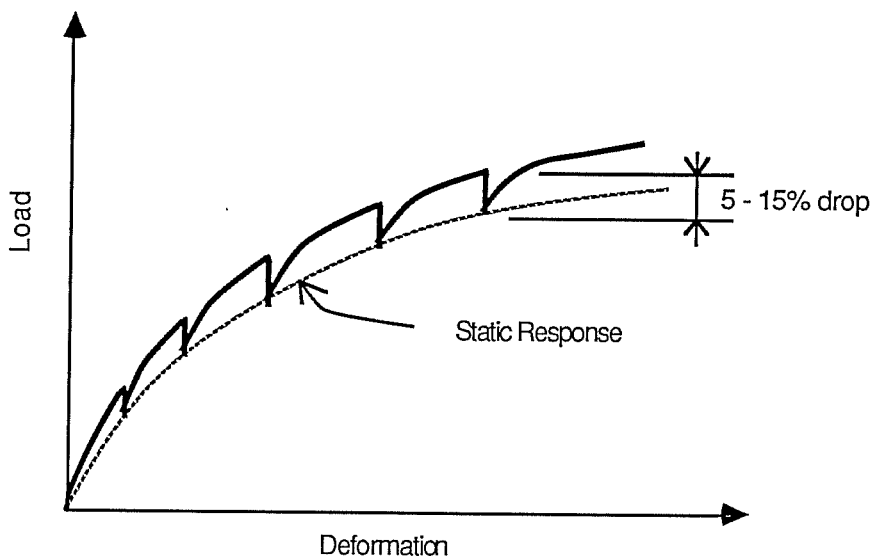

Fig. 2.20 Response Curve

CHAPTER 3 - EXPERIMENTAL RESULTS

3.1 Introduction

The presentation of experimental data and observations focuses on aspects of joint behavior which demonstrate the internal load transfer mechanisms and their modes of failure. Understanding these mechanisms is essential to the subsequent task of formulating a theoretical model to predict joint strength and stiffness.

Two approaches are used to effectively present the pertinent data. Initially individual test chronologies are summarized, first for the general case and then for each specimen. These summaries provide an overview of the tests and relate the visible distress, deformations, and internal strains to basic stages of behavior. The second portion of the chapter consists of a detailed examination of separate categories of data emphasizing comparison between test specimens. These comparisons highlight differences in behavior due to the various joint details. One category of data compares nominal joint strengths of the specimens. For this comparison data from tests 3 through 9 is included along with that from tests 10 through 17. Otherwise, only data from tests 10 through 17 are included since tests 1 through 9 are described in detail by Sheikh.[1]

In Figs. 3.1, 3.2 and 3.3, some of the terminology used in subsequent discussions is presented. In Fig. 3.1 a schematic view of the test specimen depicts member stresses associated with loading in the primary (initial) direction. These member stresses are used to distinguish locations in and around the joint. A typical load versus deformation curve is shown in Fig. 3.2 where the average ram loads are plotted against the total joint distortion. Recall that the total joint distortion (TJD) is the angular rotation of the beam relative to the column, measured directly adjacent to the joint. TJD is reported in percentages where 1% corresponds to 10 milli-radians of relative rotation. For identification, data are referred to by deformation cycle (for example: 1st - 1% cycle, 2nd - 1% cycle, etc.). Unless noted otherwise such references imply loading in the primary direction. As noted previously in Chapter 2 the sequence of loading cycles are as follows:

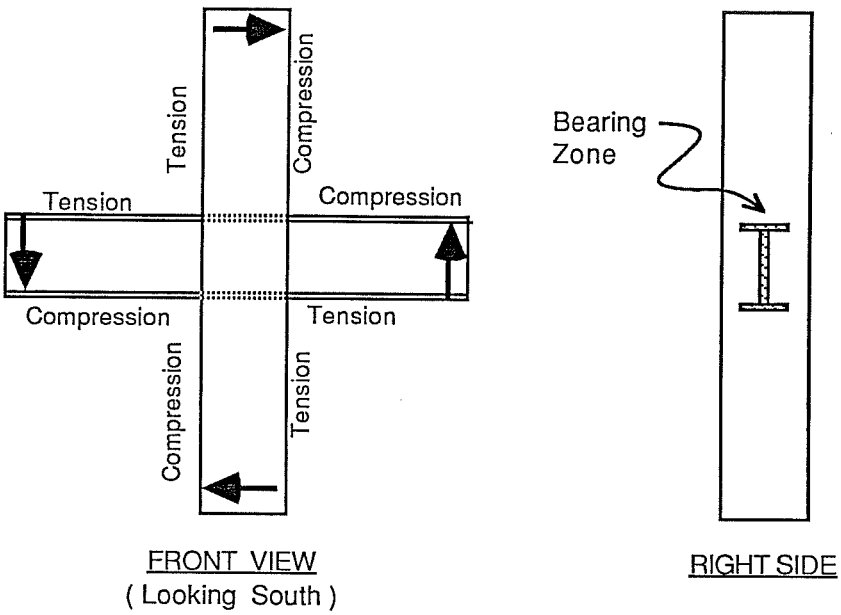

Fig. 3.1 Member Stresses Under Primary Loading

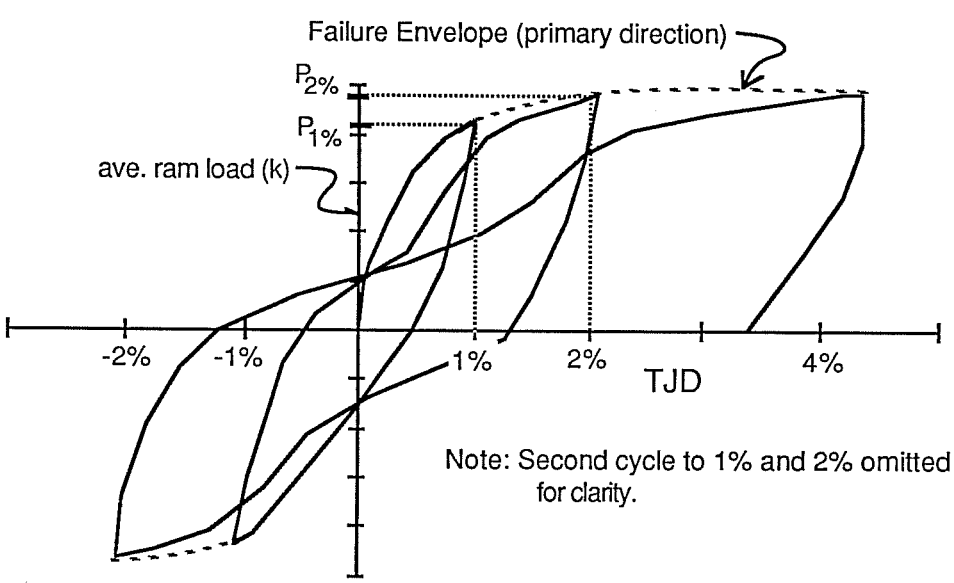

Fig. 3.2 Typical Load-Deformation Response

- Low Stress Cycle (1/2 cycle)
- 1st − 1% Cycle
- 2nd −1% Cycle
- 1st −2% Cycle
- 2nd − 2% Cycle (1/2 Cycle for Test 10 only)
- 4% Cycle (1/2 Cycle)

The distinction made between the inner and outer concrete panels is sketched in Fig. 3.3. The inner panel consists of the concrete held captive between the FBP and the beam flanges. The outer panel consists of the remaining concrete in the joint region.

Aside from measured loads and deformations, internal strain readings comprise much of the reported data. Strains measured in structural steel and reinforcing bars are given as measured stresses using elastic constitutive equations (E = 29500.0 ksi, $\nu = 0.3$). Where these reported stresses exceed the yield stress of the steel, the reader should note that such values are not the true stresses since the material is outside the elastic range. Arguably, a more correct approach might be to report strains directly, however, the stress approach is chosen since stress values are more familiar to engineers. Strains measured in the concrete are reported directly as strains since the constitutive behavior of concrete is markedly nonlinear.

3.2 Summary of Behavior

3.2.1 General. The overall behavior of the joint can be considered in three stages. The distinction between stages is not absolute, and one should be cautious not to overestimate any implied precision. However, such categorization is useful in identifying load mechanisms and key modes of failure.

The first stage occurs prior to significant cracking in the concrete and is characterized by elastic (recoverable) deformations. At low load levels, concrete is uncracked and adhesive bond transfers force between the steel beam

Table 3.1 Summary of Transition Loads and Deformations

Specimen	S_1		S_2		$P_{1\%}$	$P_{2\%}$	P_{max}
	Load	TJD	Load	TJD	Average Ram Load		
	(kips)	(%)	(kips)	(%)	(kips)	(kips)	(kips)
10 FBP (split)	14	0.2	24	0.7	29.0	34.2	39.8
11 FBP-DP-Dywi	15	0.2	40	0.8	47.0	52.7	52.7
12 Stud	12	0.2	21	0.5	28.7	34.1	34.7
13 FBP-Stud	15	0.2	31	0.6	42.8	48.0	48.0
14 WSP-Col.	13	0.2	22	0.4	33.8	37.3	37.3
15 FBP-Col.	15	0.2	26	0.5	37.0	43.2	43.2
16 FBP-Col.-Clip	15	0.2	27	0.4	37.3	41.1	41.9
17 FBP-Col.-Dywi	15	0.2	27	0.5	36.8	41.1	41.9

and concrete. During Stage 1 the adhesive bond breaks and microcracks in the concrete cause initial mobilization of lateral reinforcing ties. In general the ties begin picking up stress between 0.1% and 0.2% TJD. Stresses in such elements as FBPs, steel columns, etc. also begin increasing during this stage. For Specimens 10 through 17 the transition from Stage 1 to Stage 2 behavior occurred at loads ranging from 12 k to 15 k with associated deformations of 0.2% TJD. This transition point is termed S_1 and is listed for each specimen in Table 3.1. The initial low stress loading cycle occurs during the Stage 1 response. In practice, frequently occurring service loads should be limited to this stage.

Stage 2 commences with surface cracking of the concrete accompanied by decreased stiffness, and increasing participation of lateral ties and FBPs. Also, there is a reduction in the rate of bond mobilization around the vertical column bars with increasing load in the joint. At this stage the principle tension stresses due to shear exceed the capacity of the concrete, and strut mechanisms form which provide for shear transfer in the concrete up to ultimate load. As shown in Table 3.1 the transition between Stage 2 and Stage 3 (S_2) occurred at loads of 21 k to 40 k and deformations of 0.4% to 0.8% TJD. In actual buildings, the

Stage 2 behavior should correspond to severe service loadings beyond the range of frequent loading but below ultimate load.

The final sequence, Stage 3, begins with steel web yielding and or concrete crushing beneath the compression flanges. During this stage, changes in the relative contribution of various joint deformation modes signal readjustments in load carried by different internal mechanisms. Presumably, this occurs as the strength of joint shear mechanisms is exhausted. For example, web yielding usually causes an increase in steel panel shear (SPS) distortion. During this stage crack widths increase as there is greater mobilization of the concrete shear mechanisms (diagonal strut and diagonal compression field). Typically, web yielding is accompanied by higher stresses in FBPs and other steel elements which transfer shear into the concrete. Further evidence of this is given by increasing strains in the concrete as indicated from embedment gage data.

Typically, joints reached peak loads near 2% TJD beyond which the load was fairly constant. Table 3.1 includes loads at joint deformations of 1% and 2% along with the peak load. By 2% TJD, visible distress in the joint was severe. As shown in Fig. 3.2, specimens were loaded to a maximum deformation of roughly 4% TJD which is well beyond the useful design range. At deformations of 4%, concrete cover in the joint region was on the verge of spalling. Further discussion will be made regarding determination of the useful ultimate design load and deformation. A design limit of 1% TJD, which occurs early in Stage 3, seems to provide an appropriate index of performance.

Figure 3.4 shows a typical crack pattern. Three basic types of cracks are diagonal cracks on the front face, diagonal cracks on the side faces, and horizontal flexural cracks on the side face which extend onto the front face. Initially, flexural and diagonal cracks on the side radiate from the tension flanges of the beam. Together with diagonal cracks on the face, these cracks isolate the region of concrete shown shaded in the figure. The disengagement of this concrete results in decreased transfer of force to vertical column reinforcement in the joint. This causes vertical bar stresses adjacent to the joint to vary considerably form those predicted by bending theory. In particular, a drop in the compressive

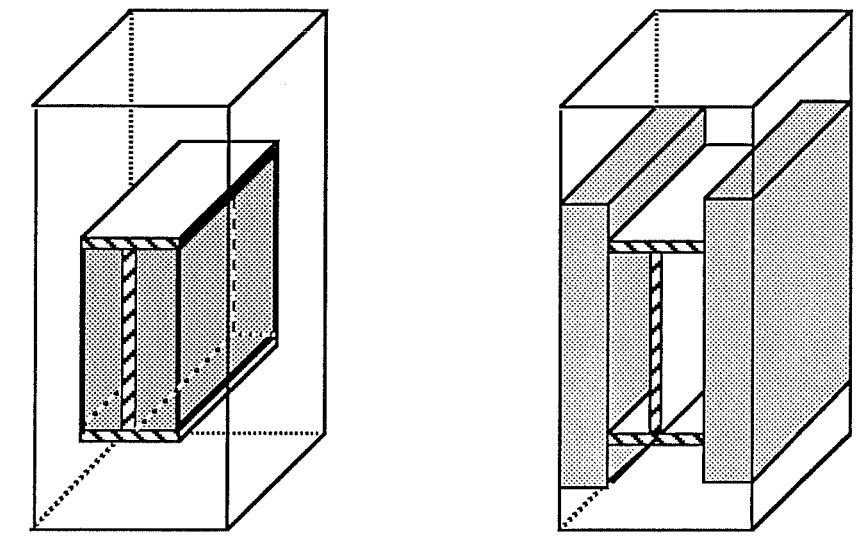

Fig. 3.3 Concrete Panel Terminolog y

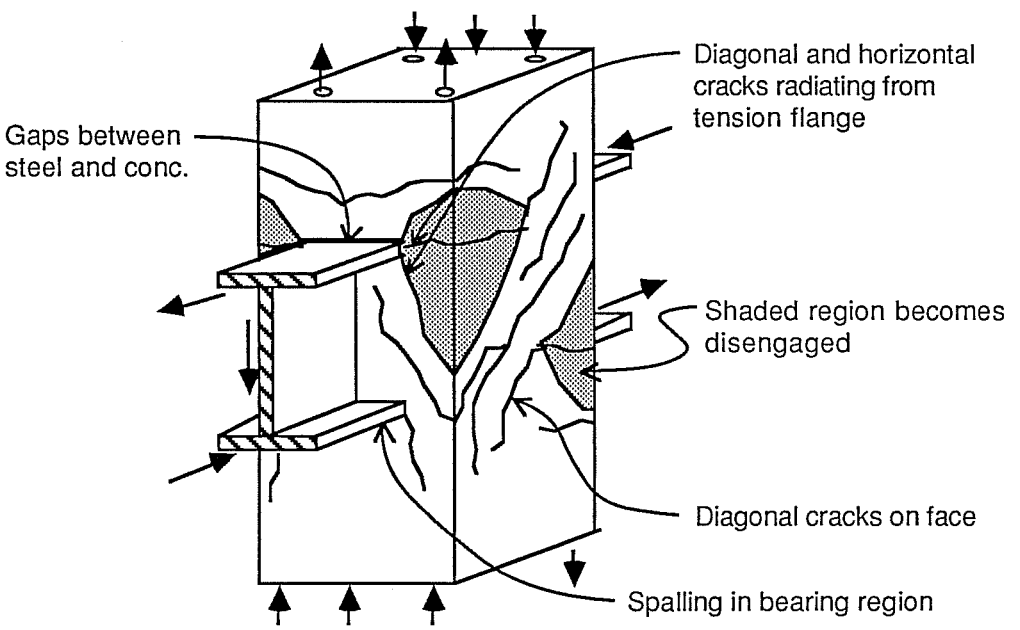

Fig. 3.4 Typical Crack Pattern

stress in bars located in the compression zone occurs at this point. Continued diagonal cracking highlights the formation of concrete compression struts. The location of gaps above (or below) the tension flanges with corresponding concrete spalling below (or above) the compression flanges is shown in Fig. 3.4. Except for Specimen 10, gaps typically measured 1/16 in. and 1/8 in. at 1% TJD and 2% TJD respectively. In Specimen 10 gaps were roughly twice the typical values from other tests.

The progression of cracking in Specimen 15, which was fairly typical of all the tests, is shown in Figs. 3.5a through d. In Fig. 3.5a, the applied load of 21 k corresponds to early Stage 2 behavior, where cracks which radiate from the tensile flange isolate the concrete encasing the vertical reinforcement. In Fig. 3.5b, an applied load of 36 k was reached at the peak of the 1st-1% cycle, signalling the beginning of Stage 3 behavior. At this point, cracks on the face highlight the flow of shear forces through the diagonal compression field. Typically, such cracks were oriented at angles of 45° to 55° with the horizon. In Fig. 3.5c, the specimen has been loaded completely through the 1st-1% cycle. As expected, the crack pattern shown in Fig. 3.5c was fairly symmetric due to opposite loadings in the primary and reverse directions. This degree of cracking is expected in practice at nominal design loads occurring at deformations of 1% TJD. During the second 1% cycle, few new cracks opened while existing cracks extended slightly. Finally, cracking after the 2nd-2% cycle is shown in Fig. 3.5d. In general, beyond 1% TJD the cracked region did not extend, but new cracks formed between those observed during the 1% cycles, and crack widths opened to 1/16 in.

The relative degree of cracking observed in different specimens is shown in Figs. 3.6 through 3.8 for Specimens 10, 12 and 13. Recall that Specimen 10 had split FBPs, Specimen 12 had welded shear studs, and Specimen 13 had both FBPs and shear studs. Specimens 10 and 12 each had one means of mobilizing the concrete shear panel, whereas Specimen 13 had two mechanisms. Hence, it follows that more severe cracking occurred in Specimen 13 due to greater concrete mobilization. Also, a close comparison of Specimens 10 and 12 reveals that 12 had slightly more cracking over a greater region of the column face. This

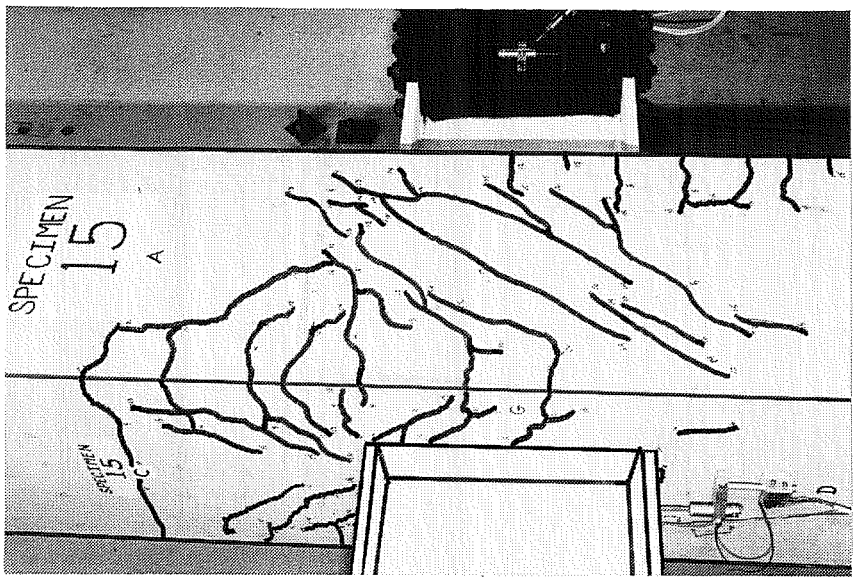

Fig. 3.5b Cracking at 1% T J D

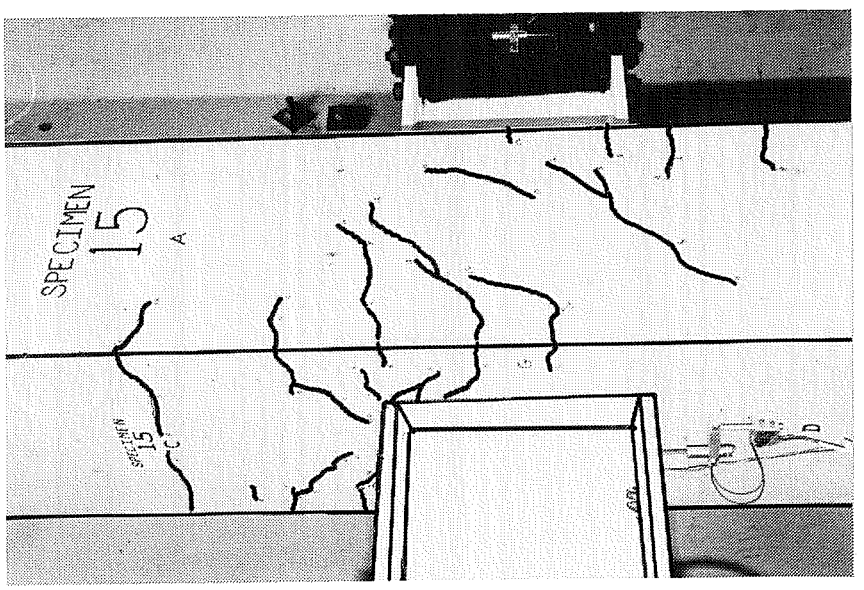

Fig. 3.5a Cracking During Stage 2

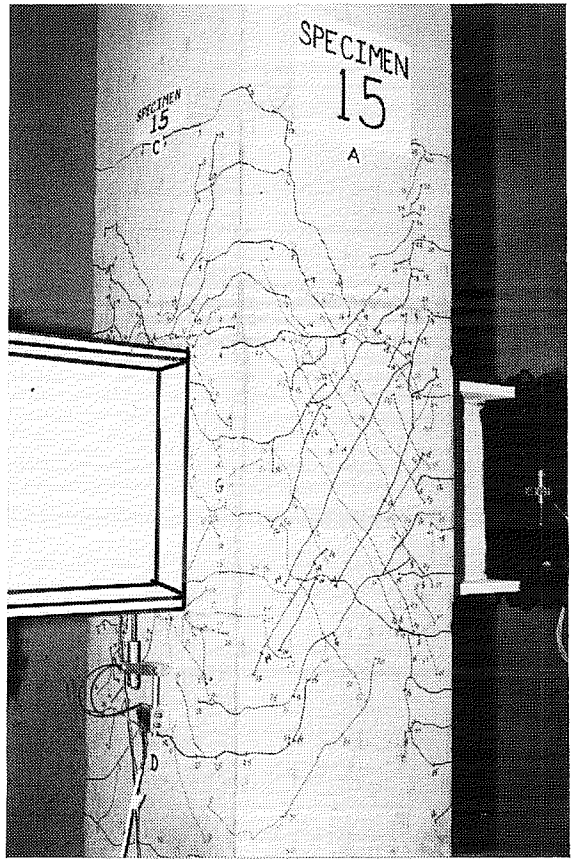

Fig. 3.5c Cracking After 1st-1% Cycle

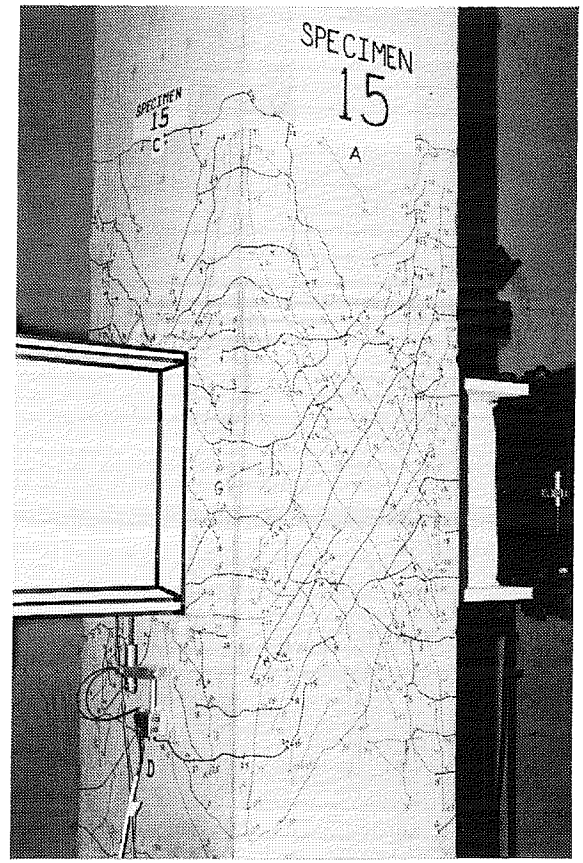

Fig. 3.5d Cracking After 2nd-2% Cycle

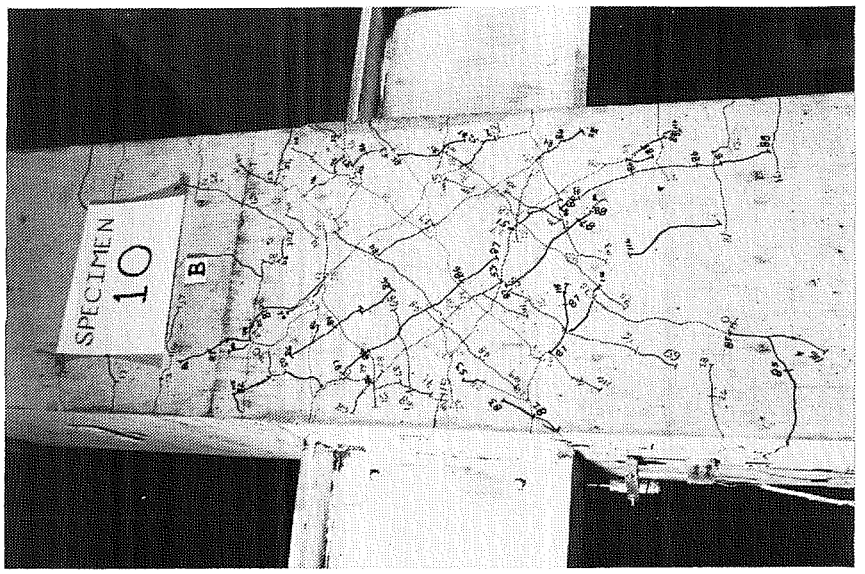

Fig. 3.7 Cracking After 2nd-2% Cycle [Specimen 10 - FBP(Split)]

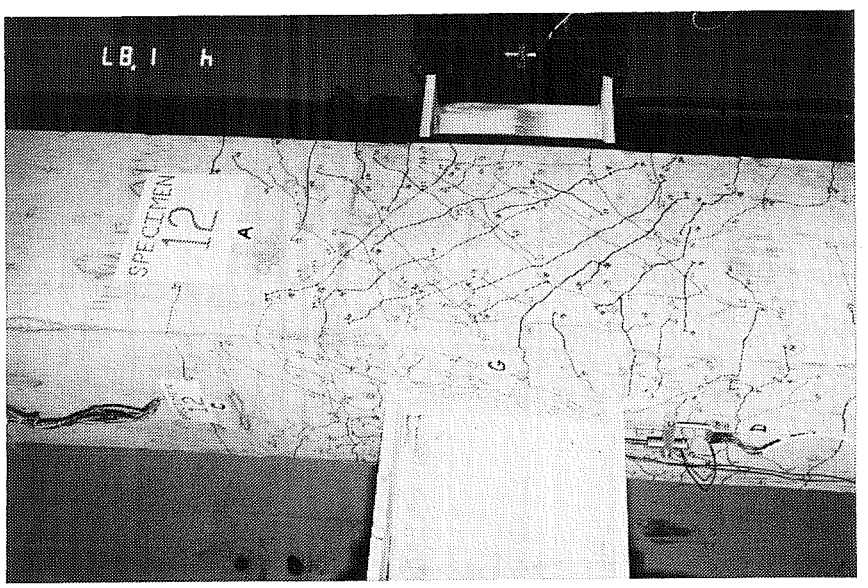

Fig. 3.6 Cracking After 2nd-2% Cycle [Specimen 12 - Studs]

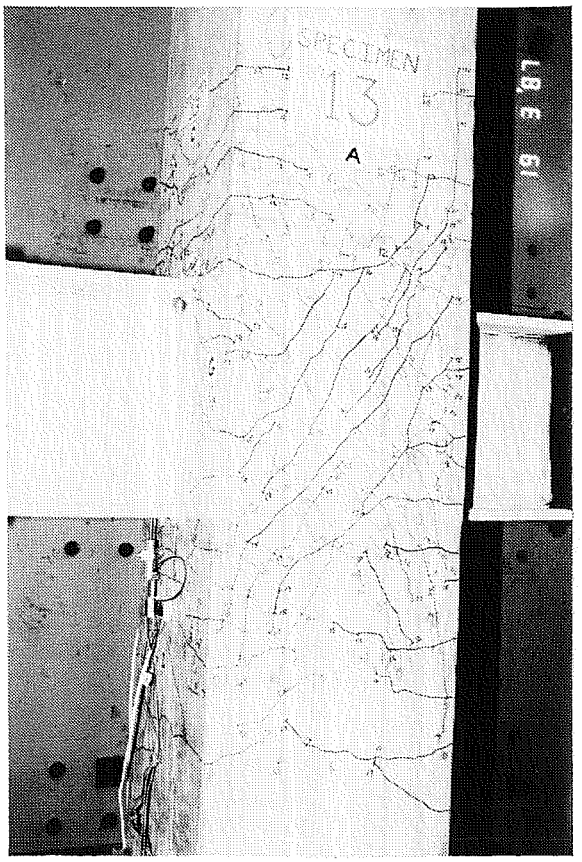

Fig. 3.8 Cracking After 2nd-2% Cycle [Specimen 13 - FBP-Studs]

is attributed to mobilization of the outer concrete panel by shear studs, whereas the FBP mobilized the inner panel. These explanations of concrete mobilization are somewhat premature based on crack patterns alone, however, subsequent comparisons of concrete strains and relative joint capacities will confirm the phenomena.

3.2.2 <u>Specimen Behavior Summaries</u>. The following is a summary of tests 10 through 17. Each test is not described in equal detail so as to

avoid repetition when results are similar to those reported previously. The load versus deformation plot for each specimen is shown in Figs. 3.9a through h. Also, for convenience, Figs. 3.10a through e show selected strain gage locations previously described in Chapter 2. These figures should be referred to throughout the test summaries.

Specimen 10, FBP(Split). The joint detail of Specimen 10 consisted of split FBPs on an otherwise plain beam. This specimen serves as a basis of comparison for other specimens which utilize a variety of details in lieu of or in addition to FBPs. The load-deformation curve is shown in Fig. 3.9a where the points S_1, S_2, and P_1% are indicated.

During Stage 1 several observations were made. At roughly 4 k (0.02% TJD), strain gage readings indicated the column ties in the bearing zone above the beam began picking up stress. Also, concrete embedment gages recorded strain in the diagonal strut with the inner gage picking up strains at 1.9 times the rate of the outer gage. This difference supports the observation previously reported by Sheikh that FBPs effectively mobilize only concrete inside the FBP width. At 9 k (0.09% TJD), ties within the beam depth began picking up load. Unlike behavior observed in other specimens, in Specimen 10 the outer panel ties outside the beam depth (Fig. 3.10b) were not mobilized until 19 k (0.4% TJD), and then to a lesser degree than in other specimens. This behavior follows from the fact that there was no positive means for joint shear to be transferred from the beam flanges to concrete above and below the beam. Finally, at 9 k bending stress in the FBP began to increase, indicating loss of adhesive bond between the steel and concrete. The FBP contribution increased further at the next loading, 14 k, when the FBP stress began increasing at over 5 times its initial rate.

Stage 2 behavior began at 14 k with opening of diagonal and horizontal cracks accompanied by an abrupt decrease in joint stiffness to 25% its initial value. Additionally, vertical reinforcing bar gages showed a decrease in compressive stress at this point. As higher loads were applied, compressive stress reversed to tension, revealing a loss of bond within the joint. This bond behavior

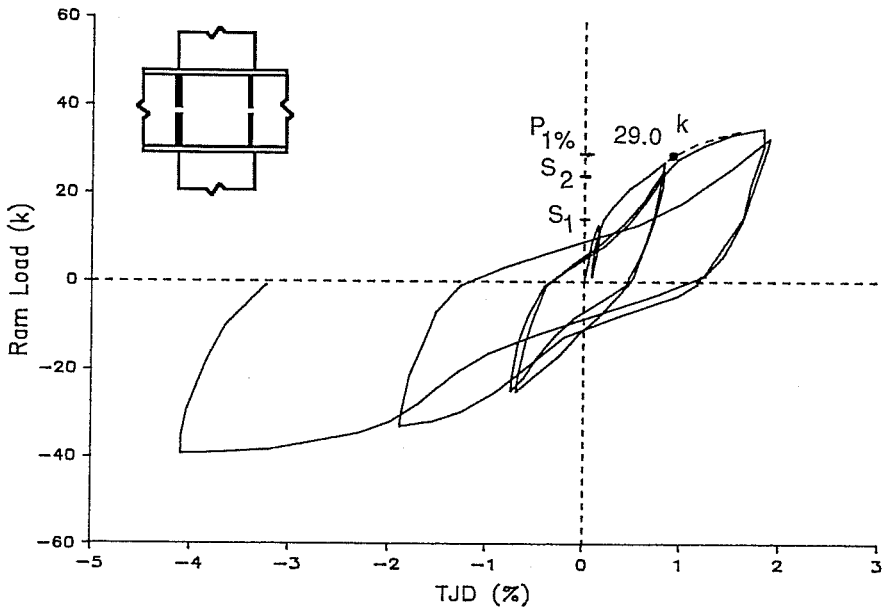

Fig. 3.9a Load-Deformation: Specimen 10 [FBP(split)]

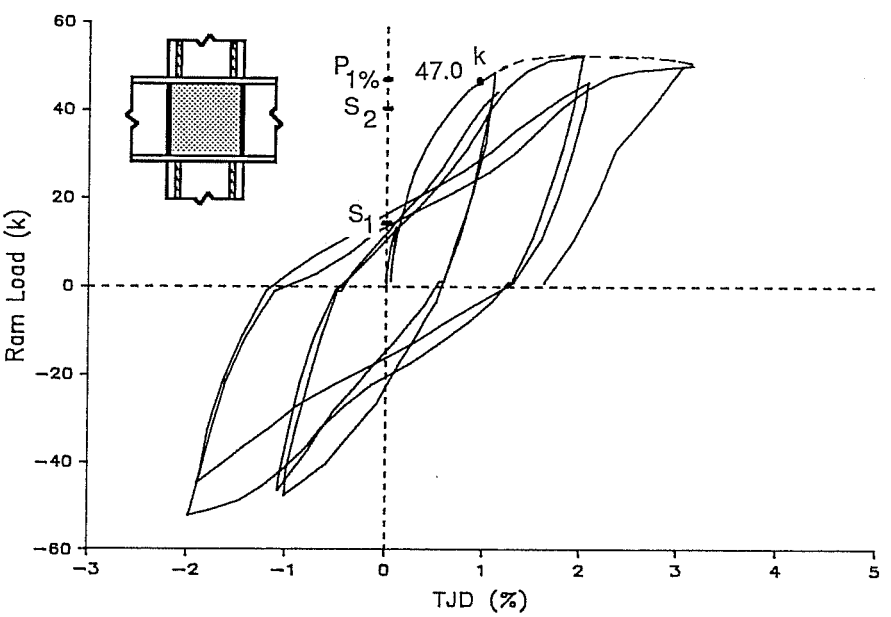

Fig. 3.9b Load-Deformation: Specimen 11 [FBP-DP-Dywi.]

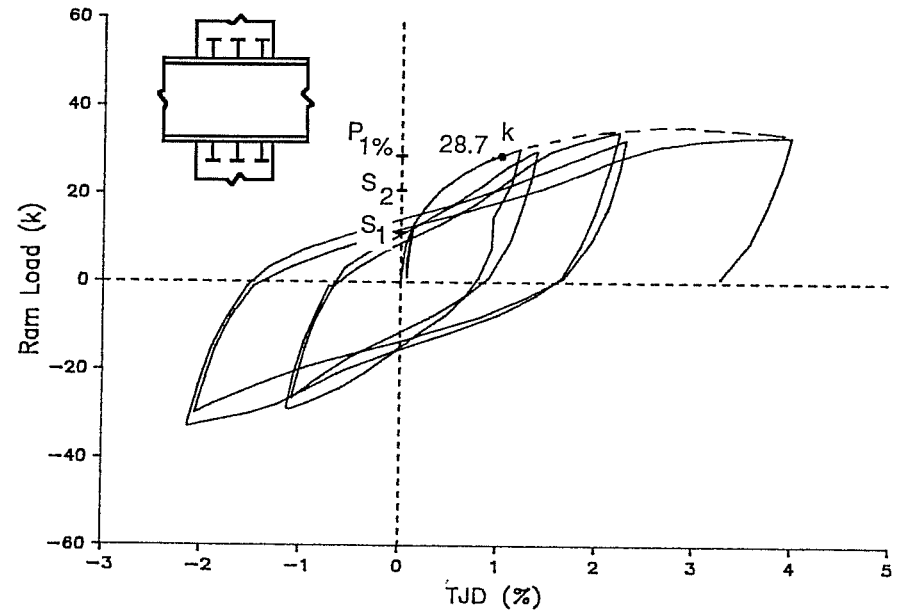

Fig. 3.9c Load-Deformation: Specimen 12 [Studs]

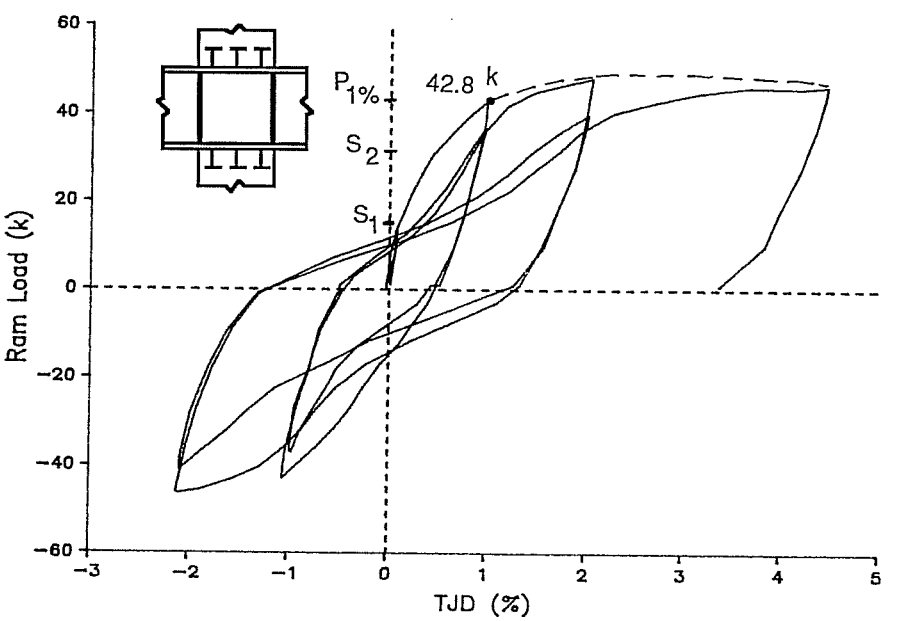

Fig. 3.9d Load-Deformation: Specimen 13 [FBP-Studs]

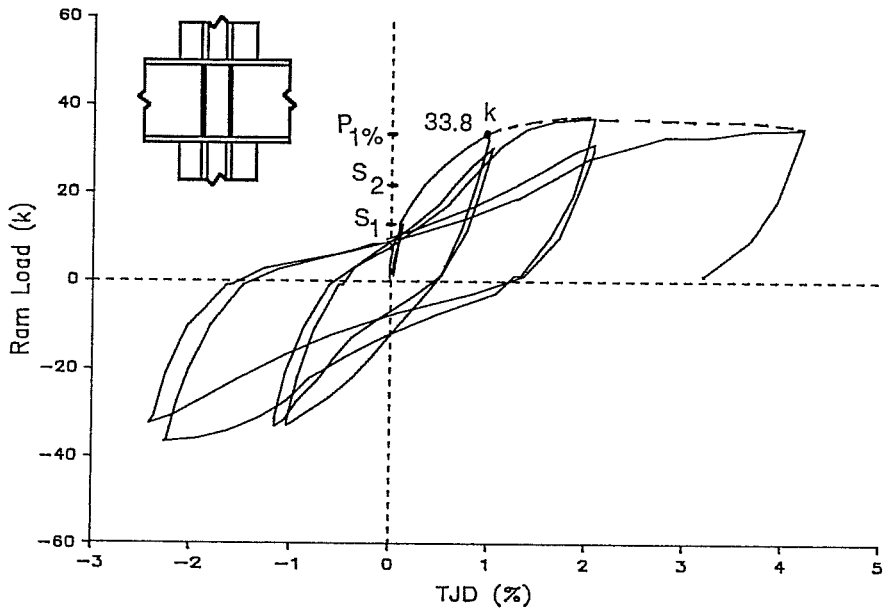

Fig. 3.9e Load-Deformation: Specimen 14 [WSP-Column]

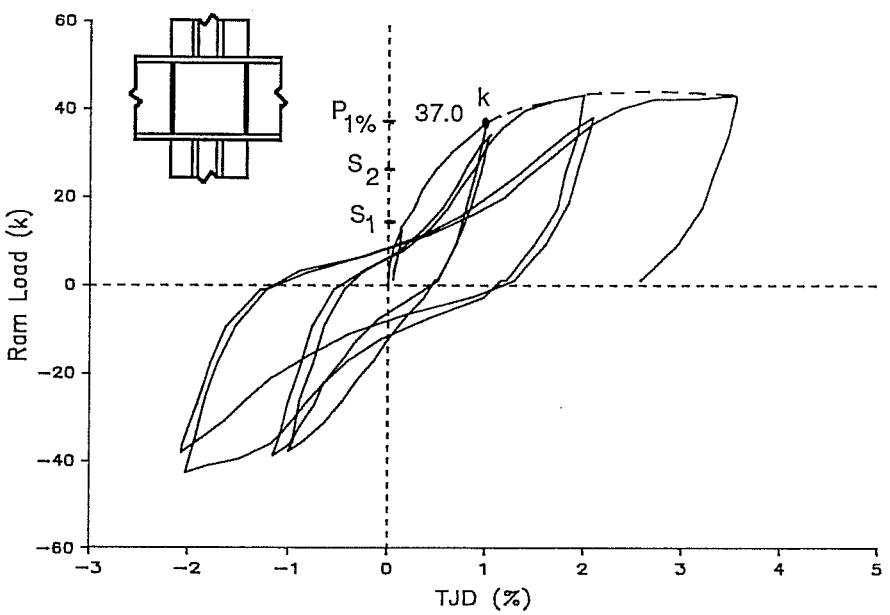

Fig. 3.9f Load-Deformation: Specimen 15 [FBP-Column]

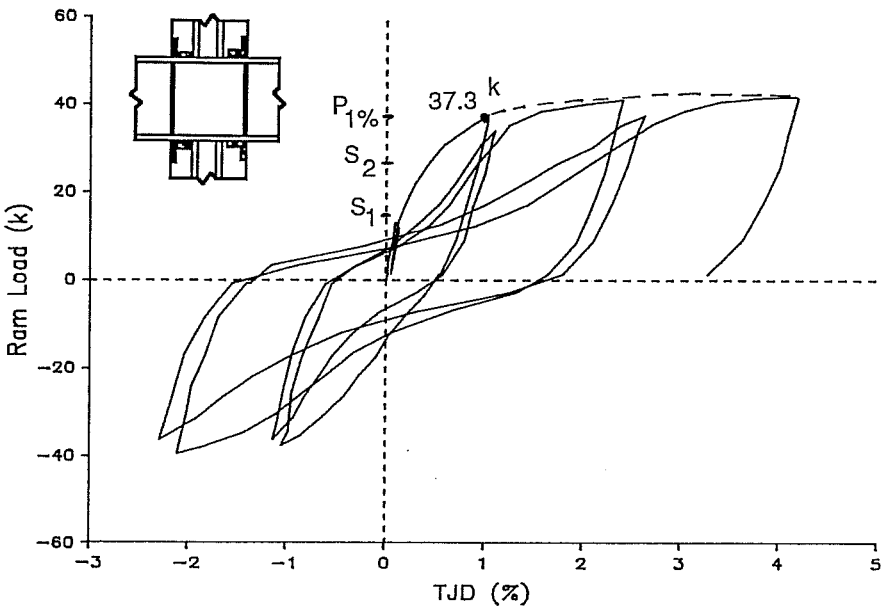

Fig. 3.9g Load-Deformation: Specimen 16 [FBP-Col.-Clip]

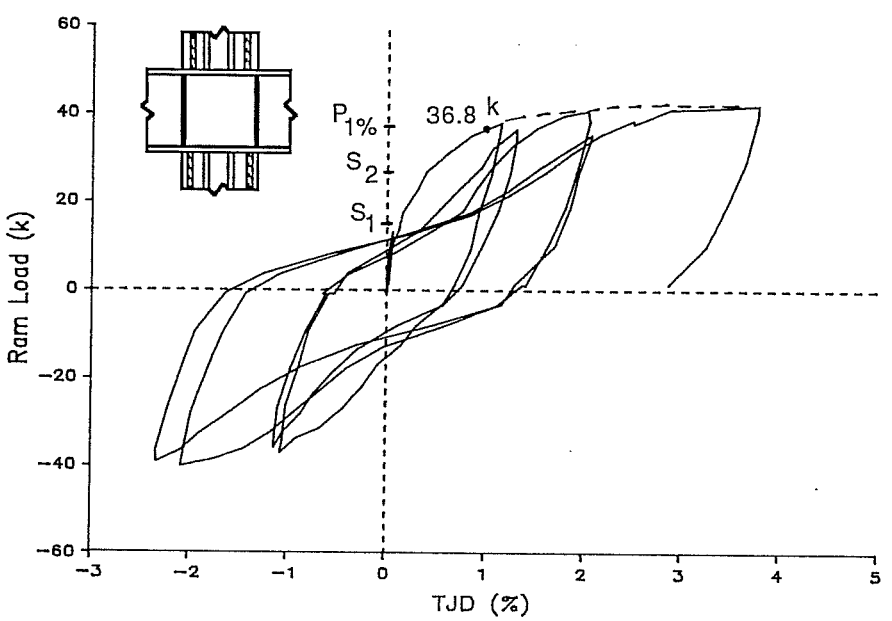

Fig. 3.9h Load-Deformation: Specimen 17 [FBP-Col.-Dywi]

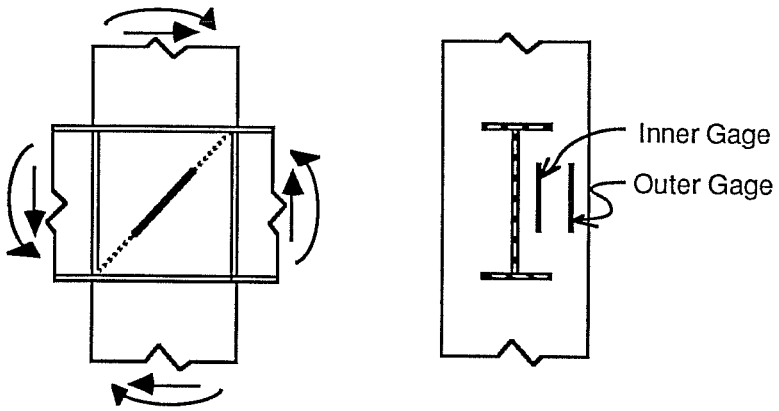

Fig. 3.10a Concrete Embedment Strain Gages

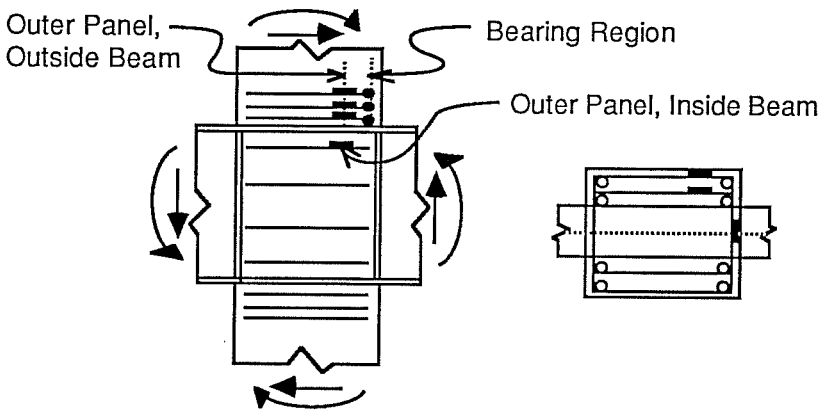

Fig. 3.10b Transverse Tie Strain Gages

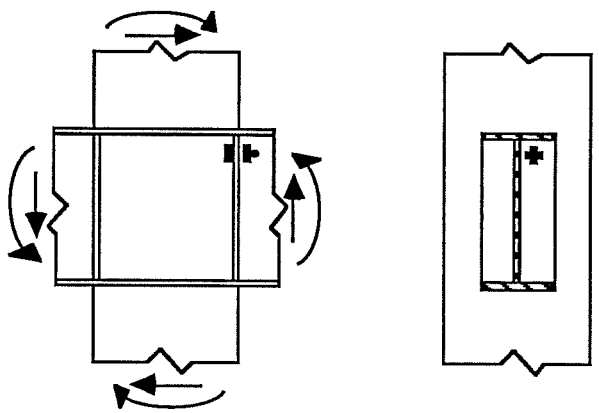

Fig. 3.10c Face Bearing Plate Strain Gages

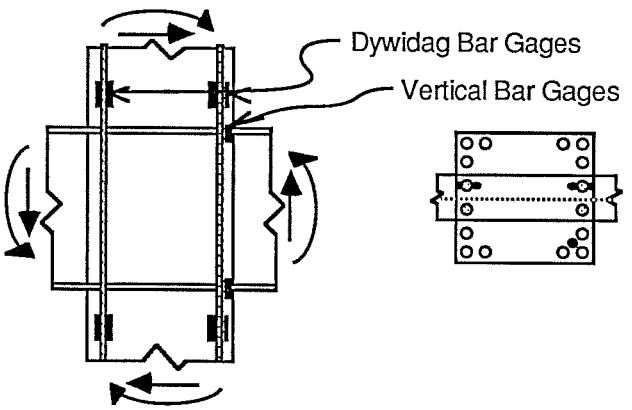

Fig. 3.10d Dywidag and Vertical Bar Gages

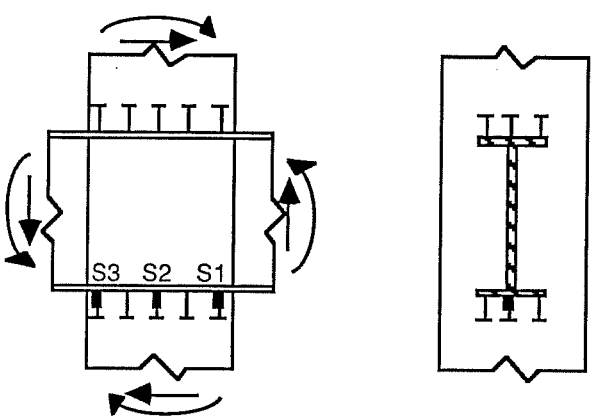

Fig. 3.10e Shear Stud Gages

is described in more detail later. Note, however, that opening of diagonal and horizontal surface cracks precipitated the change in bar stress.

The web rosette indicated web yielding at 24 k, signalling the onset of Stage 3 behavior. Accompanying this, concrete embedment gages began picking up strain at twice their initial rate. This change demonstrates increased reliance on the concrete strut to carry joint shear after the steel web yields. Spalling of the concrete cover above and below the beam was also noted at this point, probably caused by high concrete strains created by the kink which formed in the steel beam after web yielding. Based on subsequent dissection of several specimens, this kink formed approximately 2 in. inside the column face as shown in Fig. 3.11. Due to the high strain gradient caused by the beam kinking, cover spalling may not be indicative of the concrete strains inside the column ties. The peak deformation reached in the 1st-1% cycle was 0.83% TJD. This distortion was less than the targeted value of 1.0% TJD due to limited accuracy of the pen plotter used to monitor deformation during testing.

During reverse loading in the 1st-1% cycle, behavior was similar to that in the primary direction. The steel web picked up stress more rapidly in the reverse direction, and reached yield at 12 k compared to 24 k previously. This difference may be explained by observing that upon load reversal, cracks formed during initial loading reduced the stiffness of the concrete shear panel. Hence, until the cracks closed, the steel web carried a larger portion of the load. This behavior had negligible effect on the ultimate joint load in the reverse direction, which was similar to that in the primary direction. The phenomenon of crack opening and closing is inherent to concrete structures and is responsible for much of the so called "pinching" of the load-deformation curve.

Yield lines formed on the split FBPs during the 1st-2% cycle at 33 k (1.5% TJD) in the primary direction, and at 29 k (1.2% TJD) in the reverse direction. The yield line pattern is shown in Fig. 3.12. Formation of yield lines did not signal reaching of ultimate capacity, however, as strain hardening and membrane action enabled the FBPs to carry additional load. Previous tests of Specimens 4 and 5 substantiate this point, as they showed that, within reasonable

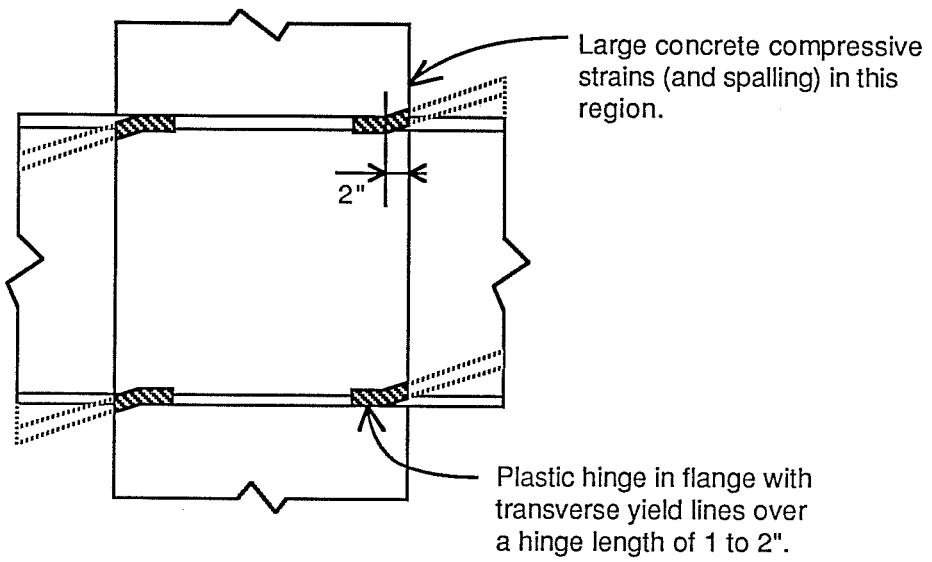

Fig. 3.11 Local Plastic Hinge (kink) in Steel Beam

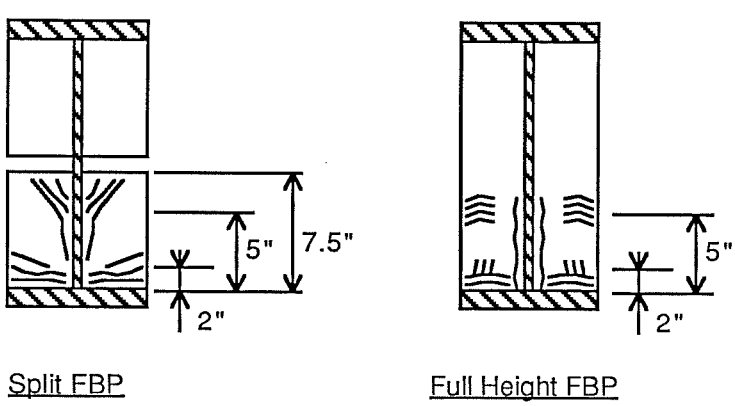

Fig. 3.12 Yield Lines on Face Bearing Plates

limits, FBP thickness (and hence, stiffness) had negligible influence on joint strength. Of course, the FBP must be designed so that it will not fracture near the perimeter weld to the beam.

The peak deformation reached during the 1st-2% cycle was 1.8% TJD. Beyond 2% TJD, Specimen 10 continued to pick up load slowly until the test was stopped at 3.5% TJD.

Specimen 11, FBP-DP-Dywi. In Specimen 11, web doubler plates were used to increase the steel panel capacity, and full height FBPs were used to mobilize the inner concrete panel. In addition, Dywidag bars (serving as vertical joint reinforcement) were expected to improve behavior in three ways. First, they served as compression reinforcement in the concrete bearing zone. Second, bars in the tension region transferred tensile forces directly from the steel beam into the concrete column. Finally, near the connection to the flange, the bars served as large shear studs which mobilized shear in the outer concrete panel. Figure 3.9b shows the load-deformation curve for Specimen 11.

Stage 1 behavior was similar to that of Specimen 10 with the variations and additions noted below. At 4 k (0.03% TJD) Dywidag bars attached to the tension flanges reached the rate of axial tensile stress increase (with respect to joint load) which then remained constant for the remaining loading. Dywidag bars which developed compressive stress also picked up load, but to a lesser degree. More detailed discussion of the Dywidag bar behavior is presented later. At low loads the inner and outer concrete gages recorded roughly equal strains. At 13 k (0.15% TJD), as the transition to Stage 2 began, concrete gages recorded strains at increasing rates: the inner gage at 2 times and the outer gage at 5 times its original rate. The large increase in the outer gage, which was not observed in other specimens, leads to suspect that this gage data may not be accurate beyond this point. The change in concrete strain mobilization was accompanied by increased FBP participation (stress increasing at 3 times its initial rate), flexural cracks radiating from the tension flanges, and an increase in the concrete panel shear (CPS) relative to other distortions.

Stage 2 behavior was evident after diagonal cracks opened and compressive stress dropped in vertical column bars at 15 k (0.2% TJD). At 30 k (0.5% TJD), vertical cracks formed on sides of the column above the tension flanges parallel to the Dywidag bars as shown in Fig. 3.13. The effect of this cracking on bond and development length for the Dywidag bars is discussed later. The pattern of yield lines which formed on the full height FBP at 36 k (0.6% TJD) is shown in Fig. 3.12.

Stage 3 commenced at 40 k (0.8% TJD) with yielding of the web panel, indicated by the rosette gage. Similar to Specimen 10, concrete spalling coincided with web yielding. Note that the cover spalled in spite of reinforcement (Dywidag bars) in the confined concrete bearing region. The peak deformation in the 1st-1% cycle was 1.2% TJD.

Similar to Specimen 10, during reverse loading the web picked up stress more quickly and yielded at a lower load, 30 k (0.5% TJD) versus 40k (0.8% TJD), than in the primary direction. Also, yielding of the FBPs occurred at 44 k (1.0% TJD).

During the 2% cycles, strain gages on the Dywidag bars showed tensile stress in some of the bars drop sharply. Subsequent dissection of the specimen revealed that 7 of the 8 welds between the steel beam and the Dywidag couplers fractured. This observation is important for two reasons. First, strain gage readings indicate that the welds were intact through the 1% cycles, and hence, data and conclusions drawn during those cycles are valid. Also, note that the load-deflection curve does not show any obvious discontinuities attributable to the weld failures. Second, the fractures raise questions regarding adequacy of the weld detail. In this case weld failure was attributed to inadequate throat thickness and to weld porosity, both of which could be avoided by more thorough supervision and inspection of welding.

The peak distortion of the 1st-2% cycle was 2.0% TJD where the peak load of 52.7 k was recorded. At the maximum distortion of 3.4% TJD the load was 96% of the peak value.

Specimen 12, Studs. The joint detail examined in Specimen 12 consisted of shear studs welded to the outside faces of the beam flanges. Like the FBP, shear studs provided a means for transferring horizontal shear directly to the concrete. However, unlike the FBP, studs mobilized the outer rather than inner concrete panel. Figure 3.9c shows the load- deformation response of Specimen 12.

Initially, concrete embedment gages picked up equal strains until the load reached 9 k (0.9% TJD) at which point the strain rates dropped to 30 - 40% of their original values. Presumably, this drop was due to the fact that Specimen 12 did not have FBPs to mobilize the diagonal compression strut after breaking of the adhesive bond. After this drop, the inner gage picked up strain at roughly 0.7 times the rate for the outer gage. At 12 k (0.2% TJD), column ties outside the beam depth began picking up load, however, ties within the joint did not pick up load until the beginning of Stage 2 at 17 k (0.40% TJD). Both the concrete and column tie strain data support results reported by Sheikh that without FBPs there is little mobilization of the inner concrete panel.

Stage 2 was marked by formation of horizontal cracks above and below the tension flanges as shown in Fig. 3.14. Prior to this point, studs directly behind the cracks (stud S1 in Fig. 3.10e) were picking up tensile stress. The crack formations resulted in sudden drops in the tensile stress, and an accompanying increase in joint distortion contributed by local flange bearing (LFB). At this point studs S1 and S2 picked up almost equal bending stresses. Gages on stud S3 malfunctioned during the test.

Early in the test the web rosette malfunctioned, however, at 21 k (1.0% TJD) alternate data indicated steel web yielding. Stage 3 behavior was identified by an increase in steel panel shear (SPS) distortion together with an indication of local beam kinking based on stress measured by a cross gage located along the beam flange center line. During Stage 3, vertical cracks shown in Fig. 3.14 opened due to the shear studs bearing on the concrete. The peak deformation in the 1st-1% cycle was 1.12% TJD.

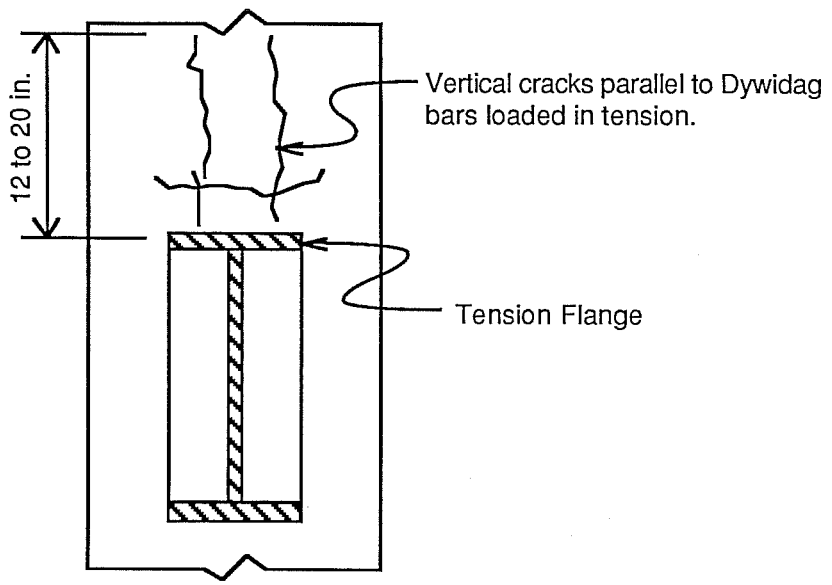

Fig. 3.13 Cracking in Specimens 11 and 17 (Dywidag bars)

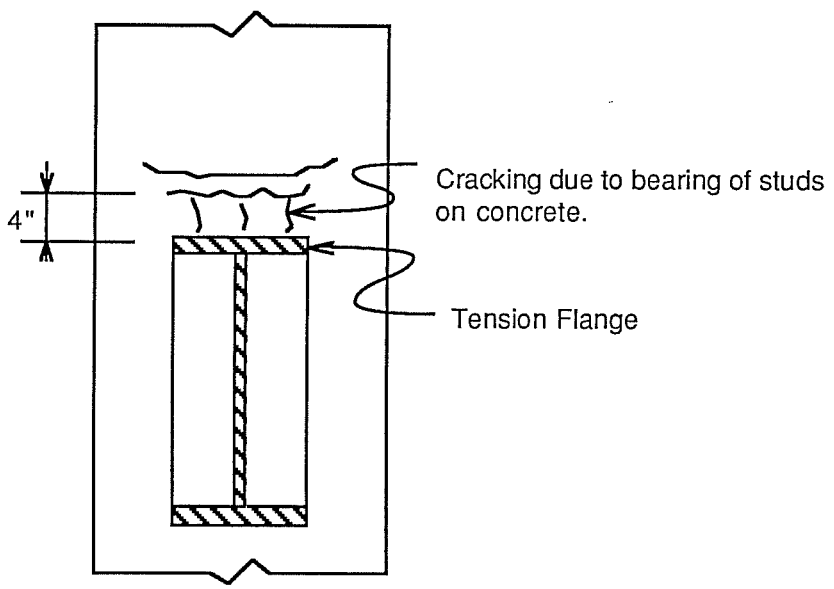

Fig. 3.14 Cracking in Specimens 12 and 13 (shear studs)

During the 1st-2% cycle, spalling of concrete adjacent to the compression flanges was noted at 30 k (1.4% TJD). The crushing coincided with formation of yield lines due to transverse bending of the beam flanges in the bearing zone. The maximum deformation in the 1st-2% cycle was 1.9% TJD. The peak load of 34.4 k was reached during the 1st-2% cycle after which the load dropped off. At the maximum joint deformation of 3.4% TJD the load reached 97% of its previous peak value.

Dissection of Specimen 12 revealed that 13 of the 15 shear studs on the bottom flange fractured during the test. It is of interest to determine when the studs fractured, and why only studs on the lower flange fractured? The fracture surfaces provided good evidence that the studs all failed during loading in the primary direction. As seen in the overall load- deformation response, joint capacity increased through the 1st-2% cycle, suggesting that the fractures occurred after this point. Fractures were located outside the puddle weld region, indicating that failures were not attributable to material or fabrication defects. Two reasons why only the lower studs fractured are as follows. First, as will be discussed later, concrete cast against the bottom of the flanges is of inferior quality due to trapped air bubbles and poor consolidation. Weak concrete in this region will induce higher bending stress in the studs as the lateral bearing stress shifts away from the flange. The second contributing cause may be the strain gage protection installed on 3 of the 15 studs (Fig. 3.10e). In effect, the soft rubber protection precludes concrete bearing for 3/4 in. of the stud adjacent to the flange. The net result is that the remaining 12 studs will carry a larger portion of the load.

Specimen 13, FBP-Studs. Specimen 13 used both FBPs and shear studs to mobilize the concrete shear panels. Essentially, these combined the mechanisms used in Specimens 10 and 12. Figure 3.9d shows the load-deformation response for Specimen 13.

The Stage 1 behavior was similar to that in previous specimens. The inner concrete gage picked up strain at 1.4 times the rate of the outer gage. This ratio lies midway between the ratios of 1.9 and 0.7 observed in Specimens 10 and

12. By 13 k (0.14% TJD) all of the ties except those in the bearing zone were picking up stress as were the FBPs.

Stage 2 began at 15 k (0.2% TJD) with formation of horizontal cracks radiating from the tension flanges and mobilization of ties in the bearing region. At 21 k (0.34% TJD), diagonal cracks opened on the column face as did horizontal cracks above the flange as shown previously in Fig. 3.14. Also, bending stress in stud S2 (Fig. 3.10e) no longer showed an increase. The rosette gage did not work in this test, however, at 26 k (0.46% TJD) the strain rate recorded by the inner concrete gage increased by 40%, indicating that the web was beginning to yield.

By 31 k (0.59% TJD), Stage 3 began as the steel panel shear (SPS) distortion, which had been negligible up to this point, abruptly began increasing. Also, vertical cracks similar to those in Specimen 12 formed above the tension flanges (Fig. 3.14). At 36 k (0.75% TJD), yield lines formed on the FBP. At 40 k (0.93% TJD), concrete spalling was noted, and also strain recorded by the inner concrete gage began increasing sharply. These observations may indicate that although the web started yielding at 26 k, the beam did not develop kinks until 40 k. The delay may have been due to greater stiffness provided by two (rather than one) concrete shear mechanisms: the FBPs and shear studs, which picked up load as the web yielded. The peak deformation in the 1st-1% cycle was 1.1% TJD.

The maximum load of 48.1 k occurred at 2.0% TJD, the peak distortion of the 1st-2% cycle. At the maximum applied distortion of 3.8% TJD the load reached 97% of the peak load recorded previously.

Specimen 14, WSP-Col. Specimen 14 was the first of four specimens with an embedded steel column. The steel column acted similarly to shear studs in mobilizing the outer concrete panel. Specimen 14 also had web stiffener plates (WSP) which, although not as effective as FBPs, mobilized the inner concrete panel. Figure 3.9e shows the load-deformation response of Specimen 14.

Strain gages on the steel column indicated transverse flange stress began increasing from initial loading due to concrete bearing forces. As will be discussed, forces originating through bearing transferred joint shear into the outer panel. As Specimen 14 had only an outer concrete gage, there was no measure of relative strain in the inner and outer panels.

Stage 2 began at 13 k (0.2% TJD) with opening of horizontal and diagonal cracks and associated dropping of compressive stress in the vertical column bars. Also, the stress picked up by ties between the flanges increased to over 3 times their initial rate at this load.

At 22 k (0.4% TJD), Stage 3 began as evidenced by an abrupt increase in the steel panel shear (SPS) distortion. The change was accompanied by a slow down in accumulation of transverse column flange stress which reduced its rate of increase to 60% of its initial rate. Also, gages on lateral ties around the column showed a similar decrease in their mobilization. These observations suggest that internal cracking had adversely affected the horizontal force transfer between the embedded steel column and outer concrete panel. At this point the force transfer mechanism may have been changing from one dominated by direct shear transfer through uncracked concrete, to transfer by a horizontal strut or shear friction mechanism as shown in Fig. 3.15. The web rosette did not indicate web yielding until 30 k (0.8% TJD), however, this data may not be indicative of overall web behavior due to close proximity with the web stiffener plates. In this case, the increase in SPS distortion at 22 k was a more reliable indication of overall web yielding. The peak deformation in the 1st-1% cycle was 1.0% TJD.

The maximum load of 37.3 k occurred during the 1st-2% cycle at the peak distortion of 1.8% TJD. The load dropped off to 93% of this value at the maximum applied distortion of 3.3% TJD.

Specimen 15, FBP-Col. Specimen 15 was similar to Specimen 14 except that in 15 the FBPs more effectively mobilized the inner concrete panel than did the WSPs in Specimen 14. Figure 3.9f shows the load-deformation response for Specimen 15.

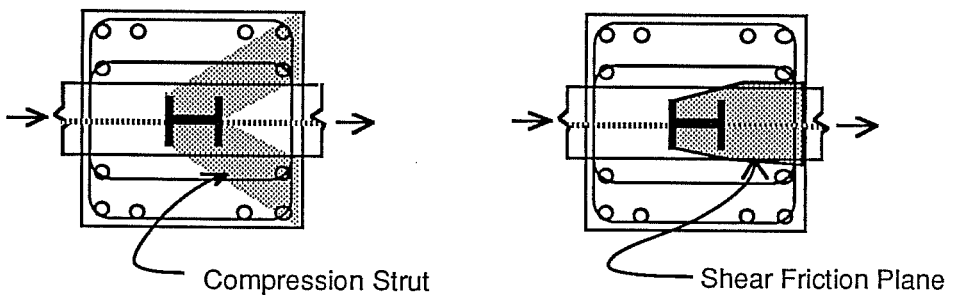

Fig. 3.15 Horizontal Transfer Mechanisms

Stage 1 behavior was similar to Specimen 14 with the following additions. The inner and outer concrete embedment gages picked up strains at an equal rate through the 1st-1% cycle. At 13 k (0.18% TJD), stress in the FBP increased in participation to over 5 times its original rate, indicating loss of adhesion between the steel beam and concrete. This change occurred with no change in the concrete strain mobilization rate.

Commencement of Stage 2, and the drop in vertical bar compressive stress, occurred at 15 k (0.2% TJD), a slightly higher load than in Specimen 14. Similar to behavior in Specimen 14, at 22 k (0.39% TJD) transverse stress in the column flange dropped to one half of its initial rate of increase.

Stage 3 is judged to have begun at 26 k (0.5% TJD). With the rosette gage malfunctioning, this estimate is based on the observation that at the next load stage of 30 k (0.70% TJD) the inner concrete gage strain began increasing at twice its original rate. As will be noted for Specimen 17, where the rosette gage was working, the onset of web yielding preceded the increase in concrete strain mobilization by one load stage. Also, at 26 k ties in the bearing zone began picking up stresses at increased rates, indicating that concrete strains

were increasing due to kinking of the steel beam. The peak deformation of the 1st-1% cycle was 1.0% TJD.

During the 1st-2% cycle the vertical bar bond began to drop at 40 k (1.3% TJD). Further discussion of bond behavior is included later in this chapter. A deformation of 1.8% TJD was reached during the 1st-2% cycle at which point the peak load of 43.2 k was recorded. During the final cycle, at the maximum applied deformation of 3.0% TJD the load equalled the previous peak of 43.2 k.

Specimen 16, FBP-Col-Clip. Specimen 16 was similar to Specimen 15 with the addition of clip angles. Clip angles were intended to provide additional confinement to the concrete bearing zone above the flanges, and also assist the steel column in transferring horizontal joint shear into the concrete. Figure 3.9g shows the load-deformation response for Specimen 16.

The outer concrete gage malfunctioned in this test, and hence there was no comparison of inner and outer concrete strains. The FBP and steel column picked up stress similarly to Specimen 15. In addition, bending stresses were evident in the clip angle from first loading.

Stage 2 and 3 behavior were similar to Specimen 15. In Specimen 16, the rosette gage indicated web yielding at 27 k (0.4% TJD) which coincided with the yield load estimated for Specimen 15. Also at 27 k, transverse bending stress in the column flange began increasing at a lesser rate. This change occurred at a load 5 k higher than in Specimens 14 and 15. The delay may have been due to formation of more effective compression struts or a larger shear friction plane than those shown previously in Fig. 3.15 owing to the clip angle.

At 31 k (0.59% TJD), the clip angle bending stress indicated yielding near its base. This coincided with an increase in steel panel shear (SPS) distortion, and increase of the inner concrete strain rate to 1.4 times its original value. Finally, at 35 k (0.8% TJD) yield lines began forming on the FBP.

The peak deformation reached during the 1st-1% cycle was 0.9% TJD and during the 1st-2% cycle 1.9% TJD. The peak load of 41.9 k was recorded at

the maximum applied deformation of 3.2% TJD. This load was only 2% higher than that recorded during the 2% cycles.

Specimen 17, FBP-Col-Dywi. Specimen 17 was also similar to 15 except for addition of vertical Dywidag bars. The function of the bars was similar to that described for Specimen 11, however, in this case utilization of the bars was less since web doubler plates were not used, and because shear stud type behavior was shadowed by the steel column. Figure 3.9h shows the load-deformation response for Specimen 17.

The behavior of Specimen 17 was similar to that of Specimens 14 through 16. During Stage 1, the Dywidag bars with tensile stress reached their full mobilization rate at 9 k (0.08% TJD). This coincided with internal cracking in the concrete as evidenced by stress increases in the lateral ties. The outer concrete embedment gage malfunctioned at an early stage, and therefore no comparison of concrete strains was available.

As in Specimen 16, the rosette gage indicated web yielding at 27 k (0.5% TJD). Also, transverse bending stress in the column flange began increasing at a slower rate at this load. At the next load of 31 k (0.63% TJD), the inner concrete gage began recording strains at over 3 times its initial rate. Also, yield lines formed on FBPs at this load. The deformation reached during the 1st-1% cycle was 1.1% TJD.

The deformation reached during the 1st-2% cycle was 1.7% TJD. The peak load of 42.1 k was recorded at the maximum applied deformation of 2.9% TJD. This load was roughly 3% above that reached during the 2% cycles.

3.3 Comparison of Test Results

The presentation in this section includes a quantitative examination of the data, with emphasis on comparative analyses between tests. Such comparison provides a reliable and convenient means to evaluate significant trends in the data. Except for general behavior, such as load-deformation response, the complex behavior in the specimens precludes reliable interpretation of isolated

pieces of data which cannot be cross referenced and checked with supporting data. In this section eleven categories of data and observations are presented.

3.3.1 Nominal Strengths. Perhaps the most important comparison is that of nominal joint strengths which clearly demonstrate the influence of different joint details and serves as the primary basis for analytic models developed to predict joint strength. In addition to considering the relative strength, three associated topics are addressed: the difference in joint deformation measured by drift versus total joint distortion (TJD); relative contribution of three joint shear mechanisms to the total connection strength; recommendation of a deformation limit for evaluating nominal joint strength based on the load-deformation behavior.

In Table 3.2, joint strengths are summarized in terms of applied ram loads at the noted deformations for Specimens 3 through 17. For Specimens 10 through 17, where cyclic loads were applied, the strengths are based on the failure envelope in the primary direction as shown previously in Fig. 3.2. In Specimens 3 through 9, TJD was not measured directly. The TJD measurement is not dependent on the specimen geometry as is the drift. A more thorough comparison of drift and TJD measurements is described below. In evaluating joint strength the difference between drift and TJD is insignificant in these tests based on data for Specimens 10 through 17. As shown in Table 3.2, the 1% drift loads are within +4% to -4% of the 1% TJD loads, and the 2% drift loads are within +0% to -3% of the 2% TJD loads.

Figure 3.16 shows the superposition of two load-deformation curves where deformation is plotted both for TJD and drift. At low deformations the two measurements agree fairly well, whereas at higher deformations, drift consistently underestimates joint distortion. A comparison of drift and TJD for Specimens 10 through 17 indicates that at 1% TJD drift differs by +12% to -13%, and at 2% TJD by +0% to -23%. A detailed analysis of the difference between drift and TJD is given by Sheikh.[1] Essentially, drift tends to overestimate TJD when member deformations outside the joint are large, and underestimate TJD when shear deformations in the joint region are large. The latter reason

Table 3.2 Summary of Connection Strengths at Given Deformations

Specimen	f'_c (ksi)	Average Ram Load (kips)			
		1% Drift	2% Drift	1% TJD	2% TJD
3 Beam	4.5	16.5	18.0	–	–
4 FBP	4.3	26.6	31.6	–	–
5 FBP (thick)	4.3	28.2	33.5	–	–
6 FBP-DP-Styr.	4.0	35.8	44.5	–	–
7 FBP (wide)	4.0	33.8	40.4	–	–
8 FBP (extended)	3.6	46.2	53.7	–	–
9 FBP (tk)-No Web	3.7	26.2	30.7	–	–
10 FBP (split)	4.7	29.5	35.4	29.0	34.2
11 FBP-DP-Dywi	4.7	45.2	52.5	47.0	52.7
12 Stud	5.0	29.0	34.5	28.7	34.1
13 FBP-Stud	5.0	41.1	48.2	42.8	48.0
14 WSP-Col.	4.0	33.7	38.0	33.8	37.3
15 FBP-Col.	4.0	36.7	43.5	37.0	43.2
16 FBP-Col.-Clip	3.8	38.8	41.1	37.3	41.1
17 FBP-Col.-Dywi	3.9	36.9	41.8	36.8	41.1

explains why drift underestimates TJD at large deformations. The purpose of this discussion is to demonstrate the advantage of calculating TJD directly from member rotations measured adjacent to the joint.

In order to accurately compare the nominal connection strengths, results are normalized to account for different concrete strengths in the specimens. The normalized values reflect loading at 1% TJD and concrete strengths of f'_c equal to 4.0 ksi. Essentially, this normalization consists of four steps. First, the steel panel contribution is subtracted from the total capacity. The steel panel strength is primarily a function of the steel section capacity, and to a lesser degree of the concrete compressive strength. The method of calculating the steel panel strength is outlined in detail in Chapter 4. Second, the remaining joint

Table 3.3 Normalized Joint Strengths

Specimen	Average Ram Load* @ 1% TJD (kips)			
	Total	Steel Panel	Concrete Panel	
			Inner	Outer
3 Beam	16.1	12.6	3.5	0
4 FBP	26.0	12.6	13.4	0
5 FBP (thick)	27.5	12.6	14.9	0
6 FBP-DP-Styr.	35.8	35.8	0	0
7 FBP (wide)	33.8	12.6	14.4	6.8
8 FBP (extended)	48.2	12.6	14.4	21.2
9 FBP (tk)-No Web	27.2	3.2	24.0	0
10 FBP (split)	27.4	12.6	14.8	0
11 FBP-DP-Dywi.	43.5	23.0	14.4	6.1
12 Stud	26.5	12.6	3.5	10.4
13 FBP-Stud	37.3	12.6	14.4	10.3
14 WSP-Col.	33.2	12.6	11.4	9.2
15 FBP-Col.	36.2	12.6	14.4	9.2
16 FBP-Col.-Clip	39.1	12.6	14.4	12.1
17 FBP-Col.-Dywi.	36.8	12.6	14.4	9.8

* Normalized to concrete strength of $f'_c = 4$ ksi.

capacity is allocated to the concrete panel for which strength is presumed to be a function of $\sqrt{f'_c}$. The concrete panel strength is then adjusted accordingly. The third step consists of allocating the concrete capacity between the inner and outer panel. Again, the inner panel consists of concrete between the flanges and within the flange width (Fig. 3.4). Typically, this panel is mobilized by the 8 in. wide FBP. The outer panel consists of remaining concrete in the joint region which is mobilized by such elements as extended or wide FBPs, steel columns, or shear studs. Allocation of strength between the panels is achieved by comparative analysis between test specimens. Finally, the normalized strength components are reassembled and summarized in Table 3.3.

The data in Table 3.3 are also presented in Fig. 3.17 where the joint strengths are expressed as relative percentages. The capacity of Specimen 5 serves as the basis of the comparisons and is set to 100%. Recall that Specimen 5 is the plain steel beam with a standard FBP (7/8 in. thick). The detailing of Specimen 5 is very similar to that of Specimens 4 and 10.

Joint strengths shown in Fig. 3.17 suggest a grouping of the tests into four categories, denoted A through D. Group A consists solely of Specimen 3 which is the plain steel beam detail. The total capacity of this specimen is 59% of Specimen 5. In Specimen 3 roughly 80% of its strength is contributed by the steel panel. Friction between the steel beam and concrete presumably mobilizes the inner concrete panel which accounts for the remaining strength.

Group B consists of Specimens 4, 5, 9, 10 and 12 whose strengths all are approximately equal to that of Specimen 5. Results of Specimens 4, 5, and 10 demonstrate the effectiveness of the standard FBP detail, where the inner concrete panel carries roughly 55% of the total load. As reported by Sheikh, the FBP mobilizes a diagonal compression strut equal in width to the FBP (8 in.) These tests also show that, within reasonable bounds, concrete mobilization inside the beam flange width is insensitive to FBP stiffness; recall that Specimen 4 has full height 3/8 in. FBPs, and Specimen 10 split 3/8 in. FBPs. Specimen 12 does not have FBPs, but instead mobilizes concrete in the outer panel through welded shear studs. In Specimen 12, a small load is also carried by the inner panel similar to Specimen 3. Specimen 9 is the final test in group B. Although, included for completeness in this discussion, the results of Specimen 9 are not used in this paper. As reported by Sheikh, the behavior of Specimen 9 suggests that in the absence of a strong steel panel the concrete compression strut width increases up to 50%. Also, increased strength in Specimen 9 may result from improved concrete quality due to better placement afforded by the large hole in the web. Since this behavior lacks a well founded explanation based on mechanics, the results will be omitted until they are verified by future tests.

Group C includes Specimens 6, 7, 13, 14, 15, 16 and 17 which have strengths ranging from 121% to 142% of Specimen 5. Specimen 7, which utilizes

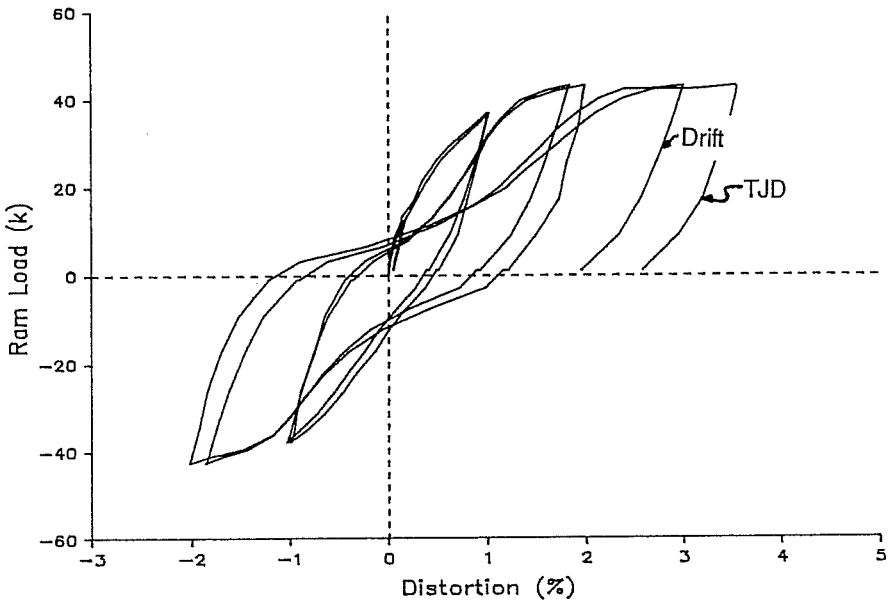

Fig. 3.16 Total Joint Distortion versus Drift (Specimen 15)

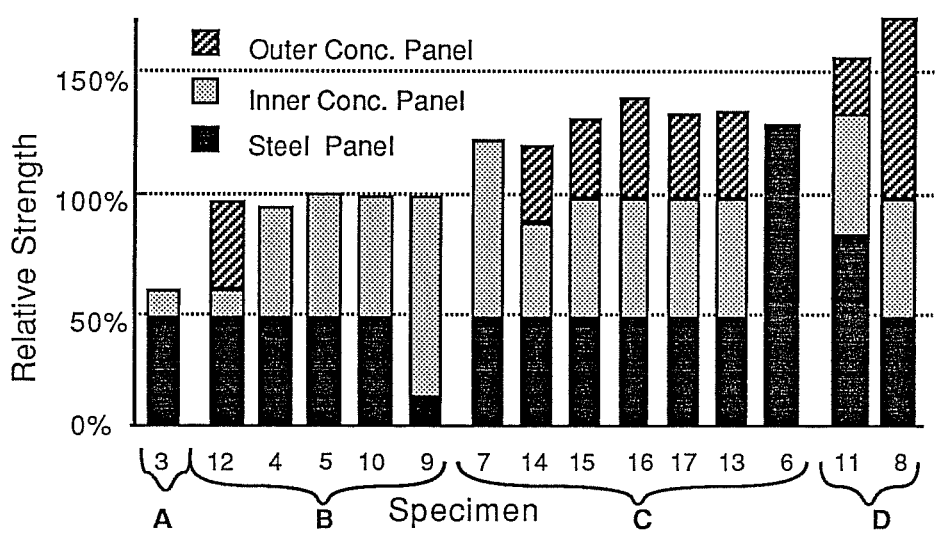

Percentages are relative to the strength of Specimen 5.

Fig. 3.17 Comparison of Normalized Joint Strengths

the 12 in. wide FBP, has a concrete panel strength approximately 42% greater than Specimen 5. As reported by Sheikh, this increase corresponds roughly to the 50% increase in compression strut width, expected from the increased FBP width. The data suggest the strength increase is not directly proportional to the plate width due to flexibility of FBPs wider than the beam flange.

Specimens 14, 15, 16 and 17 all have embedded steel columns and either FBPs or WSPs. In Specimen 15, 35% of the joint shear is carried by the steel panel, 40% by the inner concrete panel (FBP), and 25% by the outer concrete panel (steel column). Comparison of Specimens 14 and 15 reveals that the WSP detail mobilizes the inner concrete panel only 79% as effectively as the FBP. The outer concrete panel of Specimen 16 carries 30% more load than that of Specimen 15, presumably due to the clip angles. In Specimen 17 which has Dywidag bars, the outer panel strength is 7% higher than in Specimen 15. The strength increases in Specimens 16 and 17 over Specimen 15 appear to be the result of enhanced horizontal shear transfer rather than any significant improvement in vertical bearing.

Results for Specimen 13 demonstrate two points. First, the shear studs mobilize the outer concrete panel to a similar degree as the steel column. The outer panel mobilized by the studs in Specimen 13 carries about 12% more load than that mobilized by the steel column of Specimen 15. Second, the outer panel contribution mobilized in Specimen 13 is the same as that of Specimen 12. This demonstrates that within certain bounds the outer panel strength is independent of the inner panel and their respective contributions are additive.

The last specimen in group C, Specimen 6, is designed with a strong web panel to preclude shear failure and to thereby provide a basis for evaluating the crushing strength of concrete under the beam flanges. As such, direct comparisons cannot be drawn with the other specimens. However, it is instructive to note that the maximum load carried by Specimen 6 is exceeded in several specimens which mobilize the outer concrete panel. Concrete bearing failure was not apparent in these specimens as it was in Specimen 6, indicating that the vertical

bearing zone is not confined to the beam flange width for joint shear carried by the outer concrete panel.

Finally, group D includes Specimens 11 and 8 which have strengths equal to 158% and 175% of Specimen 5. Results of Specimen 11 (which incorporates FBPs, web doubler plates, and Dywidag bars) indicate that the Dywidag bars are effective in reinforcing the concrete bearing zone since the total strength exceeds that of Specimen 6 by 22%. Second, shear transfer by the Dywidag bars mobilizes the outer panel to roughly 60% of that afforded by shear studs in Specimens 12 and 13. Finally, as evidenced by comparison of tests 11, 15 and 17, the outer concrete panel strength mobilized by the steel column is not fully additive with that mobilized by the Dywidag bars. Intuitively this is reasonable since the embedded column shadows the shear effect of the Dywidag bars, or vice versa.

Specimen 8 is an important test since with very stiff extended FBPs it provides an upper bound on the outer panel strength which can be mobilized. In this specimen, relative contributions of the steel panel, inner concrete panel, and outer concrete panel to the total are 26%, 30% and 44%. Compared with Specimen 8, Specimens 13 and 15 show that shear studs and the steel column mobilize 48% and 43% (respectively) of the maximum available outer panel strength.

Finally, a reasonable limit on joint distortion for determining the nominal design strength is evaluated on the basis of load-deformation data. Previously, Sheikh has proposed 2.0% TJD as a deformation limit. A lower limit of 1.0% TJD is preferable in part based on the reasoning outlined below.

From the average specimen response, the load- deformation envelope is idealized by the tri-linear plot shown in Fig. 3.18. As indicated in the figure, doubling the joint distortion from 1% to 2% TJD results in only a modest strength gain of 15%. Additionally, if service load is considered at one half of ultimate load, the service distortion increases proportionally faster than the strength gain between 1% and 2% TJD. A design strength at 1% TJD results in service deformation of roughly 0.2%, whereas the strength at 2% TJD results in service deformations of 0.25%. Thus, for a strength increase of 15%, service deformations would increase approximately 25%.

3.3.2 Cyclic Load Behavior. The cyclic load response provides a measure of joint toughness when subjected to large inelastic deformations. Toughness is an important and sometimes overlooked aspect of structural reliability. Assessment of the cyclic response also addresses special concerns raised when the composite connection is used in structures designed for seismic loading.

The loss in strength due to reverse cyclic loading, which was similar in all the specimens, is measured from the load-deformation response. After loading through the 1st-1% cycle, the average load carried at 1% TJD was 89% of the initial strength at that deformation, and after the 2nd-1% cycle was 83% of the initial strength. Similarly, after the two additional 2% cycles, the average load was 86% and 79% (respectively) of the initial strength at 2% TJD. The modest strength loss under cyclic loading is comparable to response in well detailed reinforced concrete elements.[12]

A second measure of the cyclic behavior is the energy dissipated by hysteretic response of the joint. Hysteretic response is based on an equivalent viscous damping coefficient calculated from the area within the load-deformation curve. In Figure 3.19, calculation of the damping coefficient is described. This coefficient is the ratio of equivalent viscous damping to the critical viscous damping of the system. Clough and Penzien[13] present a derivation of this coefficient.

The average damping coefficient for all the specimens is 0.18, with values ranging from 0.15 in Specimen 15 to 0.23 in Specimen 12. These values are based on the average of the coefficients calculated for each cycle of loading.

While a rigorous appraisal of the damping coefficients is beyond the scope of this report, a comparison is made with similar values reported for reinforced concrete connections. In one study of seismic response of reinforced concrete joints, Kitayama (et.al.)[14] performed several analyses using a computer model which incorporated inelastic joint elements. In this study, joint damping coefficients of 0.10 to 0.25 were used. The 0.25 value corresponded to a well detailed joint with superior energy dissipation capability, evidenced by a wide spindle shaped load- deformation curve. According to the report, a joint detailed based on current seismic design standards would have a coefficient of 0.15. In

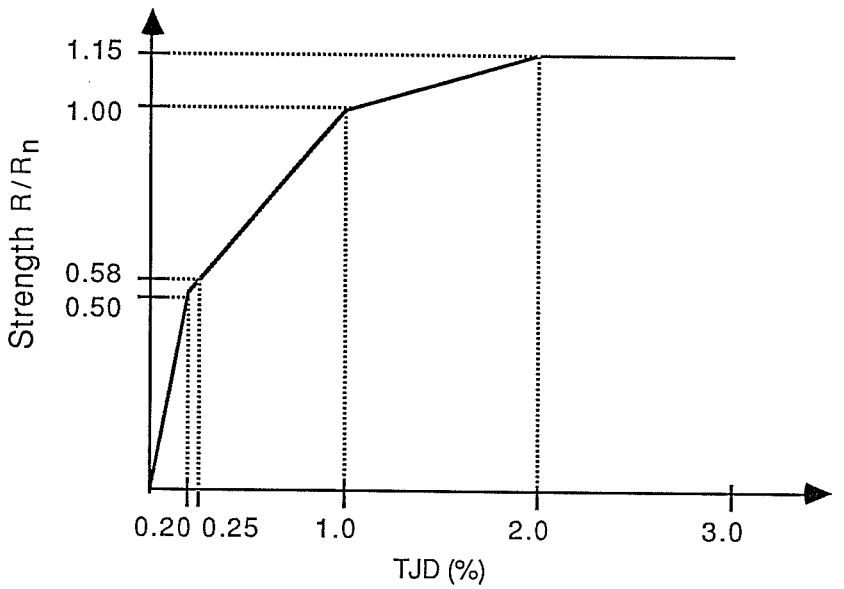

Fig. 3.18 Idealized Monotonic Joint Response

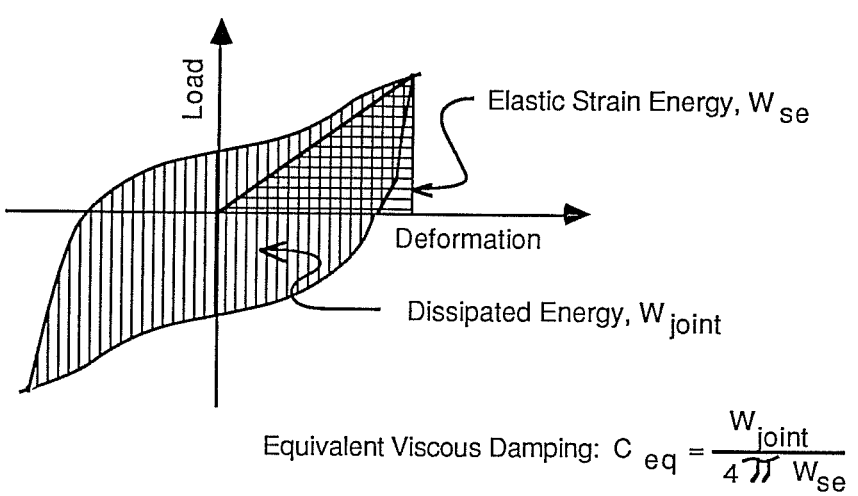

Fig. 3.19 Equivalent Viscous Damping

terms of the effect on overall behavior of structural systems, distinction between damping coefficients is minor as Kitayama reported,

> From the results of earthquake response analyses, the effect of hysteresis energy dissipating capacity on the response was found relatively small for a range of equivalent viscous damping ratios from 0.10 to 0.25 at ductility factor 4.0.

Based on this information the hysteretic response of the composite connection is comparable to that of well detailed reinforce concrete beam-column joints.

3.3.3 Components of Joint Distortion. The total joint distortion (TJD) consists of the following three components: concrete panel shear (CPS), local flange bearing (LFB), and steel panel shear (SPS). Detailed description of these modes and how they were measured is provided in Chapter 2; brief definitions are repeated here for convenience. Concrete panel shear is a measure of shear distortion of the concrete joint panel near the face of the column. Local flange bearing is a measure of relative rigid body rotation of the beam and column. This mode results primarily from high concrete strains beneath the compression flanges. Finally, steel panel shear is a measure of shear distortion of the steel panel in excess of the concrete panel shear. As noted previously, SPS is determined indirectly as the difference in measured distortion between TJD and the sum of CPS and LFB.

Component distortions are superimposed on TJD for Specimen 12 in Figs. 3.20a to c. The response shown is typical of that for Specimens 10 through 17. In the case shown, Specimen 12, SPS behavior is the most interesting. During the first loading cycle, SPS increased sharply at 21 k, indicating web yielding. Qualitative observations such as this have already been discussed in the test summaries.

Table 3.4 provides a summary of the distortion data, indicating relative percentages of each component, measured at the peak loads during the 1st-1% and 1st-2% cycles. Figures 3.20a to 3.20c indicate how the percentages are obtained from the load-deformation plots. As seen in Table 3.4, relative

Table 3.4 Components of Joint Distortion

Specimen	Percentage of TJD*					
	@ 1% TJD			@ 2% TJD		
	CPS	LFB	SPS	CPS	LFB	SPS
10	18	27	55	15	32	53
11*	34(43)	45(31)	21(26)	30(38)	47(33)	23(29)
12	25	27	48	22	24	54
13	39	46	15	33	41	26
14	41	39	20	46	33	21
15	39	41	20	40	41	19
16	36	39	25	52	33	15
17	47	29	24	56	28	16

* Normalized values in parenthesis ( ).

proportions of the component deformations did not vary significantly between 1% and 2% TJD. The table includes two sets of values for Specimen 11. The set in parenthesis is normalized to account for the thickened steel web of Specimen 11. The modified values for Specimen 11 reflect response of a similar specimen with a typical web thickness. The adjusted values are more useful for comparisons with other specimens, and are the values presented in Fig. 3.21 noted below.

The average of the values from Table 3.4 are presented graphically in Fig. 3.21 where several trends are apparent. First, Specimens 10 and 12 showed significantly larger SPS than the other specimens. Typical SPS was roughly 20% of the total, whereas in Specimens 10 and 12 SPS accounted for approximately 50%. As noted previously, Specimens 10 and 12 were different from the other specimens in that they had only one mechanism by which to mobilize the concrete shear panel. In Specimen 10, increased SPS was offset primarily by lower CPS. This behavior supports evidence that the FBP mobilizes only the inner concrete panel. Specimen 12, on the other hand, had excess SPS offset by equal reductions in both CPS and LFB. Finally, the other Specimens

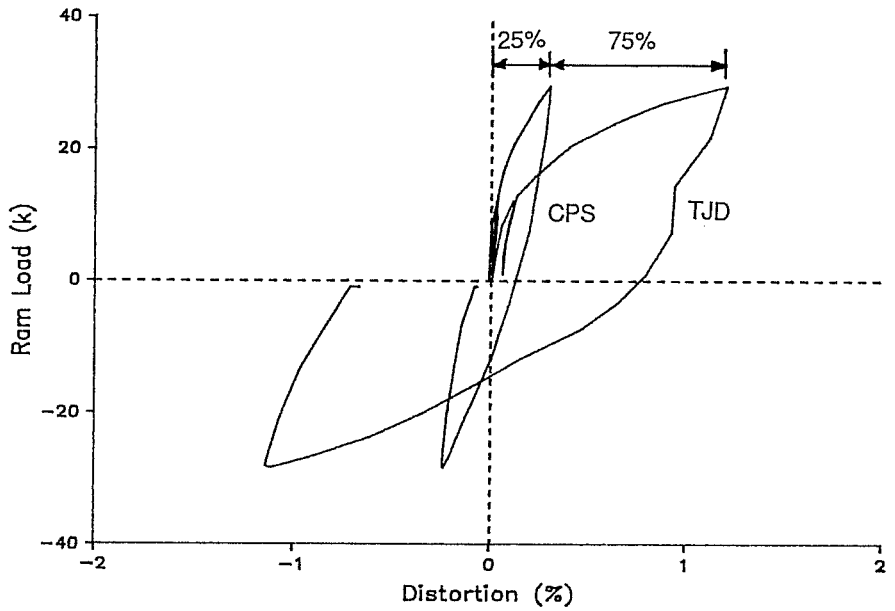

Fig. 3.20a Concrete Panel Shear (Specimen 12)

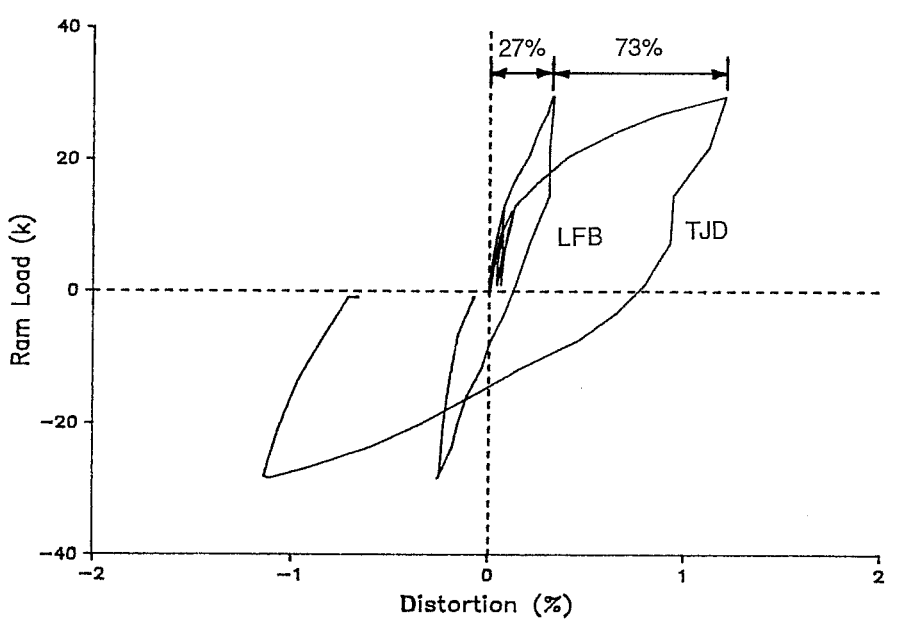

Fig. 3.20b Local Flange Bearing (Specimen 12)

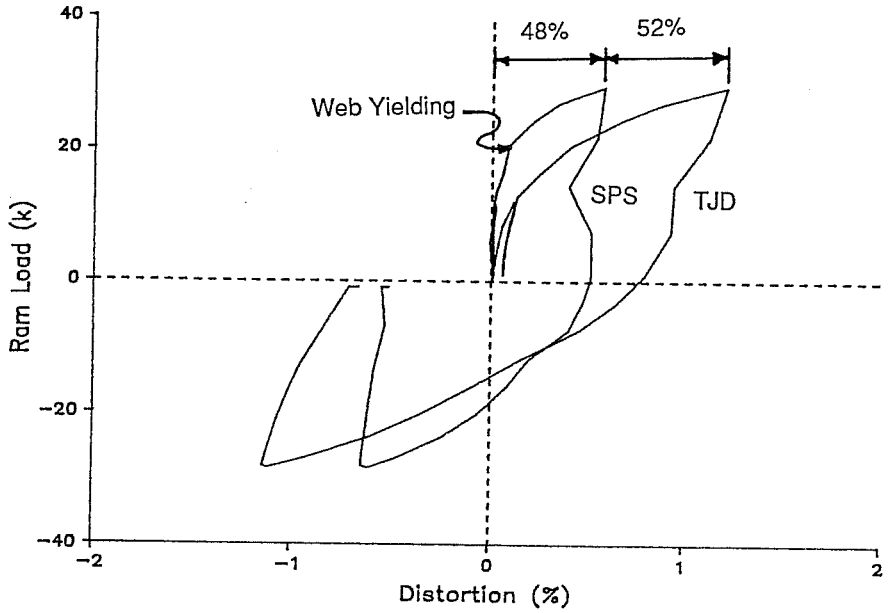

Fig. 3.20c Steel Panel Shear (Specimen 12)

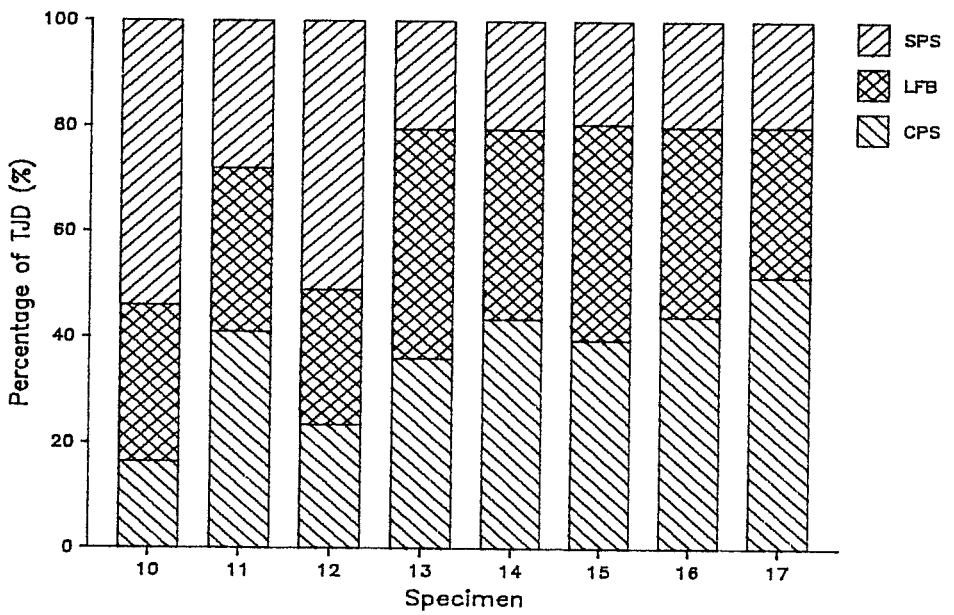

Fig. 3.21 Components of Joint Distortion

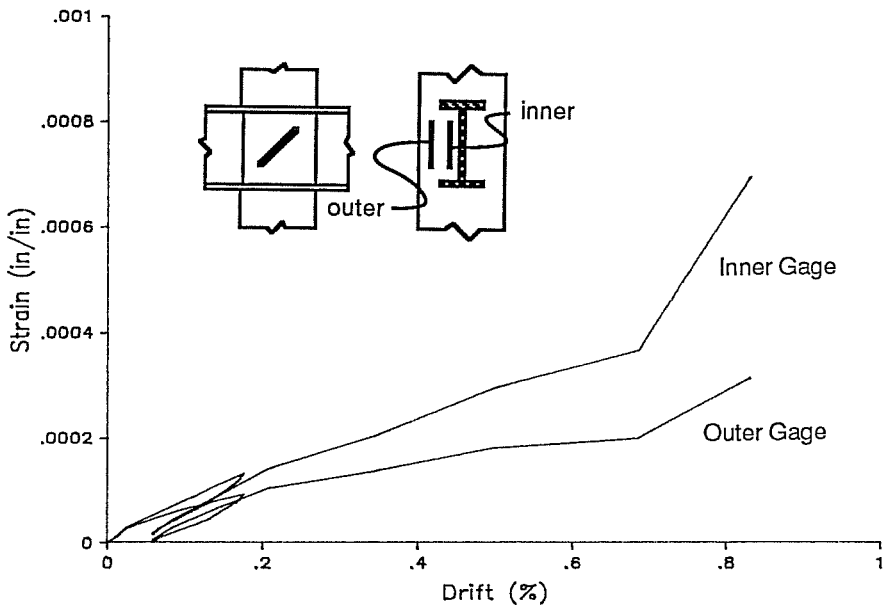

Fig. 3.22 Diagonal Strut Compressive Strains

showed more balanced behavior with the following relative distortions: CPS, 40%; LFB, 40%; and SPS, 20%.

3.3.4 Concrete Embedment Gages. Diagonal compression strain in the concrete indicating relative mobilization of the concrete panels was measured by embedment strain gages (Fig. 3.10a). Useful data from these gages was obtained during the primary direction of the 1st-1% cycle. Once loading was reversed and cracks formed perpendicular to the gages, subsequent strain data was not reliable.

In Fig. 3.22, the typical embedment strain gage response for Specimen 10 is shown. In general, strain mobilization was linearly related to overall joint deformation except at isolated points where discontinuities occurred. For example, in Specimen 10 the sharp increase in strain rate at 0.7% drift coincided with yielding of the steel web.

In Fig. 3.23a and 3.23b, embedment gage data from all the specimens are summarized. The figures show cumulative concrete strains at given deformations to demonstrate relative compression strut mobilization between specimens. The inner strain gage data reveals that in general all specimens with FBPs developed similar concrete strains with an average strain of 0.001 in./in. at 0.8% drift. Without benefit of FBPs, in Specimen 12 the strain at 0.8% drift was only 1/4 of that for specimens with FBPs.

The outer strain gage data is less conclusive than the inner gage data. Contrary to evidence provided by cracking patterns and joint distortion data, the outer gages of Specimens 10 and 12 showed roughly equal strains. Slightly larger strains in Specimens 13, 14 and 15 substantiate other evidence of increased outer concrete panel mobilization in these specimens. Increased scatter in the outer gage data may be due to the more random formation of cracks in the outer panel than in the inner panel. This occurs because joint shear in the outer panel was carried by a compression field (truss) mechanism where diagonal compression struts are not as well defined as in the inner panel where a single strut forms.

3.3.5 Longitudinal Flange Stresses. Strain gages on the beam flanges (Fig. 3.24) measured dissipation of flange force through the joint. With equal but opposite beam moments oriented as shown in Fig. 3.24, flange stress varied from tension on the left to an equal magnitude of compression on the right. The nature of stress dissipation indicates the influence of various joint shear mechanisms. For example, the steel web dissipates flange stress uniformly across the joint, whereas FBPs provide a concentrated reduction at the column face.

In Figs. 3.25a to c, flange stresses are plotted for Specimens 10, 12 and 13 at the noted ram loads. In these figures, the horizontal axis indicates the distance from the column center line, oriented with tension in the left flange and compression in the right. At 5 k the stress distribution was similar in all three specimens since the adhesive bond between the steel and concrete still transferred most of the load. At higher loads influence of the particular joint detailing becomes apparent. For example, Specimen 10 showed the highest rate

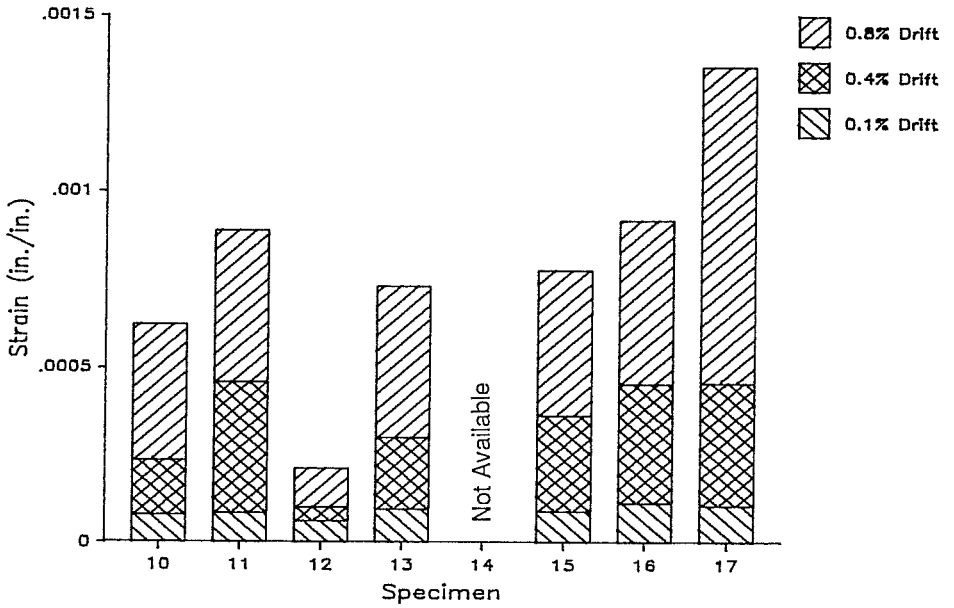

Fig. 3.23a Inner Strut Compressive Strains

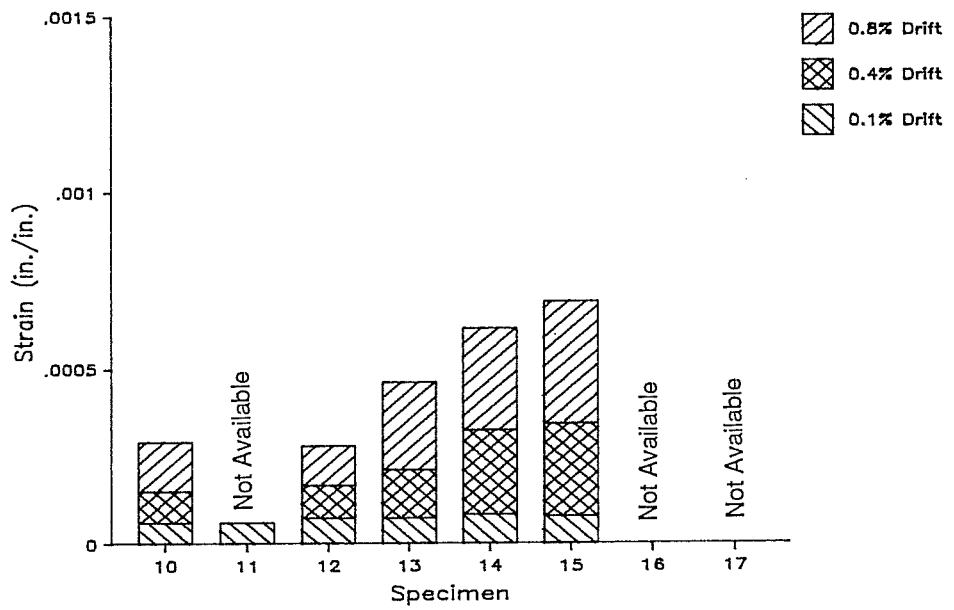

Fig. 3.23b Outer Strut Compressive Strains

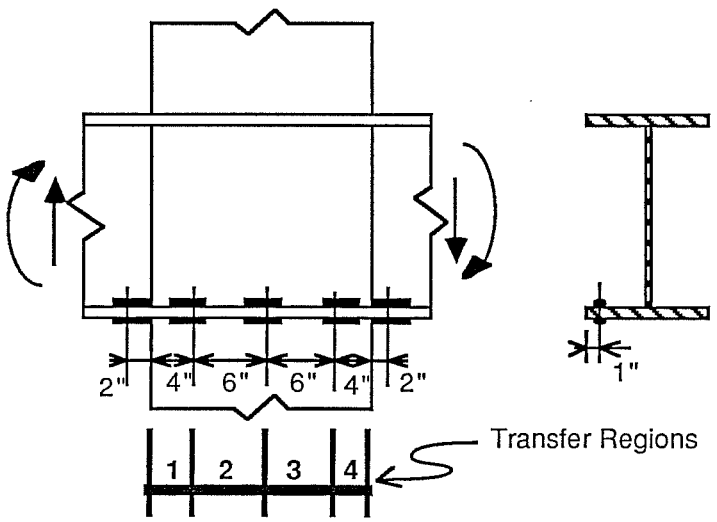

Fig. 3.24 Strain Gage Locations on Beam Flange

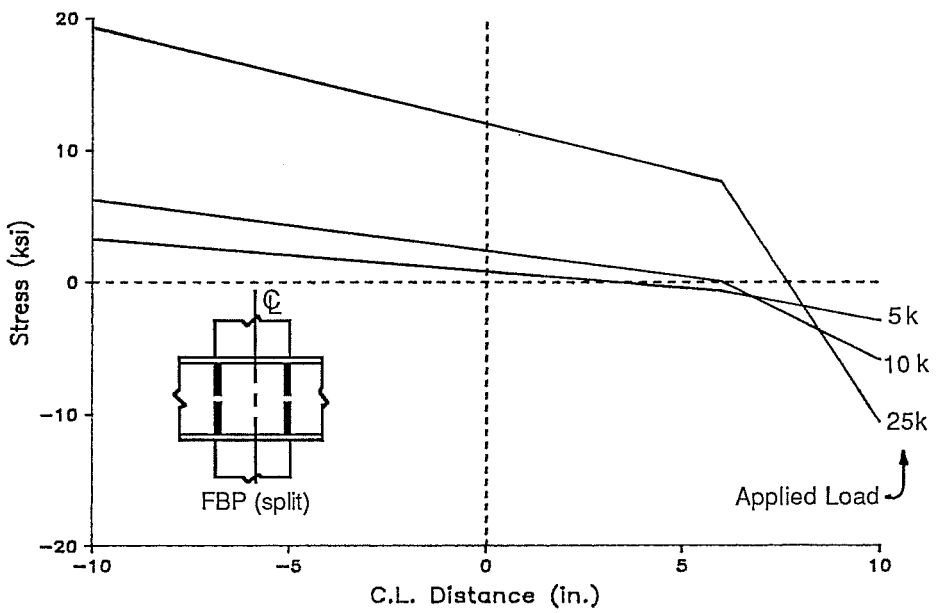

Fig. 3.25a Longitudinal Flange Stress (Specimen 10)

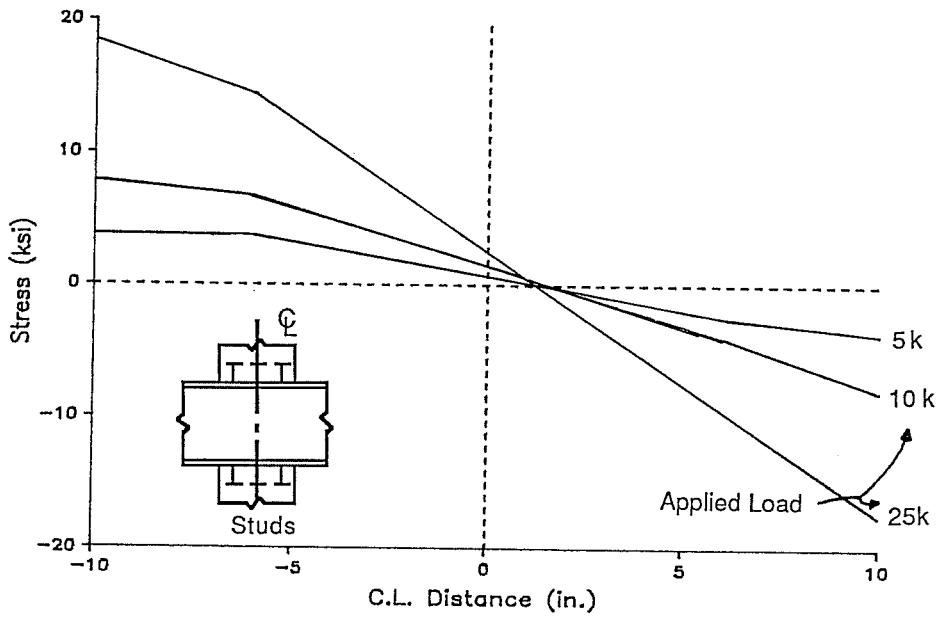

Fig. 3.25b Longitudinal Flange Stress (Specimen 12)

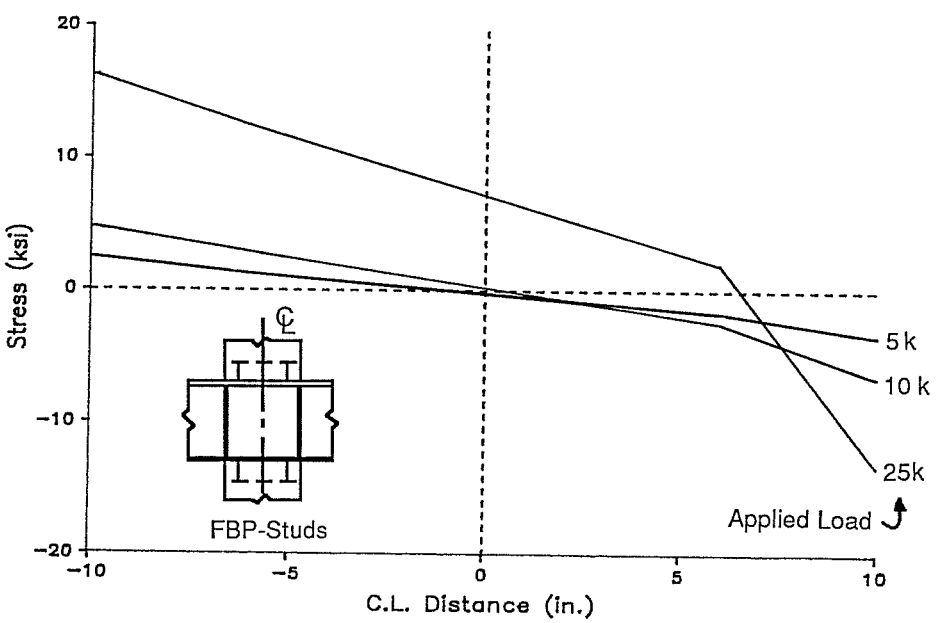

Fig. 3.25c Longitudinal Flange Stress (Specimen 13)

of transfer near the compression face due to the FBP. Specimen 12, on the other hand, displayed a fairly uniform transfer due to the steel panel and shear stud mechanisms. In Specimen 12, the slope near the tension flange is slightly less that the overall slope. Presumably, this occurs because force transferred by studs in the first row is limited by the concrete cover. Finally, as shown in Fig. 3.25c, Specimen 13 exhibited a stress gradient between that of Specimens 10 and 12. This behavior is expected since Specimen 13 utilizes both the FBP and shear studs in addition to the steel web.

A summary of the flange stress data is presented in Table 3.5a for Specimens 10 through 17, where stress dissipation gradients are given for the regions noted (see Fig. 3.24). The stress dissipation gradient indicates the axial stress dissipated per inch of length along the flange. The gradient is expressed as a percentage of the absolute difference in axial flange stress measured just outside the column. For example, the gradients for Specimen 10 are related to 100% of the dissipated stress as follows:

$$2.50\% \ (4 + 6 + 6 \text{ in.}) + 15\% \ (4 \text{ in.}) = 100\% \ (\text{over } 20 \text{ in.})$$

As expected, in specimens with FBPs, the gradients are largest in region 4. Gradients in Table 3.5a are based on stresses measured in each specimen at the maximum load reached during the 1st-1% cycle.

Relative contributions of the shear transfer mechanisms are calculated using the gradients from Table 3.5a. Relative contributions are obtained separately for each specimen by comparing the gradient in all four regions, and allocating portions of the transfer to shear mechanisms based on assumed behavior. For example, in region 1, adjacent to the tension flange, only the web mechanism transfers load and the gradient in that region is used to calculate the web contribution across the entire joint. In Specimen 10, for example, the web is calculated to transfer 50% (2.5 x 20 in.) of the axial load out of the flange.

In Table 3.5b, calculated allocations based on the flange gage data (transfer gradients) are compared with those previously determined from the nominal joint strengths. The latter is shown in parenthesis in the table. In

Table 3.5a Summary of Relative Flange Stress Dissipation (@ 1% TJD)

Specimen	Stress Transfer Gradients (% of total/in.)*			
	Region 1 (4 in.)	Region 2 (6 in.)	Region 3 (6 in.)	Region 4 (4 in.)
10	2.50	2.50	2.50	15.00
11	3.50	3.50	3.17	11.50
12	2.50	5.33	5.33	6.50
13	2.50	3.50	3.50	12.00
14	1.00	6.83	6.83	3.50
15	2.00	4.50	4.50	9.50
16	1.75	4.33	4.33	10.25
17	1.50	4.17	4.17	11.00

* Transfer regions shown in Fig. 3.24

Table 3.5b Comparison of Strength Allocation

Specimen	Percentage of Total Capacity*			
	Web	Studs	FBP, Dywi, Clip	Col., WSP
10	50(46)	–	50(54)	–
11	70(53)	–	30(47)	–
12	50(48)	50(52)	–	–
13	50(34)	13(27)	37(39)	–
14	30(38)	–	–	70(62)
15	40(35)	–	30(25)	30(40)
16	35(32)	–	34(31)	31(37)
17	30(34)	–	37(27)	33(39)

* First value based on flange gage data.
Value in parenthesis ( ) based on nominal joint strength data.

general, the two methods indicate similar trends although in some cases the percentages differ considerably. In Specimen 13, allocations between the web and studs vary significantly between methods, however, the distinction between the studs and web is difficult to distinguish using the flange gage data. Note that the sum of these values agree very well. Presumably, the nominal strength data are more reliable than the strain gage data, as the latter may contain error due to local effects which distort the measurements. However, overall agreement of the results supports general qualitative assumptions regarding the mechanisms controlling behavior.

3.3.6 Column Bar Stresses. Strain gages on the vertical bars provide measurement of the change in bar stress through the joint. This change results from vertical joint shear transferred via bond stress into the bars. Engineers have long recognized that in reinforced concrete beam-column joints high bond stress demand in the joint usually exceeds bond capacity. As a result, longitudinal bars passing through a joint have stresses quite different from those predicted by classical analysis of beam and column sections adjacent to the joint.[9]

In Fig. 3.26a, stresses for a corner bar in Specimen 11 are shown. Also shown, are theoretical stresses based on a cracked section analysis of the column adjacent to the joint. For Specimen 11 the theoretical calculation includes the Dywidag bars as longitudinal column reinforcement. In general, the tension stress increase was fairly constant, although as seen in the figure, the measured stress was less than that calculated. The stress may have been lower due to the following: unequal distribution of tension loads between all vertical column (and Dywidag) bars, errors in measurement of axial stress due to bar bending, and the influence of tension carried by the concrete.

Unlike tension stress, the compressive stress response was not constant, and typically dropped sharply as seen the figure. Evidence suggests that this drop in stress was due to cracking in the concrete which reduced transfer of joint shear forces to concrete in the vicinity of the column bars. This phenomenon was discussed previously with regard to the cracking pattern shown in Fig. 3.4.

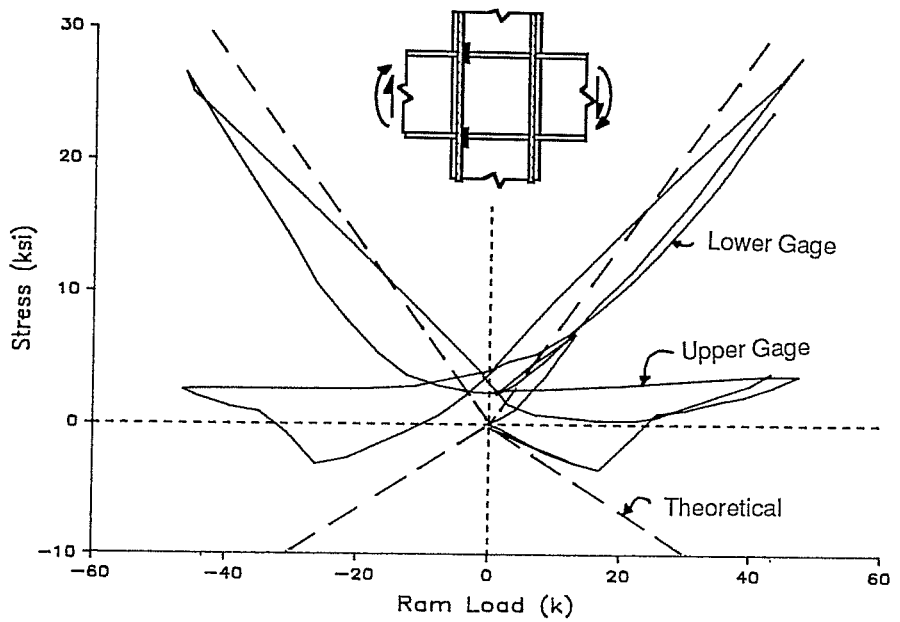

Fig. 3.26a Column Bar Axial Stress (Specimen 11)

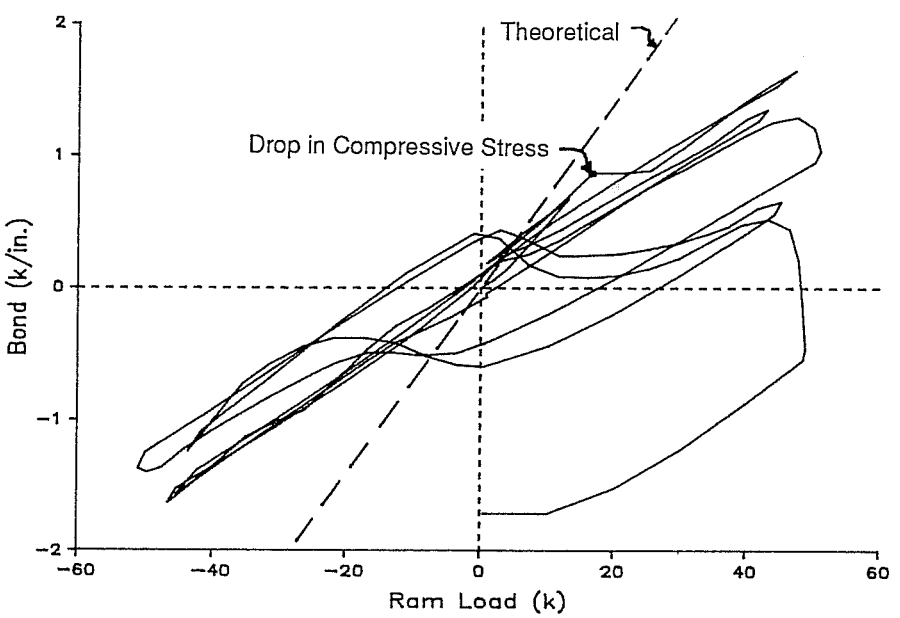

Fig. 3.26b Column Bar Bond Transfer (Specimen 11)

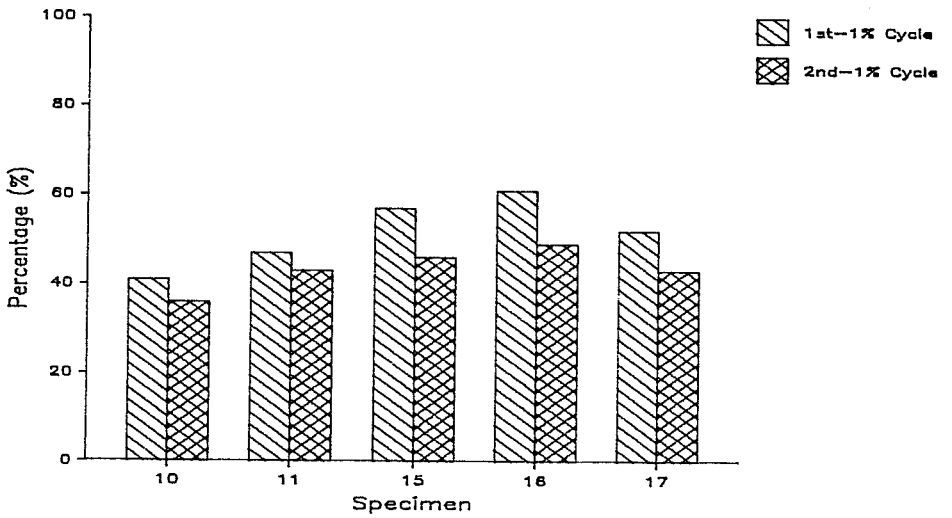

* Percentage of measured bond relative to theoretical bond calculated according to bending theory.

Fig. 3.27 Column Bar Bond Transfer - Summary

Evidence presented below also suggests that, unlike in reinforced concrete joints, this drop was not due to local bond failure around the bars.

In Fig. 3.26b, a plot of the bond transfer is shown based on the measured change in bar stress for Specimen 11. As shown, at the point where compressive stress dropped, the bond temporarily dropped, but then continued increasing with subsequent loading. This continued increase indicates that bond capacity had not been exhausted when the compressive stresses dropped. Also shown in the figure is the bond calculated according to the theoretical bar stresses shown previously in Fig. 3.26a.

In Fig. 3.27, bond transfer recorded at 30 k is summarized for tests 10, 11, 15, 16 and 17, as a percentage of the theoretical bond prediction. Data is not provided for Specimens 12, 13 and 14 as strain gages malfunctioned in these tests. As seen in Fig. 3.27, bond transfer during the 1st-1% cycle was roughly

50% of that predicted by classical bending theory. Also, bond in 11 and 17 was slightly less than that in 15 and 16. This reflects the fact that the Dywidag bars in Specimens 11 and 17 carried a larger portion of the column moment than predicted by bending theory. The low bond for Specimen 10, compared to 15 and 16, provides additional evidence of the outer concrete panel mobilization in specimens with steel columns. Finally, Fig. 3.27 also indicates that the bond drops off slightly during subsequent cycles.

3.3.7 Dywidag Bar Stresses. Stresses measured in the Dywidag bars substantiate their role in transferring both vertical force and horizontal shear between the beam and column. The stresses also provide information regarding bond transfer along the Dywidag bars, and confirmation of coupler weld fractures in Specimen 11.

Typical plots of the axial stress versus load for Dywidag bars in Specimens 11 and 17 are shown in Figs. 3.28a and b. Axial stresses were measured by a pair of gages located 4 in. from the beam flange, just beyond the threaded coupler. Dashed lines in the figures indicate the theoretical bar stresses calculated by bending theory, treating the Dywidags as typical longitudinal column reinforcement.

In both Specimen 11 and 17, tension and compression stresses exceeded the theoretical stresses through most of the test. An exception to this occurred during initial loading when, before concrete cracking, the tension stresses were less than predicted. Dywidag bars carried higher loads than predicted because of their direct attachment to the beam. Unlike the longitudinal column reinforcement, load transferred into the Dywidag bars was not reduced by concrete cracking. Upon repeated loading, Dywidag bars picked up proportionally higher load as cracking deteriorated bond transfer to the other column reinforcement.

Dywidag tensile stresses in Specimen 11 were roughly 10% to 15% higher than in Specimen 17. Presumably this was due to additional strength and stiffness of the steel panel provided by web doubler plates in Specimen 11. The difference in stress was not, however, directly proportional to the increase in web thickness.

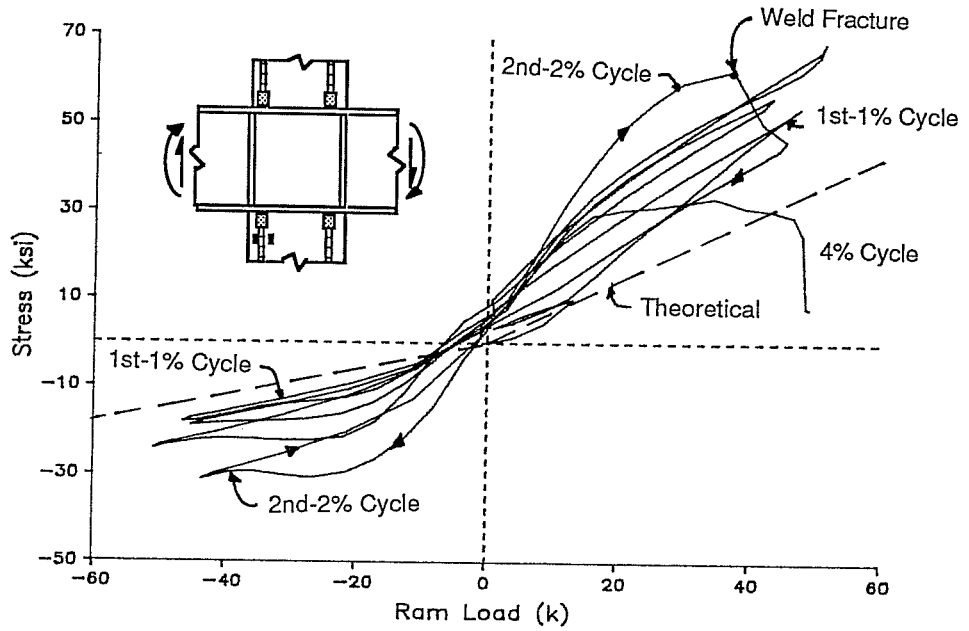

Fig. 3.28a Dywidag Bar Axial Stress (Specimen 11)

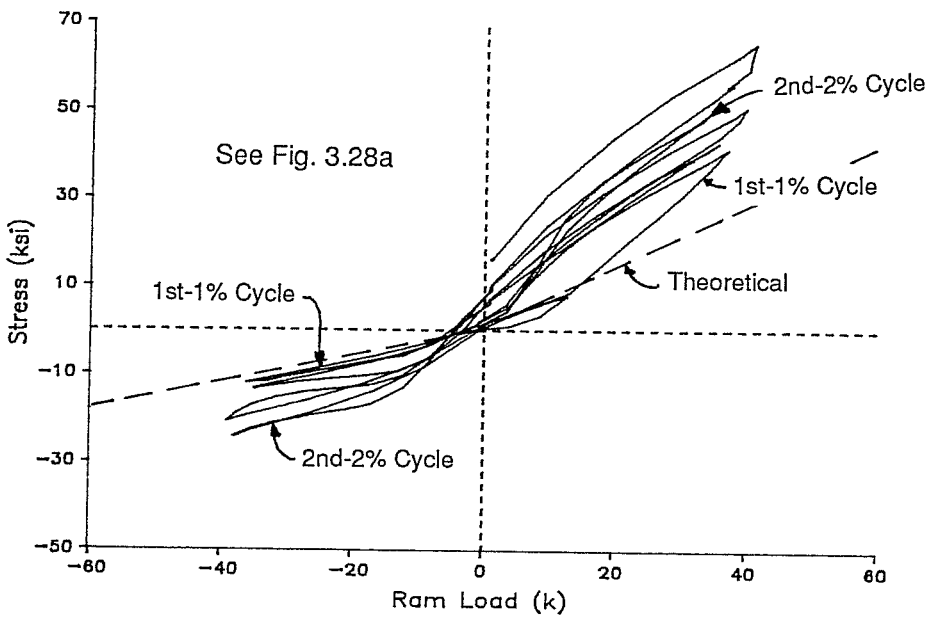

Fig. 3.28b Dywidag Bar Axial Stress (Specimen 17)

The plot in Fig. 3.28a indicates the point at which fracture of the coupler weld occurred in Specimen 11. As seen in the figure, for this bar the weld began to fracture near the peak of the 2nd-2% cycle and completely fractured during the subsequent 4% cycle. As noted previously, data from this and other bars confirm that the welds were intact well into the 2% cycles.

During the first cycle, compressive stresses closely followed those predicted by theory. In subsequent cycles, at low load levels stresses increased faster than predicted. This increase occurred while gaps adjacent to the beam were closing. Recall that these gaps formed during previous loading in the opposite direction. Once the gaps closed, concrete in the bearing zone again picked up load and the slope of the stress plot returned to the predicted slope. Finally, the bars attached to the bottom of the beam picked up slightly higher compressive stresses than bars attached to the top. This may be due to inferior quality of the concrete cast against an upper surface, in this case the bottom of the lower beam flange. Therefore, concrete above the beam is more effective in bearing than that below the beam.

In Fig. 3.29, axial stresses along the length are shown for one bar in Specimen 11. This bar had the highest recorded stresses of all the Dywidag bars. Stresses are shown in the figure at various load stages: first at 30 k, and then at peak loads of subsequent cycles. As seen in the figure, at high load there was no bond transfer over roughly the first 12 in. of bar length. This observation inspired the design recommendation given in Chapter 5 to discount a certain distance in determining development lengths for such bars. The peak bond transfer of 2.34 k/in. shown in Fig. 3.29 exceeds by 10% the ultimate bond specified by ACI-318.[15]

Pairs of strain gages at the base of the Dywidag bars indicated that bending stresses in Specimen 17 were roughly 2/3 of those in Specimen 11. The difference in bending reflects the idea that in Specimen 17 shear carried by the Dywidag bars was shared with the embedded steel column, whereas in Specimen 11 the column was not present. Bending stresses in Specimen 11 ranged up to

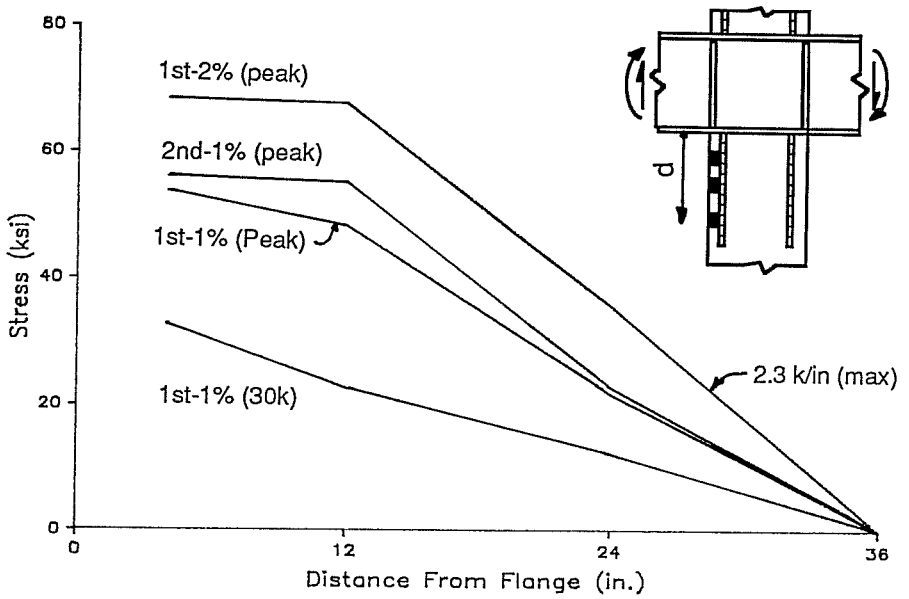

Fig. 3.29 Axial Stress Along Dywidag Bar (Specimen 11)

30 ksi during the 1% cycles, indicating the significant degree to which these bars are mobilized for shear transfer.

3.3.8 Steel Column Stresses. Stresses measured by the two cross gages on the steel column provide understanding of the horizontal shear transferred by the column. The plots in Figs. 3.30a and b show the transverse flange bending and major axis bending for the steel column in Specimen 17. These data are representative of the other three specimens with embedded steel columns.

Transverse bending shown in Fig. 3.30a indicates that the back flange carried most of the horizontal concrete bearing. As shown, this behavior holds for loading in both the primary and reverse directions. Note that the terms "back flange" and "forward flange" are defined by the loading direction. Figure 3.30a also shows that through the 1st-1% cycle, transverse bending stress in the back flange increased uniformly. During subsequent cycles, which for clarity are

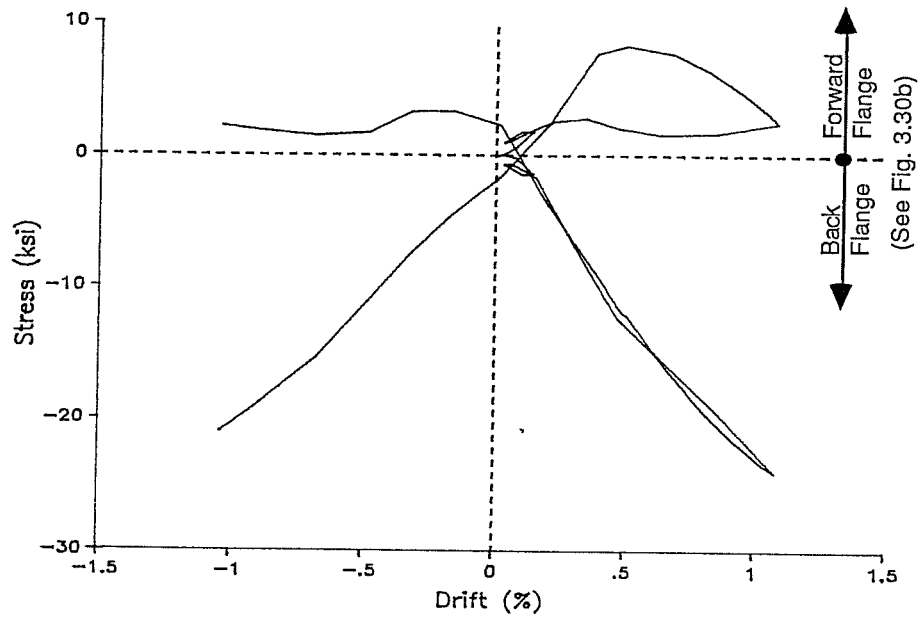

Fig. 3.30a Steel Column - Transverse Flange Bending (Specimen 17)

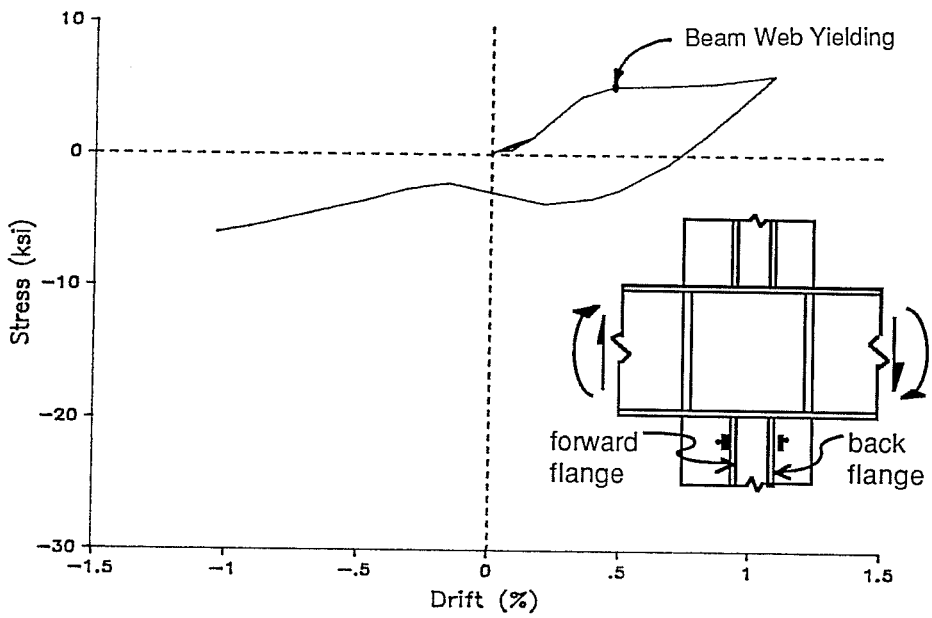

Fig. 3.30b Steel Column - Major Axis Bending (Specimen 17)

not shown, the stress dropped off, presumably due to increased cracking of the concrete. In Specimen 17, during cyclic loading, stress at 1% TJD dropped to 85%, 70% and 30% of that recorded during the initial cycle. In Specimens 14 and 15, the drop in stress was less pronounced, perhaps because in 14 and 15 there were no other structural steel attachments to the beam flanges. In Specimen 16, the drop in stress was larger than in Specimen 17. This may be due to the tendency in Specimen 16 for load to shift from the steel column to the clip angle during later cycles.

Shown in Fig. 3.30b, the plot of major axis bending stress demonstrates that the bending moment contribution of the steel column to the overall composite column was negligible. Also, as shown the bending stress in the steel column ceased to increase after the beam web yielded. The column bending stress at this point was 5.3 ksi. Assuming the bottom column response was indicative of the top column, the column moment based on the stress of 5.3 ksi corresponded to an equivalent ram load of approximately 0.6 k. Since the strength of Specimen 17 was 36.8 k, this confirms that major axis bending was important only insofar as its role in transferring horizontal load into the concrete. Of course, where the steel column size is increased relative to the concrete column, its function in primary bending will be greater.

3.3.9 Face Bearing Plate Stresses. The strain gages installed on the face bearing plates (FBP) measure both axial and bending stress in the plates. The response for Specimen 15 which was fairly typical of all the specimens is shown in Figs. 3.31a and b. As seen in Fig. 3.31a, participation of the FBP increased significantly when diagonal and horizontal cracks opened in the joint. The increased plate mobilization suggests loss of adhesive bond between the steel and concrete as the diagonal compression strut bears on the FBP. Note that the axial stresses in Fig. 3.31b did not show such an abrupt change in behavior.

In the reverse loading direction the stress response was fairly flat, indicating that only the corner of the FBP near the compression beam flange participated in forming the concrete strut. This demonstrates why the split FBP in Specimen 10 had a negligible influence on behavior, compared to specimens

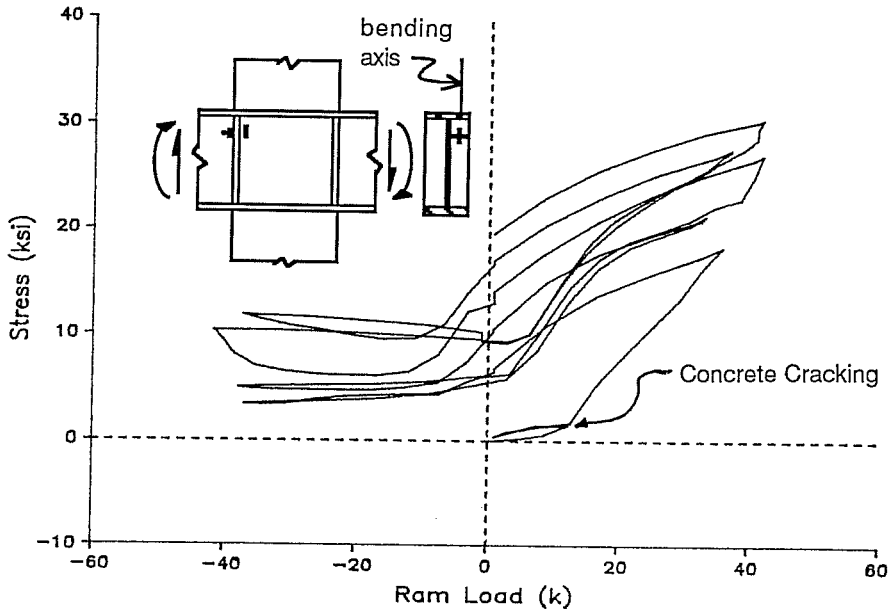

Fig. 3.31a FBP Bending Stress (Specimen 15)

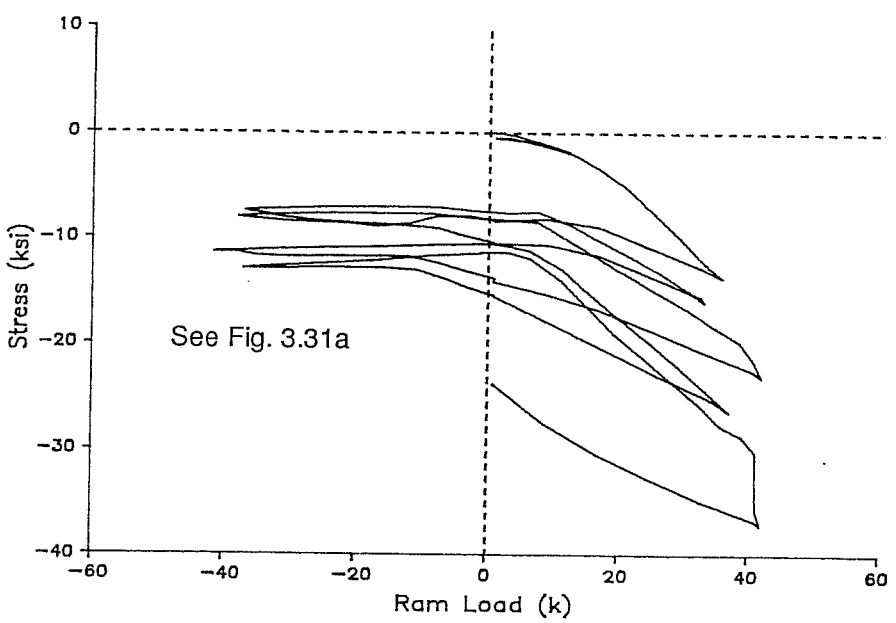

Fig. 3.31b FBP Axial Stress (Specimen 15)

with full FBPs. The strain gages did indicate, however, slightly higher bending and axial stresses in the split FBP than in the full height FBP.

3.3.10 Column Tie Stresses. Stresses in the reinforcing bar ties indicate relative participation of these ties. The response of the tie gages, T1, T6 and T9, were representative of that for all the gage data collected. As shown in Figs. 3.32a, and 3.33a gages T1 and T6 were located in the outer concrete panel with T1 within the beam depth and T6 above the beam. As shown in Fig. 3.34a, gage T9 was located in the concrete bearing region above the beam.

In general, tie data is not as conclusive as other strain gage data for two reasons. First, as the gages measured local strains, the readings were quite sensitive to crack locations. The gage data may not, therefore, be an accurate measure of the overall behavior. Second, the axial stress readings inferred from the gages may be distorted by unaccounted bending stress. In some specimens, gages were installed in pairs in order to measure the error introduced by bending. The paired gages showed an average error in the axial stress reading of $\pm 13\%$ with extremes to $\pm 28\%$.

In spite of the lack of precision, gage data do indicate several consistent trends. First, bar stresses (strains) were more directly a function of joint deformation rather than applied load. This is evident since plots of stress versus deformation yield more consistent linear behavior than stress versus load. Also, where the stress reached and exceeded the yield stress of the bars, typically, no change in the stress behavior was noted. An important question raised by this behavior is whether ties play a significant role in joint response, or whether the tie forces have little influence on the internal load mechanisms. Unfortunately, these results alone do not provide a definitive answer to this question.

The stress versus drift responses for gages T1, T6 and T9 are presented from Specimens 10 and 14 in Figs. 3.32a through 3.34b. The plots indicate that tie participation depends on the extent of concrete panel mobilization in different specimens. For example, as shown in Figs. 3.32a and b and 3.33a and b, participation for ties T1 and T6 was greater in Specimen 14 (WSP-Column) than in Specimen 10 (split FBP). During the 1st-1% cycle, participation of T1 in

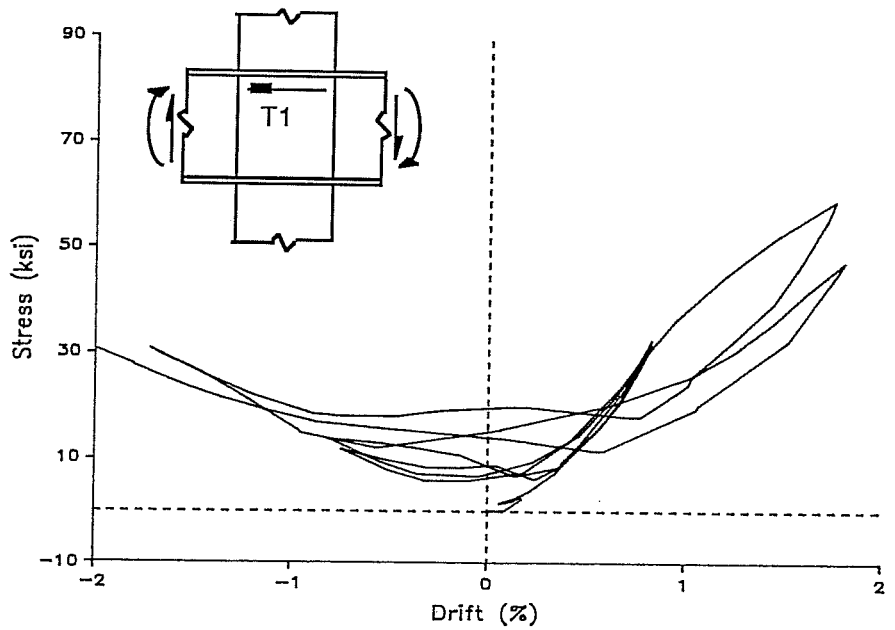

Fig. 3.32a Column Tie T1 Axial Stress (Specimen 10)

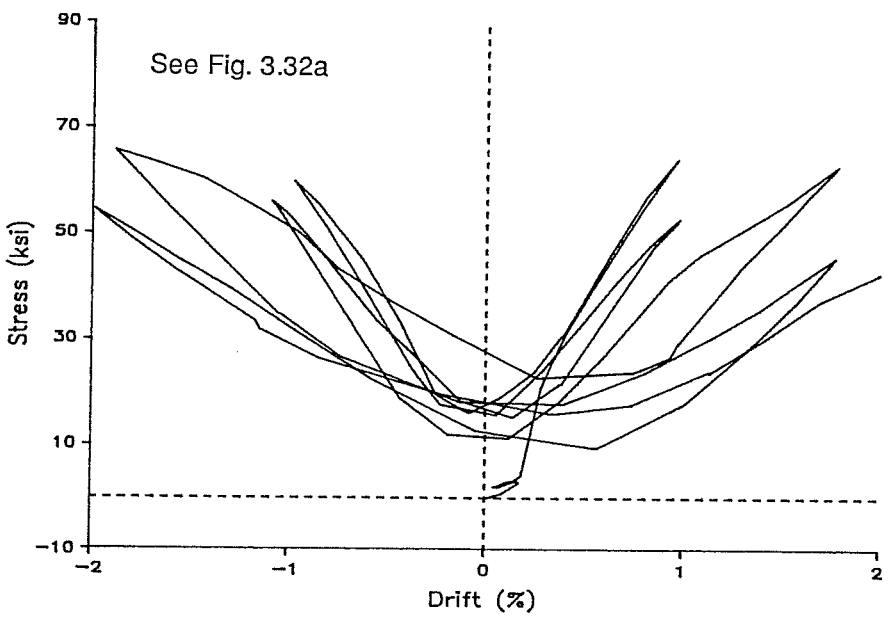

Fig. 3.32b Column Tie T1 Axial Stress (Specimen 14)

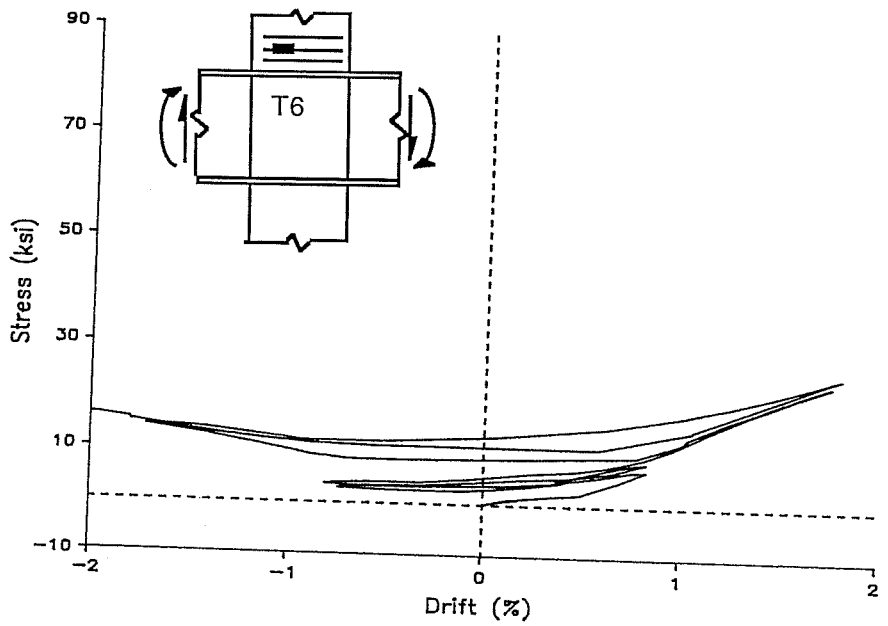

Fig. 3.33a Column Tie T6 Axial Stress (Specimen 10)

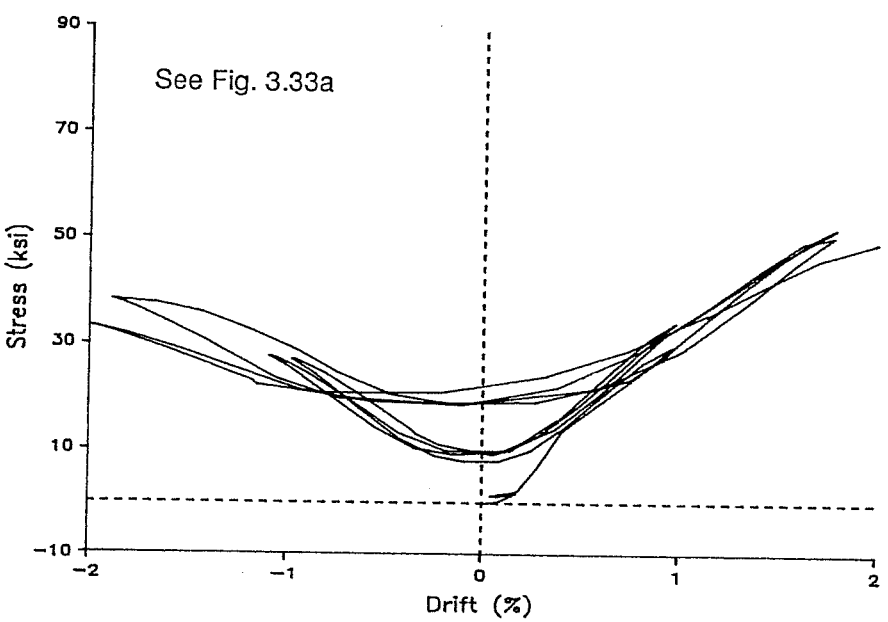

Fig. 3.33b Column Tie T6 Axial Stress (Specimen 14)

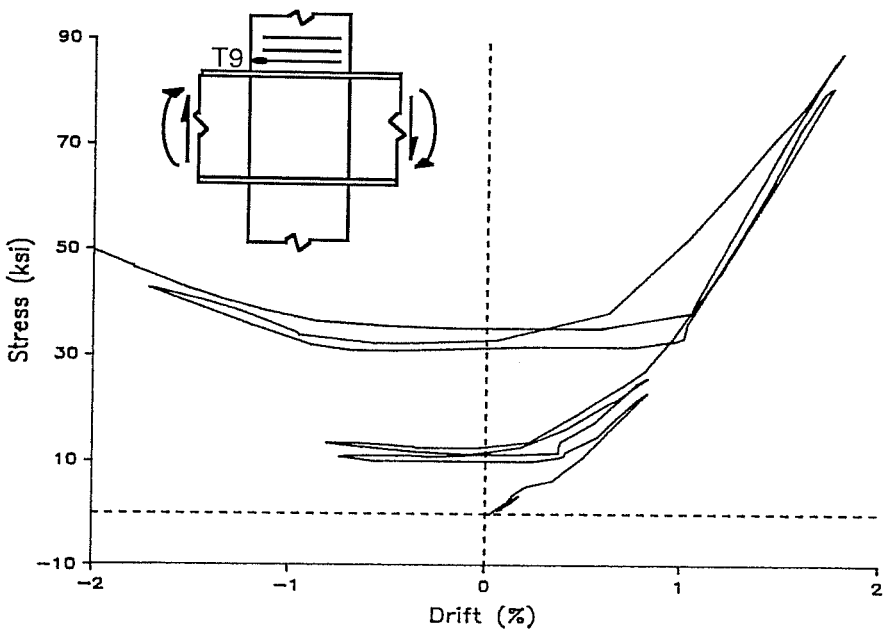

Fig. 3.34a Column Tie T9 Axial Stress (Specimen 10)

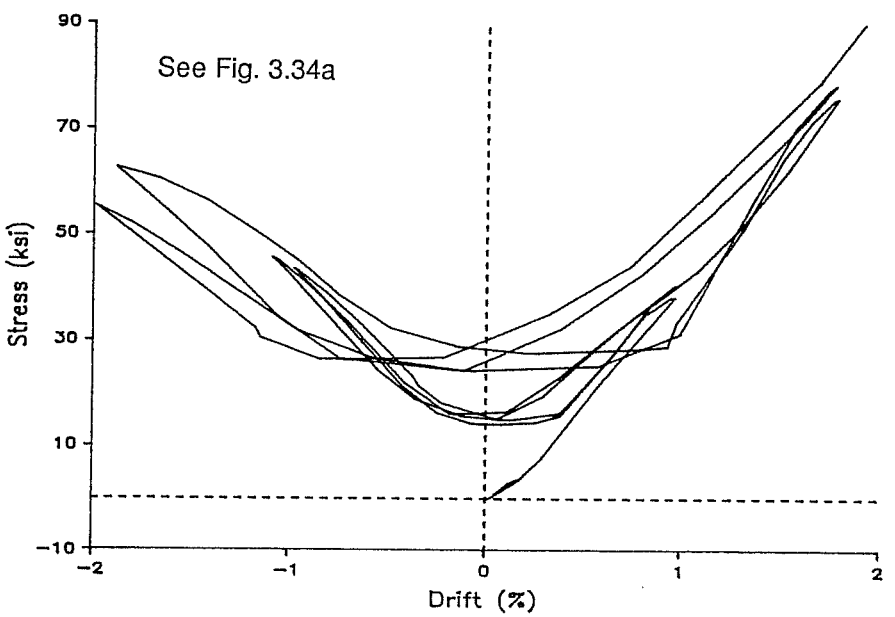

Fig. 3.34b Column Tie T9 Axial Stress (Specimen 14)

Specimens 14 through 17 was roughly 50% greater than in Specimen 10, and in Specimens 11 and 12 was 20% greater than in Specimen 10. Also, participation for T6 in Specimens 11 through 17 was approximately 150% greater than in Specimen 10.

Also seen in Figs. 3.32a through 3.33b, in the reverse direction, participation of T1 and T6 was negligible in Specimen 10, whereas in 14 it was almost equal to that in the primary direction. This behavior indicates that where joint details utilize shear capacity of the outer concrete panel, ties in that panel carry forces associated with truss action. The truss mechanism relies on the tension capacity of the ties in both directions of loading. This behavior in Specimen 14 was also seen in the other specimens.

Response of T9 demonstrates a different type of behavior. As seen in Fig. 3.34a and b, in the primary loading direction, tie participation was similar in Specimens 10 and 14 where T9 provided confinement to concrete in the bearing zone. The response of T9 in Specimens 15 and 17 was similar. In Specimens 11, 12, 13 and 16, where details such as shear studs or the clip angle also provided confinement, participation of T9 was 30% to 60% less. When loading in the reverse direction, participation of T9 was negligible in Specimen 10 as concrete in the region was no longer in compression. However, in Specimen 14 (and other specimens with attachments to the outside of the flanges), T9 participated to a similar degree as in the primary direction. In such cases, T9 presumably resisted load generated by the horizontal strut formation, shown earlier in Fig. 3.15.

Finally, ties within the beam depth showed a larger reduction in stress during subsequent cycles than those outside the beam depth. This may be due to the use of 90 degree cap ties within the beam depth and closed rectangular hoops outside. Hence, the larger stress reduction may be due to bond and anchorage deterioration of the cap ties. Another contributing factor may be that concrete within the beam depth is cracked more extensively than that outside.

3.3.11 Dissection of Specimens. Several of the specimens were dissected after testing in order to examine condition of concrete within the joint. Concrete was carefully removed with a pneumatic jackhammer. Typically, one

side of the joint was opened with the jackhammer and the beam removed, revealing the opposite side of the joint which was still intact.

The general condition of concrete in the joint is shown in Fig. 3.35. Concrete in the inner panel showed extensive diagonal cracking. With the joint opened, most of the inner panel concrete could easily be removed with a hand held chipping hammer. In Specimen 12, which did not have FBPs, concrete in the inner panel was not extensively cracked.

Between the inner and outer panels was a layer of pulverized concrete where the largest pieces were approximately 3/4 in. Presumably, such damage occurred due to rotation of the steel beam (and captive inner panel) within the outer concrete panel. Rotation during the initial cycle probably formed a crack plane between the panels. During subsequent cyclic reversals, concrete adjacent to the crack was worn through abrasion.

In the outer panel concrete was damaged to varying degrees, roughly related to the observed mobilization of the outer panel. In Specimen 10, for example, the outer panel was cracked but still rather intact. On the other hand, in Specimens 12 and 13 the outer panel was cracked so extensively such that when the lateral ties were loosened concrete fell apart in 2 to 4 in. pieces. This damage highlights the need for lateral ties which, as a minimum, provide confinement to hold damaged concrete in place.

A concrete fragment removed from below the upper flange is shown in Fig. 3.36. This sample shows the typical condition of concrete cast against an upper surface. In general, voids 1/8 in. thick and up to 2 in. diameter were found below the top and bottom flanges. These voids formed in spite of careful concrete placement and vibration, and high concrete slumps (6 to 7 in.). The condition of this concrete demonstrates the importance of casting the test components in a manner similar to actual practice. In this case, vertical casting ensures that test results will be indicative of the concrete properties expected in the field. As it is unlikely that field conditions will be better than those in the laboratory, it should be accepted that these voids will occur, and joints should be designed taking into account imperfect concrete consolidation.

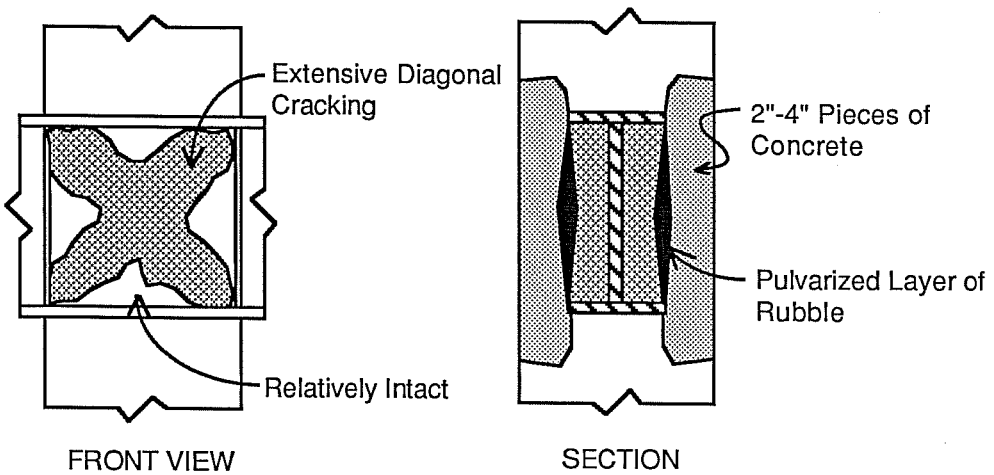

Fig. 3.35 Concrete Damage in Joint Region

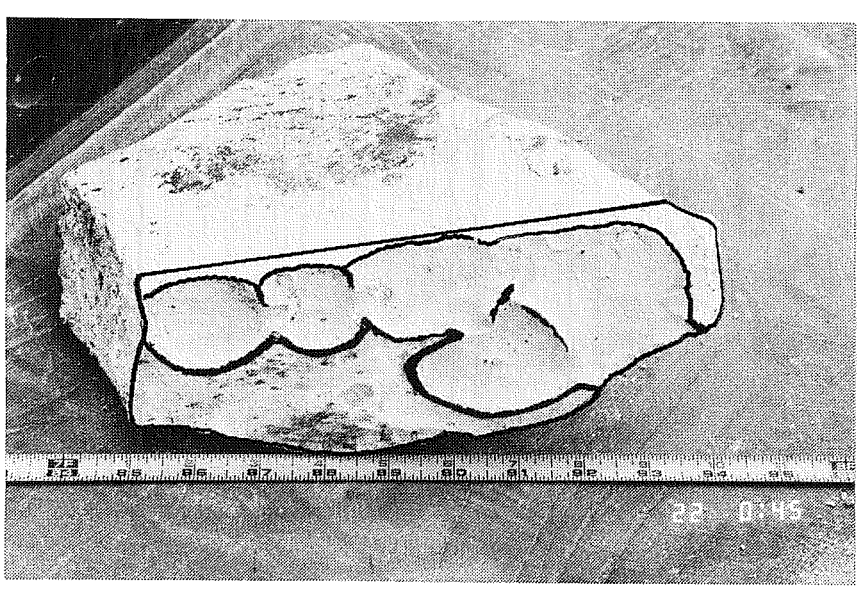

Fig. 3.36 Voids in Concrete Cast Against Flange

CHAPTER 4 - THEORETICAL JOINT CAPACITY

4.1 Introduction

In this chapter, a model developed to predict the joint capacity is assessed. The model is based in part on one previously developed and reported by Sheikh.[1] The model also draws from applicable specifications, design standards, and research for connections in reinforced concrete and structural steel. Test results of Specimens 1 through 8 and 10 through 17 provide the basis for evaluating the procedure.

4.1.1 Deformation Level. The calculated joint strength is calibrated to the measured strength at a deformation of 1% total joint distortion. As seen from the load-deformation response presented in Chapter 3, the composite joint does not exhibit a well defined limit or yield load. Consequently, a deformation level for strength evaluation is imposed for two reasons. First, selection of a specified deformation level permits comparison of results between tests and with models such as the one developed herein. Second, as this model forms the essence of the design recommendations in Chapter 5, the joint response should be accounted for in a manner consistent with the state of practice in building design.

The nominal joint strength is evaluated at a deformation of 1% TJD for several reasons to provide the desired response at service and ultimate loads. Based on the load- deformation response discussed previously, up to 1% TJD the joint is fairly stiff and beyond this point softens rapidly. This coincides with increased concrete cracking and spalling beyond 1% TJD. Also, as explained in Chapter 3, deformation beyond 1% TJD results in only marginal strength gains relative to increased distortions at service and ultimate loads.

The 1% TJD limit for nominal design strength results in roughly 0.2% TJD at service load which is consistent with deformations accepted in structural steel and reinforced concrete joints. Sheikh[1] reports that from tests reported by Meinheit[16] at the University of Texas, the typical service load deformations in reinforced concrete joints are 0.2% to 0.35% TJD. Recent tests conducted by

Guimaraes (et al.)[17] of reinforced concrete joints including the floor slab show service distortions of roughly 0.15% to 0.25%. Similarly, research of structural steel joints reported in references 18, 19 and 20 indicates service level deformations of roughly 0.2% TJD.

4.1.2 Inner and Outer Shear Panels. Shear capacity of the connection panel is a primary factor dictating joint response. Experimental observations suggest that the panel behavior can be separated into that of an inner and outer shear panel. As described previously, the inner panel consists of the steel web and concrete between the beam flanges. The outer panel consists of the reinforced concrete in the joint region outside the inner panel.

The two regions provide a convenient means to separate aspects of the joint behavior. Concrete in the inner panel participates through a diagonal compression strut formed by FBPs, WSPs, or similar details. Concrete in the outer panel participates in a combination of a single compression strut and a compression field depending on the joint detail. Figures 4.1a through c indicate the concrete regions mobilized in the various mechanisms. Figure 4.1a shows the diagonal compression strut formed in the inner panel by the FBP. In Fig. 4.1b, where a wide FBP is used, a similar strut forms in the outer panel. For convenience the strut contributions shown in Figs. 4.1a and b are incorporated together in the inner panel calculations. Shown along with the outer panel compression field, in Fig. 4.1c, is the region of concrete where shear force transfers horizontally between the embedded steel column and the outer panel. In details where the FBP is not wider than the beam, b_p equals b_f in Figs. 4.1b and c. The effective joint width, b'_j, is a function of the joint geometry and details. In Fig. 4.1c, $b'_{op}/2$ is half of the effective outer panel width.

The total joint capacity is obtained through super position of the inner and outer panel contributions. As given in Fig. 4.2a the relative proportions of beam and column moments and shears are assumed known based on a structural analysis of the overall frame. The diagrams in Fig. 4.2b indicate the portions of load carried by the inner and outer panels. The total beam and column shears are included with the inner panel calculations in order to properly reflect the

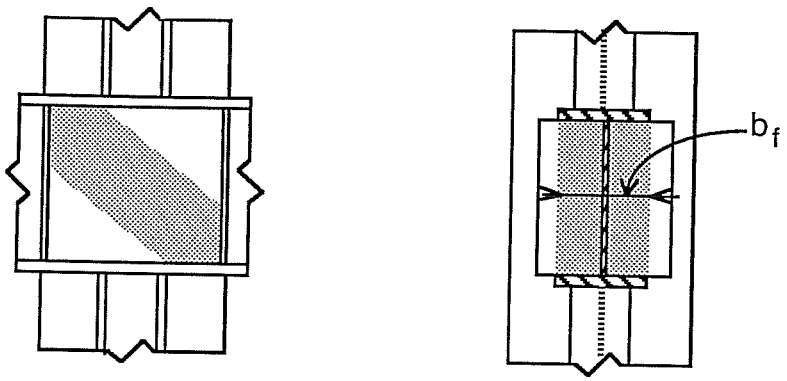

Fig. 4.1a Inner Compression Strut Region

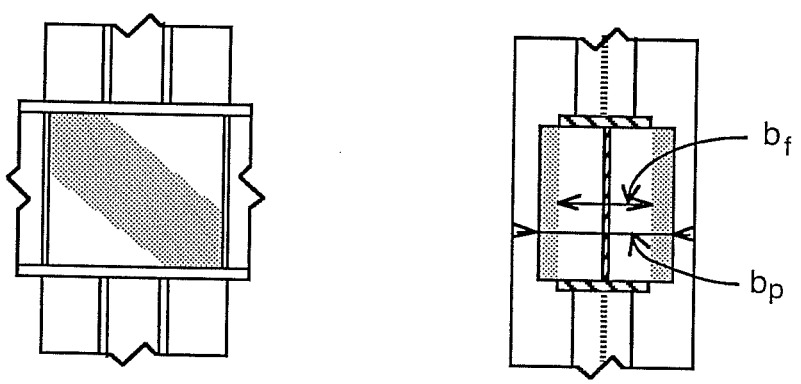

Fig. 4.1b Outer Compression Strut Region

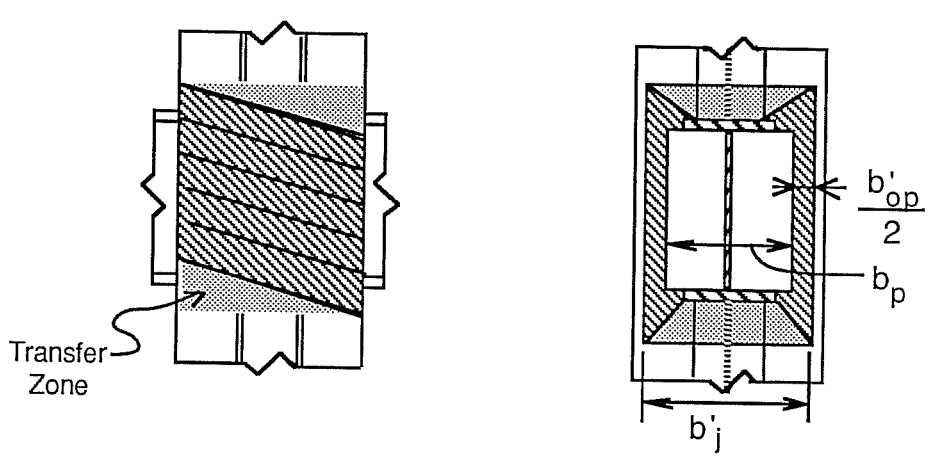

Fig. 4.1c Outer Compression Field Region

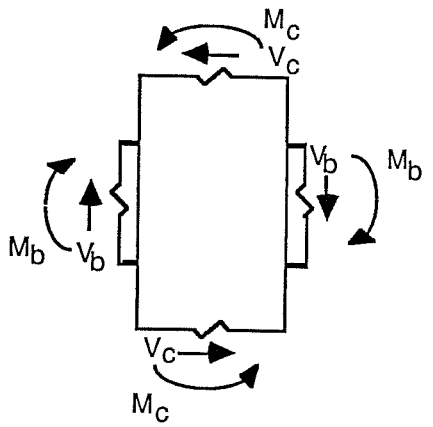

$M_b = \alpha_1 V_b$

$M_c = \alpha_2 V_b$

$V_c = \alpha_3 V_b$

Fig. 4.2a Proportional Member Forces

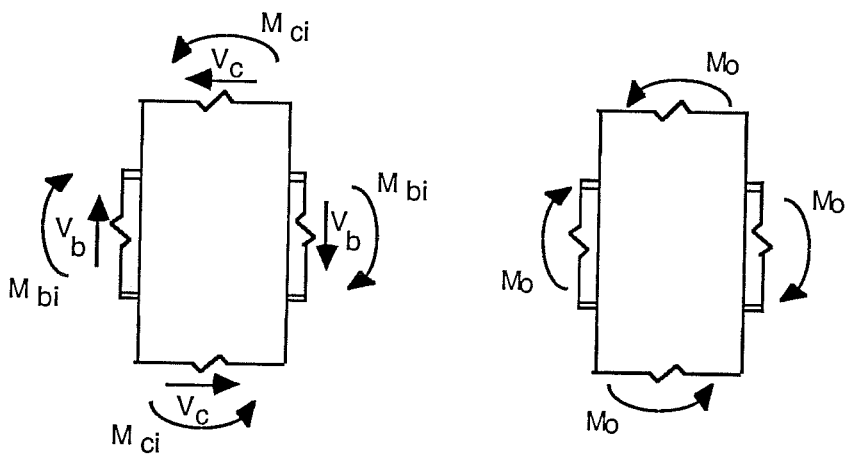

By Definition: $M_b = M_{bi} + M_o$

$M_c = M_{ci} + M_o$

$V_b = M_b / \alpha_1$

$V_c = V_b \alpha_3$

Fig. 4.2b Superposition of Inner and Outer Panel Capacities

transfer of beam shears into the column. From Fig. 4.2b the beam and column shears can be related to the beam moments as follows:

$$V_b = (M_{bi} + M_o) / \alpha_1 \qquad (4.1a)$$

$$V_c = (M_{bi} + M_o)\ \alpha_3 / \alpha_1 \qquad (4.1b)$$

4.1.3 Shear Mechanisms and Failure Modes. Analysis of the connection addresses two predominant failure modes: joint shear failure and concrete bearing failure. Joint shear failure is further distinguished between the steel panel, concrete compression strut, and concrete compression field. The analysis presented in this chapter does not consider elements and details in the joint which did not appear to contribute to joint failure in the tests. Evaluation of and recommendations for elements not involved in the joint shear and concrete bearing failure modes are considered in Chapter 5.

Steel Panel. Shear yielding of the beam web and plastic hinging of the beam flanges govern the steel panel strength. Referring to Fig. 4.3a, the steel panel strength is given by the following equations:

$$V_s = V_w + V_f \qquad (4.2a)$$

$$V_w = 0.6 F_{yw}\ t_w\ jh \qquad (4.2b)$$

$$V_f = 4\, M_{pf} / d_f \qquad (4.2c)$$

$$M_{pf} = F_{yf}\ t_f^2\ bf / 4 \qquad (4.2d)$$

The shear yield stress of 0.6 F_{yw} is based on the 1986 LRFD specification for structural steel.[10] As shown in Eq. 4.2b the web strength is dependent on the dimension jh which is the effective horizontal lever arm between the vertical force couple acting on the steel beam. This distance is a function of the concrete bearing zone length and the location of vertical reinforcement attached to the beam.

Concrete Compression Strut. The horizontal shear capacity of the concrete compression strut shown in Fig. 4.3b is calculated using the following formula:

$$V_n = 0.63 \sqrt{f'_c}\, b_e\, h \tag{4.3}$$

In this equation and throughout the report f'_c is in ksi units and dimensions in inches. The $\sqrt{f'_c}$ carries units of ksi. Except for a difference in units, Eq. 4.3 is the same as that reported in the 1985 ACI-ASCE Committee 352 recommendations[8] for calculating the shear panel strength in reinforced concrete joints. For readers familiar with reinforced concrete joint design, an alternate form of Eq. 4.3 is repeated below in terms of the units used in the ACI-ASCE report:

$$V_n = 20 \sqrt{f'_c}\, b_e\, h \tag{4.3-alt.}$$

In most concrete related design recommendations, f'_c is in psi units and dimensions in inches. In such cases the $\sqrt{f'_c}$ carries units of psi. The effective strut width, b_e, is determined from the joint geometry and details. The lever arm between the horizontal forces is equal to 0.75 d_w where the depth of the concrete panel is the distance between the steel beam flanges. The lever dimension results from the bearing zone height of 0.25 d_w shown in the figure. Sheikh[1] demonstrated that 0.25 d_w is a reasonable value where face bearing plates mobilize the compression strut.

Concrete Compression Field. The diagonal compression field strength is calculated as the combined contributions from the concrete and horizontal shear reinforcement. Referring to Fig. 4.3c the compression field strength is given by the following equations:

$$V'_n = V'_c + V'_s \leq 0.63 \sqrt{f'_c}\; b'_{op}\; h \tag{4.4a}$$

$$V'_c = 0.16 \sqrt{f'_c}\, b'_{op}\, h \tag{4.4b}$$

$$V'_s = A_{sh}\, F_{ysh}\, 0.9h \,/\, s_h \tag{4.4c}$$

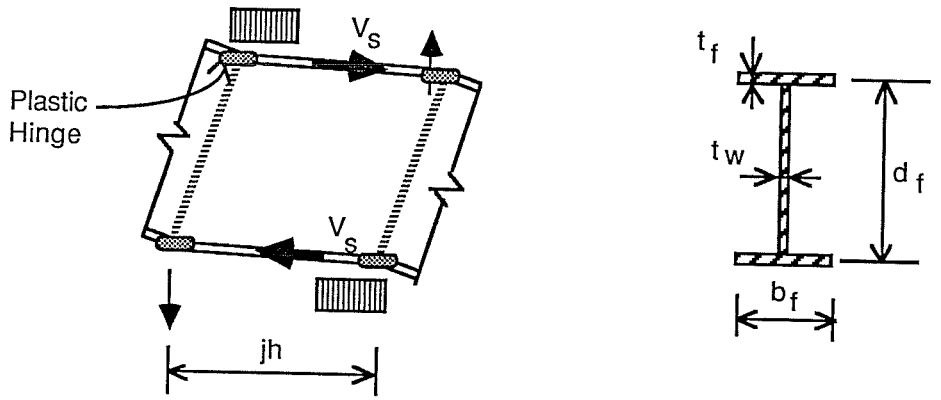

Fig. 4.3a Steel Shear Panel

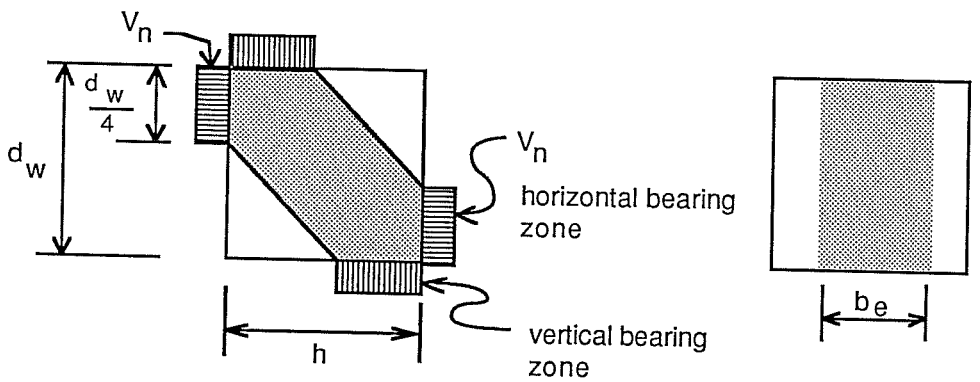

Fig. 4.3b Concrete Compression Strut

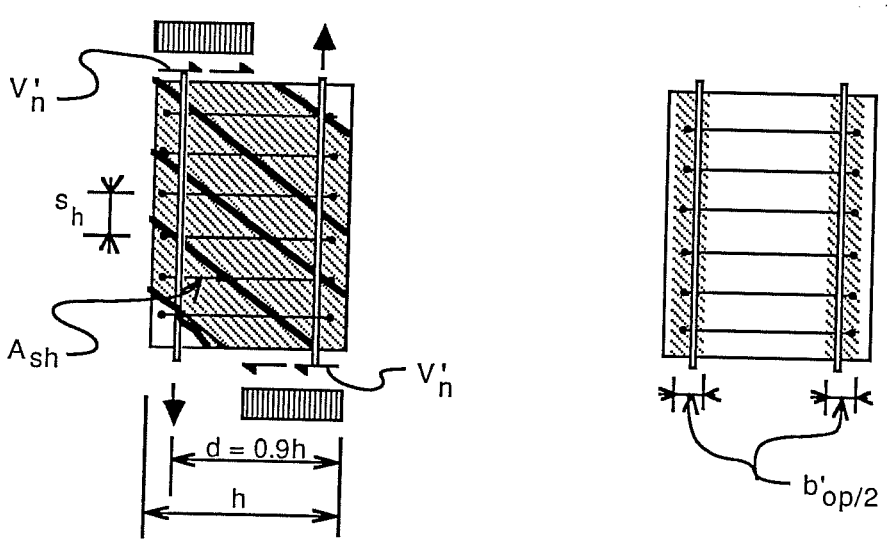

Fig. 4.3c Concrete Compression Field

These equations are derived from the 1976 ACI-ASCE Committee 352 report[21] where joint shear strength is based on a compression field model. Alternate versions of Eqs. 4.4a and b are repeated below in terms of psi and inch units used in the ACI-ASCE report:

$$V_n' = V_c' + V_s' \leq 20\sqrt{f_c'}\, b_{op}'\, h \qquad \text{(4.4a-alt.)}$$

$$V_c' = 5\sqrt{f_c'}\, b_{op}'\, h \qquad \text{(4.4b-alt.)}$$

For reinforced concrete joints, the latest ACI-ASCE Committee 352[8] report favors the compression strut model over the compression field model. However, the compression field model best represents the outer panel behavior of composite joints. An important aspect of the compression field calculation is determination of the effective panel width, b_{op}', which is a function of joint geometry and details as discussed later.

Vertical Bearing. Figures 4.4a and b show two means of transferring vertical forces between the column and inner joint panel. Figure 4.4a indicates a zone of concrete bearing against the compression flanges. Diagonal cracks observed on the side of the column suggest that vertical forces originating through bearing against the tension flange may fan out to create a bearing zone wider than the beam. At high loads, however, formation of vertical crack planes shown in Fig. 4.4a limit spreading of the bearing force. Figure 4.4b shows a shear friction mechanism which transfers load across the crack planes, and hence governs the load which fans out from the tension flange. As indicated in Fig. 4.4b, vertical force transferred by shear friction is resisted by both concrete compression stresses and bond stresses along the vertical column reinforcement. In general, compression stresses outside of the beam width are less than those within the beam width and therefore do not control the design insofar as bearing is considered.

The concrete bearing block acting on the compression flanges is proportioned based on published recommendations which correlate well with the test results. The maximum concrete bearing stress of 2 f_c' (Fig. 4.4a) relies on

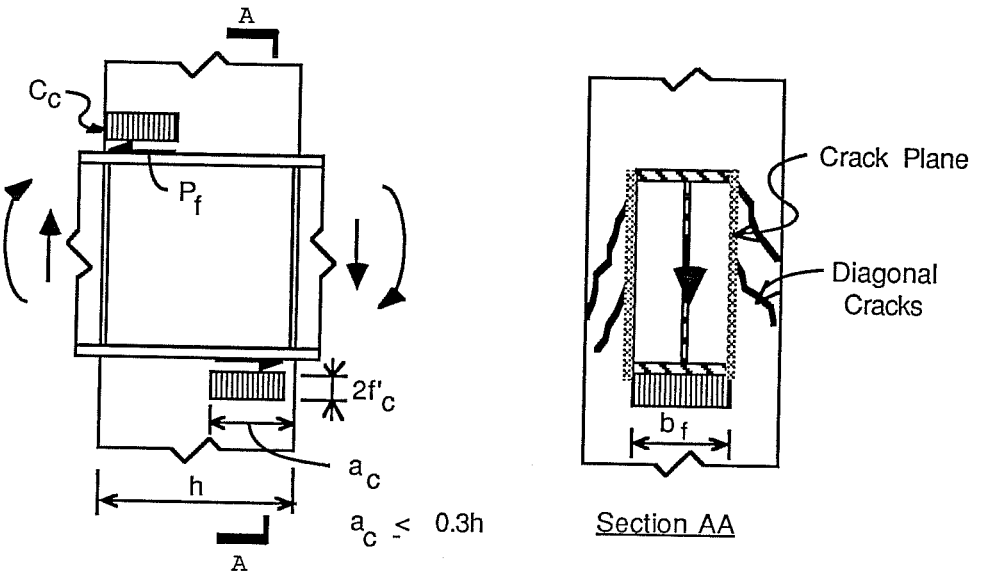

Fig. 4.4a Vertical Bearing Zone

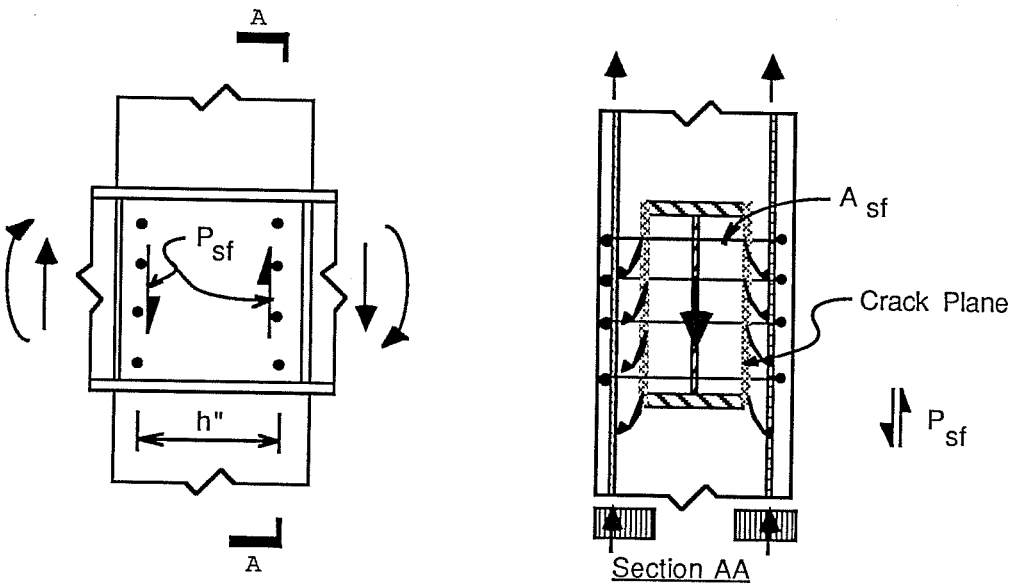

Fig. 4.4b Vertical Shear Friction

confinement afforded by the lateral ties, friction against the steel, and the surrounding concrete. Based on tests to simulate the bearing zone under a steel beam Minami[7] recommends a maximum stress of 2 f'_c. Also, ACI-318[15] specifies a maximum bearing stress of 1.7 f'_c (twice its typical value of 0.85 f'_c) when supporting concrete area is larger than the loaded area. The length of the compression block, a_c, is limited to a maximum of 0.3 h. This value is recommended in the *PCI Design Handbook*[22] for the bearing zone under embedded steel brackets. The resulting concrete bearing force, C_c, shown in Fig. 4.4a is given by the following formula:

$$C_c = 2\, f'_c\, a_c\, b_f \tag{4.5a}$$

$$\text{where } a_c \leq 0.3\, h \tag{4.5b}$$

Figure 4.4a also shows the horizontal force, P_f, transferred between the beam flange and concrete by friction. Typically, this friction force is resisted by concrete column shear. The value of P_f is derived from the ACI-318[15] shear friction recommendations where the force transfer in the bearing region is governed by the upper limit on shear stress. The resulting expression for the friction force, P_f, is as follows:

$$P_f = 0.2\, f'_c\, a_c\, b_f \leq 0.8\, a_c\, b_f \tag{4.6}$$

The expression for the vertical force, P_{sf}, shown in Fig. 4.4b is also based on the ACI-318[15] shear friction recommendations and is as follows:

$$P_{sf} = 1.4\, A_{sf}\, F_{ysf} \tag{4.7}$$

In this expression A_{sf} is the total area of reinforcement fully developed in tension across the vertical crack planes. A friction coefficient of 1.4 is used for monolithic concrete.

4.1.4 Procedure for Assessing Joint Strength. The composite joints derive their strength through interaction of several mechanisms. As demonstrated by the variety of test specimens, many joint configurations and details

which demand individual consideration are possible. Understanding basic load paths and modes of failure provides the most reliable guide to the connection analysis. Two key points in the calculations are identifying the primary joint shear mechanisms in the inner and outer panels, and evaluating the means by which these are mobilized by the connection details.

In this chapter parameters are developed for computing shear mobilized in the outer and inner joint panels, and equations are introduced which relate internal joint forces to the overall member forces. The outer panel is considered first, as the moments carried by the outer panel are required for the inner panel calculations. Included with the inner panel calculation is the influence of the vertical forces shown in Figs. 4.4a and b and of vertical joint reinforcement attached to the flanges.

In addition to the shear panel calculations, requirements for other force transfer mechanisms are considered. One such mechanism transfers joint shear horizontally between the outer panel and elements such as steel columns or extended FBPs. Also, horizontal forces and associated bearing stresses against elements such as the FBP, WSP, steel column, shear studs, and vertical joint reinforcement are considered.

Once appropriate parameters and equations are developed, a systematic approach to assessing joint capacity is presented. The solution is described through several flow charts which provide a guide to the equations for the shear strength contributed by different mechanisms and thereby help illustrate the interrelation of various parameters.

4.2 Outer Shear Panel

Outer panel contribution to joint strength is determined by resolving the effective shear resistance of the panel into equivalent beam and column moments. The shear resistance depends primarily on various joint details mobilizing concrete in the outer panel. For example, recall that the outer panel contribution in Specimens 14 through 17 was roughly 40% of that in Specimen 8, with an

extended FBP detail which resulted in greater participation of the outer panel compared with that produced by the steel column detail.

The beam and column moments, M_o, resisted by the outer panel are shown in Fig. 4.5a. As noted previously, member shears associated with these moments are included with the inner panel analysis, and therefore are not considered here. Also shown in Fig 4.5a is the panel height extension, d_{op}, provided by attachments to the beam flange. In calculations this dimension, d_{op}, is restricted to less than d/4 based on limits of the test data.

In Fig. 4.5b the beam moments, M_o, are resolved into equivalent horizontal force resultants in the concrete compression field. The strength of the joint is determined from the compression field capacity, V_n'. The vertical forces shown in Fig. 4.5b are not labeled as they are not required for calculating the compression field strength.

The strength of the concrete compression field, V_n', is dependent on the total effective joint width. The largest width observed was in Specimen 8 with the extended FBPs. Using Eq. 4.4a for the panel capacity, the effective outer panel width, b_{op}', is calculated as 6 in. for Specimen 8. The resulting effective joint width is 14 inches which coincides with the effective width specified by the 1985 ACI-ASCE Committee 352[8] for reinforced concrete joints. Using the recommendations of Committee 352, the equation for the maximum joint width is as follows:

$$b_j = (b_f + b)/2 \leq b_f + h \leq 1.75\, b_f \qquad (4.8a)$$

The limit of 1.75 b_f imposed on b_j is based on available test data where the smallest ratio of b_f/b is 0.4. Referring to Fig. 4.1c, the resulting maximum width of the outer panel is as follows:

$$b_{op} = b_j - \max(b_p\,,\ b_f) \leq 2\, d_{op} \qquad (4.8b)$$

The upper limit of 2 d_{op} for b_{op} reflects concerns regarding the horizontal transfer mechanism addressed later in this chapter.

In details with attachments other than the extended FBP the full width given by Eq. 4.8b is not realized. In such cases the joint width is reduced to an effective width by the coefficient, C, described in Fig. 4.6. This coefficient reflects the variation in strength and stiffness of the horizontal transfer strut which is a function of joint geometry. The mechanics of this transfer mechanism is described with more detail subsequently in Sec. 4.4.1. As seen in the figure the coefficient C equals 1.0 in details where an extended FBP over the full beam width is present. It is important to recognize that full effectiveness of the extended FBP requires it to have adequate strength and stiffness. Such requirements are considered later in this chapter and in Chapter 5. For details other than the extended FBP the coefficient C is related to the width and location of the shear transfer element. Referring to Fig. 4.6 the coefficient is calculated using the following equation:

$$C = (x\,/\,h)\;(y\,/\,b_f) \geq 0.25 \qquad (4.9)$$
$$\text{but } C = 0 \text{ for } (x/h)\;(y/b_f) < 0.25$$

Since no data is available for low values of C, this equation should be limited to values of C greater than 0.25. Where C is calculated to be less than 0.25 it should be set to zero since the effectiveness of the shear transfer element is minimal. Also, where two or more transfer elements are provided, the value of C may be taken as the largest of the values calculated for each separate element. This situation occurs in Specimen 17 where both a steel column and Dywidag bars are used. Since the more effective element will shadow the other, the contribution from each of the elements should not be added together.

In Fig. 4.7 outer panel mobilization coefficients are shown for the steel column, shear stud, and vertical joint reinforcement details used in the test specimens. Note that for cases such as the shear studs the dimension, y, in Eq. 4.9 is taken as the center to center dimension of the studs. Also, in figuring the center of stiffness of the stud group, studs near the tension face of the column are neglected since they have inadequate cover to develop significant load. Finally, as described in Chapter 3, the back flange of the steel column carries most of the horizontal load, and hence the dimension, x, is measured from the back flange.

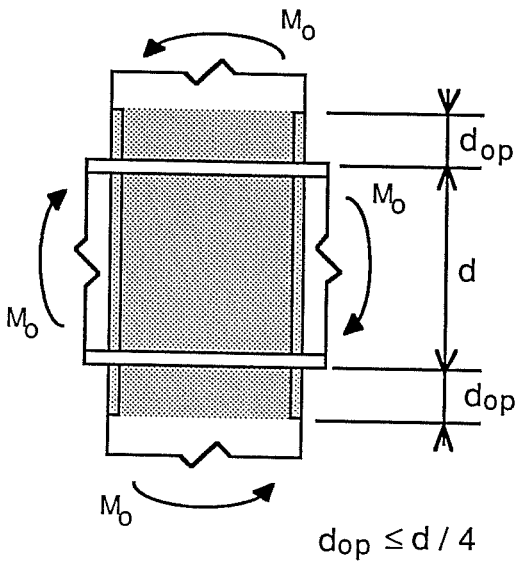

Fig. 4.5a Outer Panel: Member Forces

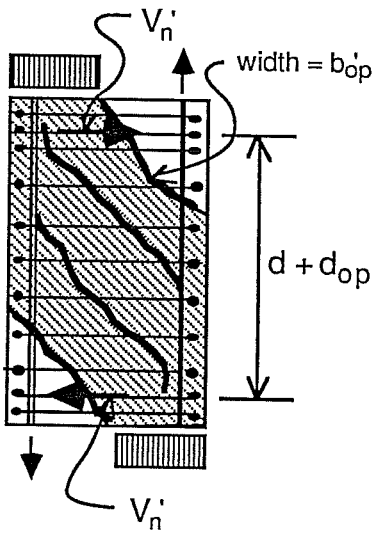

Fig. 4.5b Compression Field Shear

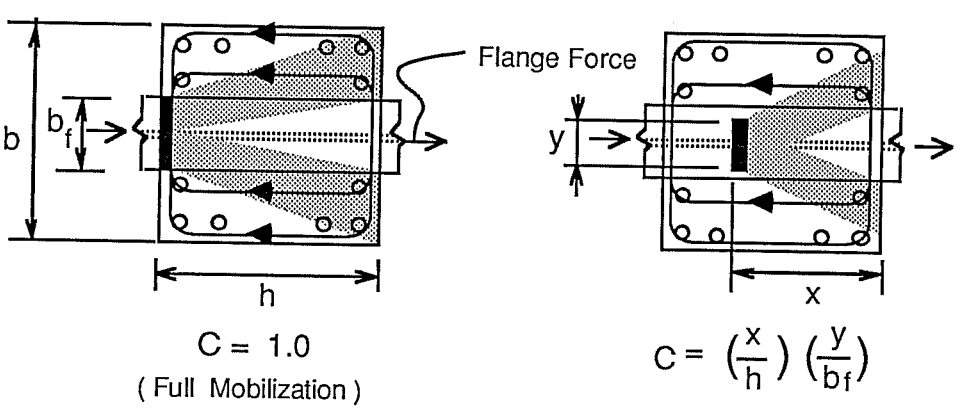

Fig. 4.6 Outer Panel Mobilization Coefficient

In Fig. 4.7 along with the calculated coefficients, values based on the experimental results are shown. The experimental values are obtained from the normalized outer panel contributions listed previously in Table 3.3. For Specimens 15 and 12 (Fig. 4.7), the calculated coefficients are slightly less than the experimental values. For Specimen 11 with the Dywidag bar detail, the computed coefficient overestimates considerably the test data value. This discrepancy is most likely due to local crushing of the concrete around the Dywidag bars which limits the shear panel contribution. Criteria for assessing such local failures is addressed later.

The coefficient given by Eq. 4.9 is used to modify the maximum outer panel width given by Eq. 4.8b, resulting in the following expression for the effective compression field width:

$$b'_{op} = C\, b_{op} \tag{4.10}$$

This dimension is used with the general compression field Eqs. 4.4a through c, to determine the effective compression field strength.

While it may seem reasonable to increase the maximum panel width in the presence of both wide FBPs and attachments to the flanges (steel columns, etc.), no data is available to verify such behavior. Therefore, the equations already developed for the outer panel strength provide a conservative result. Depending on the compression field mobilization coefficient, C, a higher joint capacity may result if the contribution of wide FBPs is neglected in calculations, since it is conservatively assumed that there is no positive interaction of the mechanisms. In such cases the FBP width used for calculations may be set equal to b_f (See Fig. 4.1). The result is that the compression strut formed by the wide FBP outside the flanges is neglected and this area of concrete is considered to participate in the outer panel compression field. As will be noted later, for calculation purposes the maximum WSP width is limited to b_f and hence should also be set to b_f in outer panel calculations.

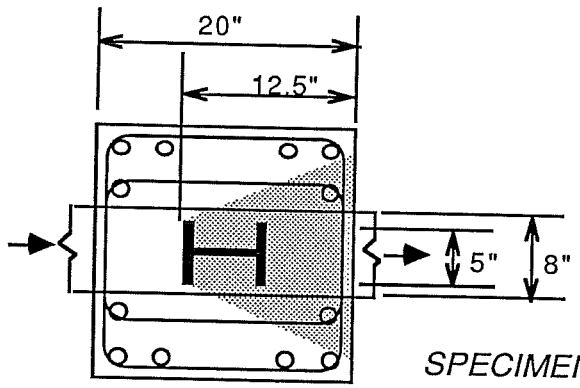

$C = \left(\frac{5}{8}\right)\left(\frac{12.5}{20}\right) = 0.39$

$C_{measured} = 0.43$

SPECIMEN 15 - Column

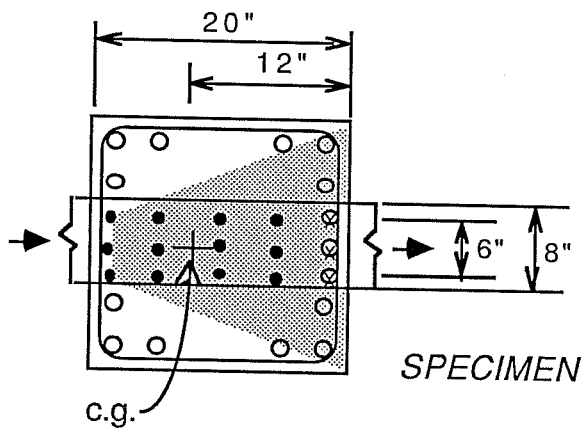

$C = \left(\frac{6}{8}\right)\left(\frac{12}{20}\right) = 0.45$

$C_{measured} = 0.49$

SPECIMEN 12 - Welded Shear Studs

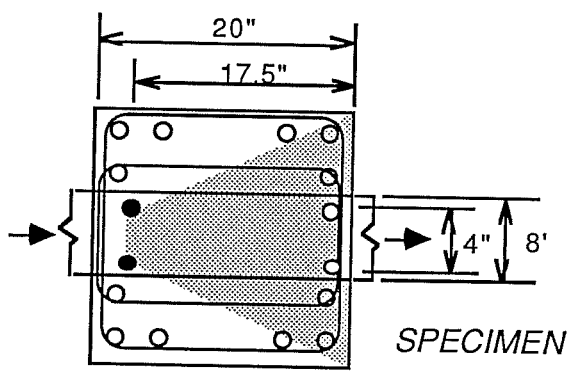

$C = \left(\frac{4}{8}\right)\left(\frac{17.5}{20}\right) = 0.44$

$C_{measured} = 0.29$

SPECIMEN 11- Vertical Joint Reinforcement

Fig. 4.7 Outer Panel Mobilization Coefficients

Once the effective horizontal shear capacity, V_n', has been established, the outer panel strength can be calculated in terms of member forces. By satisfying equilibrium between the beam moments in Fig. 4.5a and the joint shear in Fig. 4.5b the following equation results:

$$M_o = (d + d_{op})\, V_n' / 2 \tag{4.11}$$

4.3 Inner Shear Panel

The inner shear panel contribution is a function of the steel panel and concrete compression strut capacities. As the steel panel capacity is dependent on the horizontal distance, jh, shown in Fig. 4.3a, location of the vertical force couple influences the inner panel strength. Also, inner panel strength calculations include the transfer of beam and column shears through the joint region.

Figure 4.8a shows the member forces carried by the inner panel. Recall that the beam and column shears, V_b and V_c, can be expressed in terms of the beam moments, M_o and M_{bi}, according to Eqs. 4.1a and b. The beam moment carried by the outer panel, M_o, should be determined prior to calculations for the inner panel.

Member forces are resisted by the steel and concrete panels through vertical and horizontal force couples shown in Figs. 4.8b and c. Horizontal forces which reduce the panel shear by transferring column shear into the beam flanges are shown in Fig. 4.8d.

The strength of the steel panel mechanism, V_s, shown in Fig. 4.8c is determined according to Eqs. 4.2a through d presented previously. The effective length of the web shear region, jh, is the distance between the vertical column forces, P_{eq}, shown in Figs. 4.8b and c.

The inner concrete panel shown in Fig. 4.8c is mobilized in one of the three ways shown in Figs. 4.9a, b and c. The diagonal compression strut formed

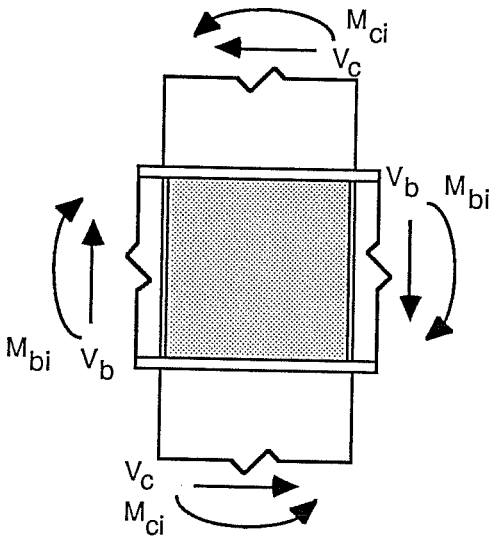

Fig. 4.8a Inner Panel: Member Forces

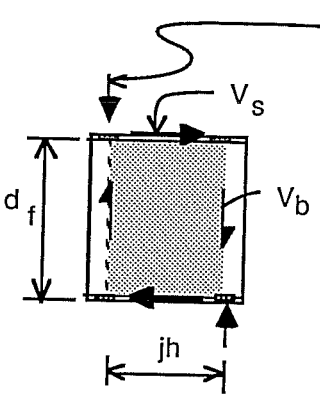

Fig. 4.8b Steel Panel Shear

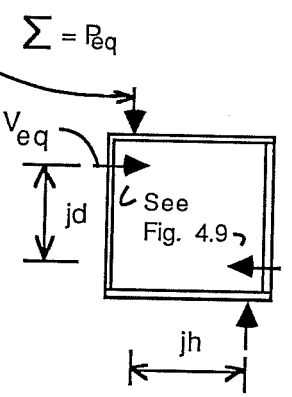

Fig. 4.8c Concrete Panel Shear

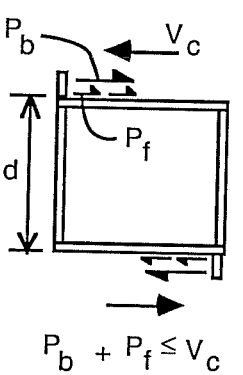

Fig. 4.8d Concrete Column Shear

by FBPs is shown in Fig. 4.9a. Comparing Figs. 4.8c and 4.9a the horizontal force and lever arm associated with the FBP detail are as follows:

$$V_{eq} = V_n \tag{4.12a}$$

$$jd = 0.75\, d_w \tag{4.12b}$$

The strut shear capacity, V_n, is calculated using Eq. 4.3 in which the strut width, b_e, is generally set equal to b_p except in cases where the FBP extends beyond the beam flanges. Test results of Specimen 7 indicate that the strut does not develop fully over the entire wide FBP width, hence, b_e is equal to the reduced width, 0.95 b_p. This behavior is presumably due to the inherent flexibility of the FBP extending outside the beam width.

Figure 4.9b shows the means by which shear friction between the concrete and steel web can mobilize the inner concrete panel where no FBPs or WSPs are present such as in Specimens 3 and 12. The normalized strengths in Table 3.3 indicate that in Specimens 3 and 12 the inner concrete panel participation is approximately 23% of that in specimens with FBPs. Such participation is accounted for through horizontal shear friction developed by column ties passing through the web. The total horizontal force generated by shear friction is generally small relative to the shear capacity of the inner concrete panel. Therefore, the panel remains essentially uncracked as the principal tensile stress does not exceed tensile capacity of the concrete. For this reason the force, P_{h_i}, shown in Fig. 4.9b is included for all of the ties. Comparing Figs. 4.9b and 4.8c, the horizontal shear force and lever arm associated with the shear friction mechanism are given as follows:

$$V_{eq} = \sum P_{h_i} \tag{4.13a}$$

$$P_{h_i} = 1.4\, A_{wf}\, F_{ysh} \tag{4.13b}$$

$$jd = \sum \left(P_{h_i}\, jd_i\right) / V_{eq} \tag{4.13c}$$

Equation 4.13b is based on ACI-318[15] recommendations for shear friction with a friction coefficient of 0.7 between the concrete and steel. In Eq. 4.13b, A_{wf} is

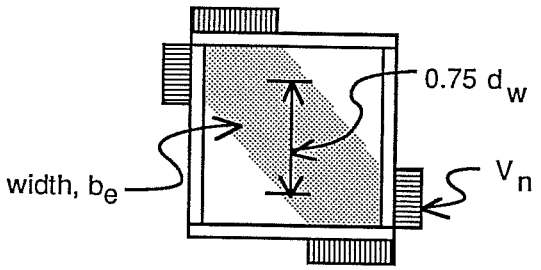

Fig. 4.9a FBP Mechanism (Specimen 5)

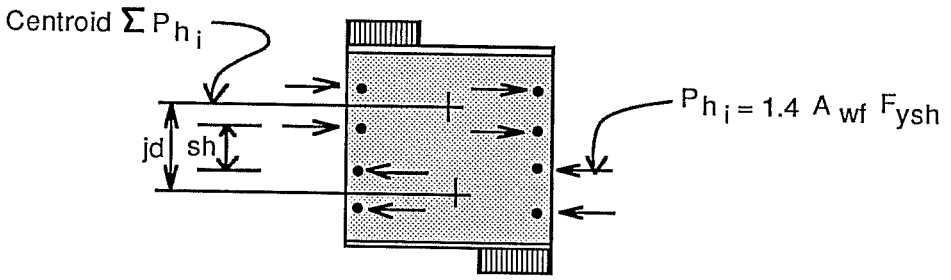

Fig. 4.9b Shear Friction Mechanism (Specimens 3 & 12)

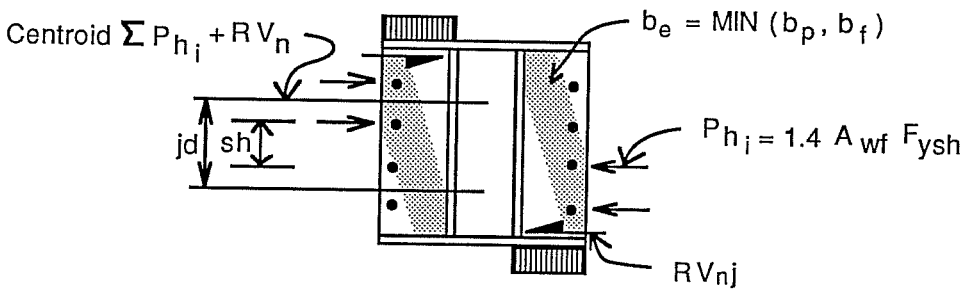

Fig. 4.9c WSP and Shear Friction Mechanisms (Spec. 14)

the total cross sectional area of reinforcement developed in tension at the steel web.

Figure 4.9c shows inner panel mobilization, such as in Specimen 14, where both WSPs and shear friction play a role. In this case compression struts form through direct bearing against the WSP on the inside and by friction against the web and the flanges. Web shear friction forms through action of transverse reinforcement and flange shear friction through the vertical bearing force developed by the diagonal strut. Comparing Figs. 4.9c and 4.8c, the horizontal shear force and lever arm associated with the WSP and shear friction mechanism are given as follows:

$$V_{eq} = \sum P_{h_i} + R\,V_n \tag{4.14a}$$

$$jd = \left[\left(\sum \left(P_{h_i}\ jd_i\right)\right) + \left(R\,V_n\ d_w\right)\right] / V_{eq} \tag{4.14b}$$

$$R = 0.5 \text{ (for WSP)} \tag{4.14c}$$

In these equations P_{h_i} is calculated using Eq. 4.13b and R is a coefficient to account for reduced strut mobilization by the WSP. The value of R is obtained by comparing the observed inner concrete panel contribution in Specimen 14 to that in Specimen 5. The strut shear capacity, V_n, is calculated using Eq. 4.3 where the strut width, b_e, is set equal to the lesser of b_p or b_f. The WSP width is limited to b_f since no test data is available to confirm effectiveness of larger widths.

Figure 4.8d shows the forces, P_f and P_b, which transfer load from the beam flange into the column where they are resisted by column shear. The sum of P_f and P_b is limited by V_c as noted in Fig. 4.8d. P_f is developed by friction between the steel flange and concrete in the compression bearing region and is calculated using Eq. 4.6. P_b is transferred through concrete bearing against attachments to the steel beam flange. Typically, where such attachments exist P_b is assumed not to control the design, and the joint is analyzed with the sum of P_f an P_b set equal to V_c. Once the joint capacity is established, P_b is checked to see that it does not exceed the available capacity of attachments to the beam

flange such as the steel column, extended FBP, etc. For simplicity, both P_f and P_b are conservatively assumed to act with a vertical lever distance equal to d.

The vertical force, P_{eq}, shown in Figs. 4.8b and c is the resultant force resisted by concrete bearing stresses, vertical joint reinforcement (attached to the beam), and shear friction provided by the ties within the beam depth. Figure 4.10 illustrates the contribution of each of these components to P_{eq}. The bearing zone capacity is determined using Eq. 4.5a and b. The vertical reinforcing components, C_{vr} and T_{vr}, are based on the nominal compression and tension strength of the steel reinforcement attached to the beam. The shear friction component, P_{sf}, is determined from Eq. 4.7. Referring to Fig. 4.10, the resultant, P_{eq}, and horizontal lever arm, jh, are given by the following expressions:

$$P_{eq} = C_c + T_{vr} + C_{vr} + P_{sf} \qquad (4.15a)$$

$$jh = \left[C_c\,(h - a_c) + (T_{vr} + C_{vr})\,h_{vr} + P_{sf}\,(h'')\right] / P_{eq} \qquad (4.15b)$$

In evaluating P_{eq}, the vertical joint reinforcement and shear friction are assumed to be stressed to full capacity. Where the connection is not governed by bearing, the concrete bearing region is not fully stressed and the length, a_c, is some value less than the maximum permissible length of 0.3 h.

Referring again to Figs. 4.8a through d, the force equilibrium between the member forces (Fig. 4.8a) and internal forces (Fig. 4.8b, c, and d) is developed. From moment equilibrium, the beam moments and shears, M_{bi} and V_b, are related to the horizontal joint shear forces by the following equation:

$$2M_{bi} + V_b\,(h - jh) = V_s\,d_f + V_{eq}\,jd + (P_f + P_b)\,d \qquad (4.16a)$$

The total applied moment given by the left side of Eq. 4.16a is calculated at the edge of the effective steel shear panel. Hence, the beam moment at the column face, M_{bi}, is increased by V_b as indicated. This increase is relatively small and is neglected in the simplified design equations presented in Chapter 5.

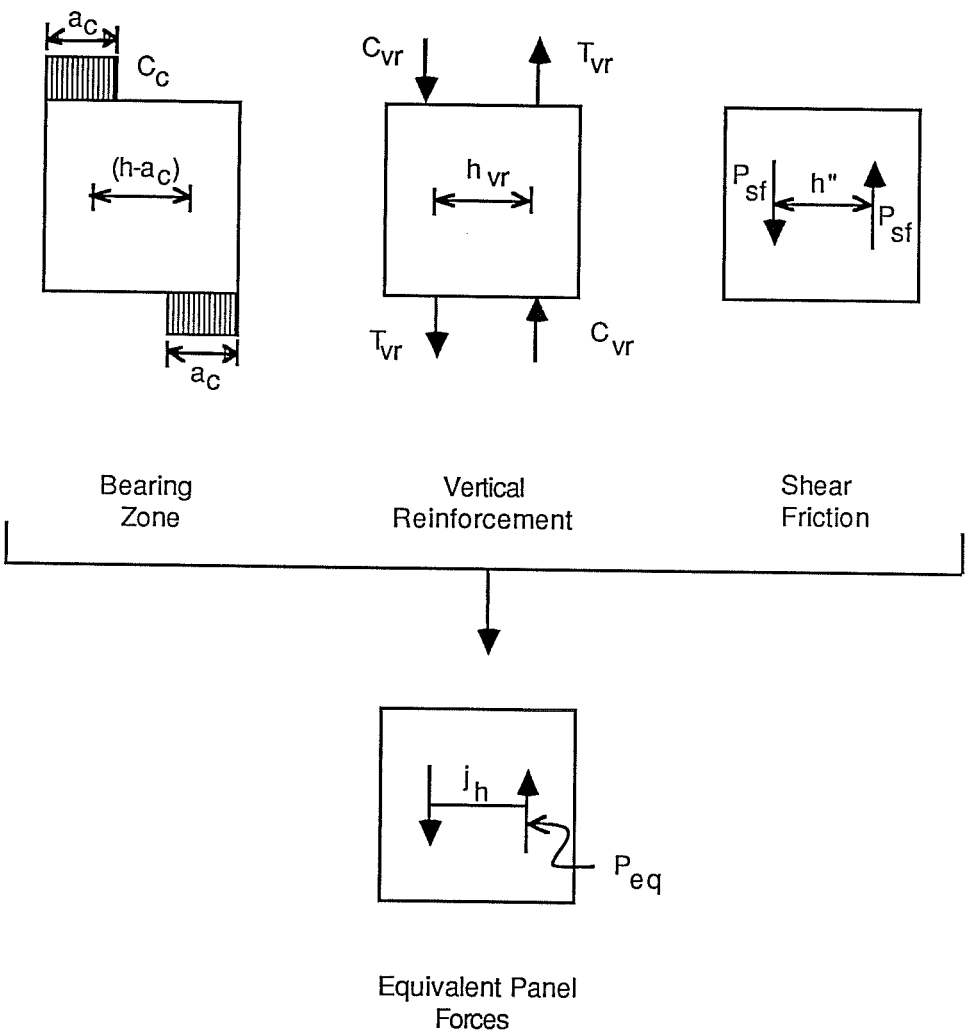

Fig. 4.10 Equivalent Vertical Forces on Inner Panel

In order to solve Eq. 4.16a for M_{bi}, the beam shear, V_b, is expressed in terms of M_{bi} and M_o using the relation given in Eq. 4.1a. Recall that M_o is the outer panel contribution calculated previously. With this substitution, Eq. 4.16a is rewritten as follows:

$$M_{bi} = \frac{V_s\, d_f + V_{eq}\, jd + (P_f + P_b)\, d - M_o\, (h - jh) / \alpha_1}{2 + (h - jh) / \alpha_1} \qquad (4.16b)$$

Solution for M_{bi} using Eq. 4.16b will be simplified by considering two extreme cases regarding the sum of the forces P_b and P_f. Recall that P_b and P_f are the horizontal forces transferred out of the beam flange and resisted by column shear as shown in Fig. 4.8d. In the first case, this sum is assumed to be less than the total column shear, V_c. Since this assumption usually applies in details without attachments to the beam flange, the force P_b is set to zero. With P_b set to zero, Eq. 4.16b is rewritten as follows:

$$M_{bi} = \frac{V_s\, d_f + V_{eq}\, jd + P_f\, d - M_o (h - jh) / \alpha_1}{2 + (h - jh) / \alpha_1} \qquad (4.17a)$$

The second case occurs where the sum of P_b and P_f equals the column shear. Typically this occurs in joints having attachments to the beam flange, but may occur in other cases where P_f is large. In this case the sum of P_b and P_f is set equal to V_c. With V_c expressed in terms of the beam moments, M_{bi} and M_o, as given in Eq. 4.1b, Eq. 4.16b is rewritten as follows:

$$M_{bi} = \frac{V_s\, d_f + V_{eq}\, jd + M_o\, (d\,\alpha_3 - h + jh) / \alpha_1}{2 - (d\,\alpha_3 - h + jh) / \alpha_1} \qquad (4.17b)$$

Where the connection is controlled by the joint shear strengths, V_s and V_{eq}, Eqs. 4.17a and b can each be shown to reduce to one equation with two unknown variables, M_{bi} and a_c. Therefore, a second equation is needed to solve either of these equations. Referring to Figs. 4.8b and c the following equation can be derived from moment equilibrium of the steel and concrete shear panels:

$$jh\, (P_{eq} - V_b) = V_s\, d_f + V_{eq}\, jd \qquad (4.18a)$$

Expressing V_b in Eq. 4.18a in terms of M_{bi} and M_o using Eq. 4.1a yields the following equation:

$$M_{bi} = \frac{-\alpha_1}{jh}(V_s\ d_f + V_{eq}\ jd) - M_o + P_{eq}\ \alpha_1 \qquad (4.18b)$$

Like Eqs. 4.17a and b, Eq. 4.18b also reduces to one equation with two unknown quantities, M_{bi} and a_c. Equation 4.18b is used with either Eq. 4.17a or b to solve for the connection strength in terms of M_{bi}. When shear panel strength governs the connection capacity, the concrete bearing zone length, a_c, is some value less than 0.3 h. Discussed subsequently in Sec. 4.5, where a_c is unknown Eqs. 4.17a or b and 4.18b are conveniently solved by iteration.

Where joint capacity is controlled by vertical concrete bearing, the bearing length, a_c, is equal to its maximum value of 0.3 h. For this case, Eqs. 4.17a and b are combined with Eq. 4.18b to eliminate the joint shear terms, V_s and V_{eq}. First, Eq. 4.18b is rewritten to obtain the following expression for V_s and V_{eq}:

$$V_s\ d_f + V_{eq}\ jd = jh\ (P_{eq} - (M_{bi} + M_o)\ /\ \alpha_1) \qquad (4.19)$$

The expression in Eq. 4.19 is substituted into Eq. 4.17a to obtain the following equation when concrete bearing controls:

$$M_{bi} = \frac{P_{eq}\ jh + P_f\ d - M_o\ h\ /\ \alpha_1}{2 + h\ /\ \alpha_1} \qquad (4.20a)$$

Since Eq. 4.20a is obtained from 4.17a, Eq. 4.20a applies to the case where P_b is set to zero and P_f is less than V_c.

When Eq. 4.19 is substituted into Eq. 4.17b the following equation is obtained where concrete bearing controls:

$$M_{bi} = \frac{P_{eq}\ jh + M_o\ (d\,\alpha_3 - h)\ /\ \alpha_1}{2 - (d\,\alpha_3 - h)\ /\ \alpha_1} \qquad (4.20b)$$

Similar to Eq. 4.17b, Eq. 4.20b applies where the sum of P_f and P_b is set equal to V_c.

In summary, where the connection is controlled by joint shear, M_{bi} is obtained using either Eq. 4.17a or b solved simultaneously with Eq. 4.18b. Where concrete bearing controls, M_{bi} is obtained directly from either Eq. 4.20a or b. Equations 4.17a and 4.20a apply where P_b is set to zero and P_f is less than the resulting column shear, V_c. Equations 4.17b and 4.20b apply where the sum of P_b plus P_f is set equal to the column shear, V_c.

Once the inner panel contribution, M_{bi}, is determined, the total joint capacity is given as the sum of the inner and outer panel capacities according to the expressions given in Figs. 4.2a and 4.2b.

4.4 Internal Transfer Mechanisms

Development of equations for calculating joint capacity from the inner and outer panel strengths is based on the premise that joint detailing is adequate to resist internal forces generated. In this section, examination of the internal force transfers focuses on critical components in the connections. The intent herein is not to introduce a detailed design method for such components, but rather to look in general terms at relevant design parameters and imposed forces.

4.4.1 Horizontal Transfer to Outer Panel. Previous discussion of the outer panel mobilization coefficient (Sec. 4.2) did not directly address strength aspects of the horizontal load transfer to the outer panel. Figures 4.11a and b illustrate two models to assess this transfer: a strut mechanism and a shear friction mechanism.

In Fig. 4.11a a pair of compression struts resist the lateral flange force through bearing on the extended FBP. Similar struts will form when a steel column, shear studs, or other detail is attached to the steel beam flange. Strut formation requires lateral ties to resist the transverse thrust, P_{t1}. Also, longitudinal column reinforcing bars serve to distribute tie forces vertically over the strut as shown in Fig. 4.11c. As indicated in Fig. 4.11c, ties outside the height d_{op} probably carry some load, and hence, in calculations ties within the height 1.5 d_{op} above the beam are considered effective. Ties are also required to drag the horizontal force, $P_{\ell 1}$, across the column where it is resisted by the outer

panel compression field. This transfer sequence is indicated in Figs. 4.11a, c and d.

Figure 4.11b shows a shear friction mechanism which offers more direct transfer of horizontal load into the outer panel. The sequence of this transfer is shown in Figs. 4.11b, 4.11c, and 4.11d. The shape and size of the shear plane shown in Fig. 4.11b is an idealization of the actual plane based on the observed surface cracking. As shown in the figure, shear transfer relies upon the tensile force, P_{t2}, provided by ties crossing the shear plane.

The two models of the horizontal transfer help explain why details other than the extended FBP are not as effective in transferring load into the outer panel. For example, the steel column detail transfers the horizontal force primarily by transverse bending of the back flange as indicated previously in Fig. 4.7. In such a case two factors affect behavior. First, the strut mechanism will not spread out as far and the load $P_{\ell 1}$ will be smaller. Also, the transverse tie force, P_{t1}, will be larger for a given horizontal load as the strut angle, θ, increases. Second, the shear friction mechanism will not be as effective since the column transfers horizontal load into concrete away from the shear plane shown in Fig. 4.11b. Similar assessments can be made for other details.

Load transferred by the strut mechanism is governed by the weakest component in the system. The three components are the longitudinal tie force, $P_{\ell 1}$, the transverse tie force, P_{t1}, and crushing strength of the strut. By comparing the width of struts in the outer compression field to those of the horizontal struts, premature crushing of horizontal struts is prevented by limiting the total effective outer panel width, b'_{op}, to 2 d_{op}. Typically, ties which carry the load $P_{\ell 1}$ will control the strut mechanism capacity since the strut angle, θ, is usually less than 45 degrees. Thus, the resulting load transfer strength is equal to $P_{\ell 1}$, calculated as the following:

$$P_{\ell 1} \leq A_\ell \, F_{ysh} \qquad (4.21a)$$

In Eq. 4.21b, A_ℓ is the total cross sectional area of ties parallel to the beam and located with a distance 1.5 d_{op} from the beam.

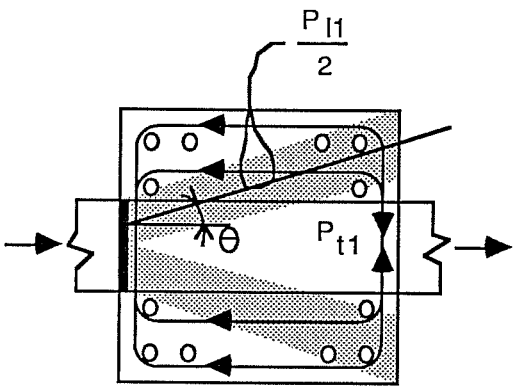

Fig. 4.11a Horizontal Strut

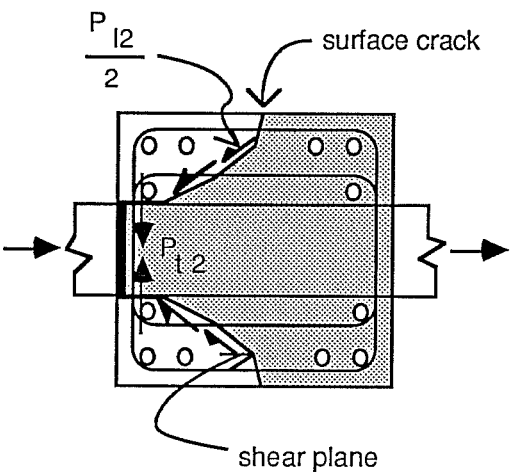

Fig. 4.11b Shear Transfer

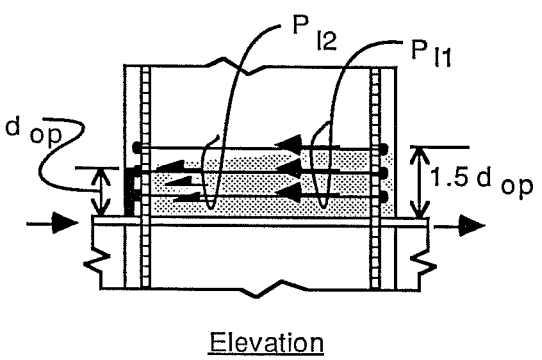

Fig. 4.11c Forces on Flange

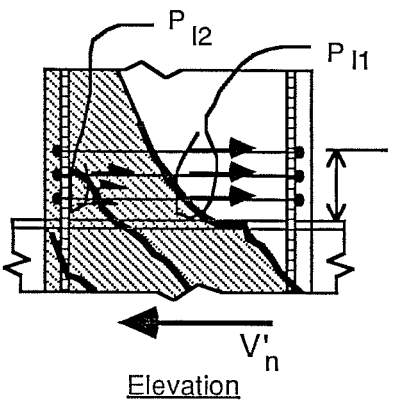

Fig. 4.11d Forces on Outer Panel

Table 4.1 Horizontal Transfer Forces

Specimen	$P_{\ell 1}$	$P_{\ell 2}$	$P_{\ell 1} + P_{\ell 2}$	P_t	V'_n
8 FBP (extended)	101	142	243	152	143
11 FBP-Db.Pl.-Dywi.	81	0	81	81	59
12 Studs	81	0	81	81	76
13 FBP-Studs	81	0	81	81	76
14 WSP-Column	81	0	81	81	60
15 FBP-Column	81	0	81	81	60
16 FBP-Col.-Clip	81	0	81	81	69
17 FBP-Col.Dywi.	81	0	81	81	66

The shear friction contribution, $P_{\ell 2}$, is limited by the force, P_{t2}, provided by the ties crossing the failure plane. Typically, this mechanism is only applicable for the extended FBP detail owing to the location of the crack plane and ties crossing that plane. The shear transfer capacity is based on the ACI-318[15] provisions for shear friction. Referring to Fig. 4.11b the capacity of $P_{\ell 2}$ is given as the following:

$$P_{\ell 2} \leq 1.4\, A_t\, F_{ysh} \qquad (4.21b)$$

In this equation A_t is the total area of transverse tie reinforcement developed in tension across the assumed shear failure planes within the transfer region.

The sum of the strut and shear friction contributions determines the total available transfer capacity, P_t. In order that the transfer mechanism not govern the connection capacity, the total capacity, P_t, must exceed the outer panel shear, V'_n (Fig. 4.11d). Based on capacities calculated according to Eqs. 4.21a and b, the transfer mechanism did not control the strength of the test specimens. Table 4.1 provides a summary of the calculated values of $P_{\ell 1}$, $P_{\ell 2}$, and V'_n in specimens where the outer panel is mobilized. Note that in all details except the extended FBP (Specimen *) the shear friction force, $P_{\ell 1}$, is conservatively taken as zero. The total capacity, P_t, listed in Table 4.1 is calculated using the following equation:

$$P_t = P_{\ell 1} + P_{\ell 2} \leq 1.5\, P_{\ell 1} \qquad (4.21c)$$

The upper bound on P_t of 1.5 times the strut contribution, $P_{\ell 1}$ is imposed to limit reliance on the shear friction mechanism, based on test results for Specimen 8. In Table 4.1, the value of P_t for Specimen 8 determined by Eq. 4.21c is close to the calculated strut capacity for Specimen 8.

Equations 4.21a, b, and c provide a means to determine the outer panel participation as limited by the capacity of the transfer mechanism. Where the mobilized outer panel shear, V_n', (calculated according to the effective compression field strength) exceeds the transfer capacity, the effective outer panel shear should be reduced accordingly.

4.4.2 Concrete Bearing Stresses. Force transfers between the steel and concrete elements may be controlled by concrete bearing stresses. The vertical bearing stress against the steel flanges is one example where such stresses often control the design. For this reason, vertical bearing stress is directly incorporated with the inner panel calculations. bearing may be critical for horizontal stresses against FBPs, steel column flanges, shear studs, and vertical joint reinforcement (Dywidag bars).

The maximum concrete bearing stress in such cases is limited to 2 f_c', following the rationale already presented with regard to the vertical bearing stress against the flanges. Subsequent design recommendations in Chapter 5 outline the effective bearing areas for each of the particular transfer elements and the load to considered in each case. When the bearing capacity of a component cannot develop the load associated with the calculated shear panel capacity, the shear panel capacity should be reduced. The only test where horizontal bearing limited the strength was Specimen 11 with the vertical Dywidag bars.

4.5 Solution of Joint Shear Equations

The stepwise procedure given herein for determining the joint strength is intended as a general guide and should not replace engineering judgment essential to proper design of such connections. The procedure is summarized in

Figs. 4.12 through 4.14f in which references for appropriate equations from this chapter are given. In Fig. 4.12 a flow chart outlining the overall approach is presented. The procedure begins with given information which includes the joint details and geometry and known proportions of adjacent beam and column forces. The beam moments resisted by the inner and outer joint panels are calculated next. From these the connection capacity is found in terms of the total moments and shears in the beam and column. The final step in the analysis is a check to see if various transfer elements can carry the imposed internal forces. If this check does not confirm assumptions made in the previous calculations, those calculations should be revised accordingly.

Outer panel calculations are summarized in Fig. 4.13. The flow chart outlines a convenient sequence to calculate various parameters with the applicable equations from this chapter noted. The three basic steps consist of evaluating first, the effective outer panel width, second, the compression field shear strength, and finally, the resulting beam moment, M_o.

Figures 4.14a through f outline the inner panel calculations. Figure 4.14a presents an overview of the procedure, referencing sub procedures given in Figs. 4.14b through f. In Fig. 4.14a the process begins by evaluating the shear contribution of the concrete panel. As indicated in Fig. 4.14b, this evaluation depends on the specific joint detail used. Next, in Fig. 4.14a, contributions of the vertical joint reinforcement and vertical shear friction are determined. After this step the remaining solution is part of an iterative process, beginning with an assumed value for the concrete bearing zone length, a_c. Using a_c the equivalent vertical force, P_{eq}, and moment arm, jh, are calculated as outline in Fig. 4.14c. The moment arm, jh, is then used in the next step where the steel panel strength, V_s, is calculated following the procedure in Fig. 4.14d. M_{bi} is then calculated using either Eq. 4.17a or b as shown in Fig. 4.14e, depending on the assumption regarding the forces P_f, P_b and V_c. Referring to Fig. 4.14c, in details where there are no flange attachments, the assumption that the sum of P_f and P_b is less than V_c usually governs. In other cases, the sum of P_f and P_b is assumed to be equal to the column shear, V_c. Referring again to Fig. 4.14a, a second value of M_{bi} is calculated using Eq. 4.18b, and this value is compared to that calculated

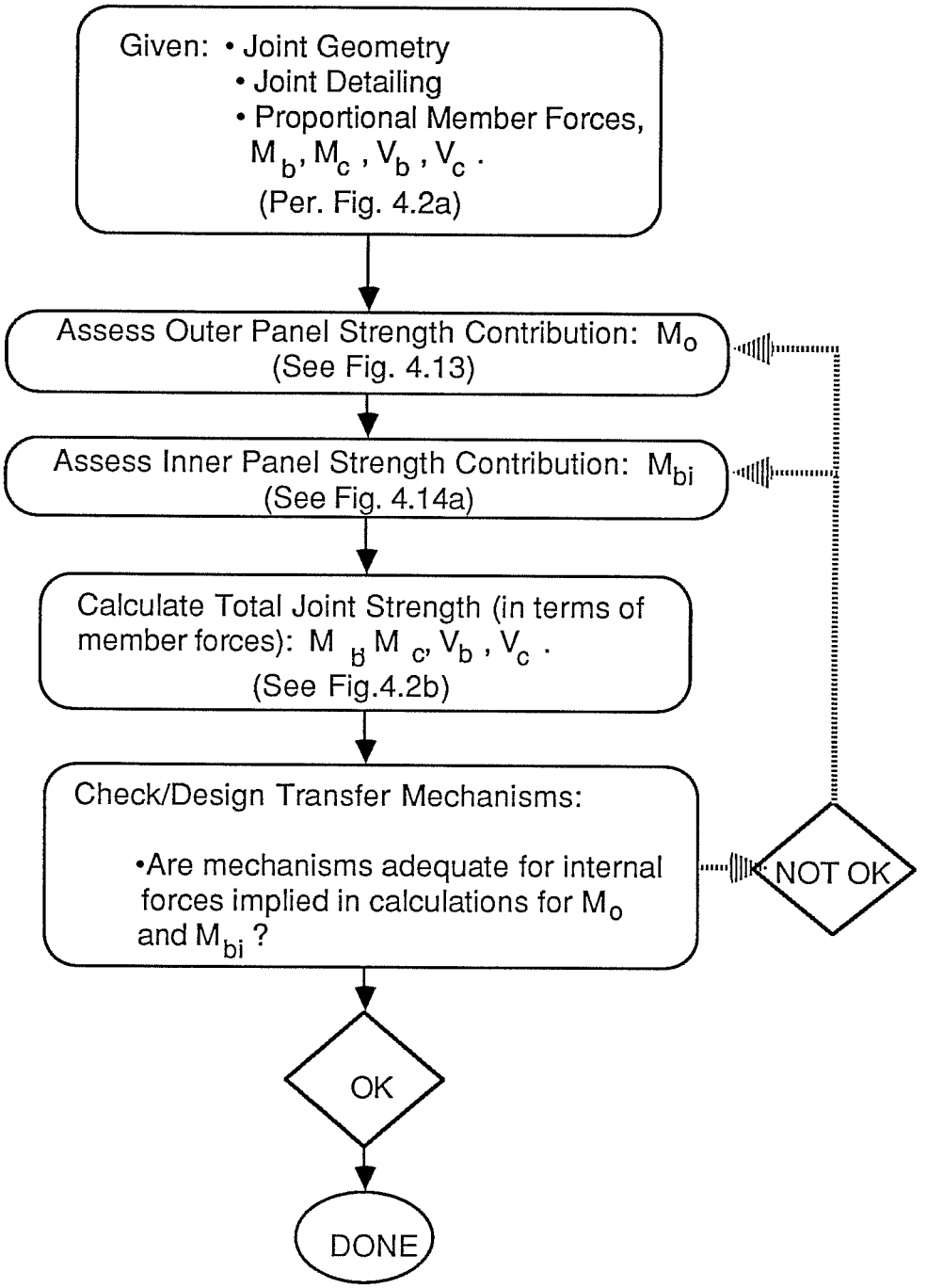

Fig. 4.12 General Procedure for Joint Assessment

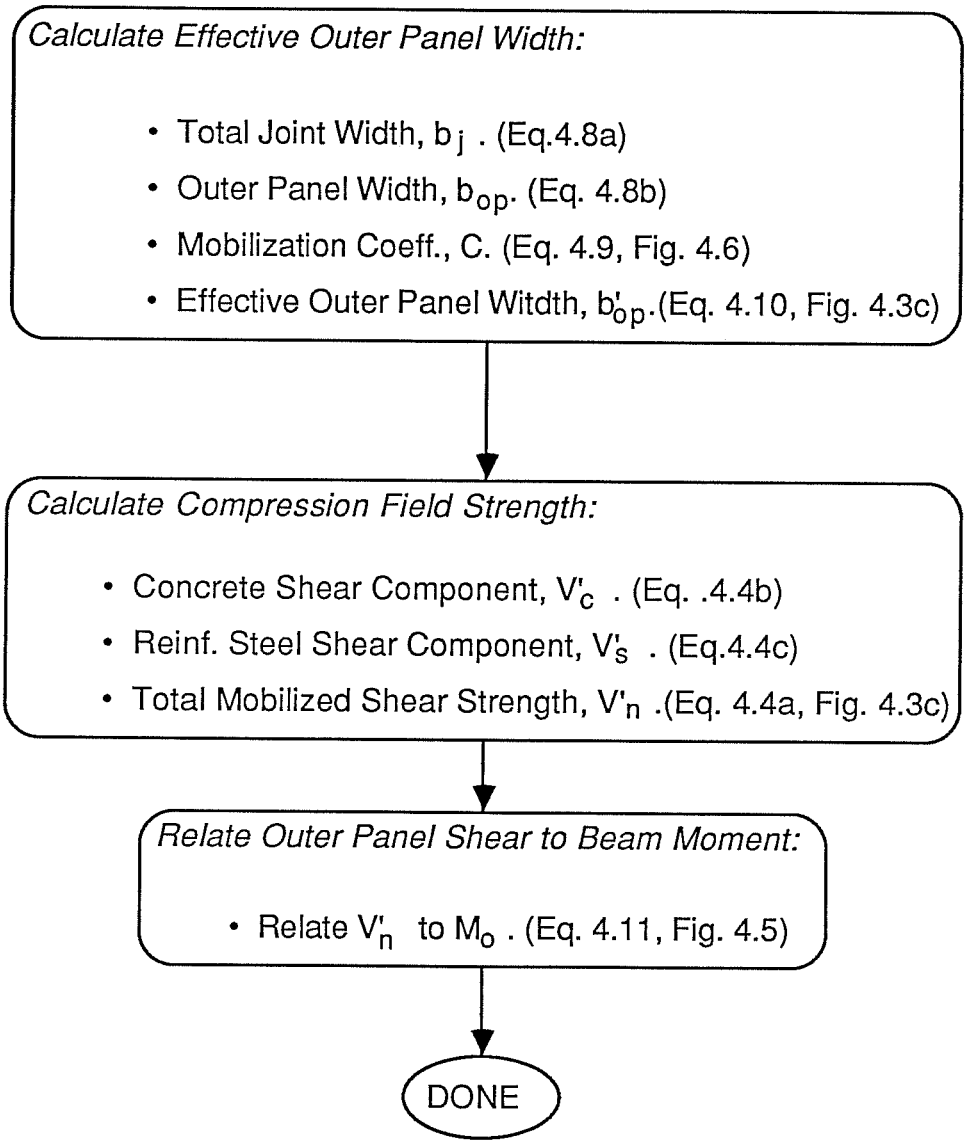

Fig. 4.13 Outer Panel Strength Calculation

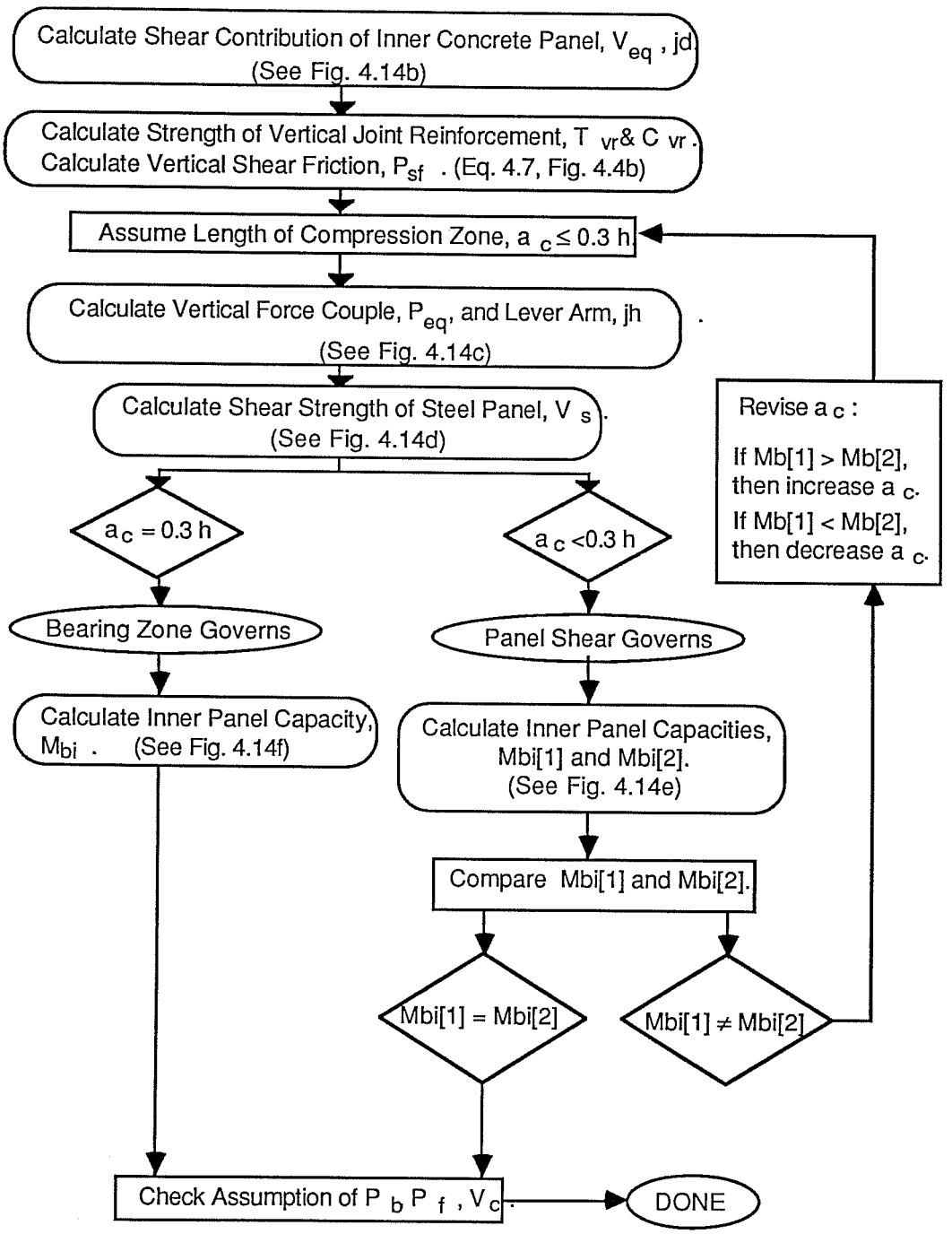

Fig. 4.14a Inner Panel Calculation for Mbi.

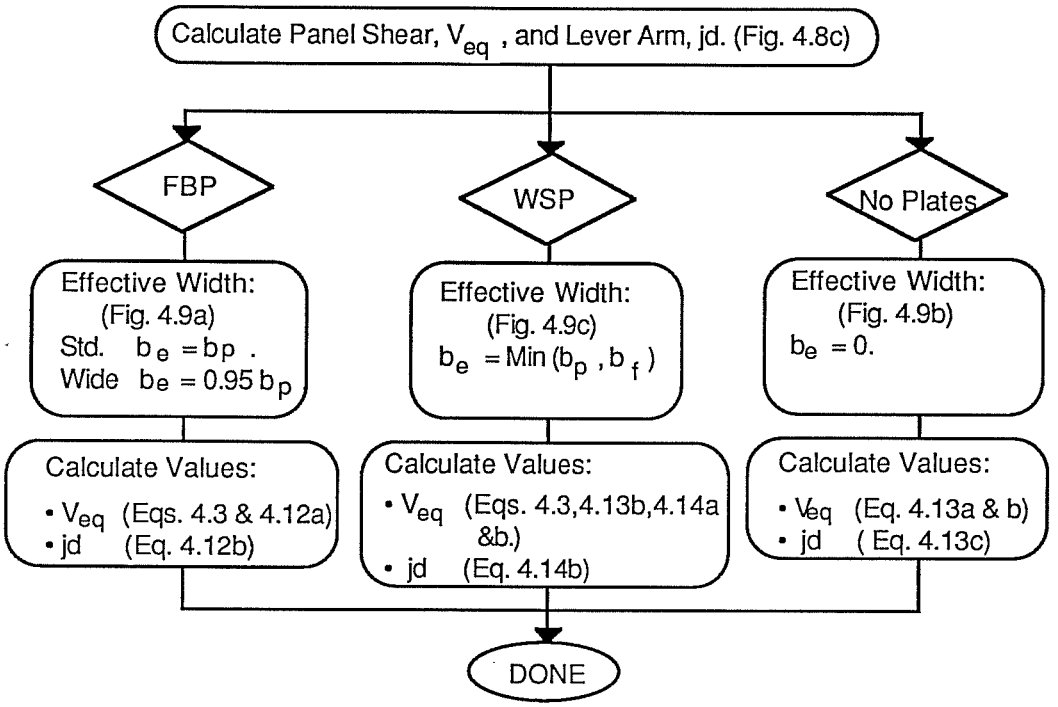

Fig. 4.14b Inner Panel Calculation for Veq and jd.

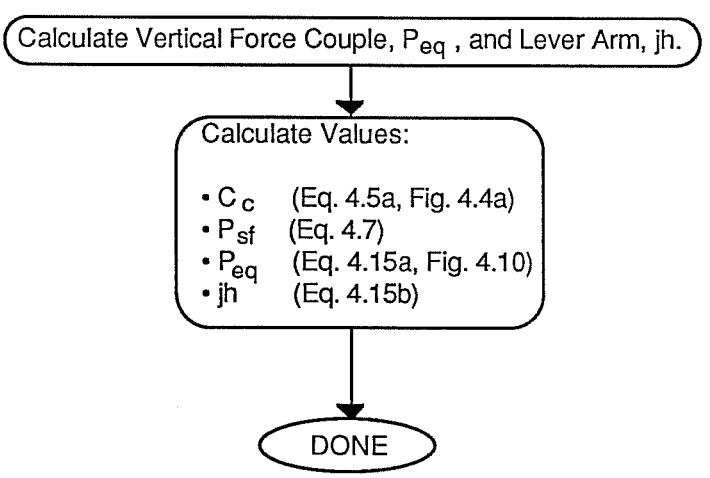

Fig. 4.14c Inner Panel Calculation for Peq and jh.

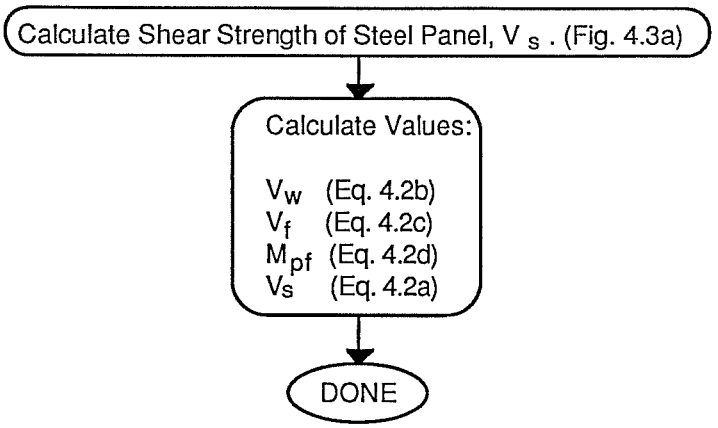

Fig. 4.14d Inner Panel Calculation for Vs

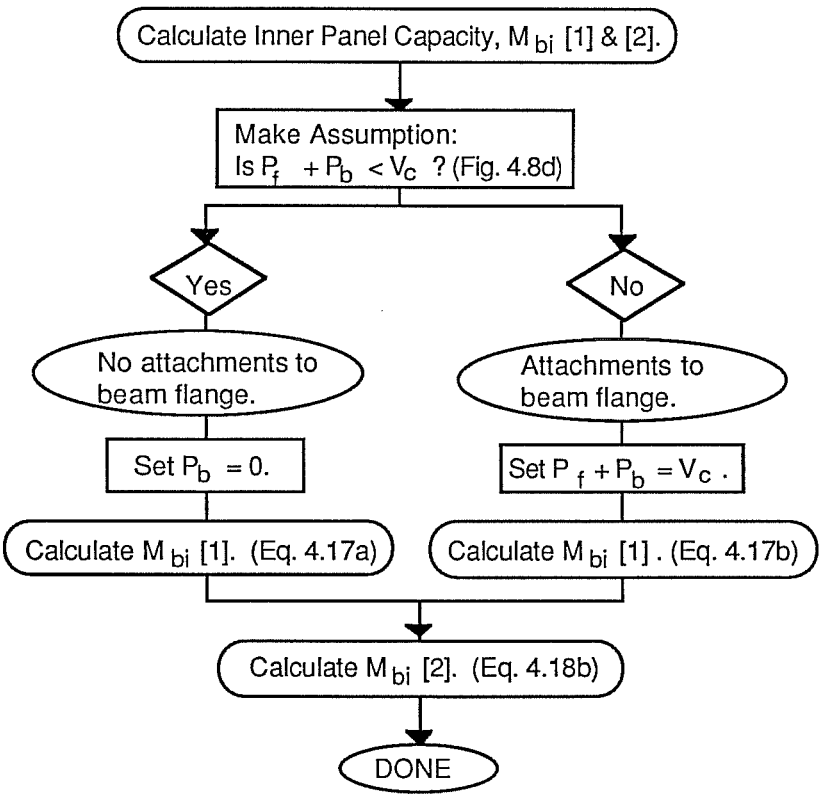

Fig. 4.14e Inner Panel Capacity, Mbi (Shear Governs)

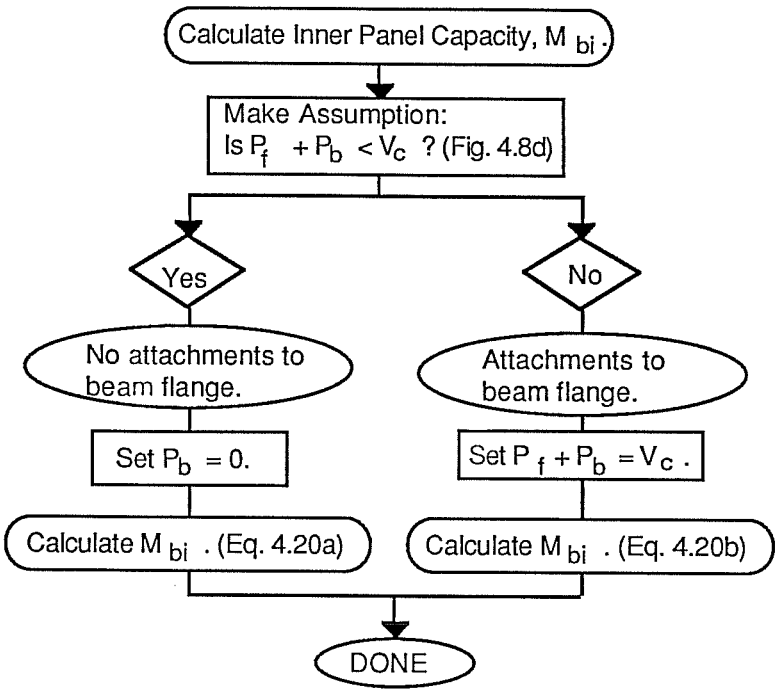

Fig. 4.14e Inner Panel Capacity, Mbi (Bearing Governs)

previously by Eq. 4.17a or b. The convergence check of M_{bi} determines whether a solution has been reached or the iteration continues with a new value for a_c. If a_c reaches its maximum limit of 0.3 h, and convergence has not been reached, then the connection is governed by concrete bearing stresses. In such cases, M_{bi} is calculated directly as outlined in Fig. 4.14f, using the value of jh calculated with a_c equal to 0.3 h. Once a solution has been obtained the assumption regarding P_f, P_b and V_c must be verified.

4.6 Comparison of Measured and Calculated Strengths

Table 4.2 is a summary of the measured and calculated joint strengths for Specimens 1 through 8 and 10 through 17. Joint strengths are expressed in terms of the applied beam shears. The test data corresponds to loading at

Table 4.2 Summary of Measured and Calculated Loads

Specimen	f'_c (ksi)	Beam Load @ 1% Drift (kips) Measured	Calculated	Failure Mode
1 Beam	3.6	17.0	17.9 (+5%)	Panel Shear
2 FBP	3.6	22.5	21.0 (−7%)	Vert. Bearing
3 Beam	4.5	16.5	15.9 (−3%)	Panel Shear
4 FBP	4.3	26.6	27.1 (+2%)	Panel Shear
5 FBP(thick)	4.3	28.2	27.1 (−4%)	Panel Shear
6 FBP-DP-Styr.	4.0	35.8	39.0 (+9%)	Vert. Bearing
7 FBP(wide)	4.0	33.8	32.5 (−4%)	Panel Shear
8 FBP(extend)	3.6	46.2	47.7 (+3%)	Panel Shear
10 FBP(split)	4.7	29.0	28.2 (−3%)	Panel Shear
11 FBP-DP-Dywi.	4.7	47.0	48.9 (+4%)	Horiz. Bearing
12 Stud	5.0	28.7	28.9 (+1%)	Panel Shear
13 FBP-Stud	5.0	42.8	41.8 (−2%)	Panel Shear
14 WSP-Col.	4.0	33.8	34.3 (+1%)	Panel Shear
15 FBP-Col.	4.0	37.0	37.3 (+1%)	Panel Shear
16 FBP-Col.-Clip	3.8	37.3	38.2 (+3%)	Panel Shear & Clip Yielding
17 FBP-Col.Dywi.	3.9	36.9	37.3 (+1.0%)	Panel Shear

1% TJD. Also shown in Table 4.2 are the controlling modes of failure for each specimen.

Calculated values compare quite well with the measured results. Typically, the calculated values range between -7% and +5% of the experimental values. Specimen 6 is an exception, with its computed load exceeding the measured value by 9%. The discrepancy in this specimen may be due to Styrofoam backing on the FBPs which adversely affects the lap splice of the cap ties within the beam depth. As vertical concrete bearing governs in Specimen 6, the vertical shear friction (Fig. 4.4b) contributed by the cap ties directly affects the

strength. If vertical shear friction is neglected, the capacity of Specimen 6 is 31.5 kips. Thus, if one supposes that the cap ties are only 50% effective because of the Styrofoam, the predicted strength is the average of 31.5k and 39.1 k, 35.3 k. This value is within -2% of the measured value.

As shown in Table 4.2, in most cases strength is controlled by joint panel shear. The panel shear is typically governed by yielding of the steel beam and by the concrete panel capacity. In Specimens 1, 3 and 14 the concrete panel capacity is limited by shear friction between the concrete and steel beam web. Otherwise, where panel shear controls, the concrete contribution is controlled by concrete strength and effective panel width. Where the outer panel compression field mechanism participates, in none of the specimens does shear reinforcement (lateral ties) control the panel strength. In all cases, the minimum shear reinforcement exceeds the amount required to develop the maximum width of the compression field. Minimum requirements for transverse reinforcement are recommended in Chapter 5.

Vertical concrete bearing controls the predicted joint strength in Specimens 2 and 6. This agrees with Sheikh's experimental observation[1] that at 1% TJD the steel web panels had not yielded in these specimens. In Specimen 11 the outer panel capacity is limited by the maximum horizontal concrete stress against the Dywidag bars and couplers.

In Specimens 16 and 17, calculated outer panel capacities are based on the details which offer largest mobilization of concrete. In Specimen 17, calculations based on the Dywidag Bar detail indicate about 12% more outer panel participation than those based on the steel column detail (see Fig. 4.7). Upon first inspection the clip angle detail in Specimen 16 appears to mobilize the outer panel as effectively as the extended FBP in Specimen 8. However, as noted both experimentally and analytically, the force transferred by the clip angle is limited by plastic hinging near its base. The predicted load for Specimen 16 is obtained by adding the small contribution of the clip angle to that of the steel column detail.

CHAPTER 5 - DESIGN RECOMMENDATIONS

5.1 Introduction

Design recommendations for composite beam-column connections are presented in this chapter. The underlying design philosophy follows that of the 1986 AISC LRFD specification[10] where the margin of safety is provided through load and resistance factors. The recommendations include a simplified version of the analytic model described previously in Chapter 4 to calculate the nominal connection strength. Detailing recommendations are based on the results of the research herein and on applicable standards for reinforced concrete and structural steel connections. The design guidelines also draw in part from recommendations for composite joints proposed by Sheikh.[1] Finally, practical concerns involving construction considerations, limitations of the design guidelines, and applicability of the design concepts to other joint configurations are addressed.

5.2 Design Philosophy

The objective in connection design is to proportion and detail a beam-column joint which insures satisfactory frame behavior under both service and ultimate loads. In evaluating design criteria for the composite joint one of two approaches may be taken. One approach is to assess the influence of joint response on overall frame behavior through a rigorous analysis accounting for joint flexibility. Results of such an analysis should be assessed using realistic standards to define satisfactory behavior. This approach is rarely if ever used in practice for two reasons. First, sophisticated computer modeling tools are not readily available to perform the analysis. Second, having evolved gradually the standards which define satisfactory behavior are closely linked to assumptions inherent in the analysis. Hence a rigorous analysis would involve not only advanced structural analysis techniques but also careful reassessment of environmental loadings and the more basic criteria and standards which define satisfactory behavior. For example, in tall buildings traditional drift indices which serve as rule of thumb to control wind induced deformations and motion are inextricably tied to the

level of sophistication in the analysis. A second approach for evaluating composite joint design criteria involves comparing behavior with that of structural steel and reinforced concrete joints. This argument implies that since current standards for designing structural steel and reinforced concrete joints result in satisfactory structures, similar standards and performance in composite joints will produce satisfactory response. The second approach is followed in this report because it utilizes the established reliability of successful joint design in structural steel and reinforced concrete.

As discussed in Chapter 4, load-deformation behavior of composite joints is similar to that of structural steel and reinforced concrete joints. Based on a deformation of 1% total joint distortion (TJD) for the design strength deformations of about 0.2% TJD are expected at service load. The composite joint deformation at service load is comparable to that reported for structural steel or reinforced concrete joints. One can reason, therefore, that currently accepted design practice for structural steel or reinforced concrete joints is applicable to composite joints.

Since composite connections occur most frequently in buildings consisting primarily of structural steel, the design recommendations incorporate design methodology of the American Institute of Steel Construction's LRFD specification.[10] In this specification load and resistance factors provide for a factor of safety against member and connection failures at ultimate load. The relationship between applied loads and required strength is given by the following equation[10]:

$$\gamma_i \, Q_i \leq \phi \, R_n \tag{5.1}$$

The left side of this equation is the required strength given as the summation of applied loads, Q_i, multiplied by the appropriate load factors, γ_i. The design strength given on the right sides is equal to the product of the nominal (calculated) resistance, R_n, and a capacity reduction or resistance factor, ϕ. Equations for calculating the nominal connection strength are given in Sec. 5.3.

AISC specifications for steel design have traditionally been developed to provide connections with a larger margin of safety than members. In the LRFD

specification, reliability indices (β factors) incorporated in the development of resistance (ϕ) factors provide the relative difference in safety. The relationship between reliability and resistance factors is described subsequently. Essentially, however, the resistance factors in the current LRFD specification are calibrated to the previous AISC Allowable Stress Specification[23] where the factor of safety for connections is roughly 1.2 times that of members (F.S. Connection = 2.0, F.S. Member = 1.67).

The LRFD specification does not address serviceability criteria directly. Traditionally, serviceability criteria and the evaluation of such have been left to the judgment of structural designers. When assessing serviceability it is recommended that composite joints be treated like welded joints in steel frames. Sheikh[1] summarizes the current state of practice regarding treatment of joint flexibility in building design.

5.2.1 Required Strength. The connection design should distinguish between cases where lateral loading due to either wind or seismic forces governs. Under wind loading the structural response is assumed to remain essentially elastic. For seismic loading, however, most building code provisions specify lateral loads based on the premise that under severe earthquakes the structure will undergo inelastic cyclic loading. The energy dissipation provided by inelastic response allows the use of equivalent static design loads which are roughly 1/3 of those required for the structure to remain elastic.[13]

Wind Loading. For wind and other loadings where elastic response is assumed, the connection should be designed for the most severe combination of forces in adjacent members following Eq. 5.1 using load factors given in the LRFD specification. The LRFD specification has adopted load factors from the American National Standard: *Minimum Design Loads for Buildings and Other Structures, ANSI A58.1.*[24] Where wind loading governs the load factor of 1.3 specified in LRFD is nearly the same as the factor of 1.28 (1.7×0.75) specified by ACI-318-83.[15].

Earthquake Loading. For seismic loading and other cases where inelastic response is envisioned, the connection should be designed to resist moments

and shears associated with plastic hinging of adjacent members. Following the ACI-318-83 provisions for seismic design, the concrete (or composite) columns framing into the joint should have a moment capacity at least equal to 1.2 times that of the beams framing into the connection. Using such criteria, the composite connection forces are limited by plastic hinging of the steel beams. The LRFD load and resistance factors (Eq. 5.1) apply in determining the minimum beam capacity based on the design lateral loads. For seismic forces the LRFD load factor of 1.5 exceeds that of 1.4 ($1.7 \times 1.1 \times 0.75$) specified by ACI-318-83. The design capacity of the connection, $\phi\, R_n$, should exceed that required to carry the beam moments and shears associated with the nominal beam capacity, M_p. Since the capacity reduction factors as described below provide a larger average factor of safety in the connection, the nominal beam capacity does not need to be increased above M_p to account for such factors as strain hardening which may increase applied forces due to beam hinging.

5.2.2 **Design Strength.** The design strength of the connection is obtained by reducing the nominal strength by a resistance factor, ϕ. The nominal joint strength is calculated using the design model and recommendations presented later in this chapter. The resistance factor for the composite joint should be taken as 0.7, the basis for which is described below. This factor is applied to the overall joint strength.

Theoretically, the LRFD resistance factors are developed on a statistical basis which provides a consistent and known level of reliability for structural components. The statistical derivation for the resistance factor is given by the following equation[10]:

$$\phi = \frac{R_m}{R_n} e^{-0.55\beta V_r} \tag{5.2}$$

In this expression R_m and R_n are the actual and calculated mean resistances (strengths) of the component under consideration, and V_r is the coefficient of variation of the resistance. The β value is a reliability index which calibrates the ϕ factor to provide a desired level of safety. In the LRFD specification connections are targeted for a reliability index (β) of 4.5 while member values range between

1.75 and 3.0. The difference in these values provides the additional margin of safety for connections.

In reality, current LRFD resistance factors were determined largely by calibration to provide similar factors of safety with the previous AISC Allowable Stress specification.[25] This is evidenced by the fact that the reliability factors (β) for connections are scattered between values of 1.9 and 5.9. In developing a resistance factor for composite joints the derivation is similarly based largely on calibration to currently established resistance factors for other elements. Statistical theory is only addressed insofar as to tie the calibration back to the resulting reliability, mean value, and coefficient of variation factors.

The capacity reduction factor of 0.7 is obtained through a comparative analysis of ϕ factors currently accepted for other components. First, the premise that the joint should have an additional margin of safety of 1.2 over the adjacent members is considered. Again, this margin is the same as that implied in Allowable Stress Design of steel structures. In this case the adjacent members are considered to be a composite column and a steel beam. The respective ϕ factors given by LRFD for these elements are 0.85 and 0.9. Dividing these by 1.2 results in maximum connection ϕ factors of 0.71 to 0.75.

A second approach to considering the connection ϕ factor is by relating it to factors associated with individual elements and modes of failure in the joint. Such factors range from a maximum of 0.9 for steel yielding to a minimum of 0.6 (LRFD) or 0.7 (ACI-318) for concrete bearing. The minimum factor of 0.7 is considered adequate based on the following reasoning. The 0.6 LRFD factor is derived directly from ACI by adjusting the ACI value of 0.7 based on the ratio of dead load factors between the specifications. The respective dead load factors in the LRFD and ACI specifications are 1.2 and 1.4 which result in an adjustment factor of 0.86. For composite connections this derivation is overly conservative since the connection is typically governed by wind or seismic loads where the LRFD load factors in fact exceed those of ACI by the ratios 1.02 (1.3/1.27) to 1.07 (1.5/1.4).

Finally, the ϕ factor of 0.7 can be tied to statistical theory using Eq. 5.2. Where there is not sufficient data to provide a reasonable statistical basis assumed values are used in Eq. 5.2 to estimate the results. By setting ϕ to 0.7, the ratio of mean strengths (R_m/R_n) to unity, and β to 4.5, the resulting coefficient of variation, V_r, is 0.144 from Eq. 5.2. This coefficient of variation implies that in a normally distributed data set roughly 49% of the values will be at least 10% away from the mean value and 17% at least 20% away. In other words, the desired β value can be achieved with a population of data having fairly wide scatter. Typically, the situation will be better than that assumed since the analytic design models underestimate the nominal strength, R_n, and hence the ratio of R_m/R_n is greater than unity. Based on comparison to test data made in Sec. 5.3, the ratio of R_m/R_n is 1.06 which when used in the calculation above results in a coefficient of variation of 0.168.

5.3 Calculation of Nominal Joint Strength

The nominal joint strength is calculated using a simplified version of the model previously developed in Chapter 4. (Simplifying modifications for the design model are summarized below.) Description of the design model is limited to those aspects needed to understand and apply the model; further background information is given in Chapter 4.

In the model two primary connection failure modes are considered: joint shear failure and vertical bearing failure. In order for the model to correctly estimate joint strength, structural steel and reinforcing bar details must be designed to carry the imposed forces. Where such details cannot carry the internal forces, the joint capacity should be reduced accordingly. Specific detailing requirements and recommendations are discussed later.

5.3.1 Simplifications to Model for Design In formulating the design model several modifications are made to the model presented previously in Chapter 4. The end result of the simplifications outlined below is to make the design model slightly more conservative and easier to use.

In the design model contribution of the plastic hinging of the beam flanges to the steel panel strength is neglected. This change has a more significant affect on the calculated strength of the experimental joint details than on details typically used in practice. The hybrid steel beam flange in this study contributes roughly 12% to the steel panel strength. For rolled beam shapes the flange contribution is in the range of 2% to 7%. Hence, neglecting the flange in rolled sections will have less effect.

Also neglected in the design model is the contribution of horizontal shear friction between the concrete and steel web mobilized by ties passing through the web. This change will significantly influence the calculated capacity of Specimens 1 and 3 without FBPs or WSPs between the flanges. For most steel details and erection procedures, some type of web stiffener is usually included in the joint region. Neglecting the shear friction contribution eliminates the uncertainty or concern regarding proper tie arrangements for developing shear friction.

The vertical component of shear friction provided by the ties is also neglected in design, thus decreasing computed strength of joint details governed by concrete bearing. This again eliminates uncertainty or concern regarding special tie detailing requirements, and encourages use of vertical reinforcement attached to the beam flanges. Such reinforcement will provide a stiffer and more reliable means than shear friction to transfer vertical loads into the concrete.

To further simplify the procedure, the inner and outer panel calculations are combined into one step. To accomplish this the concrete bearing zone calculation is modified to reflect a width equal to the effective joint width rather than the beam flange width. The net result is that the bearing calculation is slightly less conservative, which happens to partially offset the conservative effect of neglecting the vertical shear friction.

5.3.2 <u>Comparison with Phase I Model</u>**.** Aspects of this design model are similar to one presented previously by Sheikh,[1] however, there are several major differences in the models. First, this model is calibrated to the

joint strength at 1% TJD whereas Sheikh's is calibrated at 2% TJD. As discussed in Chapter 3, the load at 2% TJD is roughly 10% to 20% higher than that at 1% TJD. Second, this model is more comprehensive in that it includes provision for contribution of the steel column, shear studs, WSP and vertical joint reinforcement in addition to the FBP configurations addressed by Sheikh's model. In order to handle these details this model divides the concrete participation between inner and outer panels. Sheikh's model includes only the inner panel mechanisms.

5.3.3 Effective Joint Width. The effective joint width measures the region of concrete mobilized to resist joint shear in the connection panel. The joint width is a function of how effectively particular joint details transfer force into the concrete outside the beam width.

The joint width is shown in Fig. 5.1a. The effective joint width , b'_j, is determined by the following expression:

$$b'_j = b_i + b'_{op} \tag{5.3}$$

The terms, b_i and b'_{op}, refer to the width of concrete allocated to the inner and outer panel shear mechanisms respectively. The inner panel width, b_i, is typically the greater of the beam flange width, b_f, or stiffener plate width, b_p. Where stiffeners are used in a WSP or split FBP configuration, in calculations the plate width, b_p, should not be taken greater than the flange width, b_f. Also, where a wide FBP configuration is used, the plate width beyond the flanges may be ignored in calculations if it is beneficial to allocate a greater width to the outer panel region. In such cases b_p is set equal to b_f, thereby reducing the calculated inner panel width to the beam flange width.

The outer panel width, b'_{op}, is given by the following expression:

$$b'_{op} = C\,(b_j - b_i) \;\leq\; 2\,d_{op} \tag{5.4a}$$

$$b_j = (b_f + b)/2 \;\leq\; b_f + h \;\leq\; 1.75\,b_f \tag{5.4b}$$

$$C = (x/h)\,(y/b_f) \tag{5.4c}$$

The term, b_j, in Eqs. 5.4a and 5.4b is the joint width based on the ACI-ASCE[8] recommendations for reinforced concrete joints. The upper bound of 1.75 b_f on b_j is based on the limits of the composite joint experimental data. The outer panel mobilization coefficient, C, in Eqs. 5.4a and 5.4c indicates effectiveness of the joint detail in transferring force to the outer panel. The variables used to calculate C in Eq. 5.4c are shown in Fig. 5.1b. Where an extended FBP of width b_f is used, C has a value of 1.0. Where a steel column is used C has a value less than 1.0, based on the geometry shown in Fig. 5.1b. Calculation of C for details other than the extended FBP and the steel column are described in Chapter 4. Finally, the joint panel height is equal to the beam depth, d, plus twice the panel extension, d_{op}. The dimension, d_{op}, depends on the specific joint detail but should not be taken larger than 25% of the beam depth.

5.3.4 Joint Shear Mechanisms. The joint shear mechanisms include the steel web panel, the concrete compression strut, and the concrete compression field. The capacity of each of these elements is indicated by its horizontal shear strength as shown in Figs. 5.2a through 5.2c. The steel web panel strength, V_s, is given by the following formula:

$$V_S = 0.6\, F_{yw}\ t_w\ jh \tag{5.5}$$

The effective panel width, jh, is a function of the vertical bearing region discussed in the next section. The horizontal steel panel shear forces are separated by the vertical distance, d_f, measured between the flange center lines.

The concrete in the inner panel carries shear through a compression strut mechanism (Fig 5.2b) whose strength is calculated by the following equations:

$$V_n = 0.63\sqrt{f'_c}\ R\, b_p\, h \tag{5.6a}$$

$$\text{FBP Detail: } b_p \le b_f \qquad R = 1.0 \tag{5.6b}$$

$$b_p > b_f \qquad R = 0.95 \tag{5.6c}$$

$$\text{WSP Detail: } b_p \le b_f \qquad R = 0.7 \tag{5.6d}$$

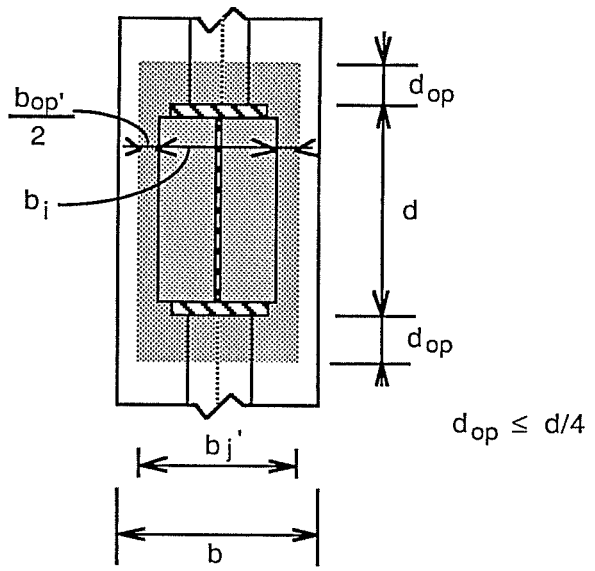

Fig. 5.1a Effective Joint Width

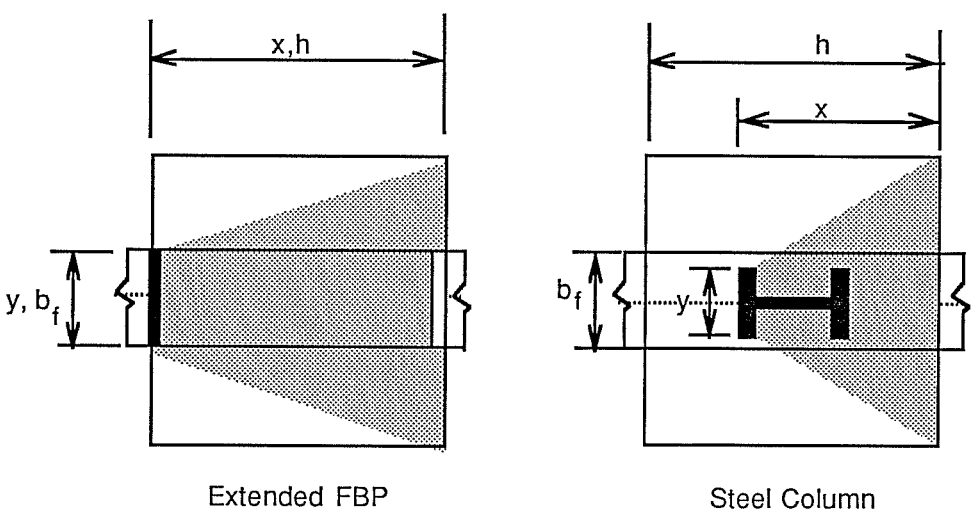

Fig. 5.1b Outer Panel Mobilization Coefficient

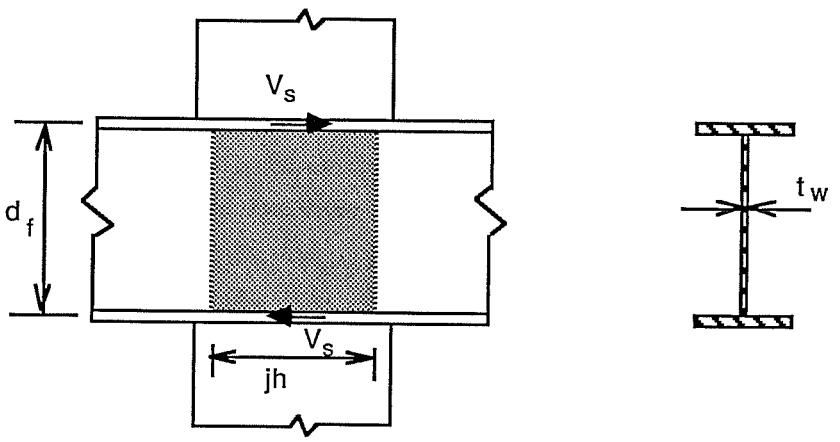

Fig. 5.2a Steel Web Panel

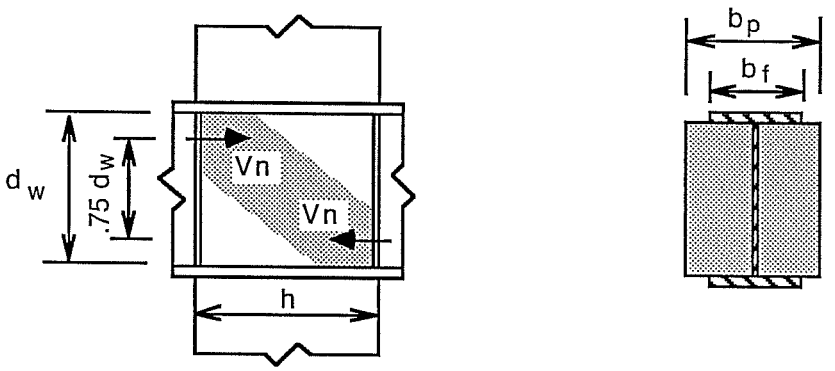

Fig. 5.2b Concrete Compression Strut

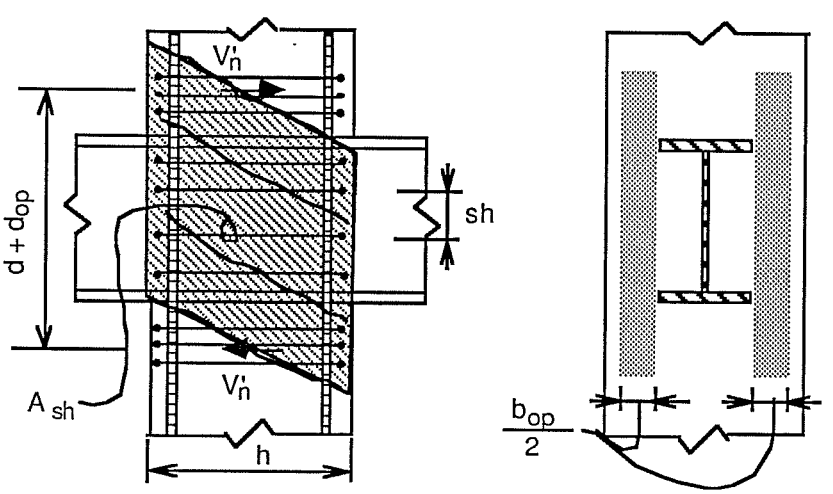

Fig. 5.2c Concrete Compression Field

With regard to the joint width calculations, the WSP and Split FBP widths should not be taken larger than the beam flange width as noted previously. Also, a consistent value of the FBP width should be used in the joint width and compression strut calculations. The R factors given above reduce the strut capacity for WSPs and wide FBPs to reflect test results. Where there are no stiffeners between the flanges the strut capacity is taken as zero. The vertical distance between the horizontal strut resultant, V_n, is equal to 3/4 of the web height ($0.75\ d_w$) as shown in Fig. 5.2b.

Concrete in the outer panel is mobilized in a compression field (Fig. 5.2c) where strength is calculated according to the following equations:

$$V_n' = V_c' + V_s' \leq 0.63\ \sqrt{f_c'}\ b_{op}'\ h \tag{5.7a}$$

$$V_c' = 0.16\ \sqrt{f_c'}\ b_{op}'\ h \tag{5.7b}$$

$$V_s' = 0.9\ A_{sh}\ F_{ysh}\ h/s_h \tag{5.7c}$$

As given by Eq. 5.7a the compression field capacity is the sum of contributions of the concrete and horizontal steel reinforcement. As shown in Fig. 5.2c, the horizontal force couple for the compression field acts with a vertical lever arm distance equal to $d + d_{op}$.

5.3.5 Vertical Force Couple. In the joint shear mechanisms, the horizontal beam flange forces are resolved into a vertical force couple in the column. The transfer of vertical load between the joint and the column is achieved primarily through the concrete bearing zone and the vertical joint reinforcement shown in Figs. 5.3a and 5.3b. Vertical joint reinforcement typically consists of steel reinforcing bars or rods attached to the steel beam.

The concrete bearing zone is treated as an equivalent rectangular stress block as shown in Fig. 5.3a. The total force transferred through bearing, C_c, is given by the following equation:

$$C_c = 2\ f_c'\ a_c\ b_j' \tag{5.8a}$$

$$a_c \leq 0.3\ h \tag{5.8b}$$

In calculating C_c the bearing zone length, a_c, is varied while the bearing zone width, b_j', and concrete stress, $2f_c'$, are kept constant. The width of the zone equals the effective joint width, b_j'. The length, a_c, is limited to a maximum value of 0.3 times the column depth. A uniform concrete bearing stress of $2f_c'$ is used to reflect confinement of the concrete by steel reinforcement and surrounding concrete. This concrete stress is more conservative than the value of $3f_c'$ recommended by Sheikh.[1]

Contribution of the vertical joint reinforcement is shown in Fig. 5.3b, indicated by the forces C_{vr} and T_{vr}. These forces are based on the joint reinforcement capacity, a topic addressed later in this chapter. Where such reinforcement is used, it is assumed that the reinforcement is fully stressed and the concrete bearing zone carries a force less than or equal to its full capacity. In other words, the bearing zone length, a_c, is less than its maximum value of 0.3h.

In the joint calculations, the concrete bearing and joint reinforcement contributions are combined into the equivalent force couple shown in Fig. 5.3c. The vertical force, P_{eq}, and the horizontal lever arm, jh, are calculated using the following equations:

$$P_{eq} = C_c + T_{vr} + C_{vr} \tag{5.9a}$$

$$jh = \left[C_c\,(h - a_c) + (T_{vr} + C_{vr})\,h_{vr}\right] / P_{eq} \tag{5.9b}$$

The horizontal lever arm, jh, is the value used in Eq. 5.5 to evaluate the steel panel capacity.

5.3.6 Joint Equilibrium. Joint equilibrium is shown in Figs. 5.4a through 5.4d. For a given joint size and structural configuration, member forces (Fig. 5.4a) are assumed to be related as follows:

$$M_b = \alpha_1\, V_b \qquad (\alpha_1,\ \text{inches}) \tag{5.10a}$$

$$M_c = \alpha_2\, V_b \qquad (\alpha_2,\ \text{inches}) \tag{5.10b}$$

$$V_c = \alpha_3\, V_b \tag{5.10c}$$

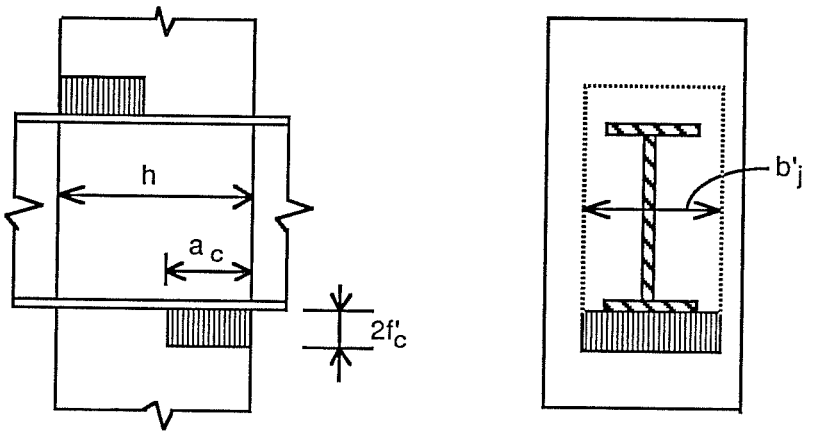

Fig. 5.3a Concrete Bearing Zone

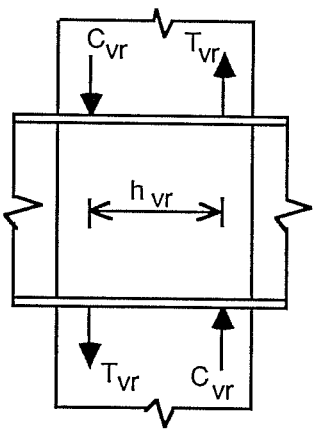

Fig. 5.3b Vertical Joint Reinforcement

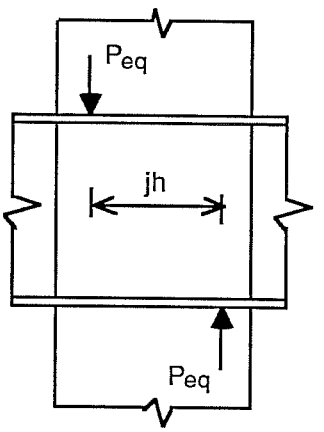

Fig. 5.3c Equivalent Vertical Force Couple

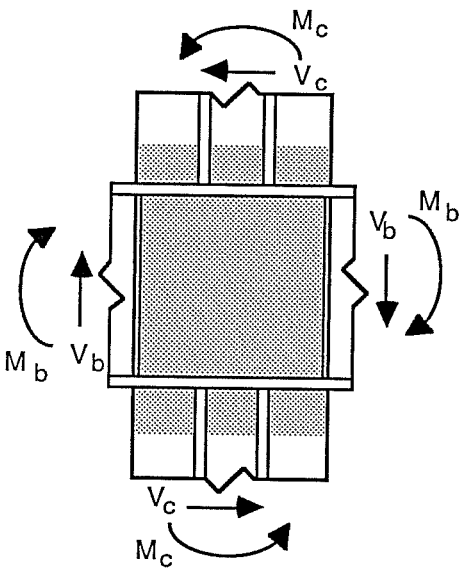

Fig. 5.4a Member Forces

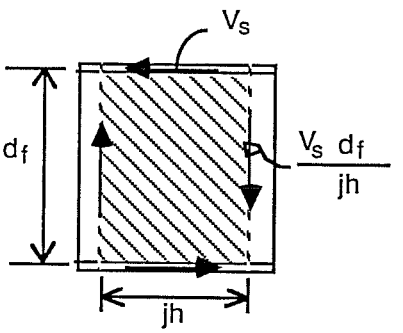

Fig. 5.4b Steel Web Panel Forces

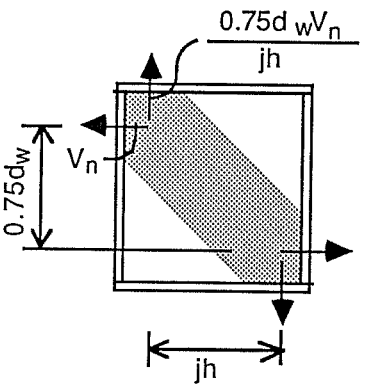

Fig. 5.4c Compression Strut Forces

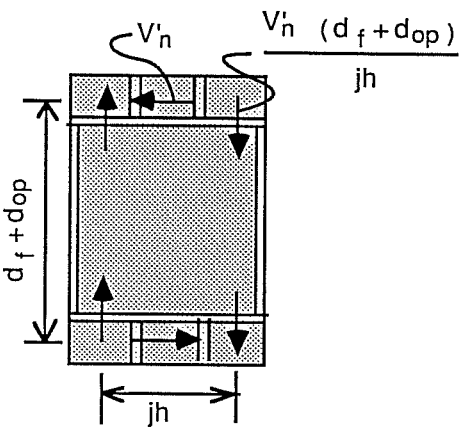

Fig. 5.4d Compression Field Forces

The internal joint forces are shown in terms of the joint shear components in Figs. 5.4b through 5.4d. In these figures the horizontal forces are the joint shear capacities shown previously in Figs. 5.2a through 5.2c. The vertical components in Figs. 5.4b through 5.4d are obtained by satisfying moment equilibrium for each panel subjected to the horizontal forces shown.

By equating beam moments at the column face to the horizontal joint shear force couples, the following equation is obtained:

$$M_b = \frac{[V_s\, d_f + V_n\, (0.75\, d_w) + V_n'\, (d + d_{op}) - (J\, V_c)\, d_f\,]}{2} \qquad (5.11)$$

The last term in Eq. 5.11 reflects the reduction in joint shear due to the horizontal force resisted by column shear, V_c. The coefficient, J, modifies the contribution of the column shear in the joint as a function of the method used for transfer of horizontal force between the beam flanges and concrete column. In connections where attachments to the beam flange, such as the steel column, provide a direct means of transferring column shear into the beam a J coefficient of 1.0 should be used. Where no direct means of transfer exists, J may be taken as 0.4 to account for force transferred via shear friction in the concrete bearing zone.

When the column shear, V_c, is expressed in terms of the beam moment, M_b, using Eqs. 5.10a and 5.10c, then Eq. 5.11 may be rewritten as follows:

$$M_b = \frac{V_s\, d_f + V_n\, (0.75\, d_w) + V_n'\, (d + d_{op})}{2 - (J\, d_f\, \alpha_3\, /\, \alpha_1)} \qquad (5.12)$$

When the connection is governed by shear capacity, the values of V_n and V_n' are known based on formulas already presented. In addition, V_s can be expressed as a function of the concrete bearing zone length, a_c. Hence, where joint shear controls, Eq. 5.12 reduces to one equation with the two unknowns, M_b and a_c.

A second equation relating the unknowns, M_b and a_c, is found by equating the vertical joint shear forces in Figs. 5.4b through 5.4d to the vertical force couple in Fig. 5.3c:

$$P_{eq} = \frac{[V_s\, d_f + V_n\, (0.75\, d_w) + V_n'\, (d + d_{op})]}{jh} + V_b \qquad (5.13)$$

When the beam shear, V_b, is expressed in terms of the beam moment, M_b, using Eq. 5.10a, then Eq. 5.13 may be rewritten as follows:

$$M_b = \alpha_1 \left(P_{eq} - \frac{V_s\, d_f + V_n\,(0.75\, d_w) + V_n'\,(d + d_{op})}{jh} \right) \qquad (5.14)$$

By substituting the joint shear capacities, Eq. 5.14 reduces to one equation with two unknowns, M_b and a_c. Thus, when the joint is controlled by shear capacity, Eqs. 5.12 and 5.14 can be solved simultaneously for a_c and M_b. As described in Chapter 4, such equations are conveniently solved through iteration.

Where the connection is controlled by concrete bearing, the concrete bearing zone length a_c is given as 0.3 h. In this case the joint shear elements are not stressed to their full capacity and hence the values for V_s, V_n and V_n' become unknowns in Eqs. 5.12 and 5.14. The equations may be combined to eliminate the unknown quantities resulting in the following equation for the beam moment:

$$M_b = \frac{jh\, P_{eq}}{2 - (J\, d_f\, \alpha_3 \,/\, \alpha_1) + jh \,/\, \alpha_1} \qquad (5.15)$$

Once the connection capacity is known in terms of the beam moments using either Eqs. 5.12 and 5.14 or Eq. 5.15, the remaining member forces can be calculated by Eqs. 5.10a through 5.10c.

5.3.7 Solution of Design Equations. A schematic diagram for calculation of the joint panel capacity is shown in Fig. 5.5. The approach outlined in Fig. 5.5 is similar to that presented previously in Chapter 4, but reflects the simplifications incorporated in the design equations. In Fig. 5.5 equation numbers are referenced in applicable steps of the solution.

5.4 Evaluation of Design Model

In this section the design model for calculating the connection strength (Sec. 5.3) is compared with measured values. Additionally, the design model is compared with more detailed, and presumably more precise, analysis described in Chapter 4. Comparison is also made with strengths calculated based on Sheikh's

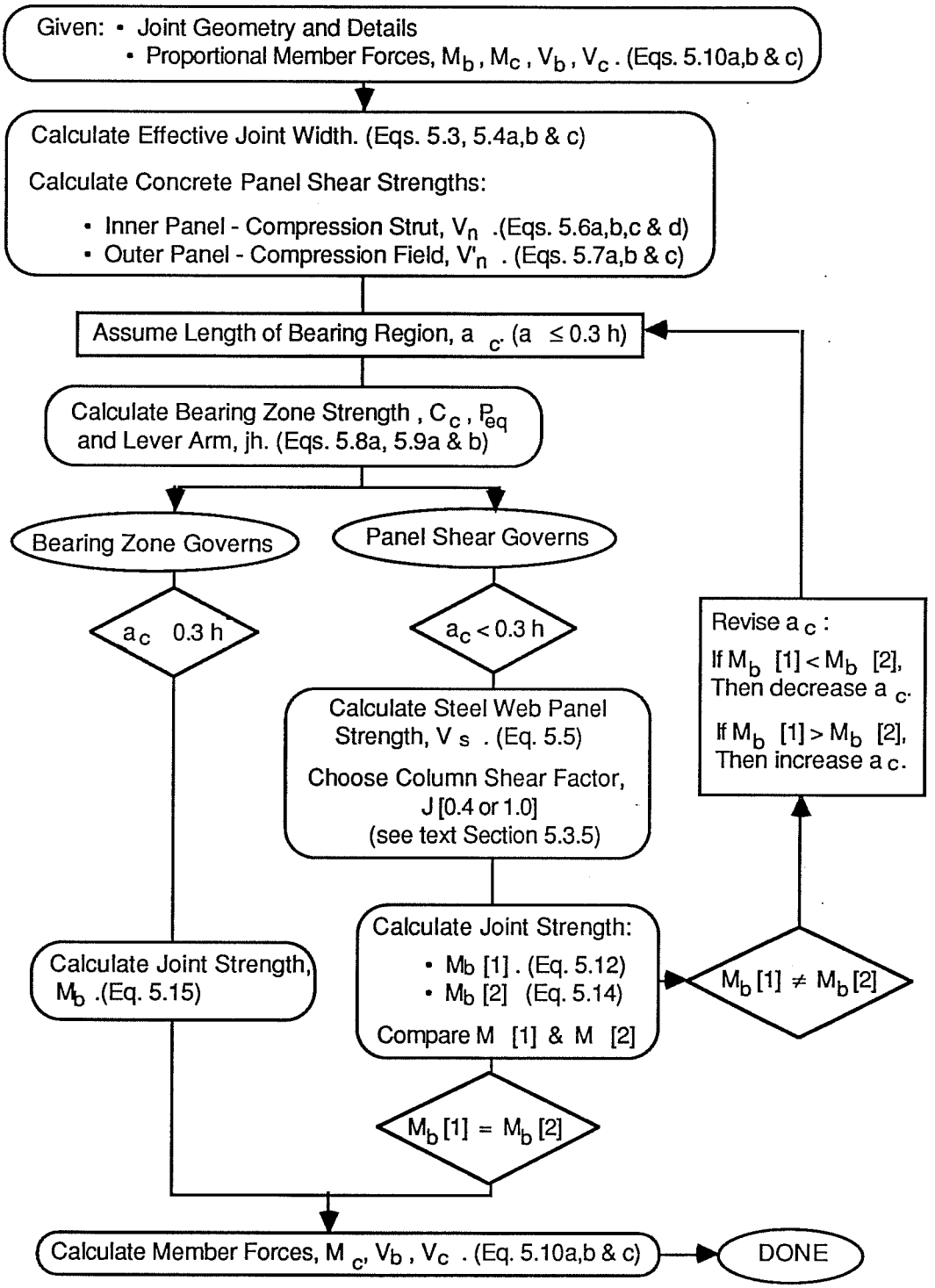

Fig. 5.5 Calculation of Nominal Joint Strength

model. Joint strengths for several representative examples of full size connections are also included. Calculations for two of the connection designs are presented in Appendix A3.

5.4.1 Test Specimens. Measured and calculated joint capacities for Specimens 1 through 8 and 10 through 17 are presented in Table 5.1. Table 5.1 also lists the percentage difference between the calculated design and measured values. The calculated design values per Chapter 5 consistently underestimate the measured strengths by 1% to 34%. Where values differ by more than 12% the discrepancy is reconciled in part by considering the particular circumstances involved. In Specimens 1, 3, and 12 where values differ by -13%, -34% and -21% respectively, the large differences arise because no FBPs or WSPs are present in the specimens. Since the design model does not incorporate contribution of the concrete strut mobilized by friction, joint capacity is purposely underestimated. Where design strength is controlled by the vertical concrete bearing in Specimens 2 and 6, a conservative estimate of the maximum bearing stress results in underestimates of -31% and -15%, respectively. The conservative bearing stress encourages use of vertical joint reinforcement which is found to be beneficial when concrete stresses are high. If the conservative results of Specimens 1, 3, 12, 2 and 6 are neglected there is good agreement between the calculated and measured strengths where the average ratio between the two is 0.95.

5.4.2 Representative Examples. Several representative joint details are designed using both Chapter 4 and Chapter 5 analyses and are compared to verify assumptions made in simplifying the model. The joints have cruciform configurations (similar to the test specimens) with 30 in. or 40 in. square columns and various rolled beam sizes. The beam sizes are chosen such that plastic moment capacities are approximately 85% of the nominal column moment capacities. The column capacities are determined by assuming typical ratios of longitudinal reinforcement, ρ, as indicated in Table 5.2. The following material strengths are used in the examples: concrete, $f'_c = 6$ ksi; reinforcement, $F_y = 60$ ksi; structural steel, $F_y = 36$ ksi.

Table 5.1 Comparison of Measured and Calculated Capacities

Specimen	Beam Load (kips)				Comparative Ratio			Comments
	Measured	Calculated			Calculated/Measured			
		Chp. 4	Chp. 5	Sheikh	Chp. 4	Chp. 5	Sheikh	
1	17.0	17.9	14.7	17.2	1.05	0.87	1.01	No FBP
2	22.5	21.0	15.6	23.6	0.93	0.69	1.05	Bearing Controls
3	16.5	15.9	10.9	11.1	0.96	0.66	0.67	No FBP
4	26.6	27.1	24.8	30.5	1.02	0.93	1.15	
5	28.2	27.1	24.8	30.4	0.96	0.88	1.08	
6	35.8	39.0	30.4	47.9	1.09	0.85	1.34	Bearing Controls
7	33.8	32.5	30.8	39.8	0.96	0.91	1.18	
8	46.2	47.7	45.7	53.2	1.03	0.99	1.15	
10	29.0	28.2	25.7	–	0.97	0.89	–	
11	47.0	48.9	45.9	–	1.04	0.98	–	
12	28.7	28.9	22.8	–	1.01	0.79	–	No FBP
13	42.8	41.8	39.8	–	0.98	0.93	–	
14	33.8	34.3	30.7	–	1.01	0.91	–	
15	37.0	37.3	35.1	–	1.01	0.95	–	
16	37.3	38.2	35.8	–	1.02	0.96	–	
17	36.9	37.3	36.4	–	1.01	0.99	–	

Joint details in Table 5.2 are chosen using the simplest detail which provides a joint strength exceeding the plastic moment capacity of the beams. The hierarchy in choosing joint details having the least to greatest strength is as follows: 1) FBP, 2) Steel Column and WSP, 3) Steel Column and FBP, and 4) Extended FBP. For each detail in Table 5.2 the ratio of joint capacity (M_j) to plastic beam capacity (M_p) is listed using both analyses. The percentage difference between the two solutions is also given.

The results in Table 5.2 show that relatively simple joint details can develop moment capacities required for a wide range of representative joint examples. For example, even in joints where the required moment capacity is based on a practical upper limit of 4% longitudinal column reinforcement, the steel column and FBP or extended FBP details suffice. The simplified design model slightly underestimates the joint capacity compared with a more detailed

Table 5.2 Comparison of Calculated Capacities For Representative Connections

Column	ρ	Beam	Detail	M_j/M_p Chp. 4	M_j/M_p Chp. 5	Diff. %	Failure Mode
40 × 40	$\frac{1}{2}$%	W27 ×84	FBP	1.24	1.28	+3%	Joint Shear
	1%	W27 × 146	Steel Column, WSP	1.34	1.290	−4%	Joint Shear
	2%	W27 × 235	Steel Column, FBP	1.06	1.04	−2%	Joint Shear
	4%	W27 × 368	Extended FBP	1.02	1.01	−1%	Joint Shear
	1%	W40 × 149	Steel Column, WSP	1.54	1.48	−4%	Joint Shear
	2%	W40 × 183	Steel Column, WSP	1.21	1.16	−4%	Joint Shear
	4%	W40 × 277	Steel Column, FBP	1.00	1.00	+0%	Joint Shear
30 ×30	$\frac{1}{2}$%	W21 × 44	FBP	1.29	1.29	+0%	Joint Shear
	1%	W21 × 73	Steel Column, WSP	1.42	1.34	−6%	Joint Shear
	2%	W21 × 122	Steel Column, FBP	1.09	1.07	−2%	Joint Shear
	4%	W21 × 201	Extended FBP	0.99	0.96	−3%	Joint Shear
	1%	W30 × 90	Steel Column, WSP	1.38	1.32	−4%	Joint Shear
	2%	W30 × 99	Steel Column, WSP	1.30	1.24	−5%	Joint Shear
	4%	W30 × 173	Extended FBP	1.13	1.13	+0%	Joint Shear
	4%	W40 × 149	Steel Column, FBP	1.12	1.03	−8%	Bearing

analysis. For the examples in Table 5.2, the difference in calculated values range between -8% and +3%. As desired, the design model is slightly conservative.

The joint strength calculation is in part a function of the ratio of beam moments to beam and column shears. By assuming inflection points at the center of the beam and column spans, the ratio of joint forces in a frame is determined by story height, center to center column spacing and column sizes. In Fig. 5.6 proportionality factors are listed for an example where the story height is set at 12 ft and the column spacings vary as shown. The examples presented previously in Table 5.2 are based on 20 ft column spacing.

Data in Tables 5.3a and b indicate sensitivity of the analysis to the ratio of member shears to moments by comparing calculated strengths for the different column spacings listed in Fig. 5.6. Values calculated using both analytic models are included. The tables show that the simplified design model is slightly

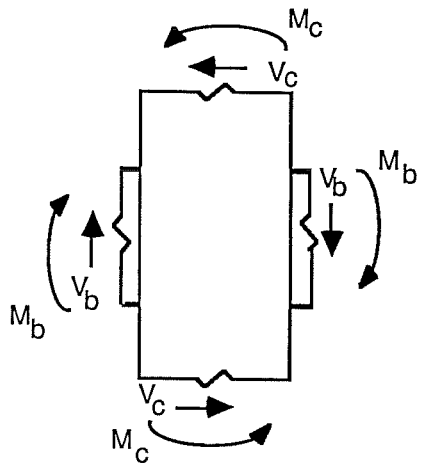

Column Size	Column Spacing (ft)	α_1 (in.)	α_3
30 X 30	10	45	0.83
	20	105	1.67
	30	165	2.50
40 X 40	10	40	0.83
	20	100	1.67
	30	160	2.50
20 X 20*	16	86	1.32

$\alpha_1 = M_b / V_b$ (inches)

$\alpha_3 = V_c / V_b$

* Values from experimental test program

Fig. 5.6 Proportional Member Forces

more sensitive than the detailed model to beam moment to beam shear ratios. However, even an extreme case (a 40 in. column with a change in beam span of 3×) results in only a 10% (1.59/1.45) change in capacity. The difference in calculated values indicates that where beam shear is large relative to beam moment (short spans), the design model sometimes results in larger joint capacities than the detailed model. As seen in Tables 5.3a and b, the difference ranges from -6% to +9%. The differences in calculated values do not warrant further refinement of the model owing to the limited base of test data upon which the analytic models are developed. This view is additionally justified by the fact that the ratio of shear to moment was not varied as a test parameter in the experimental program. Referring to Fig. 5.6 the ratios of member forces for the test specimens lie between those of the example problems with beam spans of 10 and 20 ft.

Table 5.3a Col. 40 × 40, Steel Column and WSP

Beam	Span	M_b/M_p		Diff.
		Chp. 4	Chp. 5	%
W 27 × 146	10 ft	1.32	1.36	+3%
	20 ft	1.34	1.29	−4%
	30 ft	1.34	1.27	−5%
W 40 × 149	10 ft	1.46	1.59	+9%
	20 ft	1.54	1.48	−4%
	30 ft	1.54	1.45	−6%

Table 5.3b Col. 30 × 30, Steel Column and WSP

Beam	Span	M_b/M_p		Diff.
		Chp. 4	Chp. 5	%
W 21 × 73	10 ft	1.39	1.36	−2%
	20 ft	1.42	1.34	−6%
	30 ft	1.42	1.32	−7%
W 30 × 90	10 ft	1.35	1.36	+1%
	20 ft	1.38	1.32	−4%
	30 ft	1.38	1.31	−5%

5.5 Structural Steel Detailing

Detailing requirements for structural steel components in the composite joint focus on aspects peculiar to composite connections which are not directly apparent from current design standards for steel structures. Detailing of the following components is considered: web stiffeners (FBPs and WSPs), steel column sections, steel beam flanges, welded shear studs and vertical joint reinforcement. Also developed is a general method for proportioning plates subjected to bending under concrete bearing stresses.

5.5.1 Bearing Plate Thickness. At several locations in the connection, plates subject to transverse bending under concrete bearing stresses need to be detailed. Specifically, the thickness of bearing plates supported on two or three edges must be determined. Examples include the FBP, WSP, extended FBP, steel column flange, and the steel beam flanges (Fig. 5.7a). The difficulty in determining required plate thickness is that no convenient methods are available to accurately predict the plate capacity including the effects of inelastic plate bending and membrane action. The problem is further complicated by the fact that the distribution of concrete bearing stresses against the plates is unknown.

The design method proposed for proportioning such plates is based on a dimensional analysis of the problem calibrated to the test results. The method is developed by considering a generic plate bending example shown in Fig. 5.7b with two edges supported. The two edge support provides conservative results for cases with three edges supported. Given that the plate resists a distributed load, P, with some unknown stress distribution the problem is to determine the required plate thickness.

The problem is approached by relating the applied bending moment to the resisting moment in the plate. The applied moment is proportional to the product of the applied load, P, times some characteristic length. Similarly, the moment resistance is proportional to the product of the material strength, the square of the plate thickness, and a second characteristic length. Referring to Fig. 5.7b, where L_{max} is much larger than L_{min}, the plate is essentially supported as a cantilever along L_{max}. The characteristic length of the applied

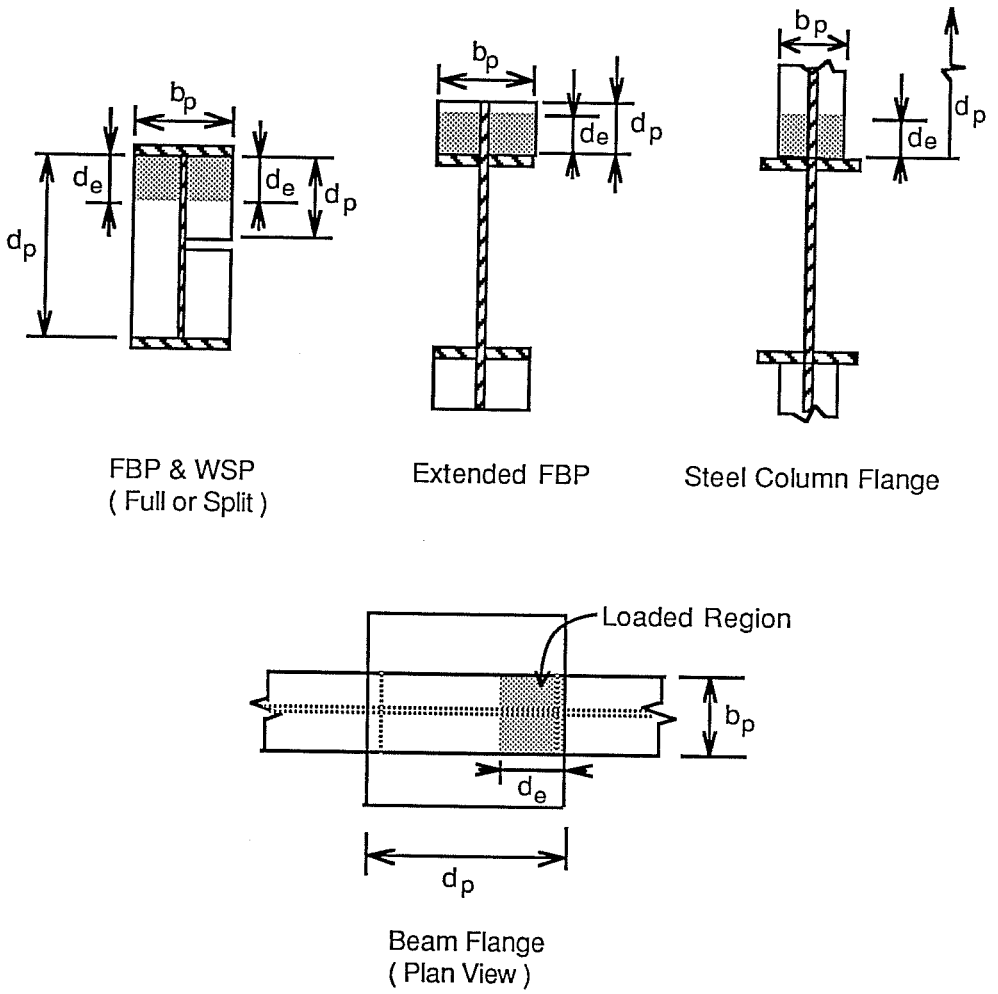

Fig. 5.7a Bearing Plate Examples

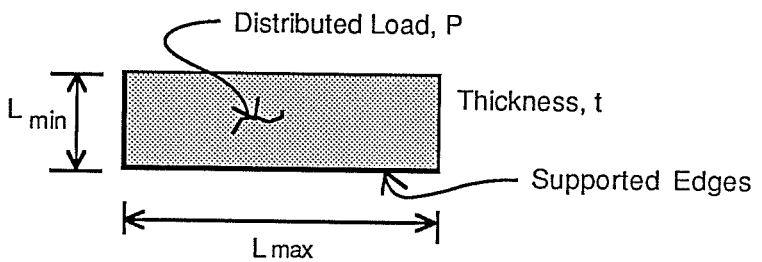

Fig. 5.7b Bearing Plate with Two Supported Edges

moment is L_{min} and that of the plate bending resistance is L_{max}. Thus the following expression can be written:

$$P\,L_{min} = K\,F_{yp}\,t_p^2\,L_{max} \tag{5.16a}$$

In this equation K is a proportionality factor. By rearranging Eq. 5.16a the plate thickness is expressed as follows:

$$t_p = K\sqrt{[P\,L_{min}/F_{yp}\,L_{max}]} \tag{5.16b}$$

The proportionality constant, K, is determined by correlating Eq. 5.16b with experimental data.

The most severe plate bending occurred in Specimen 10 where extensive yielding of the split FBP was observed. The results of this test are used to calibrate Eq. 5.16b. Referring to Fig. 5.7a the two plate lengths used in the analysis are $b_p/2$ and the concrete bearing length, d_e. Using the applied load, plate thickness, and steel properties from Specimen 10, K is 0.18. In this case, the actual plate length is longer than the loaded region (d_p exceeds d_e in Fig. 5.7a), and a K value of 0.18 is only valid where d_p/d_e is greater than 1.8. An upper bound for K where d_p equals d_e is obtained using the dimension, d_p. In this case, K is equal to 0.24.

In summary:

$$t_p = K\sqrt{[P\,L_{min}\,/\,F_{yp}\,L_{max}]} \tag{5.17}$$

$$\begin{aligned} L_{min} &= \text{Minimum } (b_p/2,\ d_e) \\ L_{max} &= \text{Maximum } (b_p/2,\ d_e) \\ P &= \text{Applied Load} \\ F_{yp} &= \text{Yield Stress of Plate} \\ K &= 0.18 \text{ where } d_p/d_e > 1.8 \\ &\quad\ 0.24 \text{ where } d_p/d_e \geq 1.8 \end{aligned}$$

Since this equation is based on a single test where the ratio of L_{min} to L_{max} is close to unity, Eq. 5.17 should be applied only to plates under concrete bearing stresses where the loaded region has a maximum aspect ratio of 2.0 ($L_{max}/L_{min} \leq 2.0$). Equation 5.17 is similar to one presented by Sheikh,[1] however, Sheikh's formulation is specifically intended only for full height FBPs supported on three edges.

5.5.2 Web Stiffeners (FBPs and WSPs). With regard to composite behavior the primary function of web stiffeners, either in a FBP or WSP configuration, is to mobilize a concrete compression strut between the flanges. The stiffeners transfer horizontal load into the concrete through direct bearing as shown in Fig. 5.8. The total horizontal load is equal to V_n as determined in the joint panel calculations using Eqs. 5.6a through 5.6d.

Required Plate Width. As described previously, in calculations the width of WSPs or split FBPs should not be taken greater than the beam flange width. Where full height FBPs are intended to mobilize concrete outside the beam flanges, the allowable plate extension is dependent on the plate thickness. The following limitation on plate extension is the same as that proposed by Sheikh[7]:

$$b_p - b_f = 5t_p \tag{5.18}$$

The intent of Eq. 5.18 is to ensure adequate stiffness for a plate extending beyond the beam flanges. Presumably, Eq. 5.18 need not apply if special measures are taken to stiffen the wide FBP.

Bearing Forces and Weld Requirements. Concrete bearing against the plate is considered using an equivalent rectangular stress block of width, b_p, and height, d_e. As noted in Chapter 4, the bearing zone height is taken as a constant value equal to 0.25 d_w. The horizontal strut capacity, V_n, is applied uniformly over the bearing area to calculate the bearing stress. The concrete bearing stress in this region should not exceed $2f'_c$. The required weld size between the beam and bearing plate should be determined with a weld length limited to the perimeter of the assumed bearing zone as shown in Fig. 5.8. The weld should be sized to transfer the force, V_n, through shear into the beam.

Plate Thickness. The FBP or WSP thickness should be determined using Eq. 5.17 developed previously. In Eq. 5.17, the load P, applied to the bearing plates on each side of the web is equal to $V_n/2$. The characteristic lengths in Eq. 5.17 are the bearing zone height, d_e (equaling 0.25 d_w), and the lesser of one-half the plate or flange width, $b_p/2$ or $b_f/2$. Finally, where a split FBP is used the ratio of d_p/d_e should be checked to determine the proper K factor to use.

5.5.3 Extended FBP. The extended FBP transfers horizontal force between the beam flange and the concrete outside the beam depth. A typical extended FBP detail is shown in Fig. 5.9. In order to be fully effective FBP height should exceed the distance d_{op} (recall $d_{op} \leq 0.25d$) indicated in Fig. 5.9. Also, to mobilize the largest outer panel shear, V_n', the FBP width should be equal to the beam flange width, b_f.

As shown in Fig. 5.9 the extended FBP resists a force equal to the sum of the outer panel shear, V_n', and the concrete column shear, V_c. Horizontal concrete bearing stresses, required plate thickness, stiffener requirements, and connection to the beam flange must be checked. The concrete stresses should be calculated by considering the applied load acting over an area of width, b_p, and height equal to the lesser of the plate height, d_p, or d_{op}. The concrete bearing stress should not exceed $2f_c'$.

In order to keep the plate to a practical thickness, stiffeners such as those shown in Fig. 5.9 are usually required. When a single stiffener at the center is used, the FBP thickness may be determined using Eq. 5.17. The characteristic lengths for Eq. 5.17 should be equal to $b_p/2$ and the lesser of d_p or d_{op}. The load, P, in Eq. 5.17 is taken equal to $(V_n' + V_c)/2$ for one half of the FBP. Since the ratio d_p/d_{op} is usually less than 1.8, a K value of 0.24 should be used in Eq. 5.17. Where an unstiffened plate is used, the required thickness is determined by considering the Extended FBP as a cantilever supported at the beam flange.

5.5.4 Steel Column Section. The only steel column requirements considered here are related to the transfer of horizontal load from the steel beam flanges into the concrete through bearing against the column.

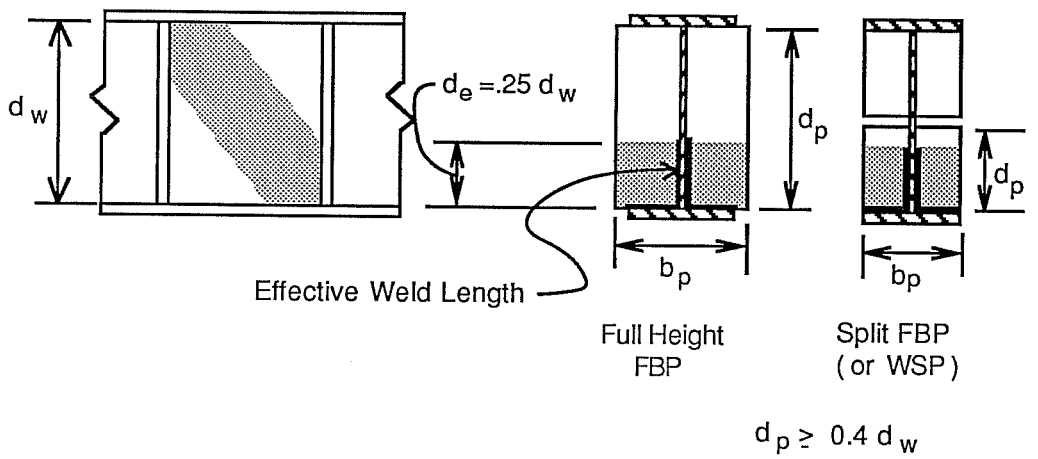

Fig. 5.8 FBP Detail

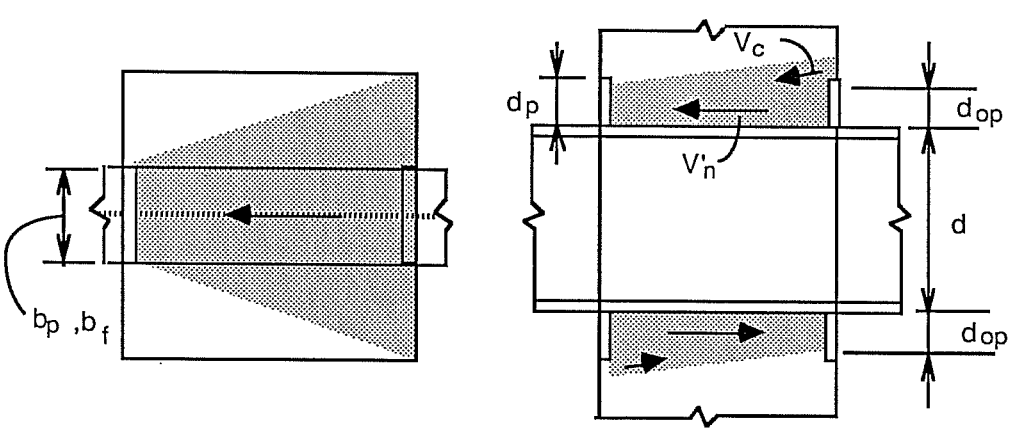

Fig. 5.9 Extended FBP Detail

As shown in Fig. 5.10 the horizontal load on the steel column is equal to the sum of the outer panel force, V_n', and the column shear, V_c. The forces are transferred to the column through concrete bearing against the flanges. Tests indicate that most of the load is carried by the back flange. Hence, the maximum bearing stress is checked by considering a bearing area over the width of the column with a height equal to d_{op}. As indicated previously the height d_{op} is limited to 0.25 times the beam depth. The concrete bearing stress over the bearing area should not exceed $2f_c'$.

Along with the bearing stress, the column flange thickness, t_f, should be checked using Eq. 5.17. The characteristic lengths for use in Eq. 5.17 are one half the column flange width, $b_f/2$, and the bearing zone height, d_{op}. The force, P, in Eq. 5.17 is taken equal to $(V_n' + V_c)/2$. Since the steel column usually extends well beyond the connection region a K value of 0.18 may be used in Eq. 5.17. The shear capacity of the column web and the connection to the beam flange should be designed to carry the sum of V_n' and V_c.

5.5.5 Welded Shear Studs. The function of the shear studs is similar to that of the Extended FBP and Steel Column in transferring horizontal shear between the steel flange and concrete. As such the shear studs should be designed to carry a load equal to the concrete column shear, V_c, plus the outer panel shear, V_n', as shown in Fig. 5.11.

As discussed in Appendix A2, the AISC-LRFD[10] specification may be used for design of the shear studs with one recommended modification. The calculated capacity of the studs per LRFD should be reduced by 20% because the available test data indicates certain cases where the LRFD provisions may overestimate the stud capacity developed in the composite joint. Also, the design strength for the connection at 1% TJD reflects roughly 85% of its ultimate capacity. Therefore, the stud design capacity should be reduced similarly to insure that the studs will not fail prematurely.

The LRFD specification should also be followed with regard to stud spacing and placement considerations. As shown in Fig. 5.11, the minimum center-center spacing of the studs is 6 stud diameters in the direction of force

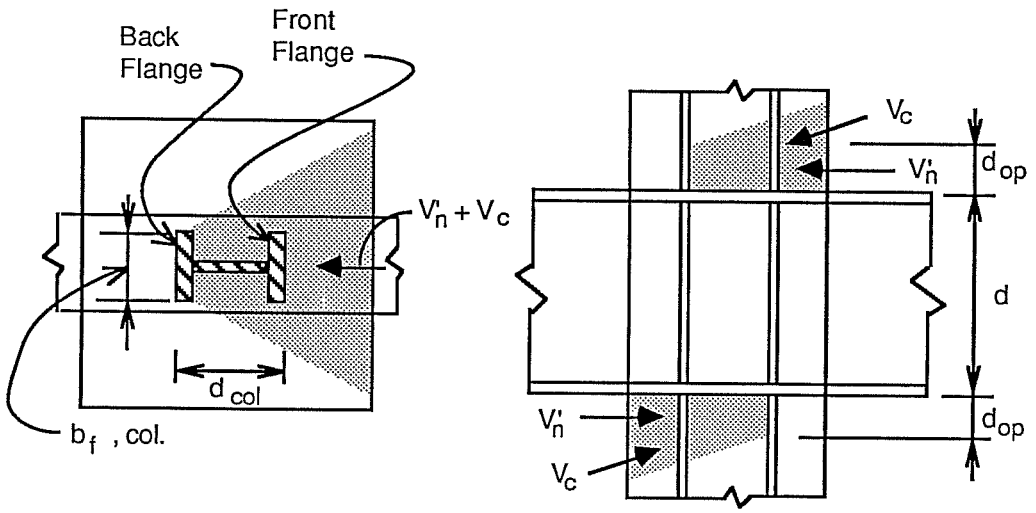

Fig. 5.10 Steel Column Detail

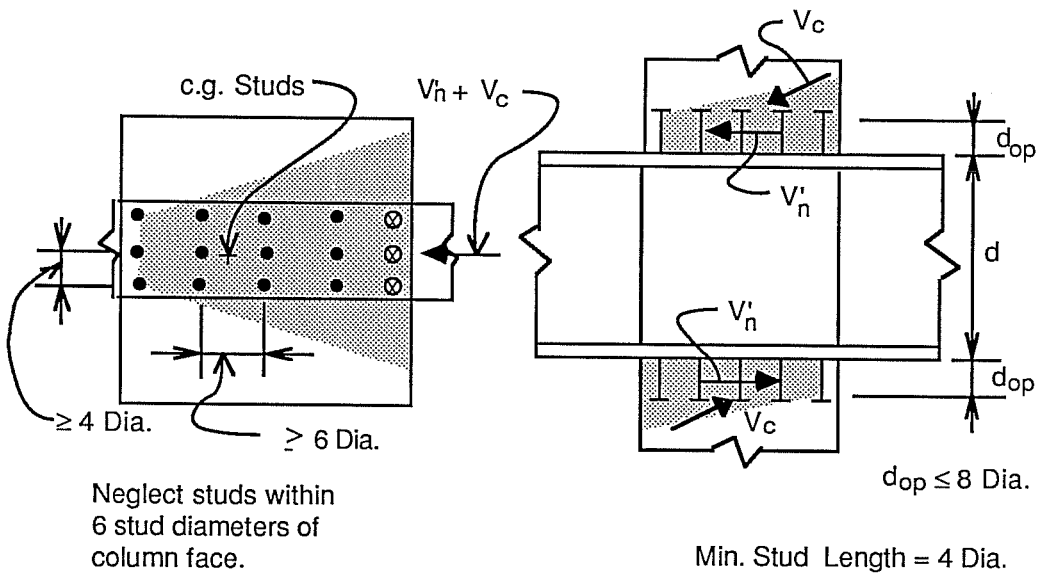

Fig. 5.11 Welded Shear Stud Detail

and 4 diameters transverse to the force. Studs within 6 diameters of the tension face of the column should not be considered as contributing to the stud group capacity since such studs have inadequate concrete cover to develop their full shear capacity. No more than 3 studs per row should be considered in strength calculations. Finally, the minimum required stud height is 4 stud diameters, and the calculated dimension of d_{op} should not exceed 8 diameters or 0.25 d.

5.5.6 Vertical Joint Reinforcement. Joint reinforcement provides for a direct transfer of vertical tension and compression forces between the beam flanges and the connection, and for horizontal load transfer in a manner similar to that of the extended FBP, steel column and shear studs.

Vertical joint reinforcement is needed when concrete bearing stresses control design. Assessment of the axial capacity of vertical reinforcement should include consideration of the mechanical connection to the beam and adequate development of the reinforcement into the concrete. Bar connection to the steel beam may be by direct welding or through welded couplers. These details should be checked using applicable standards such as the LRFD specification and the American Welding Society Standards. ACI-318 should be used to determine the required bar development length. As shown in Fig. 5.12, the development length should be evaluated after discounting a distance adjacent to the beam flange equal to the greater of the following: the connection fixture length, 1/4 of the beam depth, or 12 inches. The discounted region is based on the bond and cracking behavior discussed in Chapter 3. Finally, the reinforcement should be located within 0.2 h of the column face in order to be fully stressed prior to crushing of adjacent concrete.

The vertical joint reinforcement may also be considered to provide a horizontal force transfer similar to that of welded shear studs. Where this is the case both the shear capacity of the reinforcement and the horizontal concrete bearing stress against the reinforcement should be checked. The maximum horizontal load resisted by the vertical reinforcement is the sum of the outer panel

(compression field) shear, V_n', and the concrete column shear, V_c. The horizontal bearing stresses are evaluated using the projected horizontal width of the reinforcement over a height equal to d_{op}. The bearing stress is limited to $2f_c'$.

Reinforcement adjacent to the tension face is ineffective in transferring horizontal load due to insufficient concrete cover. Hence, this reinforcement should be neglected in considering the horizontal transfer capacity. Finally, if the horizontal transfer capacity provided by the vertical joint reinforcement does not meet the transfer force assumed in the joint panel calculations (Sec. 5.3), the joint capacity should be reduced accordingly.

5.5.7 Steel Beam Flanges. Along with carrying axial load calculated by normal beam theory, the beam flanges are subjected to transverse bending from concrete bearing and joint reinforcement which transfer vertical force between the steel beam and concrete column. Fig. 5.13 shows the forces to consider in assessing transverse flange bending. The upper bound on the vertical force transferred into the steel beam occurs where the steel web panel has yielded. In such cases the vertical force in the steel beam is equal to the following:

$$P_v = V_s \; d_f \; / jh + V_b \tag{5.19}$$

Where a strong web panel precludes its yielding, the force given by Eq. 5.19 need not exceed that calculated by the combined capacity of the concrete bearing zone and the vertical joint reinforcement.

The method of assessing the required flange thickness varies depending on specific joint detailing. For example, where no FBP or other stiffeners are used the transverse bending stress is determined by considering the flanges as simple cantilevers supported at the web. If FBPs are present, the flange thickness may be checked using Eq. 5.17 for loading by uniform concrete bearing stresses. Where vertical joint reinforcement causes flange bending, a yield line analysis may be used to determine the transverse plate capacity. Also, where joint reinforcement carries large loads, local stiffeners may be required to support

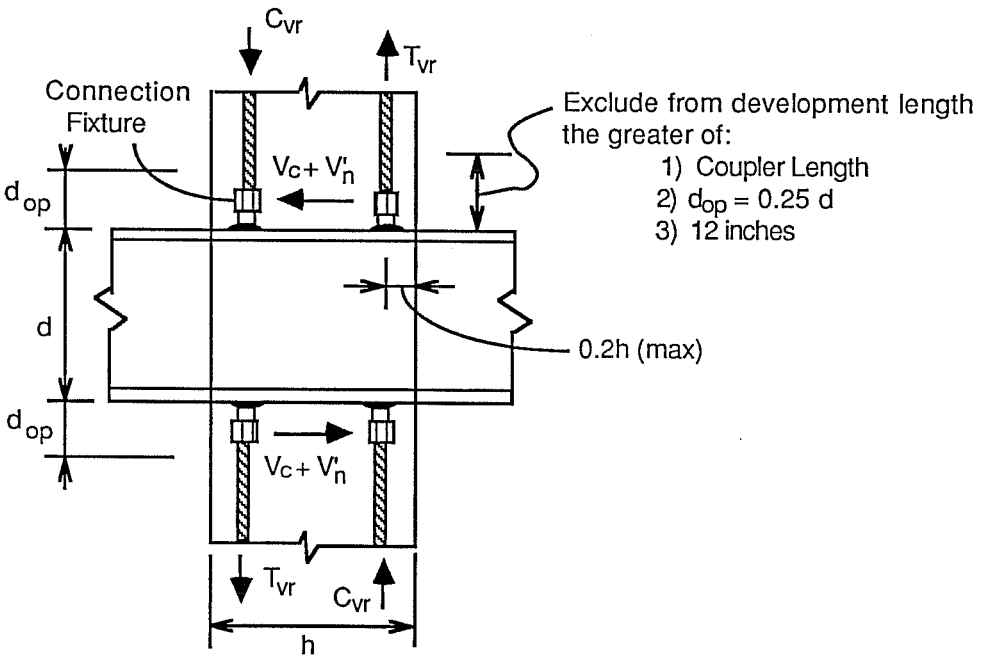

Fig. 5.12 Vertical Joint Reinforcement

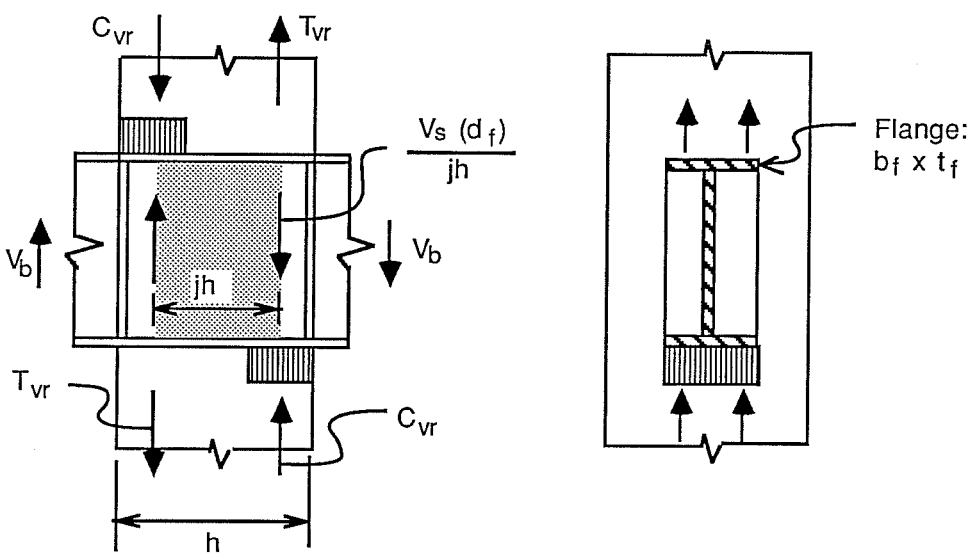

Fig. 5.13 Transverse Loads on Beam Flanges

the flange. Bearing stresses against the compression flange tend to be resisted in part by the opposite tension flange due to load transferred by concrete between the flanges. The range of possible details and configurations is large. Specific recommendations or equations cannot address properly the wide range of circumstances that determine required flange thickness and are, therefore, not attempted in this report.

5.6 Reinforcing Steel Detailing

Detailing recommendations for the lateral ties and longitudinal column bars in the joint region are intended to supplement standard detailing practice and requirements given by applicable reports and standards of the American Concrete Institute.

Most of the detailing recommendations are drawn from recent research and detailing recommendations for reinforced concrete joints. Several important differences exist, however, between composite joints and reinforced concrete joints. First, the basic joint shear behavior in the composite joint is a combination of the steel web, the compression strut and the compression field mechanisms, whereas in reinforced concrete joints typically only the compression strut mechanism is considered in design. Second, in composite joints detailing is complicated by fabrication difficulties posed by the steel beams and column passing through the joint.

5.6.1 Horizontal Column Ties. In the composite joint horizontal ties serve several functions which are considered in the detailing recommendations. One function is to carry tension forces associated with the compression field (or truss) mechanism, thereby providing shear resistance in the outer concrete panel. The ties above and below the beam must also resist tension forces associated with the horizontal strut mechanism transferring horizontal shear between beam flanges and outer panel. The second major function of the ties is in providing confinement to concrete in and adjacent to the joint region. Such confinement is particularly important for seismic design where inelastic cyclic loading is anticipated. Finally, ties in the joint region prevent local buckling of longitudinal column bars.

Lateral ties within the beam depth primarily carry joint shear in the compression field and to a lesser degree provide confinement to the joint core. The shear requirement for the ties is calculated using Eqs. 5.7a through c based on concrete controlling the compression field strength. In order for tie capacity not to govern compression field strength as given by the upper bound in Eq. 5.7c, the cross sectional tie area, A_{sh} (Fig. 5.14), should satisfy the following equation:

$$A_{sh} = \frac{0.52\sqrt{f'_c}\, b'_{op}\, s_h}{F_y} \tag{5.20}$$

To reiterate, this equation applies only when it is desired to develop the full compression field width, b'_{op}, mobilized by the joint detail.

A minimum tie area is recommended based on recent research and recommendations in the United States and Japan for minimum lateral ties in reinforced concrete joints. In the United States, the ACI-ASCE Committee 352[8] recommends a minimum tie area given by the greater of the following equations:

$$A_{sh} = \frac{0.3\, s_h\, h''\, f'_c\, (A_g/A_c - 1)}{F_y} \tag{5.21a}$$

$$A_{sh} = \frac{0.09\, s_h\, h''\, f'_c}{F_y} \tag{5.21b}$$

The area given by Eqs. 5.19a and 5.19b may be reduced by 1/2 for interior joints where orthogonally framed beams provide confinement to the joint.

In Japan, Kitayama (et al.)[14] recommend a minimum tie area which can be expressed as follows:

$$A_{sh} = 0.003\, b\, s_h \tag{5.22}$$

Equation 5.22 results in about 1/3 the steel area required by Eqs. 5.21a and 5.21b. Both the US and Japanese recommendations are specified for use in seismic design, and both primarily intend the requirements to provide a minimum concrete confinement for exterior joints. The large difference between the

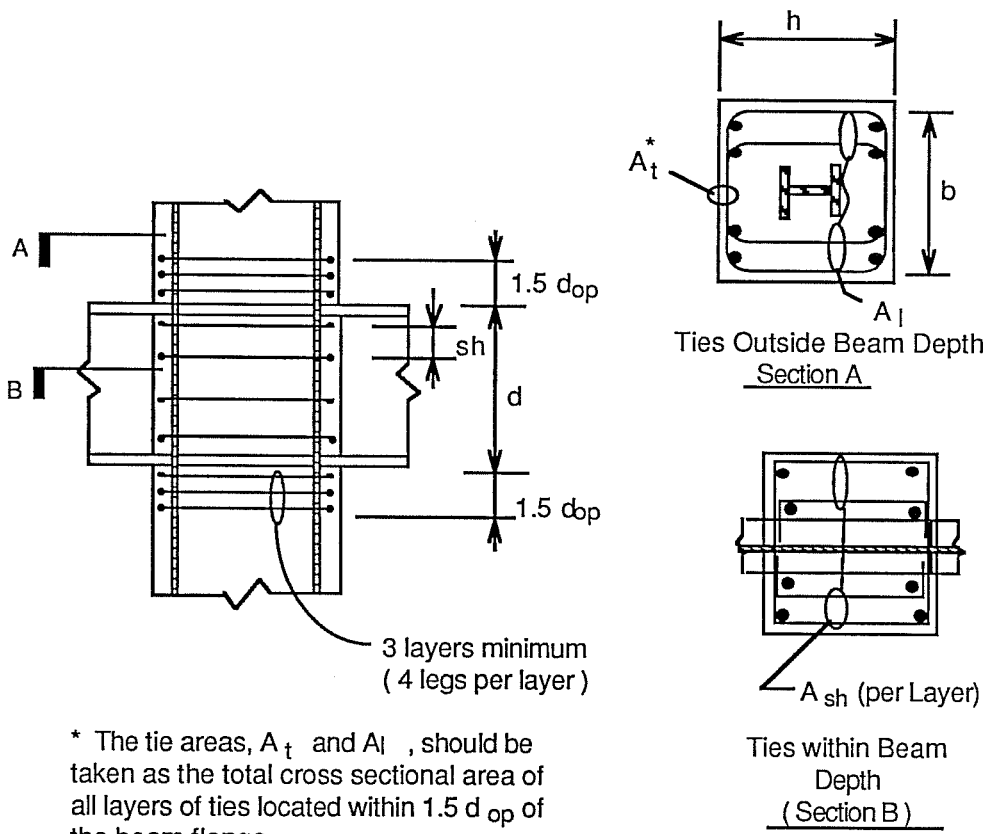

* The tie areas, A_t and A_l, should be taken as the total cross sectional area of all layers of ties located within 1.5 d_{op} of the beam flange.

Fig. 5.14 Lateral Tie Reinforcement

U.S. and Japanese recommendations is indicative of the lack of consensus regarding the function and requirements for lateral ties in reinforced concrete joints.[9] Also, the difference is in part a function of the nature of the two references. The ACI-ASCE recommendation is the consensus of a committee of engineers and researchers and Eqs. 5.21a and b in fact represent a relaxation of the tie requirement from an earlier report. Kitayama's recommendation, on the other hand, is the proposal of a single group of researchers based on a recent set of experimental data.

Based on a comparison of the aforementioned recommendations for concrete joints, the following minimum requirements are proposed for composite joints:

$$A_{sh} = 0.004\, b\, s_h \quad \text{(Non-Seismic)} \tag{5.23a}$$

$$A_{sh} = 0.007\, b\, s_h \quad \text{(Seismic)} \tag{5.23b}$$

In Fig. 5.15, Eqs. 5.21a and 5.21b are compared with recommendations for reinforced concrete joints. Note that in Fig. 5.15 the ACI-ASCE recommendation is based on the following properties: $f'_c = 6$ ksi, $F_y = 60$ ksi, column width = column depth, concrete cover = 1.5 in. As seen in the figure, both the non-seismic and seismic recommendations for the composite joint fall between the recommendations for concrete joints. Also indicated in Fig. 5.15 is the reinforcement provided in the 20 in. columns of the test specimens.

The tie areas given by Eqs. 5.23a and 5.23b are compared with values from Eq. 5.20 to determine the effective compression field width, b'_{op}, for which minimum ties provide the required steel contribution. Assuming values for f'_c and F_y of 6 ksi and 60 ksi in Eq. 5.20 results in the following compression field widths:

$$b'_{op} = 0.19\, b \quad \text{(Non-seismic)} \tag{5.24a}$$

$$b'_{op} = 0.33\, b \quad \text{(Seismic)} \tag{5.24b}$$

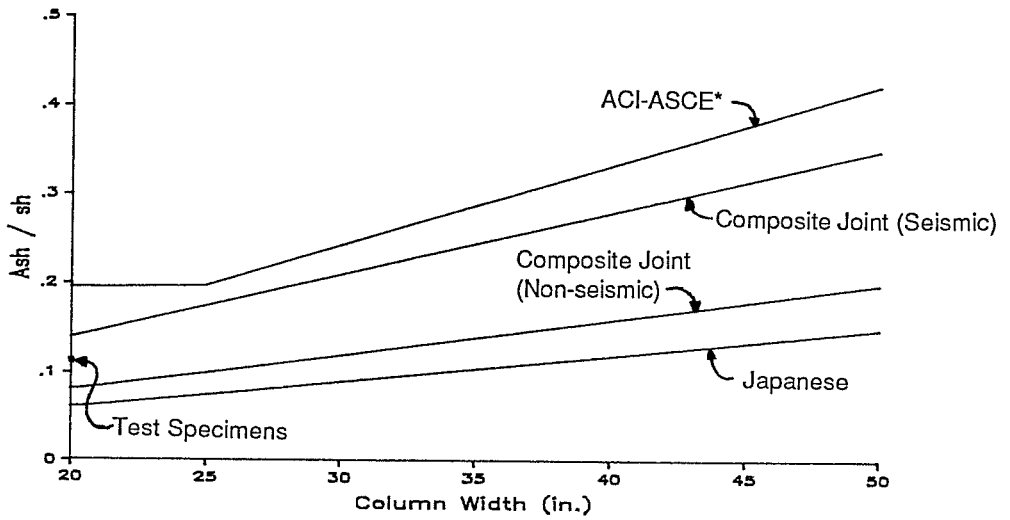

* note: ACI-ASCE curve is based on the following values used in Eqs. 5.19a and b: F_y = 60ksi, f'_c = 6 ksi, square col., 1.5 in. cover.

Fig. 5.15 Minimum Lateral Tie Areas

In a joint where the beam width is one half the column width, an extended FBP detail mobilizes a compression field width equal to approximately 0.25 b. Similarly, an embedded steel column in a similar detail would mobilize a width equal to roughly 0.12 b. Compared to the widths given in Eqs. 5.24a and 5.24b, the minimum tie area provides at least 75% of the reinforcing steel required to develop the available compression field capacity.

Column ties above and below the beam both carry tensile forces which transfer shear into the outer concrete panel and provide concrete confinement in the highly stressed bearing zone. The minimum recommended tie requirement in this region is for three layers of ties located as shown previously in Fig. 5.14. The recommended bar sizes are related to the column width, b, as follows: $b \leq$ 20 in., #3 bars; $b \leq$ 30 in., #4 bars; $b >$ 30 in., #5 bars.

Where the outer panel compression field is mobilized, additional ties may be required to transfer the shear force, V_n', between the beam flange and the outer panel. This horizontal force is transferred by combined strut and shear friction mechanisms described more completely in Chapter 4. Referring to the tie areas, A_t and A_ℓ shown in Fig. 5.14, the horizontal transfer strength is calculated by the following equations:

$$P_t = P_{\ell 1} + P_{\ell 2} \leq 1.5\, P_{\ell 1} \tag{5.25a}$$

$$P_{\ell 1} = F_{ysh}\, A_\ell \tag{5.25b}$$

$$P_{\ell 2} = 1.4\, A_t\, F_{ysh} \tag{5.25c}$$

$P_{\ell 1}$ in Eq. 5.25 is the capacity of the strut mechanism. $P_{\ell 2}$ in Eq. 5.25c is the shear friction mechanism strength which usually applies only with the extended FBP detail. The upper limit on P_t of 1.5 $P_{\ell 1}$ in Eq. 5.25a is based on the maximum horizontal transfer observed in the test specimens.

Figure 5.16 indicates the reinforcement required in a 3 ft square column based on the proposed minimum standards. As noted previously, additional ties may be required where the internal forces exceed those carried by the minimum steel areas. Also, the ties in the joint region should meet minimum requirements for the concrete or composite column adjacent to the joint.

The example in Fig. 5.16 demonstrates several practical detailing concerns in composite joints. The cross section above the beam (Sec. A) depicts a region where detailing is similar to that in reinforced concrete columns. For non-seismic designs the ties in this region may be closed rectangular hoops with 90 degree hooks or cap ties. Where loss of concrete cover is a design concern due to seismic loading, rectangular ties should have 135 degree hooks which anchor the ties in the column core. Within the beam depth (Sec. B), tie detailing is complicated by steel beam webs passing through the column. Figure 5.16 includes a transverse floor beam in order to present a realistic example of detailing considerations within the beam depth. As shown in the figure, the ties within the beam depth are made up of several pieces. The inner set of reinforcement

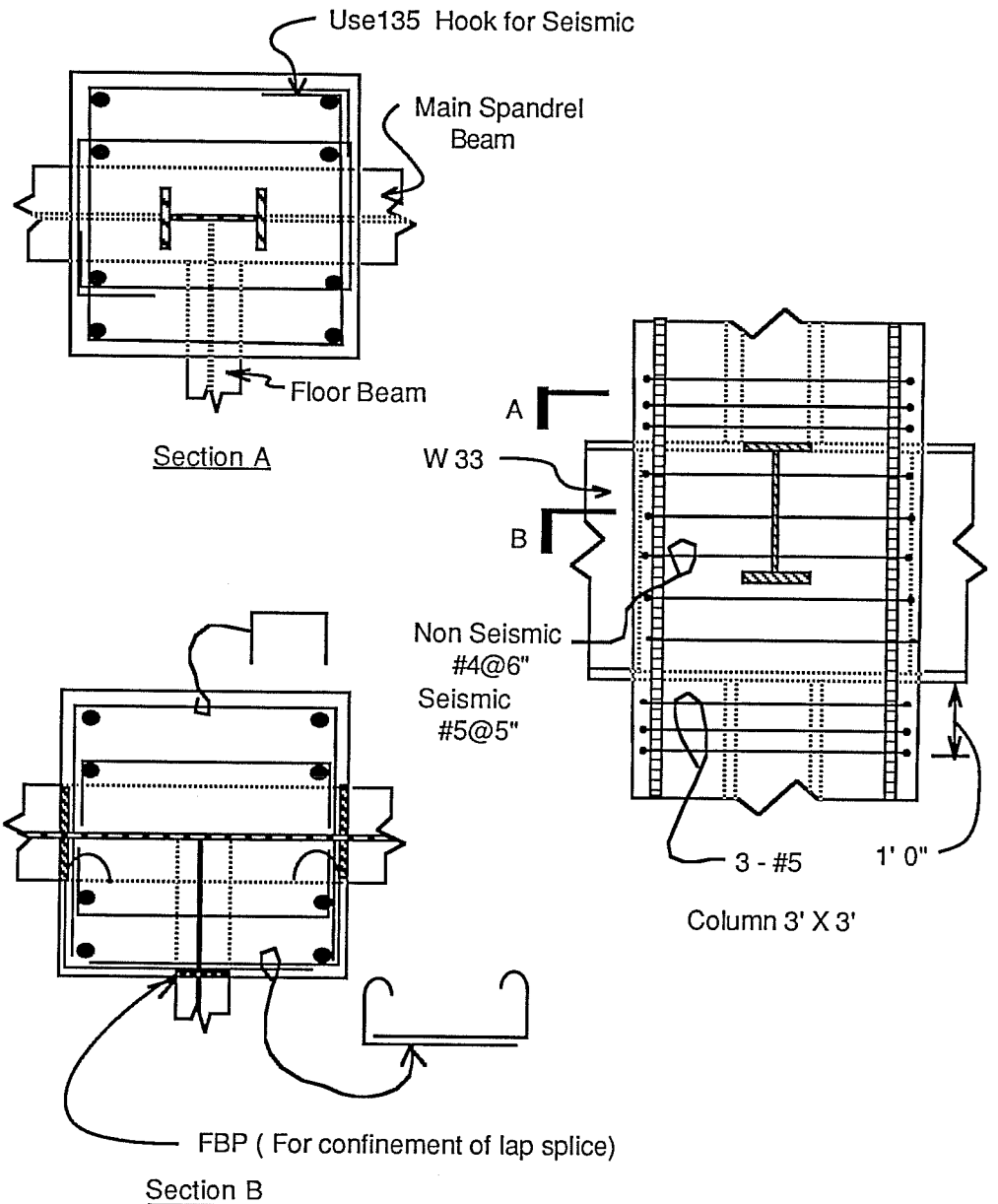

Fig. 5.16 Typical Joint Reinforcement

consists of hairpin ties which do not pierce the main spandrel beam web. For seismic design the hairpin ties should have a 135 degree hook on at least one of the ends. The outer tie is fabricated in three pieces as shown. In such cases bars should be lap spliced or hooked to provide full tension development of ties around the column perimeter. Note that particularly for seismic design, the FBP on both the spandrel and floor beam is recommended to provide confinement for lap splices of the ties.

5.6.2 Vertical Column Bars. Where vertical column bar sizes are controlled primarily by column bending moments, the bond stress around the bars is quite large through the joint region. As observed in the experiments, typically at a load equal to roughly 1/2 the nominal design load, the rate of increase in bond stress drops off. This results from concrete cracking which isolates the vertical bars and surrounding concrete from the joint panel. This phenomenon is aggravated by reinforcing bar layouts where vertical steel is concentrated in column corners to provide clearance for steel beams.

In reinforced concrete joints where there is concern over loss of bond through the joint, the vertical bar sizes are limited as a function of the connection height. ACI-ASCE Committee 352[8] recommends that in joints subjected to seismic loading the bar diameter be limited by the beam depth, d, as follows:

$$d_b \leq d / 20 \tag{5.26}$$

A similar set of recommendations is proposed for composite joints with two variations. First, separate requirements are proposed for seismic and non-seismic loadings. Second, the joint height should be taken as the beam depth, d, plus the joint extension, d_{op}, where elements such as the steel column extend the region of concrete mobilization. The maximum bar sizes are given as follows:

$$d_b \leq (d + d_{op}) / 15 \quad \text{Non-seismic} \tag{5.27a}$$

$$d_b \leq (d + d_{op}) / 20 \quad \text{Seismic} \tag{5.27b}$$

The less stringent value for the non-seismic case is based on Specimens 3 through 17 in which the ratio of beam depth to column bar diameter was 14.2 and performance was satisfactory. In addition to the bar size limitation, bundled bars should not be used where high bond stresses are of concern.

The limitations on the vertical bars need not apply where the column reinforcement is provided primarily to carry axial loads. In such cases the bond stress in the joint is not as critical due to the smaller moment transfer relative to the size and number of vertical reinforcing bars. Where axial load is significant, bond requirements may be checked by comparing the actual bond area provided with that which would exist if axial load were ignored and the vertical bars detailed to satisfy Eqs. 5.27a and 5.27b. In other words, in the hypothetical case the bars would be designed for moment only and smaller bar sizes than maximum permitted size chosen. The bond areas should be calculated as the product of the bar perimeter and the connection height.

5.7 Limitations of Recommendations

The design recommendations presented herein should not be indiscriminately applied to composite connections substantially different from the test specimens upon which the guidelines are based. Since the test specimens considered in this study are all of similar geometry and concrete strength, limitations are given to restrict applicability of the design recommendations. The recommendations may provide useful and reliable information for connections not included within the limitations, however, careful judgment must be exercised in extrapolating the results.

The design equations presented in this report directly apply only to planar connections of cruciform shape such as those tested in the experimental program. The basic component strengths for the steel and concrete joint shear mechanisms may be adapted for use in other joint configurations. When used for other geometries the internal load paths must be examined in order to properly calculate the joint strengths. Discussion regarding the analysis of alternate configurations is outlined later in this chapter.

Design equations for the concrete panel and compression zone are limited to normal weight concrete with compressive strengths (f'_c) equal to or less than 6 ksi. This limitation follows that given by the ACI-ASCE Committee 352 recommendations, which cite lack of experimental data for light weight and high strength concrete. Research in progress at the University of Texas[26] involving use of high strength concrete in reinforced concrete joints may yield data to increase the applicability of these recommendations for higher strength concretes.

Finally, the recommendations in this report are limited to connections where the geometry conforms to the following ratios:

$$\text{Column Depth/Beam Depth:} \quad 0.75 \leq h/d \leq 1.5 \tag{5.28a}$$

$$\text{Beam Width/Column Width:} \quad 0.3 \leq b_f/b \leq 0.6 \tag{5.28b}$$

Equation 5.28a is the same as that proposed by Sheikh.[1] Equation 5.28b limits the recommendations to geometries similar to those tested. Also, limitations on the maximum beam width address practical concerns regarding concrete placement and passage of column reinforcement through the joint.

5.8 Additional Considerations

Thus far the design recommendations have focused on assessing influence of joint details on the strength of planar cruciform configurations. Equally important to successful design of such connections are construction concerns related to fabrication and erection of the composite system and placement of concrete in the joint region. Since buildings require joint configurations other than the cruciform configuration studied, analysis of alternate joint configurations is considered in this section.

5.8.1 Concrete Placement. Structural steel members passing thru the joint pose an obstruction to concrete placement. Special measures should be taken to insure against voids in the concrete. Such measures include special attention to detailing to avoid congestion and careful selection of concrete mixes, vibration procedures, and an adequate inspection program.

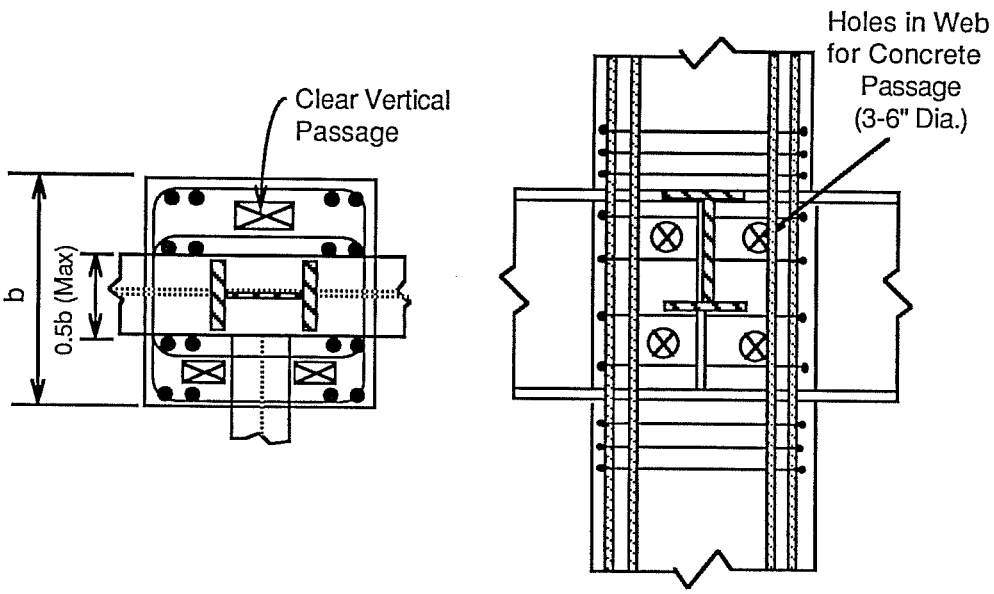

Fig. 5.17 Detailing Recommendations for Concrete Placement

Joint congestion is best avoided by limiting the beam flange width to roughly 1/2 of the column width as shown in Fig. 5.17. Limitation to even smaller widths is advised in three dimensional configurations where wide beams run in orthogonal directions. The flange width in the test specimens was 40% of the column width. The lateral tie and vertical bar layout should provide clear vertical passages for concrete placement as shown in Fig. 5.17. Finally, where the steel beam depth is large, holes through the beam web will facilitate placement of the concrete. Where such holes are used their effect on reducing the steel web panel strength should be considered.

The concrete mix should be specified with consideration for the degree of congestion, method of placement and vibration, access to the joint region, and the anticipated inspection program. Based on the specimens cast in the laboratory, high concrete slumps on the order of 6 in. are recommended. With

such slumps concrete lift heights should be limited to approximately 1 ft between vibration. In addition, air entrainment of about 5% improves the workability of the concrete. Where high strength concretes are used, super-plasticizers (water reducers) may offer the most economical solution to reliable placement of the concrete.

5.8.2 Coordination. Recommendations regarding the coordination of detailing, fabrication, and construction are beyond the scope of this report other than to advise that such considerations be addressed early in the design process. Particularly in the joint region, composite construction requires close coordination of the structural steel, reinforcing steel, and formwork details. Coordination of detailing needs to be addressed in the design specifications by either requiring one agency to be responsible for all the work, or to carefully outline the detailing responsibilities and channels of communication between different contractors and detailers. In design, the proposed erection sequence must be examined to insure that the envisioned structure can be built. In the joint region, the main fabrication concern relates to detailing of reinforcing steel such that it can be conveniently installed around the structural steel. Further discussion of coordination and construction concerns for composite frames is presented in references 2, 3, 5 and 27.

5.8.3 Alternate Joint Configurations. As presented in this chapter the design equations are directly applicable to the cruciform (planar interior) joint configuration as shown in Fig. 5.18a. The design recommendations may be adapted for other configurations through examination of the internal forces and joint shear mechanisms. In order to demonstrate application to alternate configurations several representative examples of other joint details are discussed.

Figures 5.18a through 5.18d show four connection configurations considered in this section. In these figures beam forces associated with lateral frame loading are shown along with the proportional column forces. Figures 5.18a, b, and c include the following planar connections: interior, corner and top corner. Figure 5.18d shows a three dimensional corner connection which occurs in perimeter framed tube structures.

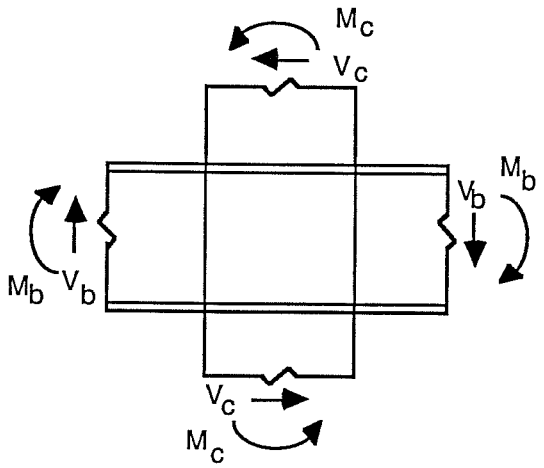

Fig. 5.18a Planar Interior

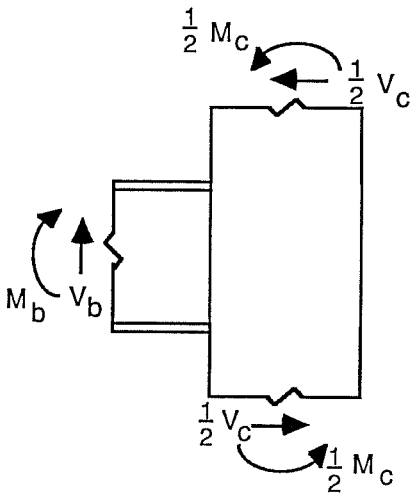

Fig. 5.18b Planar Corner

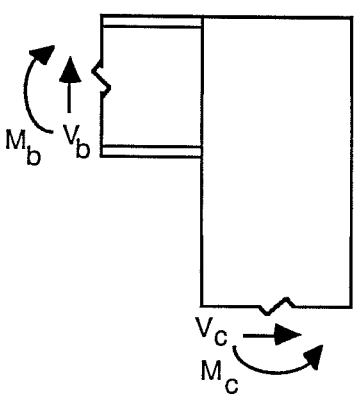

Fig. 5.18.c Planar Top Corner

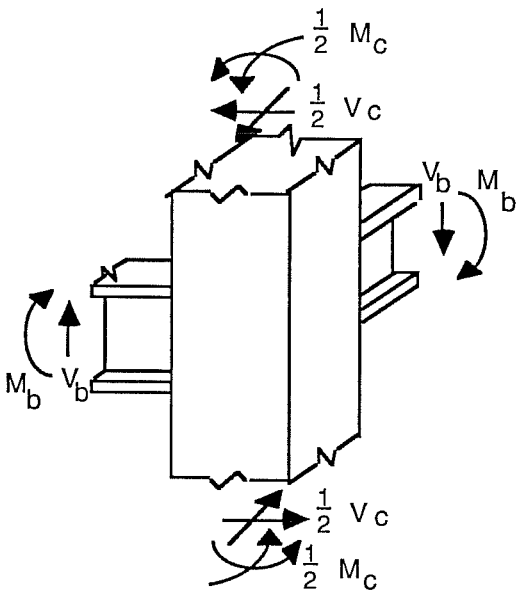

Fig. 5.18d Three Dimensional Corner

The required joint shear strength is essentially a function of the total unbalanced beam moment transferred into the columns. Referring to Figs. 5.18a through 5.18d, the unbalanced moment in the interior connection is twice that of the planar corner connections. The total unbalanced moment for the three dimensional corner connection is equal to the planar joint, however, since the loads are applied about two axes the internal forces in each direction are smaller. The three dimensional corner is reasoned to be less critical than the planar case by considering an analogy to biaxial bending of concrete columns. Figure 5.19 shows a typical failure envelope for biaxial bending in reinforced concrete members. As indicated in this figure biaxial loading equal to 1/2 of the ultimate capacity in each of the two directions is within the safe design region.

By comparison the planar interior joint (Fig. 5.18a) is assumed to be as critical as any of the other three connection types in a given structure. Strictly speaking, this may not always be the case since connection forces will vary depending on location in the structure. However, this observation implies that in a given structure the nature of details required for interior joints will probably be adequate elsewhere. Hence, analysis of interior joints will suffice for feasibility studies used for determining what special connection details will be required for a given project.

Planar Corner Detail. The internal shear mechanisms are similar in the four connection configurations, however, some important differences must be addressed in detailing the connections. A planar corner detail shown in Fig. 5.20a is most like an internal joint. The primary difference is that in the corner detail the unbalanced beam moment enters the joint though only one side of the column. Also, the unbalanced beam shear alters the joint equilibrium slightly. Note that in order for the joint shear mechanisms to be fully effective the beam must extend the entire width of the column as indicated in Fig. 5.20a. Another difference between the interior and corner details is support of the FBP. As shown in Fig. 5.20b, where the beam extends outside the connection, the horizontal beam transfers forces into the bearing plate from the web and flange on both sides of the plate. Where the beam does not extend outside the joint, force is transferred only from the web and flange inside the joint. Transfer from one side may not be

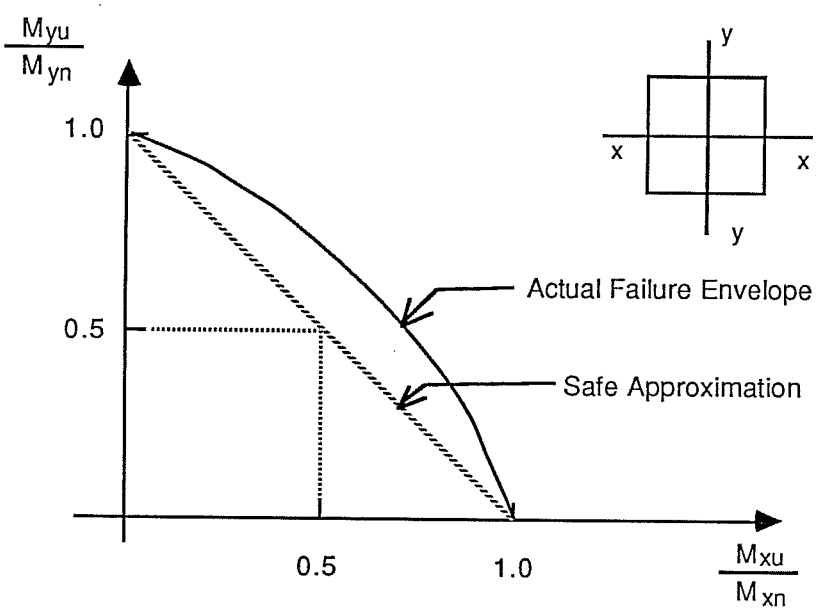

Fig. 5.19 Failure Envelope For Biaxial Flexure in Concrete Members

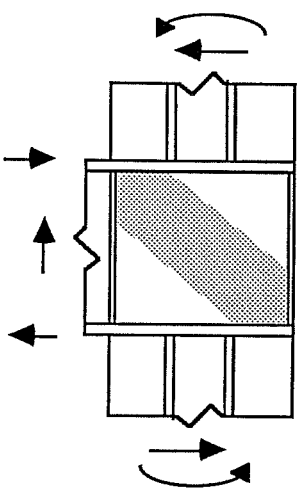

Fig. 5.20a Planar Corner Joint

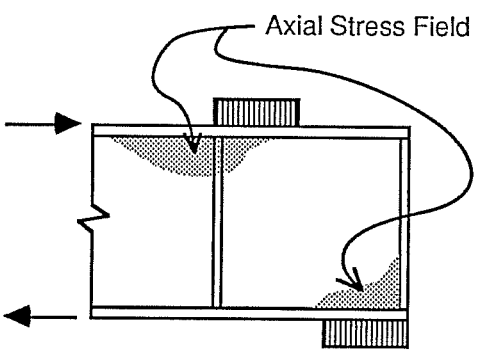

Fig. 5.20b Force Transfer to FBP

as effective, particularly considering that the web inside the joint may be yielded in shear. Whether or not this condition significantly affects behavior was not examined in the experiments.

Top Corner Detail. The top corner joint shown in Fig. 5.21a is similar to the typical corner detail with several variations. Vertical joint reinforcement must be provided to transfer tension from the joint panel directly into the column. Such vertical reinforcement should resist tension associated with the total column moment. As shown in Fig. 5.21a, web stiffeners or other structural steel reinforcement may be required to locally strengthen the beam. In particular, the full tension of the vertical joint reinforcement must be carried through the beam depth in the region denoted "a" in Fig. 5.21a. Also, at point "b" in Fig. 5.21a the vertical component of the concrete strut bears on the beam flange, thereby inducing bending stresses. Finally, the outer panel (compression field) mechanism cannot be mobilized in this detail unless measures are taken to provide a vertical compression resultant at the top of the column. For example, Fig. 5.21b shows how mechanical anchorage of the longitudinal column reinforcement would resist the vertical component of the diagonal compression field. Solutions to the joint detailing problems are not limited to those shown in Figs. 5.21a and b, but, the details demonstrate basic force transfers required in the top corner joint.

Three Dimensional Corner Detail. Figure 5.22a shows a three dimensional corner configuration. As in a planar corner connection, steel beams should extend fully through the column in order to form the steel web and concrete strut mechanisms. As evident from the plan view in Fig. 5.22a, the beam configuration requires steel details which provide continuity of both beams through the connection. The specific strength requirements of the steel details should be evaluated based on joint shear equilibrium. As noted previously, the three dimensional corner detail in a given structure typically will have smaller forces in each direction than the planar interior joint.

Transverse Beams. The three dimensional corner configuration raises the question of whether joint mechanisms are affected by transverse beams and

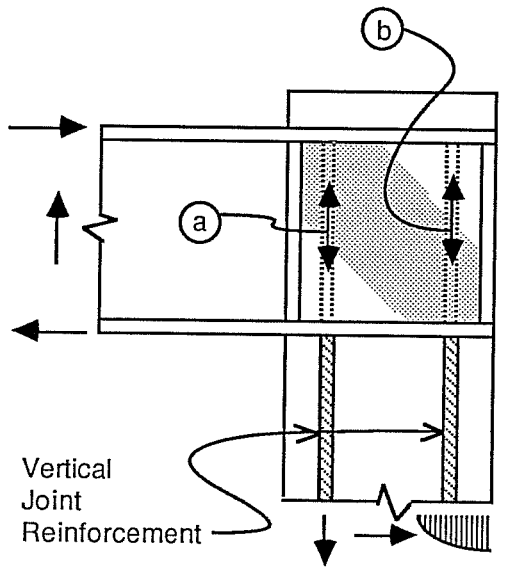

Fig. 5.21a Top Corner Joint (Inner Panel)

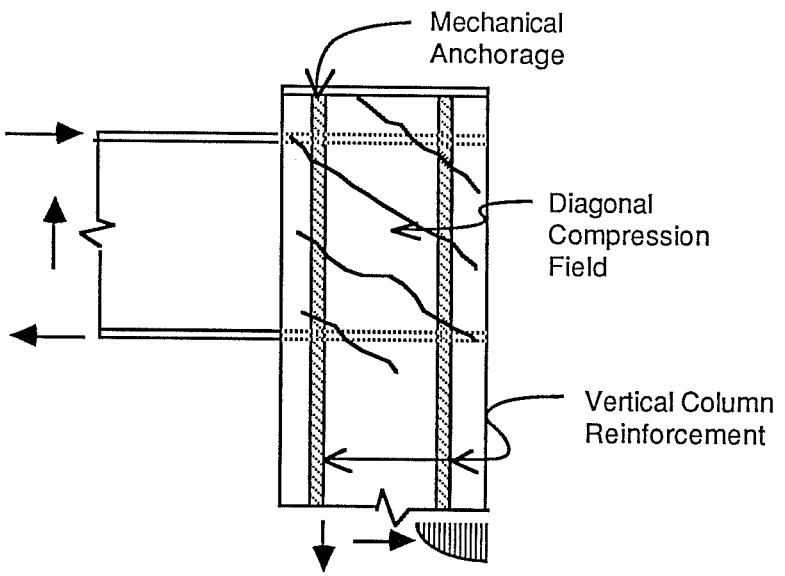

Fig. 5.21b Top Corner Joint (Outer Panel)

biaxial loading in the joint. The transverse beams have both beneficial and negative influences on the joint shear capacity. First, the beam configuration presents more difficult fabrication of column ties and placement of concrete. Transverse beams also create additional planes of discontinuity through the joint. Whether such discontinuities will decrease the joint strength by forming slip planes is not known. Referring to Fig. 5.22a, concrete confinement in the compression strut region tends to mitigate the influence of discontinuities. On the other hand, in Fig. 5.22b, the discontinuities appear to be of more concern in the less confined concrete in the outer panel compression field. The transverse beam may have a positive influence due to out of plane web bending induced by joint shear deformations. In this instance, web bending helps resist joint shear. Another advantage of the transverse beam is in adding confinement to concrete in the joint region particularly when FBPs are used. The current ACI-ASCE recommendations[8] for reinforced concrete connections indicate that transverse beams increase the joint shear capacity by 20% through confinement. Also, transverse compression struts will induce a biaxial compression state (in the horizontal plane) which theoretically increases the maximum compression failure stress in the concrete. Transverse beam effects outlined for the three dimensional corner joint also exist to a degree in planar connections where transverse floor beams frame into the connection. The floor beams do not induce significant biaxial joint forces, but do influence behavior by their presence in the joint region.

Floor Slab. Incorporation of the floor slab in the joint shear mechanisms offers another means of improving the connection strength. The effect of a concrete slab in mobilizing the outer concrete panel is similar to that of extended FBPs as shown in Fig. 5.23. In the detail shown the floor slab above the beam works with the extended FBP below the beam. In utilizing the concrete slab several factors should be kept in mind. First, the horizontal load transferred into the joint by the slab cannot exceed the load developed by shear studs along the beam outside the connection. Second, the effective slab area in compression is based on a width, b, equal to that of the concrete column. Where the slab is utilized, the construction details must insure that no gap exists between the floor slab and column. Third, slab reinforcement continuous through the column will

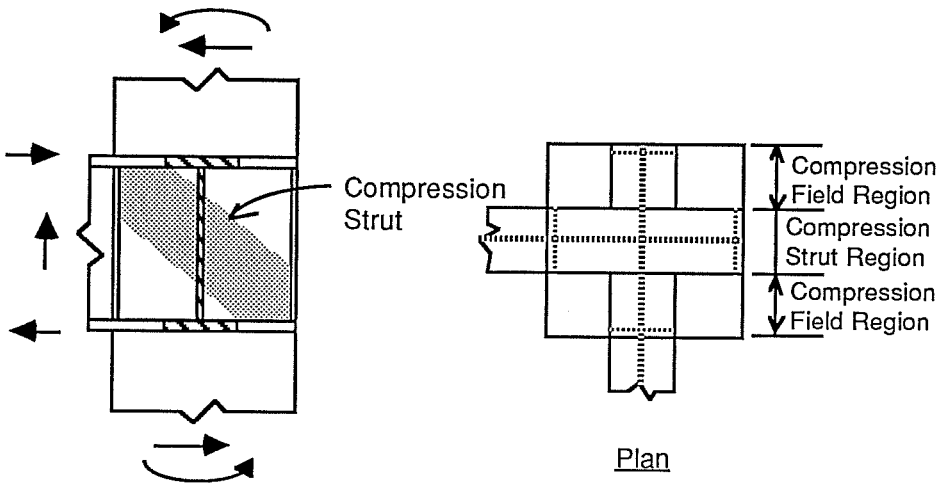

Fig. 5.22a Three Dimensional Corner Joint

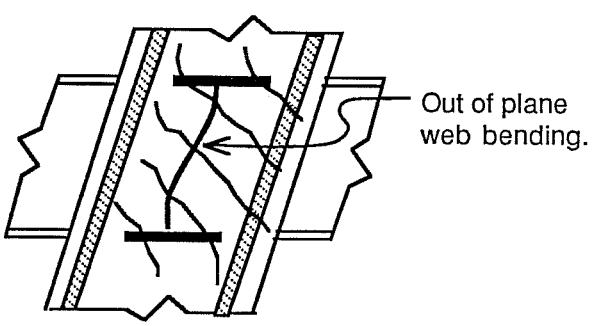

Fig. 5.22b Compression Field With Transverse Beam

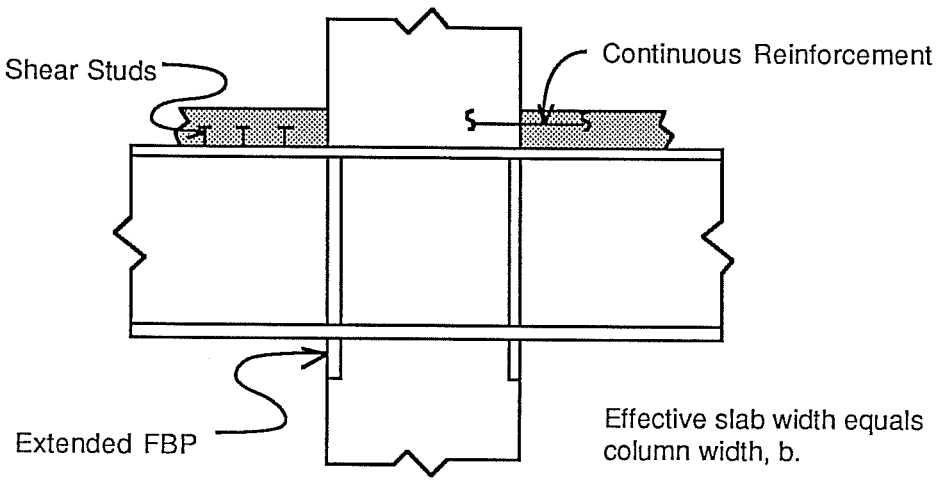

Fig. 5.23 Utilization of Concrete Floor Slab

be beneficial to behavior. Contribution of such reinforcement is limited by the force which can be transferred into the concrete column by bond stresses along the bars. The bond stress transfer may be evaluated using ACI-318[15] provisions for bar anchorage and development length. The LRFD specification[10] for composite beams provides guidance regarding the shear stud transfer and the axial capacity of the concrete slab.

CHAPTER 6 - SUMMARY AND CONCLUSIONS

6.1 Summary

Test were conducted on eight 2/3 scale connections between steel beams and reinforced concrete columns. The specimens were tested under reverse cyclic loading. Various structural steel details were tested in order to assess their influence on the connection strength and stiffness. Details examined include face bearing plates (FBP), web stiffener plates (WSP), embedded steel columns, welded shear studs, steel doubler plates, and vertical joint reinforcement. Additionally, results of nine similar tests previously documented by Sheikh[1] were summarized for comparison purposes. The tests were analyzed, both qualitatively and quantitatively, to determine the internal mechanisms which govern joint behavior.

Based on the experimental results, joint behavior and design were described in terms of two primary modes of failure: joint panel shear and vertical bearing. Joint panel shear strength was calculated as the sum of contributions from the following three elements: the steel (web) panel, inner concrete panel, and outer concrete panel. The steel panel strength consisted primarily of the shear capacity of the beam web which can be increased by doubler plates. The inner concrete panel was mobilized in a diagonal compression strut by face bearing plates or inset web stiffener plates. Finally, outer panel shear was resisted by a concrete compression field, mobilized through such details as steel columns, shear studs, or extended face bearing plates. The compression field strength was a function of both the concrete strength and horizontal column ties.

Vertical bearing failure occurred when the concrete crushing strength was exceeded in the column adjacent to the beam flanges in compression. Vertical joint reinforcement, such as Dywidag bars used in the tests, provided an effective means of strengthening the bearing zone. Also, confinement provided by column ties and extended face bearing plates (or clip angles) to some degree enhanced the concrete compression strength.

Design recommendations were presented for joint configurations such as those tested along with discussion of alternate configurations. The recommendations were drawn in part from recommendations presented previously by Sheikh, and from current specifications for structural steel and reinforced concrete connections. A key component of the recommendations is an analytic design model for calculating the connection capacity. This model addressed the primary modes of failure previously discussed, and was calibrated to test results based on joint deformations at service and ultimate loads of 0.2% and 1.0% total joint distortion, respectively.

6.2 Conclusions

6.2.1 General. The tests demonstrate that the composite beam-column connection is a reliable detail with behavior characterized by reasonable stiffness at service load and ductile failure at ultimate load. Deformations of the composite joint at service and ultimate load are comparable to those in reinforced concrete and welded structural steel connections. Additionally, under reverse cyclic loading, the connection showed toughness comparable to reinforced concrete joints detailed for seismic design.

6.2.2 Strength Behavior. The strength of the connection can be accurately assessed by applying simple principles of mechanics in analyzing the governing internal mechanisms and modes of failure. Two major conclusions addressing aspects of behavior are described below.

Mobilization of Concrete Panel. Details examined in the tests indicate that joint shear strength was enhanced considerably by mobilization of concrete in the joint region. Further, this concrete participation was achieved through simple details which added little complication to the connection. The basic requirement of such details was that they provide a path for transferring horizontal force between the steel beam flange and the inner or outer concrete panel.

In the test specimens, addition of face bearing plates and web stiffener plates mobilized the inner joint panel, with resulting strength increases of 70% and 50% (respectively) over the plain steel beam. In general, the bearing plate

effectiveness was not affected by plate thickness or by splitting the plates at midheight. Also, strength enhancement was roughly proportional to the bearing plate width.

Attachments to the beam flange, such as the steel column, shear studs, and extended face bearing plates mobilized concrete in the outer panel. In the tests, the steel column and shear studs provided roughly a 60% strength increase over the plain steel beam, and the extended face bearing plates provided a 130% increase. The difference in strength increase was related to how effectively the details transfer shear from the beam flange through horizontal struts to the outer joint panel.

The strength increase provided by separate details mobilizing the inner and outer panels was additive. For example, the strength increase afforded by the face bearing plates (inner panel) and shear studs (outer panel) was equal to the sum of contributions which each detail provides separately. However, strength gains achieved by details which mobilize the same region of concrete should not be added together.

Compression Zone Enhancement. Vertical joint reinforcement attached to the beam flange enhanced connection strength where concrete crushing in the zone adjacent to the compression flanges controls. The enhanced strength of the bearing region equals the sum of the tension and compression strength of reinforcement attached to the beam flanges.

Where concrete crushing did not control design, vertical joint reinforcement did not noticeably improve the connection strength or stiffness. Vertical joint reinforcement did, however, reduce the intensity of bond stress on longitudinal column bars through the joint and may be desirable for seismic design where large inelastic load reversals are of concern. Finally, the tests did not provide a clear measure of how much concrete bearing strength was improved by additional confinement provided by clip angles or extended face bearing plates.

6.2.3 Attractive Design Alternative. Several representative design examples showed that relatively large connection forces could be developed by such details as the steel column combined with face bearing plates or web

stiffener plates. Typically, these or similar details would already exist in connections due to erection sequence requirements for composite frames. Composite connections, therefore, were shown to offer an attractive alternative to structural steel or reinforced concrete connections.

6.3 Future Research

While the experimental results reported both herein and previously by Sheikh provide answers to many questions, several areas remain where additional research is needed to more fully understand joint behavior. Topics are presented below in descending order of priority or importance. Included for completeness, several of the items listed below were suggested previously by Sheikh.

Horizontal Ties. The role of horizontal ties in the joint region is not well understood, and deserves investigation since tie detailing and fabrication are significant costs in the connection. Based on the presumed internal force mechanisms, the ties appear to serve three functions peculiar to the connection: 1) joint shear reinforcement in the outer panel compression field, 2) participation in horizontal transfer mechanisms above and below the beam, 3) confinement of concrete in the joint region.

Alternate Configurations. Alternate joint configurations and aspect ratios (width – length – height) should be tested to verify the general applicability and accuracy of design recommendations presented herein. Alternate configurations may include corner and three dimensional details, and connections with composite beams where slab effects are considered.

High Strength Concrete. In practice, concrete strengths of up to 12 ksi are becoming common, particularly for columns in tall buildings. Currently, there is no published research data for composite (or reinforced concrete) connections where concrete strengths higher than 6 ksi are reported.

Axial Load Effects. In this research, no axial load was applied to the column, however, obviously axial loads will exist in practice. As reported by Sheikh, other research has shown that compressive axial load should improve

connection behavior. Such improvement may be considerably beneficial for reducing horizontal tie requirements in the connection, since both the axial load and ties resist opening of diagonal shear cracks.

Seismic Design. The research herein was not intended to specifically address the many particular concerns related to seismic design, and hence, further work focusing on seismic considerations is warranted. In particular, such research should assess whether the restrictions in the Japanese SRC standards are appropriate based on current seismic design practice.

THE END

APPENDIX A1
Summary of Phase I: Specimens 1 through 9

The test results of Specimens 1 through 9 which comprise Phase I of the composite joint project have been reported by Sheikh.[1] For convenience, descriptions and results of the Phase I tests which are used in developing and calibrating the design model are summarized herein.

Details tested in Specimens 1 through 9 are summarized in Fig. A1.1. The strengths for these specimens at given deformation levels are listed in Table A1.1. Definition of the joint deformation (drift) is the same as that given in Chapter 2 of this report. Connection strengths in Table A1.1 are modified from the values reported by Sheikh to reflect an updated calibration of the load setup used in the experiments. Discussion of relative specimen strengths is included in Chapter 3 of this report. Plots of the load-deformation response and a summary of the testing procedure for Specimens 1 through 9 are presented in Sheikh's report. Tables A1.2 and A1.3 indicate the material properties for the structural steel, reinforcing steel and concrete used in fabricating the Phase I specimens.

Specimens 1 and 2 are 1/2 scale pilot tests designed to examine the influence of the FBP detail. The overall geometry and the reinforcing bar layout for these two specimens are shown in Figs. A1.2 and A1.3. Figure A1.4 shows the steel details for Specimens 1 and 2. As seen in this figure, the difference between the two is addition of FBPs in Specimen 2.

Specimens 3 through 9, considered as 2/3 of full scale, all have the same basic geometry and reinforcing bar arrangements which are also common to Specimens 10 through 17 tested in Phase II. Figures A1.5 and A1.6 show the overall geometry and reinforcing bar layout for Specimens 3 through 9. Further discussion of the specimen configuration is the same as that given for Specimens 10 through 17 in Chapter 2.

Figure A1.7 shows the structural steel details used in Specimens 3 through 5. Specimen 3 consists of a plain steel beam which is continuous through the column. The built-up beam section which is identical for Specimens 3 through

Table A1.1 Summary of Connection Capacities at Given Deformations

Specimen	f'_c (ksi)	Average Ram Load (kips)* 1% Drift	2% Drift
1 Plain Beam	3.6	17.0 (17.0)	17.8 (17.8)
2 FBP	3.6	22.5 (22.5)	26.2 (26.2)
3 Plain Beam	4.5	16.5 (17.4)	18.0 (18.8)
4 FBP	4.3	26.6 (27.4)	31.6 (32.5)
5 FBP (thick)	4.3	28.2 (29.1)	33.5 (34.3)
6 FBP-DbPl-Styr.	4.0	35.8 (36.7)	44.5 (45.3)
7 FBP (wide)	4.0	33.8 (34.6)	40.4 (41.2)
8 FBP (extended)	3.6	46.2 (47.0)	53.7 (54.5)
9 FBP-No Web	3.7	26.2 (27.0)	30.7 (31.5)

* Note: Loads given in parenthesis ( ) are values taken directly from Sheikh's report. The second value shown has been modified to account for friction losses in the rams. This modification is based on the ram calibration used in reporting Phase II results.

9 is similar to that used in Specimens 10 through 17. In Specimens 10 through 17 a slightly thicker flange (7/8 inch versus 3/4 inch) is used in order to provide a greater bending capacity. Specimens 4 and 5 are the same as 3 with the addition of FBPs. The 3/8 inch thick plates in Specimen 4 represent a practical thickness for typical construction. In Specimen 5, very thick (7/8 inch, Fy 50 ksi) plates are used to determine whether connection performance is sensitive to the plate's bending strength and stiffness.

Figure A1.8 shows details for Specimens 6 and 7. In Specimen 6, thick web doubler plates are used to preclude joint shear failure. The purpose of this test is to assess the mode of failure due to concrete crushing against the flanges. Additionally, Specimen 6 had Styrofoam blocking behind the FBPs to eliminate formation of a diagonal compression strut in the concrete. In Specimen

Table A1.2 Material Properties – Steel Coupons and Reinforcing Bars

Specimens	Description	Static Yield Stress (ksi)	Ult. Stress (ksi)	Gauge Length (in.)	% Elong.	Strain Hardening E_{sh} (ksi)	Strain Hardening ϵ_{sh} (in./in.)
1 - 2	Long. Web	55.6	71.5	2	34.0	290	.024
1 - 2	Tranv. Web	56.3	71.7	2	28.2	245	.020
1 - 2	Flange & FBP	44.5	66.3	2	37.7		
3 - 9	Long. Web	36.5	56.5	2	40.5	335	.022
3 - 9	Tranv. Web	35.9	56.1	2	33.1	27.0	.020
3 - 9	Flange	50.6	76.3	8	25.1		
3 & 6	3/8–in. FBP	43.4	68.5	2	38.0		
4, 5, 7-9	7/8–in. FBP	58.9	87.3	2	33.3		
1 - 2	#3 bars	62.1	92.1	8	17.0		
1 - 2	#9 bars	62.2	99.1	8	18.6		
3 - 7	#3 bar	65.0	101.8	8	15.3		
3 - 7	#4 bars	61.6	90.2	8	18.3		
3 - 7	#10 bars	65.7	104.2	8	16.1		
8 - 9	#3 bars	77.0	112.4	8	11.0		
8 - 9	#4 bars	60.0	101.8	8	11.6		
8 - 9	#10 bars	65.3	104.5	8	15.8		

7, the FBPs are wider than the beam flanges to determine whether the diagonal concrete compression strut capacity increases proportionally with plate width.

Figure A1.9 shows details for Specimens 8 and 9. In Specimen 8, extended FBPs above and below the flanges are intended to mobilize concrete outside the beam depth. Specimen 9 was built using a beam section recycled from Specimen 5. In Specimen 9, a large portion of the web section is cut out in order to reduce the steel panel contribution to the strength. The reasoning

Table A1.3 Concrete Cylinder Strength

Specimen	28-day Strength (psi)	Day of Testing Age (days)	Day of Testing Strength (psi)
1	3300	93	3550
2	3300	106	3550
3	4400	42	4500
4	4100	48	4300
5	4100	56	4300
6	3900	74	4000
7	3900	81	4000
8	3600	28	3600
9	3600	39	3700

behind this experiment is to isolate the joint shear contribution of the concrete strut.

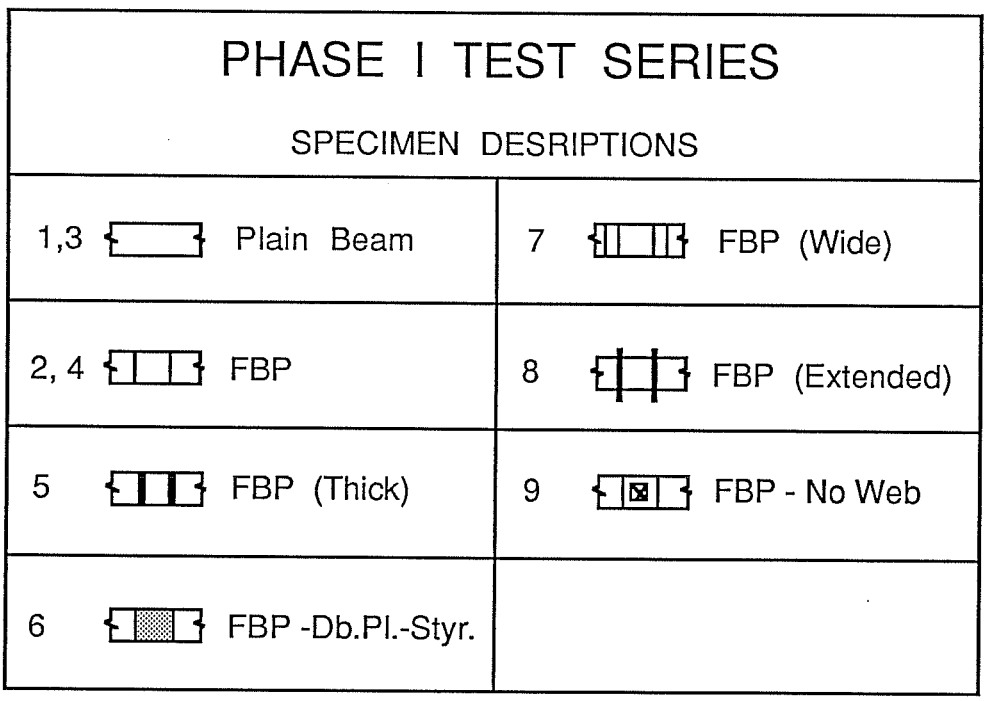

Fig. A1.1 Summary of Phase I

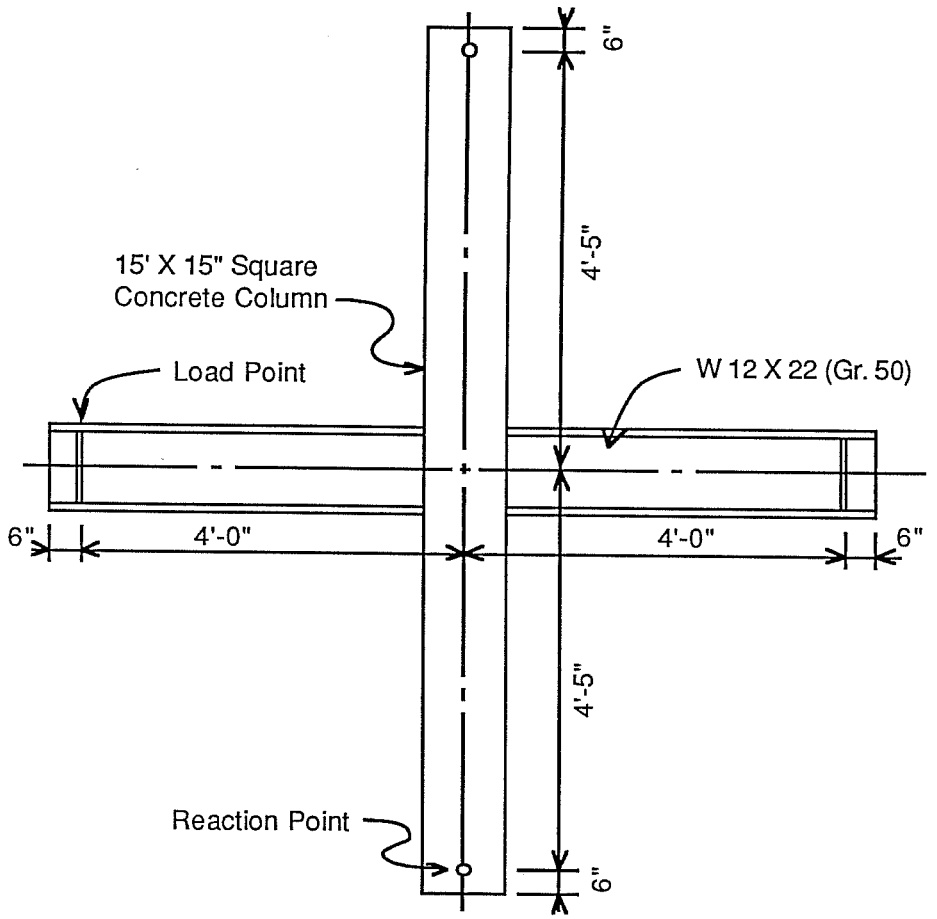

Fig. A1.2 Test Specimens 1 and 2

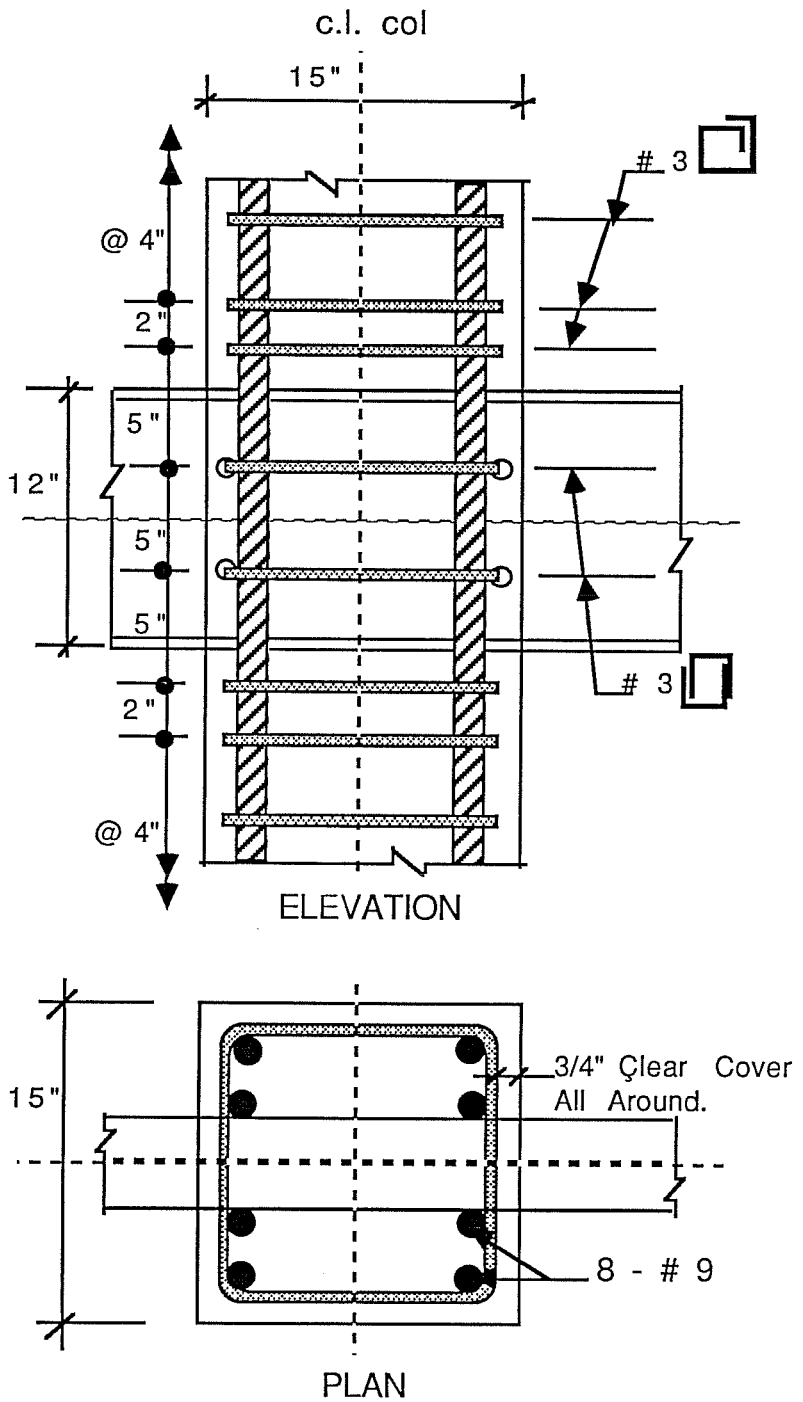

Fig. A1.3 Joint Reinforcement for Specimens 1 and 2

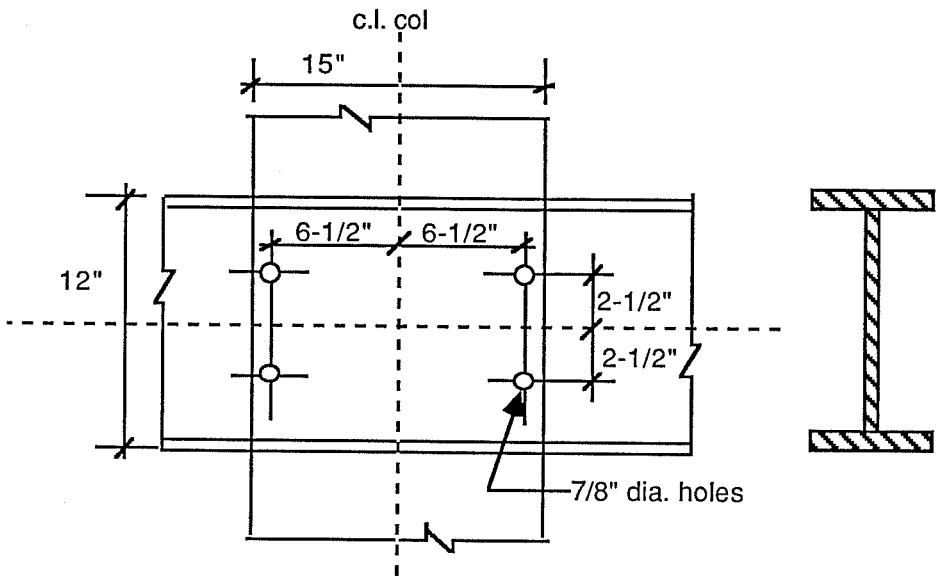

Specimen 1

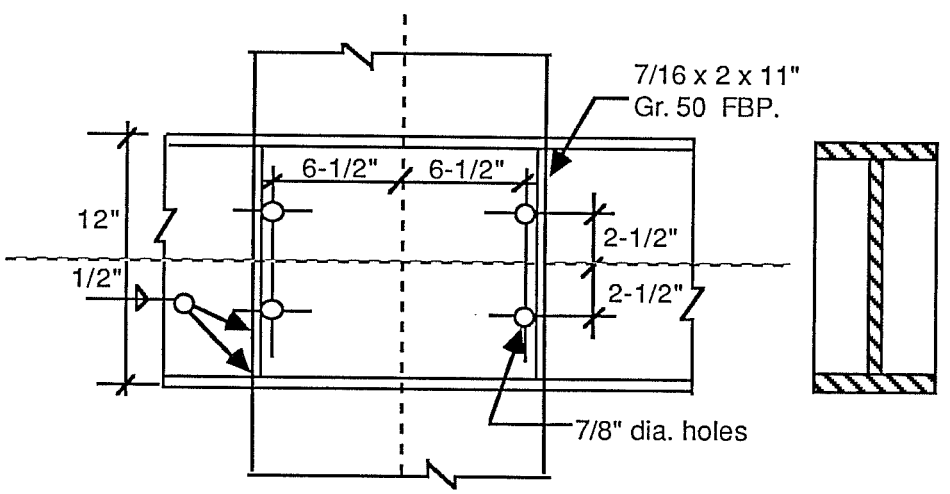

Specimen 2

Fig. A1.4 Joint Details for Specimens 1 and 2

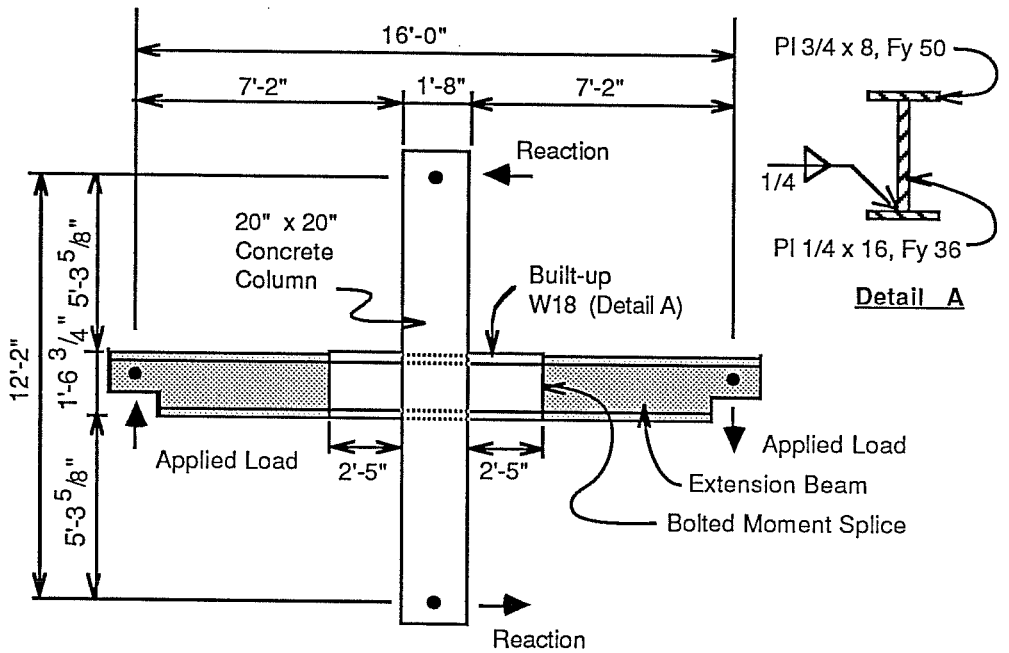

Fig. A1.5 Typical Test Specimen (Specimens 3 to 9)

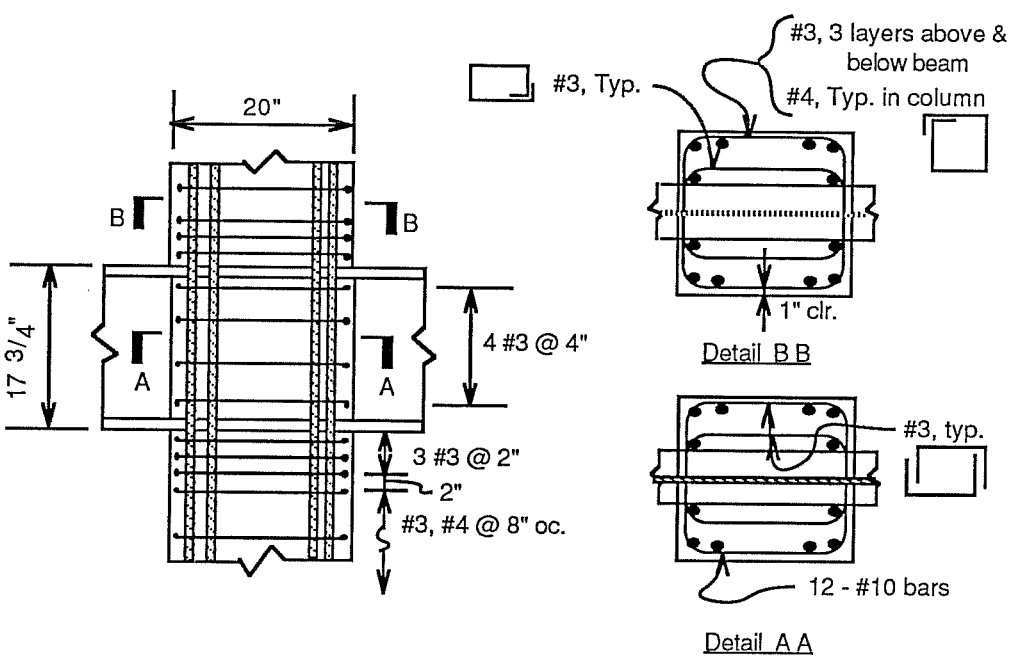

Fig. A1.6 Typical Reinforcing Steel Detail (Specimens 3 to 9)

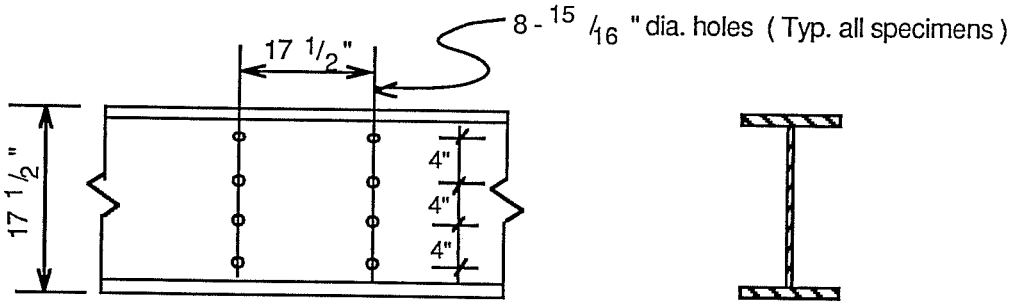

Specimen 3: Plain Beam

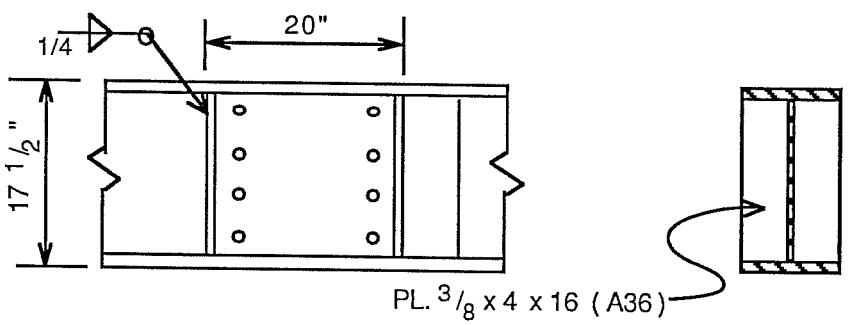

For information not shown see Spec. 3.

Specimen 4: FBP

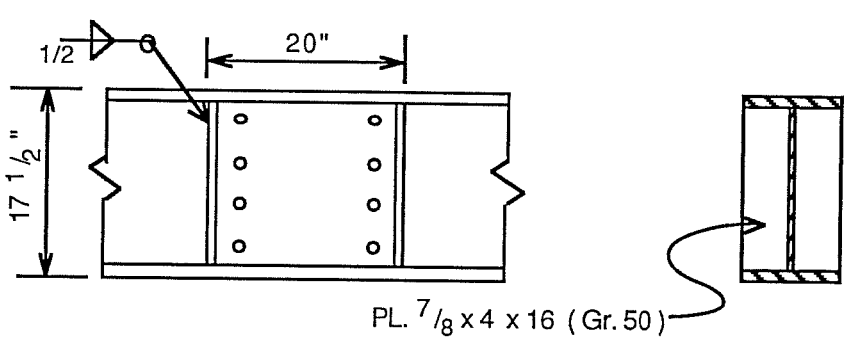

For information not shown see Spec. 3.

Specimen 5: FBP (thick)

Fig. A1.7 Joint Details for Specimens 3, 4, and 5

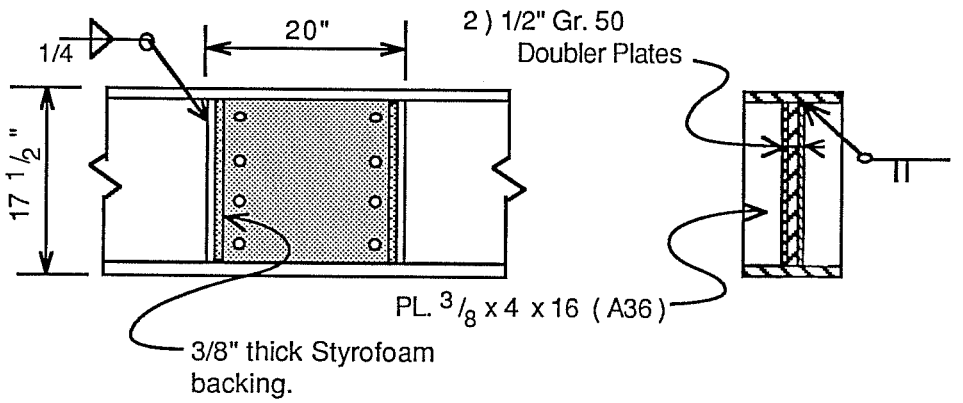

For information not shown see Spec. 3. (Fig. A1.7)

Specimen 6: FBP - DbPl. - Styrofoam

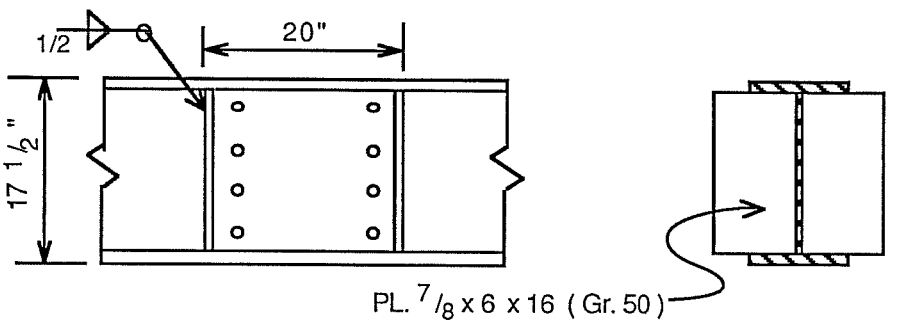

For information not shown see Spec. 3 (Fig. A1.7).

Specimen 7: FBP (wide)

Fig. A1.8 Joint Details for Specimens 6, and 7

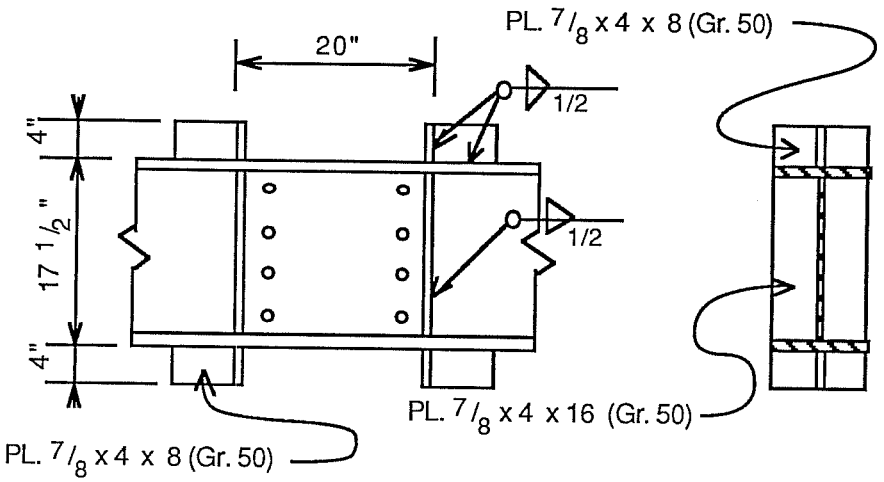

For information not shown see Spec. 3 (Fig. A1.7).

Specimen 8: FBP (Extended)

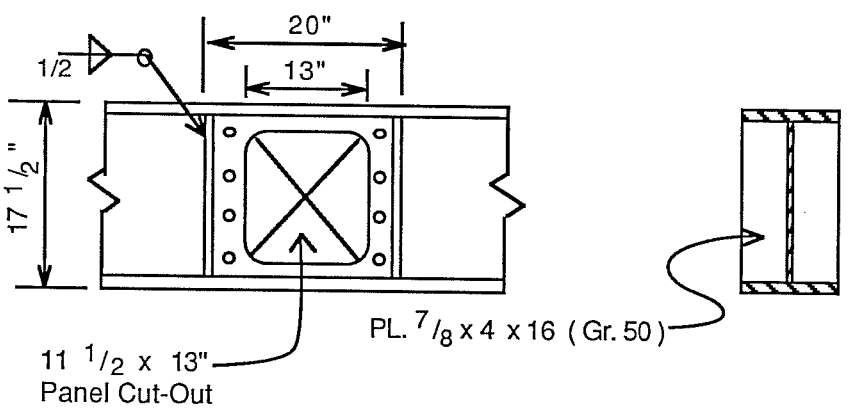

For information not shown see Spec. 3 (Fig. A1.7).

Specimen 9: FBP (thick) - No Web

Fig. A1.9 Joint Details for Specimens 8 and 9

APPENDIX A2
Evaluation of Shear Stud Group Strength

This section provides examination of the strength of the shear stud groups which were used in joint Specimens 12 and 13. Included is data both from Specimens 12 and 13, and also from four push out tests described herein. Additionally, the measured stud group strengths are related to values calculated using the AISC-LRFD[10] specification for shear studs in composite beams.

A2.1 Push out Tests. Four push out tests were conducted to obtain more direct measurement of the shear stud group capacity used in Specimens 12 and 13. The push out test specimen and experimental set up are shown in Figs. A2.1 and A2.2. The specimen was fabricated by recycling the flange plates and attached studs from the joint Specimens 12 and 13. As reported previously, in Specimen 13 the shear studs were still intact after the test. In Specimen 12 the shear studs attached to the top flange were intact, but those attached to the lower flange fractured during the joint test. Using the intact studs, three push out tests were conducted on full stud groups and one on a single stud. The reason for reusing the shear studs was a practical one related to economy. The influence of the recycled studs was probably insignificant with regard to ultimate load, but may have reduced the ductility in the push out tests.

The push out specimen shown in Fig. A2.1 was designed to simulate the local environment of the stud groups in the composite joint. The steel reinforcement was similar to that used in the joint, and the specimen was cast in the vertical position shown in Fig. A2.1. Two of the stud groups were cast facing downward in order to examine the effect of casting position on stud capacity. The steel flange plates were painted with a thick coat of primer paint to reduce significant contribution of concrete adhesion and friction against the plates.

The test set up is shown in Fig. A2.2 along with the sequence in which the stud groups were tested. Load was applied by a 600 k screw type testing machine through a spherical loading head as shown. The deformation or slip of the flange plate relative to the concrete was monitored with two 1 in. dial gages. Load was applied quasi-statically at increments of 10 to 20 k during the initial

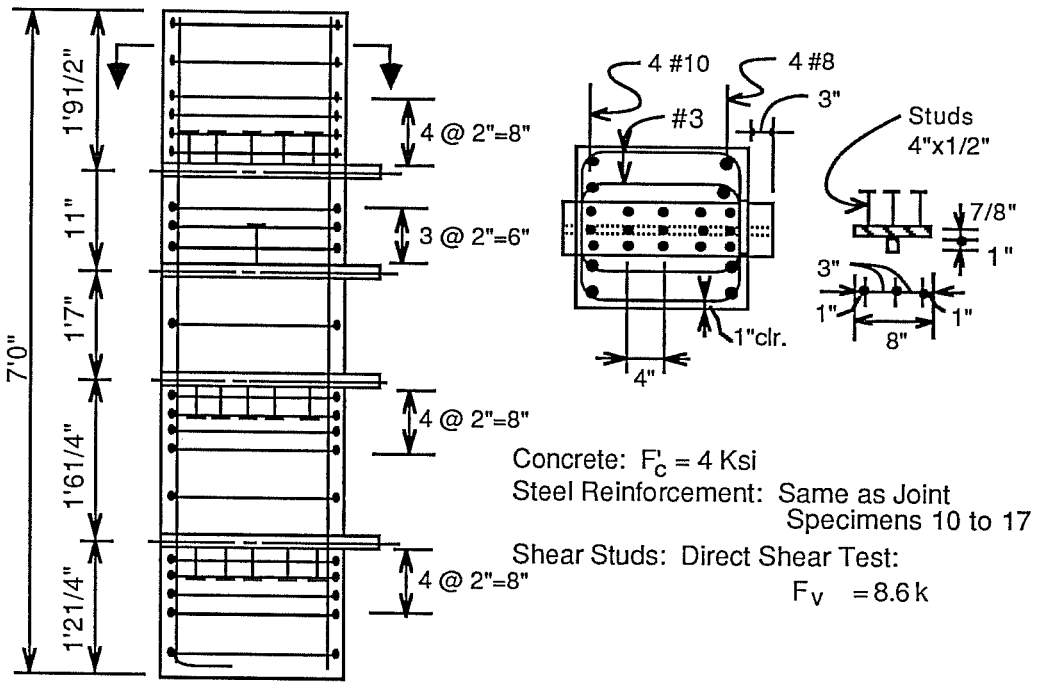

Fig. A2.1 Push Out Test Specimen

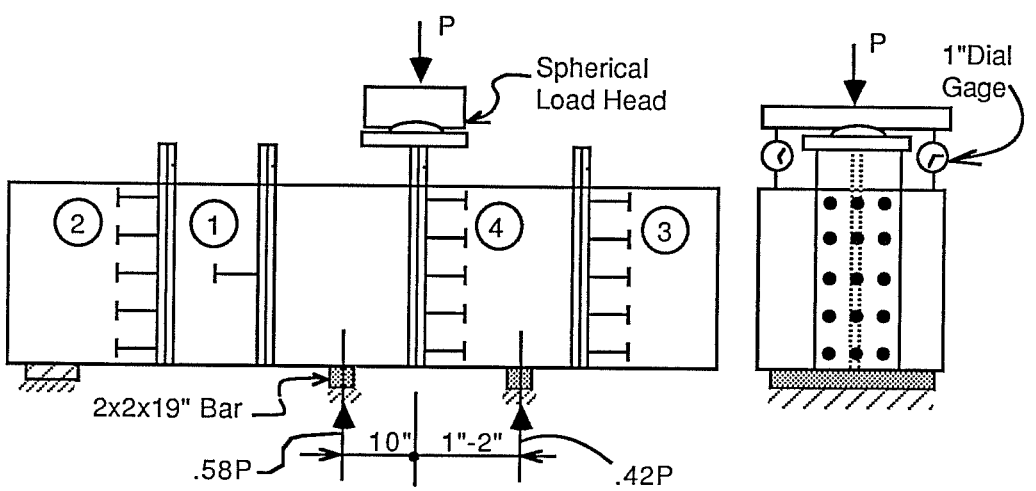

Fig. A2.2 Stud Pushout Test Setup

stages, and at displacement increments of 0.01 in. to 0.02 in. at higher loads when the stiffness reduces. As shown in Fig. A2.3, in general not all of the studs fractured during the push-out tests. Typically, only the studs near the loaded side of the plate failed, while the remaining studs pushed through the concrete.

The load-slip response of the tests are shown in Fig. A2.4. The results of the three tests (Tests 2, 3 and 4) with the full stud groups show similar behavior during the initial loading stages. Above 100 k, Tests 3 and 4 which were bottom cast have less stiffness than Test 1 which was cast upright. This behavior supports the notion that concrete cast against an upper surface is inferior to other concrete. The difference in peak loads between Tests 3 and 4 is not readily explained. Test 4 may have a lower strength since it was loaded after Test 3. Hence, cracking of concrete in the vicinity of Test 4 during loading of Test 3 may have reduced the capacity of Test 4.

A2.2 Direct Shear Tests. In order to determine the capacity of the shear studs based on the steel strength, direct shear tests were conducted on six studs. The direct shear tests were conducted in a 600 k hydraulic testing machine. During testing the studs were loaded through a fixture which insured that no bending was induced in the stud, and that a shear failure occurred across a single plane.

From the direct shear test, the average shear strength of the studs was 8.6 kips which results in a ultimate nominal shear stress of 43 ksi. Assuming the ultimate shear stress is related to the ultimate tensile stress by the Von Mises criterion ($F_v = F_t / \sqrt{3}$), the ultimate tensile stress is 75 ksi (43 $\sqrt{3}$ ksi). The resulting tensile capacity of the stud is 14.9 kips.

A2.3 Calculated Stud Capacity. In the AISC-LRFD[10] specification, the following equations are used for calculating shear stud capacity for composite beams with solid slabs:

$$Q_n = 0.5\, A_{sc} \sqrt{f'_c}\, E_c \;\leq\; A_{sc}\, F_u \qquad (A2.1a)$$

$$E_c = w^{1.5} \sqrt{f'_c} \qquad (A2.1b)$$

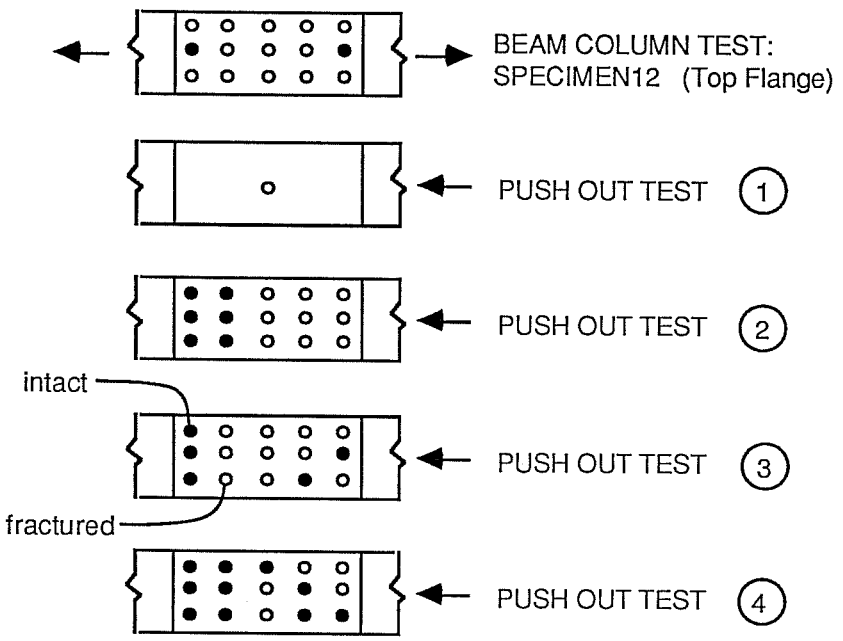

Fig. A2.3 Diagram of Stud Fractures

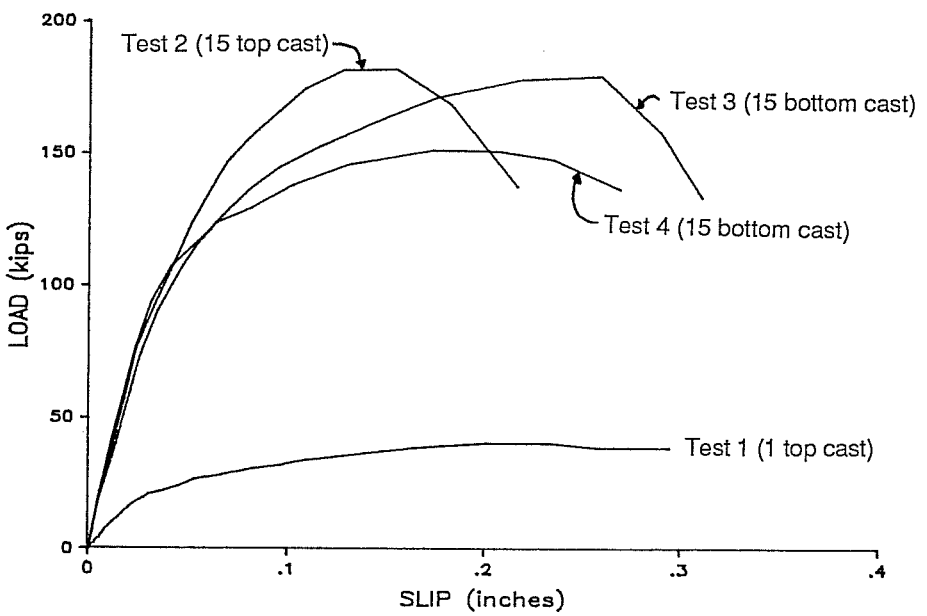

Fig. A2.4 Load-Deformation Response of Push Out Tests

Using concrete properties from the push out tests the stud capacity according to Eqs. A2.1a,and b is 11.8 kips. The upper limit on the stud capacity in Eq. A2.1a is based on tensile fracture of the stud. Based on the direct shear tests, the tensile capacity of the stud is 14.9 k, and hence does not control. According to Eqs. A2.1a and b the direct shear strength of the stud does not control design. This implies that behavior is governed by a shear friction mechanism which is limited only by concrete strength and the tensile strength of the stud.

A2.4 Analysis of Test Results. Comparison of the calculated single stud capacity of 11.8 kips with the maximum measured load of 40.7 kips in push out Test 1 (single stud) indicates that a significant load is carried by adhesion and friction between the flange plate and concrete. Assuming that the load carried by friction and adhesion is constant in all the tests, the shear stud capacity in each of Tests 2, 3 and 4 may be determined using the following equations:

$$\text{Test 1:} \qquad X + C = P_1 \qquad (A2.2a)$$

$$\text{Tests 2,3 \& 4:} \quad 12X + C = P_i \qquad (A2.2b)$$

In each equation X is the capacity of a single stud, C is the force carried by adhesion and friction, and P_i is the measured peak load in each test. Arguably, the friction may not be the same in all tests, however, this simplification is assumed in light of the available data. In Eq. A2.2b, only twelve studs are assumed to carry load since studs in the first row have insufficient cover to develop significant force. This assumption is supported by the observed stud fractures shown in Fig. A2.3 for the push out tests.

By combining Eq. A2.2a for Test 1 with Eq. A2.2b for Tests 2,3 and 4, three measurements of the single stud capacity are obtained. The three values are listed in Table A2.1 along with values calculated using the AISC-LRFD[10] specification. Also shown in Table A2.1 are single stud strengths calculated from the load carried by joint Specimens 12 and 13.

As shown in Table A2.1, for Specimen 12 the calculated stud capacity ranges from 10.8 k to 14.5 k depending on the assumptions used in the calculation.

Table A2.1 Summary of Calculated and Measured Stud Strengths

Calculated	Measured	Single Stud Strength (kips)
AISC–LRFD	–	11.8
–	Push out 2	12.8
–	Push out 3	12.6
–	Push out 4	10.1
–	Joint Spec. 12	10.8 to 14.5
–	Joint Spec. 13	12.3

The lower bound is obtained by assuming that the shear stud group carried a load equal to the outer panel shear plus the column shear according to the breakdown of component strengths given in Table 3.3 of Chapter 3. The upper bound value adds to the stud force the horizontal shear force associated with the inner concrete panel since friction is the only other means of transferring this force. For Specimen 13 the single value of 12.3 k is based on studs carrying the outer panel and column shear since in this case the inner panel shear is directly transferred into the beam by the FBP detail.

In determining the shear stud strengths noted in Table A2.1 for Specimens 12 and 13, peak connection loads are used rather than the 1% TJD loads. This is done because the stud loads calculated from the connection tests are compared with those from the push out tests where no deformation criterion is imposed on the measured strength. Also, the stud strengths for Specimens 12 and 13 were based on normalized joint strengths to reflect the same concrete strength as the push out tests ($f'_c = 4$ ksi).

The summary of results in Table A2.1 indicates that the AISC-LRFD[10] specification provides a reasonable value for the shear stud strength in composite joints. For design purposes stud strengths equal to 80% of the AISC values are recommended. There are two reasons for reducing the nominal strength by 20% for composite joint design. First, as indicated by the data in Table A2.1, there is evidence that the AISC strength may not be reached in some cases (Specimen 12

and Push out test 4). In both instances where the AISC values were not reached the studs were located in regions where concrete was cast against an upper surface. The second reason for the reduction is related to the deformation criteria in determining the connection design strength. As presented in Chapters 4 and 5 the joint design equations estimate the joint forces at an implied deformation of 1% TJD. Since the measured peak capacity may exceed the design capacity by 15% to 20%, it is prudent to design the studs with a similar margin between design and ultimate capacity. In other words, the additional margin of strength in the stud design should preclude stud failure prior to the connection reaching its ultimate capacity.

APPENDIX A3
Design Examples

Two design examples are included which demonstrate application of the design equations and recommendations from Chapter 5. Also, in the first example the joint strength is also calculated according to the model from Chapter 4. In each example the nominal strength of the connection is calculated given a beam and column size and type of detail. Column sizes are chosen to be representative of actual practice. Beam sizes are chosen such that their plastic moment is roughly 80% of the nominal column bending strength.

Design Example 1 is shown in Fig. A3.1. In this example a FBP and steel column detail provide a nominal connection strength which can transfer a beam moment that is roughly 4% higher than the plastic moment of the W27 $\times$ 235 steel beam. Note, however, that this comparison is based on nominal strengths where the capacity reduction factors have not been considered. If the respective ϕ factors for the connection and beam are 0.7 and 0.9, then the connection design strength is roughly 80% of the beam design strength. If required, the connection strength could be increased through the use of extended face bearing plates, with face bearing plates or web doubler plates. In Example 1, along with calculating the nominal joint strength (per Chapters 4 and 5) the following items are determined (checked): horizontal tie requirement, maximum size of vertical column bars, FBP size and thickness, and minimum required steel column flange and beam flange thicknesses.

Design Example 2 is shown in Fig. A3.2. In this case the nominal connection strength is calculated for a similar detail (FBP, steel column) but with and without vertical joint reinforcement. Without vertical joint reinforcement the connection strength is governed by bearing failure, whereas with reinforcement joint panel shear controls the strength. As shown in Fig. A3.2 the vertical joint reinforcement increases the joint strength by roughly 11%. In both cases the nominal connection strength exceeds the plastic moment capacity of the beam by the ratios, 1.03 and 1.14, respectively. In Example 2 other aspects such as detailing of the connection are not considered.

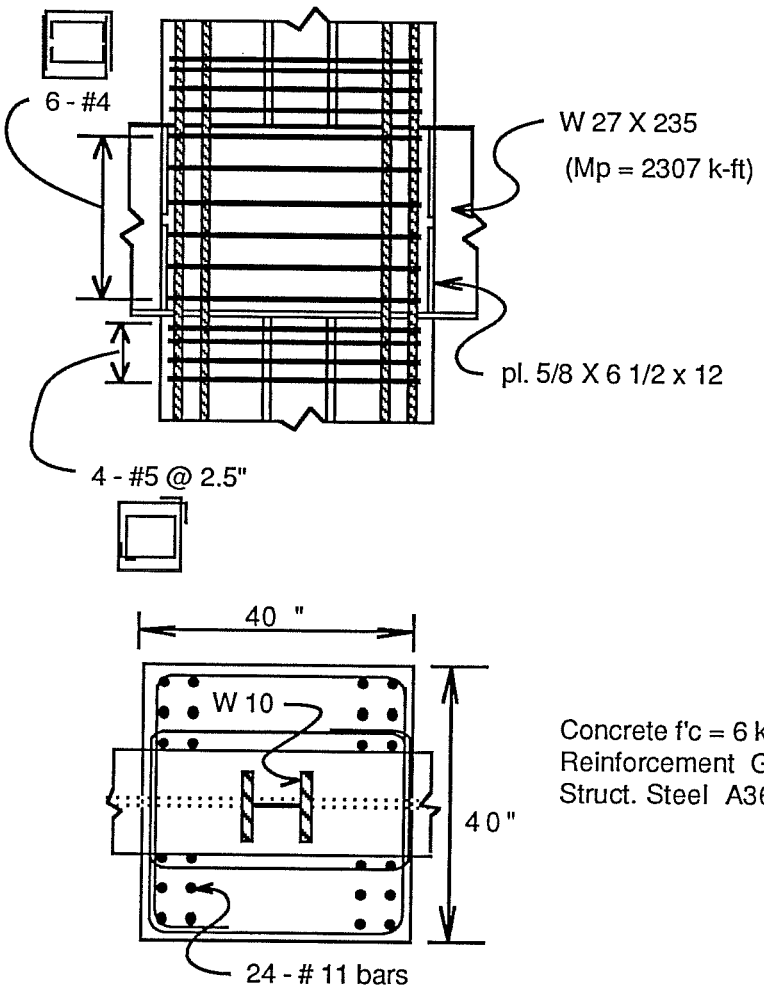

Nominal Joint Strength (ϕ = 0):

Vb = 288 k
Mb = 2396 k-ft (Per Chapter 5)

Vb = 294k
Mb = 2446 k-ft (Per Chapter 4)

Fig. A3.1 Design Example 1

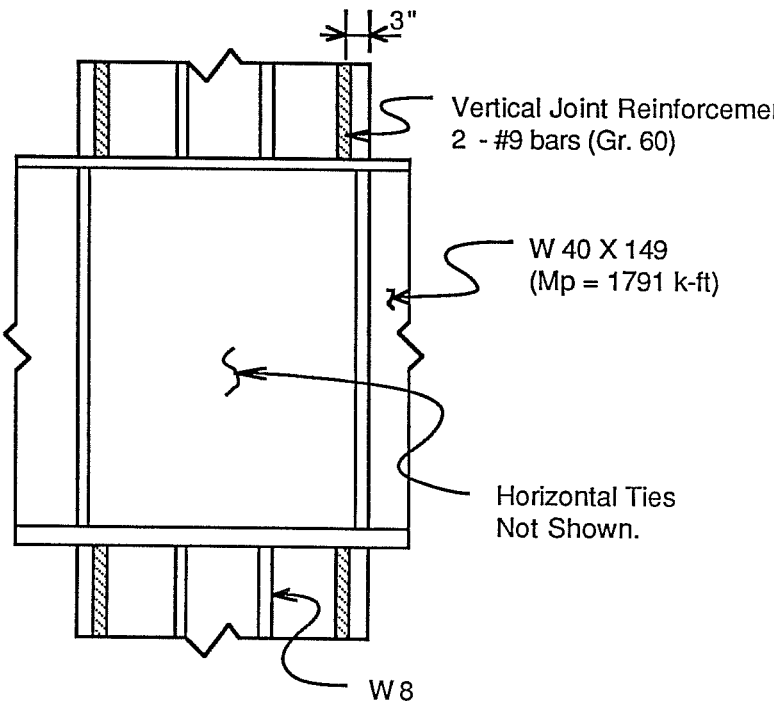

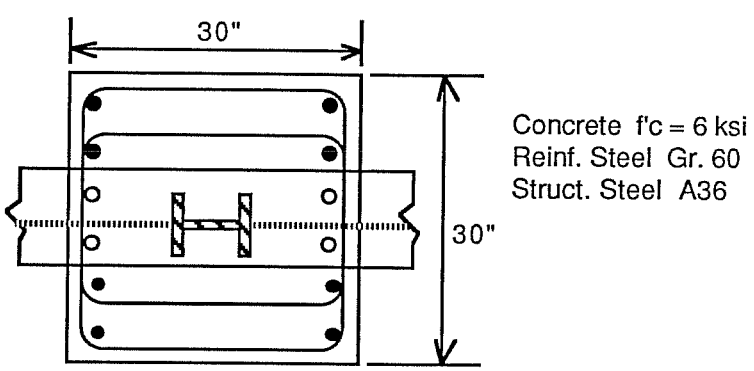

Nominal Joint Strength (ϕ = 0):

Without Vertical Joint Reinforcement: Vb = 210 k
Mb = 1837 k-ft

With Vertical Joint Reinforcement: Vb = 234 k
Mb = 2047 k-ft

Fig. A3.2 Design Example 2

EXAMPLE 1 – SPLIT FACE BEARING PLATE WITH STEEL COLUMN

Given:

1) Joint geometry and layout shown in Fig. A3.1

2) Reinforced Concrete Column: 40 × 40 in. square

$24 - \#11$ bars ($\rho = 2.2\%$)

$f'_c = 6$ ksi

$F_y = 60$ ksi

3) Steel Beam: W27 × 235 (A36)

$M_p = 2307$ k-ft

d = 28.66 in.

$b_f = 14.19$ in.

$t_w = 0.91$ in.

$t_f = 1.61$ in.

4) Proportional Member Forces:

$$M_b = \alpha_1 V_b \qquad (5.10a)$$

$$V_c = \alpha_3 V_b \qquad (5.10c)$$

$\alpha_1 = 105$ in.

$\alpha_3 = 1.67$

Calculate:

1) Connection strength in terms of maximum beam moment and shear (M_b and V_b). Calculate strength using models from Chapters 4 and 5.

2) Horizontal tie requirement.

3) Maximum size of vertical column bars.

4) FBP size and thickness

5) Minimum steel column flange thickness.

6) Minimum beam flange thickness.

1. Calculate Connection Strength in Terms of M_b and V_b

I - Strength Per Design Model (Chapter 5–Ref. Fig. 5.5)

Determine effective joint width:

Max. joint width:

$$b_j = (b_f + b)/2 \leq b_f + h \leq 1.75\, b_f \qquad (5.4b)$$

$$b_f = 14.19 \text{ in.}$$

$$b = 40 \text{ in.}$$

$$h = 40 \text{ in.}$$

$$\underline{b_j = 24.8 \text{ in.}}$$

Mobilization coefficient:

$$C = (x/h)\,(y/b_f) \qquad (5.4c)$$

$$x = 25 \text{ in.}$$

$$h = 40 \text{ in.}$$

$$y = 10 \text{ in.}$$

$$b_f = 14.2 \text{ in.}$$

$$\underline{C = 0.44}$$

Effective outer panel width:

$$b'_{op} = C(b_j - b_i) \leq 2\, d_{op} \qquad (5.4a)$$

$$C = 0.44$$

$$b_j = 24.8 \text{ in.}$$

$$b_i = b_f = 14.2 \text{ in.}$$

$$d_{op} = 0.25d = 7.2 \text{ in.}$$

$$\underline{b'_{op} = 4.7\text{in.}}$$

Effective joint width:

$$b'_j = b_i + b'_{op} \tag{5.3}$$

$$b_i = 14.2 \text{ in.}$$

$$b'_{op} = 4.7 \text{ in.}$$

$$\underline{b'_j = 18.9 \text{ in.}}$$

Calculate shear panel strength:

Inner panel:

$$V_n = 0.63\sqrt{f'_c}\, R\, b_p\, h \tag{5.6a}$$

$$R = 1.0 \qquad (5.6b)$$

$$b_p = 14.2 \text{ in.}$$

$$h = 40 \text{ in.}$$

$$f'_c = 6 \text{ ksi}$$

$$\underline{V_n = 877 \text{ k}}$$

Outer panel (Assume ties do not govern):

$$V'_n = V'_c + V'_s \leq 0.63\sqrt{f'_c}\, b'_{op}\, h \tag{5.7a}$$

$$f'_c = 6 \text{ ksi}$$

$$b'_{op} = 4.7 \text{ in.}$$

$$h = 40 \text{ in.}$$

$$\underline{V'_n \leq 290 \text{ k}}$$

Calculate tie area req'd:

$$V'_n = V'_c + V'_s = 290 \text{ k}$$

$$V'_c = 0.16\sqrt{f'_c}\, b'_{op}\, h = 73 \text{ k} \tag{5.7b}$$

$$V'_s \geq V'_n - V'_c = 217 \text{ k}$$

$$V'_s = 0.9\, A_{sh}\, F_{ysh}\, h/s_h \tag{5.7c}$$

$$F_{ysh} = 60 \text{ ksi}$$

$$\underline{\frac{A_{sh}}{sh} \geq 0.10 \text{ in.}}$$

1st Iteration:

Assume Length of Bearing Region

$$a_c \leq 0.3\,h\,(12 \text{ in.}) \tag{5.8b}$$

Try $\underline{a_c = 7 \text{ in.}}$ (panel shear governs)

Calculate P_{eq} and jh:

$$P_{eq} = C_c + T_{vr} + C_{vr} \tag{5.9a}$$

$$T_{vr} = C_{vr} = 0$$

$$C_c = 2 f'_c\, a_c\, b'_j \tag{5.8a}$$

$$f'_c = 6 \text{ ksi}$$

$$a_c = 7 \text{ in.}$$

$$b_j = 18.9 \text{ in.}$$

$$\underline{P_{eq} = C_c = 1588 \text{ k}}$$

$$\underline{jh = h - a_c} \tag{5.9b}$$

$$h = 40 \text{ in.}$$

$$a_c = 7 \text{ in.}$$

$$\underline{jh = 33 \text{ in.}}$$

Calculate steel panel, V_s:

$$V_s = 0.6\,F_{yw}\,t_w\,jh \tag{5.5}$$

$$F_{yw} = 36 \text{ ksi}$$

$$t_w = 0.91 \text{ in.}$$

$$jh = 33 \text{ in.}$$

$$\underline{V_s = 649 \text{ k}}$$

Column shear factor:

$$J = 1.0 \text{ (since steel column is present)}$$

Calculate resulting beam moment, M_b:

$$M_b[1] = \frac{V_s\, d_f + V_n\,(0.75\, d_w) + V_n'\,(d + d_{op})}{2 - (J\, d_f\, \alpha_3/\alpha_1)} \tag{5.12}$$

$$V_s = 649 \text{ k}$$
$$V_n = 877 \text{ k}$$
$$V_n' = 290 \text{ k}$$
$$d_f = 27.05 \text{ in.}$$
$$d_w = 25.44 \text{ in.}$$
$$d = 28.66 \text{ in.}$$
$$d_{op} = 0.25\, d = 7.2 \text{ in.}$$
$$J = 1.0$$
$$\alpha_3 = 1.67$$
$$\alpha_1 = 100 \text{ in.}$$

$$\underline{M_b[1] = 28,860 \text{ k-in.}}$$

$$M_b[2] = \alpha_1 \left[P_{eq} - \frac{V_s\, d_f + V_n (0.75\, d_w) + V_n'\,(d + d_{op})}{jh} \right] \tag{5.14}$$

$$\underline{M_b[2] = 23,380 \text{ k-in.}}$$

Compare $M_b[1]$ and $M_b[2]$:

$$M_b[1] > M_b[2], \text{ therefore, increase } a_c.$$

$$\text{Try } \underline{a_c = 7.27 \text{ in.}}$$

2nd Iteration:

$$P_{eq} = 1649 \text{ k}$$

$$jh = 32.73 \text{ in.}$$

$$V_s = 643 \text{ k}$$

$$M_b[1] = 28,760 \text{ k-in.}$$

$$M_b[2] = 28,860 \text{ k-in.}$$

$M_b[1] = M_b[2]$ (Close enough)

$\underline{M_b = M_b[1] = 28,760 \text{ k-in.} = 2396 \text{ k-ft}}$

I - Solution Per Design (Chapter 5) Model:

Nominal Joint Strength:

$M_b = 2396$ k- ft $\quad (M_b/M_p = 1.04)$

$V_b = 288$ k

Design Joint Strength:

$M_d = \phi M_n$, $\phi = 0.7$

$M_d = 1677$ k-ft

$V_d = 202$ k-ft

II - Strength Per Chapter 4 Model (Ref.- Figs. 4.12 thru 4.14f)

Assess outer panel strength, M_o:

Total joint width:

$$b_j = (b_f + b)/2 \leq b_f + h \leq 1.75\, b_f \qquad (4.8a)$$

$$b_f = 14.19 \text{ in.}$$

$$b = 40 \text{ in.}$$

$$h = 40 \text{ in.}$$

$\underline{b_j = 24.8 \text{ in.}}$

Outer panel width:

$$b_{op} = b_j - max(b_p\,,\, b_f) \leq 2\, d_{op} \qquad (4.8b)$$

$$b_j = 24.8 \text{ in.}$$

$$b_p = 14.2 \text{ in.}$$

$$b_f = 14.19 \text{ in.}$$

$$d_{op} = 0.25\,d = 7.2 \text{ in.}$$

$$\underline{b_{op} = 10.6 \text{ in.}}$$

Mobilization Coefficient:

$$C = (x/h)\,(y/b_f) \tag{4.9}$$

$$x = 25 \text{ in.}$$

$$h = 40 \text{ in.}$$

$$y = 10 \text{ in.}$$

$$b_f = 14.2 \text{ in.}$$

$$\underline{C = 0.44}$$

Effective outer panel width:

$$b'_{op} = C\,b_{op} \tag{4.10}$$

$$C = 0.44$$

$$b_{op} = 10.6 \text{ in.}$$

$$\underline{b'_{op} = 4.7}$$

Calculate compression field strength (Assume ties do not govern):

$$V'_n = V'_c + V'_s \leq 0.63\sqrt{f'_c}\,b'_{op}\,h \tag{4.4a}$$

$$f'_c = 6 \text{ ksi}$$

$$b'_{op} = 4.7 \text{ in.}$$

$$h = 40 \text{ in.}$$

$$\underline{V'_n \leq 290 \text{ k}}$$

Calculate M_o:

$$M_o = (d + d_{op})\,V'_n/2 \tag{4.11}$$

$$d = 28.66 \text{ in.}$$

$$d_{op} = 7.2 \text{ in.}$$

$$V_n' = 290 \text{ k}$$

$\underline{M_o = 5200 \text{ k-in.}}$

Assess inner panel strength, M_{bi}:

Shear contribution of inner concrete panel, V_{eq} & jd:

FBP detail $\therefore b_e = b_p = 14.2$ in.

$V_{eq} = V_n = 0.63\sqrt{f_c'}\, b_e\, h$ (4.12a, 4.3)

$$f_c' = 6 \text{ ksi}$$

$$b_e = 14.2 \text{ in.}$$

$$h = 40 \text{ in.}$$

$\underline{V_{eq} = 877 \text{ k}}$

$jd = 0.75\, d_w$ (4.12b)

$$d_w = 25.44 \text{ in.}$$

$\underline{jd = 19.1 \text{ in.}}$

Vertical shear friction:

$P_{sf} = 1.4\, A_{sf}\, F_{ysf}$ (4.7)

A_{sf} : 2 shear planes

$6\#4$ bars

$A_b = 0.2 \text{ in.}^2$

$A_{sf} = 2.4 \text{ in.}^2$

$F_{ysh} = 60 \text{ ksi}$

$\underline{P_{sf} = 202 \text{ k}}$

1st Iteration:

Assume bearing zone length, a_c:

$$a_c \leq 0.3\,h = 12 \text{ in.} \tag{4.5b}$$

$$\text{Try } \underline{a_c = 7 \text{ in.}}$$

Calculate vertical force couple, P_{eq} & jh:

$$P_{eq} = C_c + T_{vr} + C_{vr} + P_{sf} \tag{4.15a}$$

$$C_c = 2\,f'_c\,a_c\,b_f \tag{4.5a}$$

$$f'_c = 6 \text{ ksi}$$

$$a_c = 7 \text{ in.}$$

$$b_f = 14.2 \text{ in.}$$

$$C_c = 1193 \text{ k}$$

$$T_{vr} = C_{vr} = 0$$

$$P_{sf} = 202 \text{ k}$$

$$\underline{P_{eq} = 1395 \text{ k}}$$

$$jh = \left[C_c\,(h - a_c) + (T_{vr} + C_{vr})\,h_{vr} + P_{sf}\,(h'')\right]/P_{eq} \tag{4.15b}$$

$$C_c = 1193 \text{ k}$$

$$h = 40 \text{ in.}$$

$$a_c = 7 \text{ in.}$$

$$T_{vr} = C_{vr} = 0$$

$$P_{sf} = 202 \text{ k}$$

$$h'' = 37 \text{ in.}$$

$$\underline{jh = 33.6 \text{ in.}}$$

Calculate steel panel strength, V_s:

$$V_s = V_w + V_f \tag{4.2a}$$

$$V_w = 0.6\,F_{yw}\,t_w\,jh \tag{4.2b}$$

$$F_{yw} = 36 \text{ ksi}$$

$$t_w = 0.91 \text{ in.}$$

$$jh = 33.6 \text{ in.}$$

$$V_w = 660 \text{ k}$$

$$V_f = 4M_{pf}/d_f \tag{4.2c}$$

$$M_{pf} = F_{yf}\,t_f^2\,b_f/4 \tag{4.2d}$$

$$F_{yf} = 36 \text{ ksi}$$

$$t_f = 1.61 \text{ in.}$$

$$b_f = 14.2 \text{ in.}$$

$$M_{pf} = 331 \text{ k-in.}$$

$$d_f = 27.1 \text{ in.}$$

$$V_f = 49 \text{ k}$$

$$\underline{V_s = 709 \text{ k}}$$

Calculate beam moment, $M_{bi}[1]$ & $M_{bi}[2]$:

Assume $P_b + P_f = V_c$

$$M_{bi}[1] = \frac{V_s\,d_f + V_{eq}\,jd + M_o\,(d\alpha_3 - h + jh)/\alpha_1}{2 - (d\alpha_3 - h + jh)/\alpha_1} \tag{4.17b}$$

$$V_s = 709 \text{ k}$$
$$d_f = 27.1 \text{ in.}$$
$$V_{eq} = 877 \text{ k}$$
$$jd = 19.1 \text{ in.}$$
$$M_o = 5200 \text{ k-in.}$$
$$d = 28.66 \text{ in.}$$
$$\alpha_3 = 1.67$$
$$h = 40 \text{ in.}$$
$$jh = 33.6 \text{ in.}$$
$$\alpha_1 = 100 \text{ in.}$$

$$\underline{M_{bi}[1] = 24{,}045 \text{ k- in.}}$$

$$M_{bi}[2] = \frac{-\alpha_1}{jh}(V_s\, d_f + V_{eq}\, jd) - M_o + P_{eq}\, \alpha_1 \qquad (4.18b)$$

$$\underline{M_{bi}[2] = 27{,}263 \text{ k-in.}}$$

Compare $M_{bi}[1]$ and $M_{bi}[2]$:

$$M_{bi}[1] < M_{bi}[2]$$

Decrease a_c, Try $\underline{a_c = 6.8 \text{ in.}}$

2nd Iteration:

$$C_c = 1159$$
$$P_{eq} = 1361 \text{ k}$$
$$jh = 33.8$$
$$V_w = 664 \text{ k}$$
$$V_s = 713 \text{ k}$$
$$M_{bi}[1] = 24{,}150 \text{ k}$$
$$M_b[2] = 24{,}175 \text{ k}$$

$M_{bi}[1] = M_{bi}[2]$ (close enough)

$\underline{M_{bi} = M_{bi}[1] = 24{,}150 \text{ k-in.}}$

Total Capacity: $M_b = M_{bi} + M_o = 29{,}350$ **k-in.** $= \underline{\mathbf{2446 \text{ k-ft}}}$

II - Solution Per Chapter 4 Model:

Nominal Joint Strength:

$M_b = 2446$ k-ft $\quad (M_b/M_p = 1.06)$

$V_b = 294$ k

2. Tie Requirements

Inside joint:

Minimum to carry panel shear:

$$\frac{A_{sh}}{s_h} = 0.100 \text{ in.}$$

Minimum recommended: (non-seismic) (5.23a)

$$\frac{A_{sh}}{s_h} = 0.004\,b = \underline{0.160} \text{ in.} \quad \text{(Governs)}$$

Say 4 leg $-$ #4; $\quad A_{sh} = (0.2 \text{ in.}^2)\,(4) = 0.8 \text{ in.}^2$

$$\therefore \; s_h \text{ max} = 0.8/0.160 = 5 \text{ in.}$$

Inside Joint:
USE 4 - #4 @ 5 in. max

Outside joint:

Minimum recommended: (Fig. 5.14)

3 layers - 4 leg # 5 bars

$$A_t \,,\, A_\ell = 3 \times 4 \times 0.31$$
$$= 3.72 \text{ in.}^2$$

Requirement for horizontal transfer:

Required $P_t \leq V'_n = 290$ k

$$P_t = P_{\ell 1} + P_{\ell 2} \leq 1.5\, P_{\ell 1} \tag{5.25a}$$

$$P_{\ell 1} = F_{ysh}\, A\ell \tag{5.25b}$$

$F_{ysh} = 60$ ksi

$A\ell = 3.72$ in.^{2} (min)

$P_{\ell 1} = 223$ k

$P_{\ell 2} = 0$ (for column detail)

$P_t = 223$ k $<$ 290 k (No Good)

Increase A_t , $A\ell$

USE 4 layers of #5 bars:

$$P_t = P_{\ell 1} = 297 \text{ k} > 290 \text{ k} \qquad (OK)$$

Outside Joint (within $10\frac{1}{2}$ in. of beam)
4 layers - 4 leg - #5 bars

3. Maximum Size of Vertical Bars

Non-seismic:

$$d_b \leq (d + d_{op})/15 \tag{5.27a}$$

$$d_{op} = \frac{1}{4}\, d$$

$d_b \leq 2.38$ in.

#11 bars $<$ 2.38 in. (OK)

4. FBP Size and Thickness

Horizontal force, $V_n = 877$ k

Split FBP: $t_p = K\sqrt{PL_{min}/F_{yp}\, L_{max}}$ (5.17)

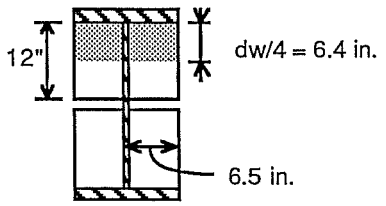

Loaded area:

$L_{min} = 6.4$ in.

$L_{max} = 6.5$ in.

$d_p = 12$ in.

$d_e = 6.4$ in.

$d_p/d_e = 1.88$, so K = 0.18

$F_{yp} = 36$ ksi

$P = 877/2 = 439$ k

$t_p = 0.622$ in. USE $\frac{5}{8}$ in.

Face Bearing Plate $\frac{5}{8} \times 6\frac{1}{2} \times 12$ in.

Check bearing stress:

$F_b = P/A$

$P = 439$ k

$A = 41.6$ sq.in.

$F_b = 10.6$ ksi $< 2f'_c$ (OK)

5. Minimum Steel Column Flange Thickness

Force on flange: $V'_n + V_c = 290 + 481 = 771$ k

Bearing area: $(b_{f\,col})\,(d_{op}) = (10)\,(7.2) = 72.$ sq.in.

Bearing stress: $768/72 = 10.7$ ksi $< 2f'_c$ (OK)

Plate thickness:

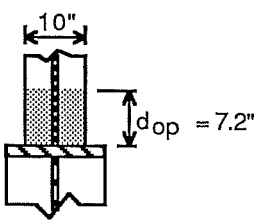

$$t_p = K\sqrt{PL_{min}/F_{yp}\,L_{max}} \qquad (5.17)$$

$K = 0.18$

$P = 771/2 = 386$ k

$L_{min} = 5$ in.

$L_{max} = 7.2$ in.

$F_{yp} = 36$ ksi

$t_p \leq 0.49$ in. min. flange thickness

6. Check Beam Flange Thickness

Force on flange:

$$P_v = V_s\, d_f \,/\, jh + V_b \qquad (5.19)$$

$V_s = 643$ k

$d_f = 27.05$ in.

$jh = 32.7$ in.

$V_b = 288$ k

$P_v = 820$ k

Plate thickness:

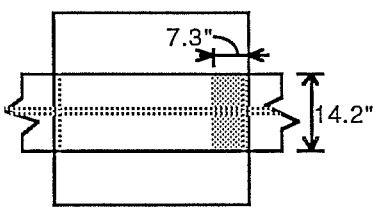

$$t_p = K\sqrt{PL_{min}/F_{yp}\,L_{max}} \qquad (5.17)$$

$K = 0.18$

$P = 820/2 = 410$ k

$L_{min} = 7.1$ in.

$L_{max} = 7.3$ in.

$F_{yp} = 36$ ksi

$t_p \leq 0.601$ in.

$t_p = t_f = 1.61$ in. $>$ 0.601 in. (OK)

EXAMPLE 2 – FACE BEARING PLATE WITH STEEL COLUMN AND VERTICAL JOINT REINFORCEMENT

Given:

1) Joint geometry and layout shown in Fig. A3.2

2) Reinforced Concrete Column: 30 × 30 in. square

$\rho = 4\%$ (max)

$f'_c = 6$ ksi

$F_y = 60$ ksi

3) Steel Beam: W40 × 149 (A36)

$M_p = 1791$ k-ft

d = 38.2 in.

$b_f = 11.81$ in.

$t_w = 0.63$ in.

$t_f = 0.83$ in.

4) Proportional Member Forces:

$$M_b = \alpha_1 V_b \qquad (5.10a)$$

$$V_c = \alpha_3 V_b \qquad (5.10c)$$

$\alpha_1 = 105$ in.

$\alpha_3 = 1.67$

Calculate:

1. Connection strength in terms of maximum beam moment and shear (M_b and V_b). Calculate strength based on design model (Chapter 5) for two cases: one without and one with vertical joint reinforcement.

1. Calculate Maximum Beam Forces, M_b & V_b

Determine effective joint width:

Maximum joint width:

$$b_j = (b_f + b)/2 \leq b_f + h < 1.75\, b_f \qquad (2.4b)$$

$$b_f = 11.81 \text{ in.}$$

$$b = 30 \text{ in.}$$

$$h = 30 \text{ in.}$$

$\underline{b_j = 20.7 \text{ in.}}$

Mobilization coefficient (Neglect vertical joint reinforcement):

$$C = (x/h)\,(y/b_f) \qquad (5.4c)$$

$$x = 19 \text{ in.}$$

$$h = 30 \text{ in.}$$

$$y = 8 \text{ in.}$$

$$b_f = 11.81 \text{ in.}$$

$\underline{C = 0.43}$

Effective outer panel width:

$$b'_{op} = C(b_j - b_i) \leq 2\, d_{op} \qquad (5.4a)$$

$$C = 0.43$$

$$b_j = 20.7 \text{ in.}$$

$$b_i = b_p = 11.8 \text{ in.}$$

$$d_{op} = 0.25d = 9.55 \text{ in.}$$

$\underline{b'op = 3.8 \text{ in.}}$

Effective joint width:

$$b'_j = b_i + b'_{op} \qquad (5.3)$$

$$b_i = 11.8 \text{ in.}$$

$$b'_{op} = 3.8 \text{ in.}$$

$\underline{b'_j = 15.6 \text{ in.}}$

Calculate shear panel strength:

Inner panel:

$$V_n = 0.63\sqrt{f'_c}\, R\, b_p\, h \qquad (5.6a)$$

$$R = 1.0 \qquad (5.6b)$$

$$b_p = 11.8 \text{ in.}$$

$$h = 30 \text{ in.}$$

$$f'_c = 6 \text{ ksi}$$

$\underline{V_n = 546 \text{ k}}$

Outer panel: Assume ties do not govern:

$$V'_n = V'_c + V'_s \leq 0.63\sqrt{f'_c}\; b'_{op}\, h \qquad (5.7a)$$

$$f'_c = 6 \text{ ksi}$$

$$b'_{op} = 3.8 \text{ in.}$$

$$h = 30 \text{ in.}$$

$\underline{V'_n \leq 176 \text{ k}}$

I - Consider Case WITHOUT Vertical Joint Reinforcement

Assume length of bearing region:

$$a_c \leq 0.3\, h = 9 \text{ in.} \qquad (5.8b)$$

Try $\underline{a_c = 9 \text{ in.}}$

Calculate $P_{eq}\; jh$:

$$P_{eq} = C_c = 2\, f'_c\, a_c\, b'_j \qquad (5.9a,5.8a)$$

$$f'_c = 6 \text{ ksi}$$

$$a_c = 9 \text{ in.}$$

$$b_j = 15.6 \text{ in.}$$

$\underline{P_{eq} = 1685 \text{ k}}$

$jh = (h - a_c)$ (5.9b)

$h = 30$ in.

$\underline{jh = 21.0 \text{ in.}}$

Calculate steel panel strength, V_s:

$V_s = 0.6 F_{yw}\, t_w\, jh$ (5.5)

$F_{yw} = 36$ ksi

$t_w = 0.63$ in.

$jh = 21.0$ in.

$\underline{V_s = 286 \text{ k}}$

Column shear factor:

$J = 1.0$ (since steel column is present)

Calculate resulting beam moment, M_b

Assuming shear governs:

$$M_b[1] = \frac{V_s\, d_f + V_n(0.75\, d_w) + V_n'(d + d_{op})}{2 - (J d_f\, \alpha_3/\alpha_1)} \tag{5.12}$$

$V_s = 286$ k

$d_f = 37.4$ in.

$V_n = 546$ k

$d_w = 36.5$ in.

$V_n' = 176$ k

$d = 38.2$ in.

$d_{op} = 9.6$ in.

$J = 1.0$

$\alpha_3 = 1.67$

$\alpha_1 = 105$ in.

$$\underline{M_b[1] = 28,811 \text{ k-in.}}$$

$$M_b[2] = \alpha_1 \left[P_{eq} - \frac{(V_s\, d_f + V_n\,(0.75 d_w) + V_n'(d + d_{op})}{jh} \right] \tag{5.14}$$

$$\underline{M_b[2] = 6709 \text{ k-in.}}$$

Compare $M_b[1]$ and $M_b[2]$:

$$M_b[1] > M_b[2], \text{ so increase } a_c.$$

But, a_c, is at maximum value, therefore, <u>bearing governs</u>.

Calculate beam moment, M_b, with bearing controlling:

$$M_b = \frac{jh\, P_{eq}}{2 - J\, d_f\, \alpha_3/\alpha_1 + jh/\alpha_1} \tag{5.15}$$

$$jh = 21.0 \text{ in.}$$

$$P_{eq} = 1685 \text{ k}$$

$$\underline{M_b = 22,045 \text{ k-in.}}$$

I - Solution Per Design Model (<u>Without</u> Vertical Joint Reinforcement)

<u>Nominal Joint Strength:</u>

$$M_b = 1837 \text{ k-ft} \qquad (M_b/M_p = 1.03)$$

$$V_b = 210 \text{ k}$$

<u>Design Joint Strength:</u>

$$M_d = \phi M_n \,, \; \phi = 0.7$$

$$M_d = 1286 \text{ k-ft}$$

$$V_d = 147 \text{ k}$$

II - Consider Case WITH Vertical Joint Reinforcement

Strength of vertical joint reinforcement:

$$\underline{2-\#9 \text{ bars: } T_{vr} = C_{vr} = 120 \text{ k}}$$

$$\underline{h_{vr} = 24 \text{ in.}}$$

1st Iteration:

Assume length of bearing region:

$$a_c \leq 0.3\,h = 9 \text{ in.} \tag{5.8b}$$

$$\underline{\text{Try } a_c = 8 \text{ in.}}$$

Calculate P_{eq}, jh:

$$P_{eq} = C_c + T_{vr} + C_{vr} \tag{5.9a}$$

$$C_c = 2\,f'_c\,a_c\,b'_j \tag{5.8a}$$

$$f'_c = 6 \text{ ksi}$$

$$a_c = 8$$

$$b'_j = 15.6 \text{ in.}$$

$$C_c = 1498 \text{ k}$$

$$T_{vr} = C_{vr} = 120 \text{ k}$$

$$\underline{P_{eq} = 1738 \text{ k}}$$

$$jh = (C_c\,(h = a_c) + T_{vr} + C_{vr}\,(h_{vr}))\,P_{eq} \tag{5.9b}$$

$$\underline{jh = 22.3 \text{ in.}}$$

Calculate V_s:

$$V_s = 0.6\,F_{yw}\,t_w\,jh \tag{5.5}$$

$$F_{yw} = 36 \text{ ksi}$$

$$t_w = 0.63$$

$$jh = 22.3$$

$$\underline{V_s = 304 \text{ k}}$$

Calculate resulting beam moment, M_b:

$$M_b[1] = \frac{V_s\, d_f + V_n\,(0.75\, d_w) + V_n'\,(d + d_{op})}{2 - (J\, d_f\, \alpha_3/\alpha_1)} \tag{5.12}$$

$$V_s = 304 \text{ k}$$

$$d_f = 37.4 \text{ in.}$$

$$V_n = 546 \text{ k}$$

$$d_w = 36.5 \text{ in.}$$

$$V_n' = 176 \text{ k}$$

$$d = 38.2 \text{ in.}$$

$$d_{op} = 9.6 \text{ in.}$$

$$J = 1.0$$

$$\alpha_3 = 1.67$$

$$\alpha_1 = 105 \text{ in.}$$

$$\underline{M_b[1] = 24{,}698 \text{ k-in.}}$$

$$M_b[2] = \alpha_1 \left[P_{eq} - \frac{V_s\, d_f + V_n(0.75\, d_w) + V_n'\,(d + d_{op})}{jh} \right] \tag{5.14}$$

$$\underline{M_b[2] = 19{,}038 \text{ k-in.}}$$

Compare $M_b[1]$ and $M_b[2]$:

$$M_b[1] > M_b[2], \text{ therefore, increase } a_c.$$

$$\underline{\text{Try } a_c = 8.4 \text{ in.}}$$

2nd Iteration:

$$P_{eq} = 1813 \text{ k}$$

$$jh = 21.9 \text{ in.}$$

$$V_s = 298 \text{ k}$$

$$M_b[1] = 24,559 \text{ k-in.}$$

$$M_b[2] = 24,852 \text{ k-in.}$$

$$M_b[1] = M_b[2] \qquad \text{(Close enough)}$$

$$\underline{M_b = 24,559 \text{ k-in.} = 2047 \text{ k-in.}}$$

II - Solution Per Design Model (<u>With</u> Vertical Joint Reinforcement):

<u>Nominal Joint Strength:</u>

$$M_b = 2047 \text{ k-ft} \qquad (M_b/M_p = 1.14)$$

$$V_b = 234 \text{ k}$$

<u>Design Joint Strength:</u>

$$M_d = \phi M_n \text{ , } \phi = 0.7$$

$$M_d = 1432 \text{ k-ft}$$

$$V_d = 164 \text{ k}$$

Glossary of Nomenclature

A_c = cross-sectional area of column core confined by ties, sq. in.

A_g = gross cross-sectional column area, sq. in.

A_l = total area of ties parallel to beam in transfer zone as shown in Figs. 4.11 and 5.14, sq. in.

A_{sh} = total cross-sectional area of transverse reinforcement (including cross ties) with spacing sh and perpendicular to dimension b, sq. in.

A_{sf} = total cross-sectional area of transverse reinforcement fully developed in tension and crossing the vertical crack plane as shown in Fig. 4.4b, sq. in.

A_t = total area of ties perpendicular to beam in transfer zone as shown in Figs. 4.11 and 5.14, sq. in.

a_c = length of concrete bearing zone, in.

b = width of concrete column measured perpendicular to beam, in.

b_e = effective width of concrete panel, in.

b_f = width of steel beam flanges, in.

b_i = effective width of inner panel, in.

b_j = maximum width of joint region, in.

b'_j = effective width of joint region, in.

b_{op} = maximum width of outer panel, in.

b'_{op} = effective width of outer panel, in.

b_p = width of FBP or WSP, in.

C = mobilization coefficient as shown in Figs. 4.6 and 4.7.

C_c = nominal compression strength of bearing zone adjacent to the beam, k.

C_{vr} = nominal compression strength of vertical reinforcement, k.

d = total height of steel beam, in.

d_b = diameter of reinforcing bar, in.

d_f = distance between centerlines of the steel beam flanges, in.

d_{op} = additional effective joint depth provided by attachments to flanges , in.

d_w = distance between beam flanges (height of web), in.

e = base for natural logarithm.

F_y = specified minimum yield stress of steel, ksi.

F_{yw} = specified yield stress of beam web, ksi.

F_{yf} = specified yield stress of beam flange, ksi.

F_{yp} = specified yield stress of bearing plate, ksi.

F_{ysh} = specified yield stress of transverse shear reinforcement, ksi.

f'_c = specified compression strength of concrete, psi.

h = total depth of concrete column measured parallel to the beam, in.

h'' = total depth of column core confined by ties, in.

h_{vr} = horizontal distance between vertical joint reinforcement, in.

J = dimensionless coefficient to account for contribution of column shear in joint calculations.

jd = vertical distance between the horizontal force couple, V_{eq}, shown in Fig. 4.8, in.

jh = horizontal distance between the vertical force couple, P_{eq}, shown in Figs. 4.10 and 5.3c, in.

K = dimensionless coefficient to account for geometry in evaluating bearing plate thickness.

L_{max} = maximum characteristic length used for evaluating bearing plate thickness, in.

L_{min} = minimum characteristic length used for evaluating bearing plate thickness, in.

M_b = total moment in the steel beam adjacent to the connection, k-in. (unless otherwise noted).

M_c = total moment in the reinforced concrete or composite column adjacent to the connection, k-in. (unless otherwise noted).

M_{bi} = moment in the steel beam carried by the inner joint panel, k-in.

M_{ci} = moment in the concrete column carried by the inner joint panel, k-in.

M_o = moment in the steel beam and concrete column carried by the outer joint panel, k-in.

M_{pf} = plastic moment capacity of beam flange, k-in.

n = number of layers of transverse reinforcement within the beam depth.

P = applied load, k.

P_b = horizontal column shear transferred into the steel flanges by bearing (Fig. 4.8E), k.

P_{eq} = resultant of vertical forces acting on the inner panel, k.

P_f = horizontal column shear transferred into the steel flange by friction, k.

$P_{\ell 1}$ = strut transfer force provided by column ties in Fig. 4.11a, b and c, k.

$P_{\ell 2}$ = shear friction transfer force shown in Fig. 4.11b, c and d, k.

P_{sf} = vertical force transferred by shear friction into the inner concrete panel, k.

P_t = total strength of horizontal force transfer to outer panel, k.

P_{t1} = tension force provided by column ties in Fig. 4.11a, k.

P_{t2} = tension force provided by column ties in Fig. 4.11b, k.

P_v = maximum vertical force in steel beam associated with web panel yielding, k.

Q_i = applied load (DL,LL,W,E,S or other).

R = reduction coefficient for inner concrete panel strength.

R_m = mean value of measured component strength.

R_n = mean value of calculated component strength.

s_h = center to center spacing of transverse column reinforcement, in.

T_{vr} = nominal tension strength of vertical joint reinforcement, k.

t_f = thickness of the steel beam flange, in.

t_p = thickness of bearing plate, in.

t_w = thickness of the steel beam web, in.

V_b = total shear in the steel beam adjacent to the connection, k.

V_c = total shear in the reinforced concrete or composite column adjacent to connection, k.

V_c' = concrete contribution to the compression field mechanism, k.

V_f = contribution of local flange bending to steel panel strength, k.

V_n = nominal horizontal shear capacity of the compression strut mechanism, k.

V_n' = nominal horizontal shear capacity of the compression field mechanism, k.

V_r = coefficient of variation for ratios of resistances, R_m/R_n.

V_s = nominal horizontal shear capacity of the steel web panel, k.

V_s' = reinforcing steel contribution to the compression field mechanism, k.

V_w = contribution of web shear to steel panel strength, k.

x = dimension for calculation of C coefficient, in.

y = dimension for calculation of C coefficient, in.

α_i = proportionality constants relating beam and column forces.

β = reliability (safety) index.

γ_i = load factors as given by AISC-LRFD specification.

ϕ = resistance (capacity reduction) factor.

REFERENCES

1. Sheikh, T.M., "Moment Connections Between Steel Beams and Concrete Columns," Ph.D. Dissertation, Department of Civil Engineering, The University of Texas at Austin, Dec. 1987.

2. Griffis, L., "Some Design Considerations for Composite-Frame Structures," *AISC Engineering Journal*, 2nd Quarter, 1986.

3. Moore, W., Gosain, N., "Mixed Systems: Past Practices, Recent Experience and Future Direction," *Composite and Mixed Construction*; Proceedings of the U.S./Japan Joint Seminar, Edited by C. Roeder, ASCE, 1985.

4. Rastorfer, D., "William J. Le Messurier's Super-tall Structures: A Search for the Ideal," *Architectural Record*, Jan. 1985.

5. Iyengar, H., "Recent Developments in Mixed Steel-Concrete Systems," *Composite and Mixed Construction*; Proceedings of the U.S./Japan Joint Seminar, Edited by C. Roeder, ASCE, 1985.

6. Wakabayashi, M., "Recent Developments for Composite Buildings in Japan," *Composite and Mixed Construction*; Proceedings of the U.S./Japan Joint Seminar, Edited by C. Roeder, ASCE, 1985.

7. Minami, K., "Beam to Column Stress Transfer in Composite Structures," *Composite and Mixed Construction*; Proceedings of the U.S./Japan Joint Seminar, Edited by C. Roeder, ASCE, 1985.

8. ACI-ASCE Committee 352, "Recommendations for Design of Beam Column Joints in Monolithic Reinforced Concrete Structures," *Report ACI 352 R-85*, 1985.

9. Paulay, T., "Equilibrium Criteria for Beam-Column Joints," Interim Report: US-NZ-Japan-China Seminar on Design of RC Beam-Column Joints for Earthquake Resistance, University of Canterbury, Christchurch, NZ, Aug. 1987.

10. American Institute of Steel Construction, "Specifications for the Load and Resistance Factor Design, Fabrication and Erection of Structural Steel for Buildings," AISC, Chicago, IL, Sept. 1986.

11. Griffis, L., Consulting Structural Engineer with the firm of Walter P. Moore and Assoc., Houston, TX.

12. Gosain, N., Brown, R., & Jirsa, J., "Shear Requirements for Load Reversals on RC Members," *Journal of the Structural Division*, ASCE, July, 1977.

13. Clough, R., & Penzien, J., *Dynamics of Structures*, McGraw Hill, NY, 1975.

14. Kitayama, K., Otani, S. & Aoyama, H., "Earthquake Resistant Design Criteria for Reinforced Concrete Interior Beam-Column Joints," *Proceedings–Pacific Conference on Earthquake Engineering*, Wairakei, New Zealand, 1987.

15. American Concrete Institute, "Building Code Requirements for Reinforced Concrete (ACI-318) and Commentary," ACI, Detroit, MI, 1983.

16. Meinheit, D.F., "The Shear Strength of Reinforced Concrete Beam-Column Joints," Ph.D. Dissertation, Department of Civil Engineering, The University of Texas at Austin, Dec. 1983.

17. Guimaraes, G., et al., "Tests of Reinforced Concrete Slab-Beam-Column Connections– U.S. Designs," Interim Report: US-NZ-Japan-China Seminar on Design of RC Beam-Column Joints for Earthquake Resistance, University of Canterbury, Christchurch, NZ, Aug. 1987.

18. Krawinkler, H., Bertero, V., & Popov, E., "Shear Behavior of Steel Frame Joints," *Journal of the Structural Division*, ASCE, Nov. 1975.

19. Stelmack, T., Marley, M. & Gerstle, K., "Analysis and Tests of Flexibly Connected Steel Frames," *Journal of Structural Engineering*, ASCE, July 1986.

20. Ackroyd, M., Gerstle, K., "Behavior of Type 2 Steel Frames," *Journal of the Structural Division*, ASCE, July, 1982.

21. ACI-ASCE Committee 352, "Recommendations for Design of Beam-Column Joints in Monolithic Reinforced Concrete Structures," 1976.

22. Prestressed Concrete Institute, *PCI Design Handbook–Precast Prestressed Concrete*, PCI, Chicago, IL, 1978.

23. American Institute of Steel Construction, "Specifications for the Design, Fabrication and Erection of Structural Steel Buildings with Commentary," AISC, Chicago, IL, Nov. 1978.

24. American National Standards Institute, "Minimum Design Loads for Buildings and Other Structures, ANSI A58.1," ANSI, 1982.

25. Galambos, T., "Reliability of Connections, Joints and Fasteners," Structural Engineering Report No. 85-05, Department of Civil and Mineral Engineering, University of Minnesota, Dec. 1985.

26. Guimaraes, G., & Jirsa, J., Research in progress on the use of high strength concrete in reinforced concrete slab- beam-column connections, 1988.

27. Bjorhovde, R., "Design Considerations for Composite Frames," Las Construcciones De Acero En Zonas Sismicas (Steel Construction in Seismic Zones), Proceedings, 5th International Symposium of Steel Structures, Morelia, Michoacán, Mexico, Nov. 1987.